Universidad de Guanajuato

Division de Ciencias e Ingenierías.
Campus Leon

STRUCTURAL AND DYNAMICAL PROPERTIES OF COLLOIDS UNDER CONFINEMENT

EDITH CRISTINA EUÁN DÍAZ

IN ORDER TO OBTAIN THE DEGREE OF:

Doctor in Physics

UNDER THE SUPERVISION OF:

RAMÓN CASTAÑEDA PRIEGO

SALVADOR HERRERA VELARDE

FRANCOIS PEETERS

VYACHESLAV MISKO

December 2013 – Final version

Universidad de Guanajuato

Departamento de Ingenierías
Division de Ciencias e Ingenierías.
Campus Leon

Universiteit Antwerpen

Condensed Matter Group
Departement Fysica
Campus Groenenborger

STRUCTURAL AND DYNAMICAL PROPERTIES OF COLLOIDS UNDER CONFINEMENT

EDITH CRISTINA EUÁN DÍAZ

IN ORDER TO OBTAIN THE DEGREE OF:

Doctor in Physics

UNDER THE SUPERVISION OF:

RAMÓN CASTAÑEDA PRIEGO

SALVADOR HERRERA VELARDE

FRANCOIS PEETERS

VYACHESLAV MISKO

December 2013 – Final version

Wissenschaft und Kunst gehören der Welt an, und vor
ihnen verschwinden die Schranken der Nationalität.

Science and art belong to the whole world, and before them
vanish the barriers of nationality.

La ciencia y el arte pertenecen a todo el mundo, y ante
ellas de

-Johann Wolfgang von Goethe

Dedicated to...

To the Mexican peo
of my Education. And now, even in the
darkne

country...

To the Belgian peo

o

my PhD Education...

The loving memory of Juana Muñoz Vázquez.
1928-2006.

The loving memory of J. Guadalupe Díaz-Barriga.
1924-2008.

Xokbi Chuuy

Bóon le loolo'ob yóok'ol le iipilo' kantéen uktéen suut tu beetaj le púutso, buka'aj u puulu bin in tuukul ti' teecho' Tin wilaj a chambéel che'ej leeti' u chuka'an óolalil a úuchbenil. Te'e xaako le k'uuncho'obo' ts'o'ok u bak'ubao'ob yaan k'iine ma'atán u cha'akubao'ob; ka jan k'a'ajsik a k'iinilo'ob, ich a xaake' yaanchajtech k'uucho'ob jejelás u boonilo'b, chako'ob, booxo'ob, sako'ob, k'ano'ob yéetel ukp'éel u láak'o'ob ku síinil tu nak'le ka'ano'. Yéetel le lo'obo' ta chuyaj a k'iino'ob, ta chuyaj a náayo'ob; ich a xaake', asab yaan jejeláas k'uuch p'aatal, u boonilo'obe jujump'íit u bin u saátal le púuts'o' táan u bin u cháambetal.

Hilo Contado

Se pintaron las flores sobre el hupil, cuatro, siete veces giró la aguja, son las veces que pensé en tí. Vi tus manos que trabajan ávidamente, vi tu sonrisa lenta, es la paciencia de tus días. En la canasta, los hilos se han enredado, a veces no se desatan; en un instante rememoras tus días, en tu canasta tuviste hilos de muchos colores, rojos, negros, blancos, amarillos y siete más que se extienden hasta el cielo. Con ellos bordaste tus días, bordaste tus sueños; en tu canasta, todavía quedan varios hilos, sus colores desaparecen poco a poco y tu aguja se hace más lenta.

Counted Thread

Flowers were painted on hupil, four, seven times turned the needle, those are the times I thought of you. I saw your hands working eagerly, I saw a slow smile, is the patience of your days. In the basket, the wires have become entangled, sometimes they do not untie; instantly reminisce your days, in your basket you had threads of many colors, red, black, white, yellow and seven others that stretch to the sky. With them embroidered your days, you embroidered your dreams, in your basket there are still several threads, their colors are gradually disappearing and your needle is slowing down.

A Mayan poem.

A mi papá Luis Humberto Euán E
Irma E
hablan Maya y E

To my father Luis Humberto Euán E
grandparent
speak English but they do speak Mayan and I,

ABSTRACT

In this thesis, we focus on questions that concern the effect of confinement in colloidal suspensions. We explore the structural and dynamic properties of colloids interacting with external potentials; the latter allows us to explore the behavior of such materials when they are spatially restricted. We attack systematically several levels of confinement, going from a quasi-zero-dimension to a quasi-three-dimension. In our study, we put special emphasis on the fact that the colloidal particles are immersed in a solvent which makes this adventure more exciting.

First, we present the most basic knowledge about how Hydrodynamic Interactions (HI) affect the dynamics of the particles. This is done by studying a simple case: two and three Brownian particles highly confined, in such a way that they can only move around one point and interact just by the solvent. Here, we find that the HI couple dynamically the movements of the particles, giving rise to not-null autocorrelation functions. Negative cross-correlation functions are found for several configurations with an exception in the collinear configuration of three particles, where we find for the fist time that a third particle placed between two other outermost induces positive correlations.

Then, we gain more insight of the hydrodynamic coupling when we consider an infinite line of interacting Brownian particles. We realize that the HI allow the particles to move faster if the system is homogeneous, but if there is a spatially-periodic external field interacting with them, the dynamics changes. More specifically, we find that the inclusion of the HI give rise to counterintuitive behaviors, such as slowing down and speeding up processes in the dynamics of the system depending on the amplitude and the periodicity of the external field.

Furthermore, we show that we can induce dimensional variations by changing the confinement conditions and allowing the interacting Brownian particles to move in two dimensions. This is done by deliberatively controlling the available space in one of the directions. Thus, we find that, by mastering the level of confinement, dimensionality changes can be induced. Moreover, by geometrically relaxing or constraining the system, incredible structural an dynamical behaviors can be found, such as sudden melting, re-entrant freezing phenomena, slow and fast dynamics, and caging effects that look alike to glasses, just to mention a few.

The last system in which we focus our attention is a couple of layers of colloidal particles placed over a one-dimensional periodic field

that recreates a substrate. The latter only affects the bottom layer by inducing that the colloidal particles occupy the regions where they can minimize their energy. In a general way, our findings are that if the period of the substrate is the same as the mean particle distance, the upper layer tends to reproduce the structure of the bottom layer. When the period of the substrate is twice the previous one, the particles at upper layer fill those spaces where there is an absence of particles at the bottom. One of the exciting things about this layered system is that, for certain conditions, the colloidal particles behave like a solid in the direction where the periodic external potential is applied and, in the opposite one, they behave like a liquid.

ABSTRACT

Tegenwoordig weet de wetenschappelijke gemeenschap dat colloïdale deeltjes bijzondere eigenschappen vertonen als hun beweging beperkt wordt in de ruimte. Deze wetenschap is een gevolg van de talrijke onderzoeken die werden uitgevoerd, zowel experimenteel, theoretisch als doormiddel van computer simulaties. Niettemin, zelfs met de enorme hoeveelheid nieuwe resultaten, zijn er nog steeds veel vragen die beantwoord moeten worden. In dit doctoraat heb ik mij geconcentreerd op die vragen die betrekking hebben op de structurele en dynamische eigenschappen van colloïdale suspensies wanneer hun beweging wordt beperkt door externe potentialen. Dit stelt ons in staat om het gedrag te onderzoeken van dergelijke materialen als ze ruimtelijk worden ingeperkt. We verkennen systematisch verschillende niveaus van opsluiting, gaande van quasi–nul tot quasi–drie dimensies.In onze studies benadrukken we het feit dat de colloïdale deeltjes ondergedompeld zijn in een vloeibaar oplosmiddel wat dit avontuur nog spannender maakt.

Eerst presenteren we de basisprincipes hoe hydrodynamische interacties (HI) de dynamica van deeltjes beinvloeden. Dit wordt gerealiseerd aan de hand van het eenvoudige geval van twee en drie Brownse deeltjes wiens beweging beperkt is tot deze rond een punt en die interageren met een solvent. We vinden dat de HI aanleiding geeft tot gekoppelde dynamica waarbij de beweging van de deeltjes aanleiding geeft tot autocorrelatiefuncties die van nul verschillen. Negatieve kruis–correlatiefuncties werden gevonden voor enkele configuraties dit met uitzondering van de co–lineaire configuratie van drie deeltjes waarbij het derde deeltje geplaatst is tussen de twee deeltjes dewelke positieve correlaties induceert.

Een dieper inzicht van de hydrodynamische koppeling werd bekomen door een oneindige ketting van interagerende Brownse deeltjes te beschouwen. Het blijkt dat de HI de deeltjes sneller kan doen bewegen indien het systeem homogeen is. Maar in de aanwezigheid van een interagerend ruimtelijk periodiek uitwending veld verandert de dynamica. De HI geeft aanleiding tot contra–intuïtief gedrag zoals een vertraging en versnelling van de dynamica afhankelijk van de amplitude en periodiciteit van het uitwendig veld.

Verder tonen we aan dat we dimensionele variaties kunnen induceren door het veranderen van de inperkingscondities en door de interagerende Brownse deeltjes te laten bewegen in twee dimensies. Dit werd gerealiseerd door de beschikbare ruimte te veranderen in één van de richtingen. We vinden dat door de sterkte van de inperking te controleren we de dimensionaliteit kunnen veranderen, het

is mogelijk om een veranderde structurele en dynamische gedrag te bekomen zoals een plots smelten, een re–entrant vriezen, langzame en snelle dynamica en een kooi effect dat gelijkaardig is met een fenomeen dat waargenomen is in glazen.

Het laatste systeem dat onderzocht werd zijn gekoppelde lagen van colloïdale deeltjes die geplaatst zijn over een één–dimensionaal periodisch veld dat een periodiek substraat simuleert. Dit period substraat beinvloed alleen de onderste laag en zorgt ervoor dat de colloïdale deeltjes posities innemen die de energie minimaliseert. In het algemeen vinden we dat als de periode van het substraat hetzelfde is als de inter–deeltjes afstand, de bovenste laag de neiging heeft om de structuur van de onderste laag te reproduceren. Echter als de periode van het substraat twee keren groter is gaan de deeltjes van de bovenste laag de ruimtes vullen tussen de deeltjes van de onderste laag. Een van de merkwaardigste resultaten is dat in dit gelaagde systeem onder bepaalde condities, de colloïdale deeltjes zich gedragen als een vaste stof in de richting van de periodische potentiaal en als een vloeistof in de loodrechte richting hierop.

RESUMEN

En esta tesis nos enfocamos en aquellas preguntas que conciernen al efecto del confinamiento en suspensiones coloidales. Nosotros exploramos propiedades estructurales y dinámicas de coloides cuando éstos interactúan con potenciales externos; esto último nos permite explorar el comportamiento de dichos materiales cuando están espacialmente restringidos. Atacamos sistemáticamente varios niveles de confinamiento , yendo desde una cuasi-cero dimensión a una cuasi-tridimensional. En nuestro estudio, ponemos énfasis especial en el hecho de que las partículas coloidales están inmersas en un solvente lo cual hace esta aventura más emocionante.

Primero presentamos el conocimiento más básico de cómo las Interacciones Hidrodinámicas (HI, por sus siglas en inglés) afectan la dinámica de las partículas. Ésto es hecho mediante el estudio de un caso simple: dos y tres partículas Brownianas altamente confinadas, de ésta manera dichas partículas sólo pueden moverse al rededor de un punto e interactuan sólo por medio del solvente. Aquí, encontramos que las HI acoplan dinámicamente los movimientos de las partículas, dando lugar a funciones de autocorrelación diferentes de cero. Funciones de correlación cruzada negativas son encontradas para varias configuraciones con una excepción: el caso colinear de tres partículas, donde encontramos por primera vez que una tercera partícula, localizada entre dos que se encuentran en los extremos, induce correlaciones positivas.

Después, ganamos más intuición del acoplamiento hidrodinámico cuando consideramos una línea infinita de partículas Brownianas interactuantes. Nos damos cuenta de que las HI permiten a las partículas moverse más rápido si el sistema es homogéneo, pero si hay un campo externo espacialmente periódico interactuando con ellas, la dinámica cambia. Más específicamente, encontramos que la inclusión de las HI da lugar a comportamientos contraintuitivos, como procesos de frenado y aceleración (respecto al caso homogéneo) en la dinámica del systema dependiendo de la amplitud y la periodicidad del campo externo.

Más aún, mostramos que podemos inducir variaciones dimensionales cambiando las condiciones de confinamiento y permitiendo el movimiento en dos dimensiones de las partículas Brownianas interactuantes. Ésto es hecho controlando deliberadamente el espacio accesible en una de las direcciones. En consecuencia, encontramos que, dominanto el nivel de confinamiento, se puede inducir cambios dimensionales. Es más, relajando o restringiendo geométricamente al sistema, increíbles comportamientos estructurales y dinámicos puedes

ser encontrados, tales como fenómenos de derretimiento y congelamiento re-entrante, dinámicas lentas y rápidas, y efectos de encajuelamiento que se parecen a los que muestran los vidrios, sólo por mencionar algunos.

El último sistema de interés en en cual nosotros enfocamos nuestra atención es una pareja de capas de partículas coloidales situadas sobre un campo periódico unidimensional que recrea un substrato. Éste último sólo afecta la capa inferior, induciendo que las partículas coloidales ocupen las regiones donde pueden minimizar su energía. De manera general, nuestros descubrimientos son, si el periodo del substrato es el mismo que la distancia promedio entre partículas, la capa superior tiende a reproducir la estructura de la capa inferior. Cuando el periodo del substrato es el doble del anterior, las partćilas en la capa superior tienden a llenar aquellos espacios donde hay una ausencia de partículas en la capa inferior. Una de las cosas emocionantes de éste sistema de capas es que, para ciertas condiciones, las partículas coloidales se comportan como un sólido en la dirección en que el potencial externo periódico es aplicado y, en la dirección opuesta, se comporta como un líquido.

PUBLICATIONS

Some ideas and figures have appeared previously in the following publications:

1. "Single-file diffusion in periodic energy landscapes: The role of hydrodynamic interactions", **Edith C. Euán-Díaz**, Vyacheslav R. Misko, Francois M. Peeters, Salvador Herrera-Velarde and Ramón Castañeda-Priego, *Physical Review E*, 2012, **86**, 031123.

2. "Directed Self-Assembly of Colloids on Parallel Layers by a One-Dimensional Modulated Substrate", Salvador Herrera-Velarde, Alexandra Delgado-González, **Edith C. Euán-Díaz** and Ramón Castañeda-Priego, *Journal of Nanofluids*, 2012, **1**, 44–54.

3. "Hydrodynamic correlations in three-particle colloidal systems in harmonic traps", Salvador Herrera-Velarde, **Edith C. Euán-Díaz**, Fidel Córdoba-Valdés and Ramón Castañeda-Priego, *Journal of Physics: Condensed Matter*, 2013, **25**,325102.

4. "Structural phases and dimensional variations induced by a parabolic potential in colloidal systems", **Edith C. Euán-Díaz**, Salvador Herrera-Velarde, Vyacheslav R. Misko, Francois M. Peeters and R. Castañeda-Priego, *To be submitted*.

5. "Self-diffusion of interacting colloids in a parabolic potential", **Edith C. Euán-Díaz**, Salvador Herrera-Velarde, Vyacheslav R. Misko, Francois M. Peeters and R. Castañeda-Priego, *To be submitted*.

6. "Single-file diffusion: The role of the attractive interactions", **Edith C. Euán-Díaz**, Salvador Herrera-Velarde and R. Castañeda-Priego, *To be submitted*.

ACKNOWLEDGMENTS

Actually, I'm pretty short with words, but I feel my heart
ex
part of my Che
when I mentally go backwards, when I try to make a re
of the ex
cannot be but happy. One should think that it is the easie
part, but for me it has been the mo
think carefully, and even then, I feel that the words cannot
ex

Primero que nada quiero agradecerle
Elodia, que han e
mo
lo
todo lo que le

A mis hermana Genny que con su apoyo, amor y e
ha hecho de mi vida algo me
que siempre dibujan una sonrisa en mi cara, que me ofrecen
su amor y apoyo incondicional. Un minuto al lado de todo
mis hermano
que sea sortear las visicitude
hacer.

A mis sobrino
dan grande
me

A mis cuñado
mis hermano
me conocieron. Gracias por todo.

A mi familia, que son tanto
a todo
Co my beloved Frank; you have transformed my life in
a inde
love. Chanks for giving me the courage to go on when I felt
that I was not made for this. Chanks for your wise advise and
mo
succe
A mis ase
mado como profe
de po
cias por su confianza, apoyo y guía durante todo
Siempre e
ede
Co Francois and Slava, for giving me the big o
and the honor to work with you. Chanks for giving me your
trust and support. I have no words to de
perience in Belgium changed my profe
life.
A todo
profe
go
Co all my colleague
all over the world. Chis PhD has given me the o
to meet great peo
piece
been of constant learning, each one of you have contributed
to make me wiser and more human. Chanks everyone.
Co all my friends, all of you have given me your support in
moment
tho
thanks for being part of my life. One of the great thing

studying a PhD on Phy
gather around the world. Everyone is special, unique, lovely
and occupie
tears in laughs, loneline
weather in beach (or pool or BBQ or ice-cream) partie
beer, mistake
better place. Please, acce

To the administrative personnel that did a great job during
all the required procedure

CONTENTS

LIST OF FIGURES

LIST OF TABLES

ACRONYMS

PDF	Probability Density Function
DLVO	Derjaguin-Landau-Verwey-Overbeek
lhs	Left-Hand-Side
rhs	right-hand side
PB	Poisson-Boltzmann
1D	One-Dimensional
2D	Two-Dimensional
3D	Three-Dimensional
q1D	Quasi-One-Dimensional
q2D	Quasi-Two-Dimensional
HI	Hydrodynamic Interactions
BD	Brownian Dynamics
MSD	Mean-Square Displacement
SFD	Single-file Diffusion

1

INTRODUCTION

"The capacity to learn is a gift;
The ability to learn is a skill;
The willingne
- Dune: House Harknonnen, page 437.

Nowadays, colloids are one of the most studied fields belonging to the *Soft Condensed Matter* (a subfield of the *Condensed Matter* Physics). *Soft Condensed Matter* defines a broad class of materials including but not limited, to colloidal suspensions, liquid crystals, polymers, that are characterized by weak interactions between polyatomic constituents, by important thermal fluctuations effects, by mechanical softness and rich phase behavior. *Soft Condensed Matter* has grown as an important and interesting field, not only because its wealth of everyday applications, also because of the fact that it stimulates fruitful interdisciplinary interactions between scientists from physics, chemistry, and biology [1].

Lately, with the large number of specialized conferences organized every year on topics like polymer chemistry and physics, colloid chemistry and physics, surfactants in solutions, etc., the scientific community gave more a unified three-folded-view of foft matter systems at the *International Soft Matter Conference* held in Aachen, Germany, in October 2007 [2].

First, it was recognized over the last decades that colloids, polymers and surfactants are by far not as distinct materials as previously assumed. Indeed, there is essentially a continuum of molecules and systems spanning the gaps between these three "basic" materials, as illustrated in the "*Soft Matter* Triangle" in Fig. 1.1. The two main axes of this triangle are, roughly speaking, amphiphilicity as abscissa and elongation or flexibility as ordinate. Let us illustrate this by following the left-hand side of the triangle from colloids to flexible polymers. Traditionally, colloids are rigid particles with a spherical shape. There are, however, also colloids with other shapes, like platelets and rods. As the aspect ratio of colloidal rods (the ratio of rod length and rod diameter) becomes larger, they generally lose their rigidity and

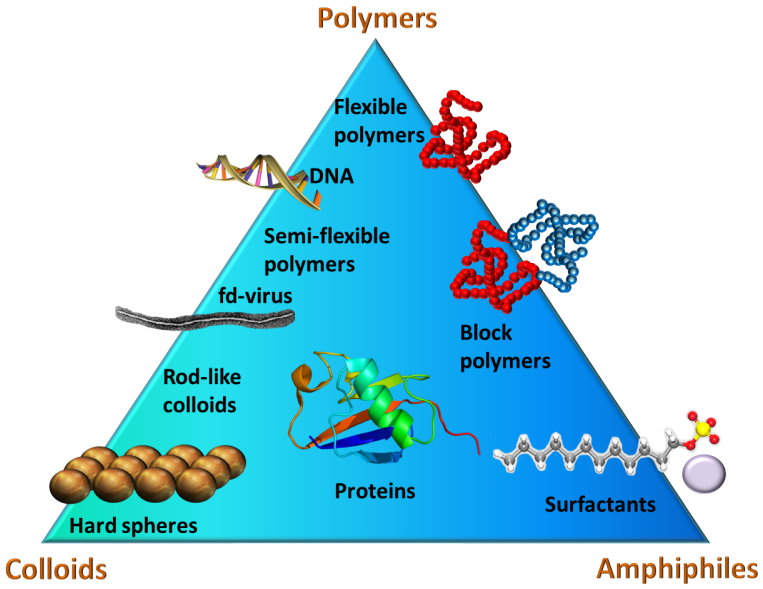

Figure 1.1: The components of modern *Soft Matter* systems can be arranged in a triangle, which shows that there is a continuum of molecules and materials which fills the space between spherical colloids, flexible polymers, and surfactants (adapted from Ref. [2]).

become somewhat flexible. An example is the *fd-virus* shown in Fig. 1.1, where the length of the particle is about a third of the persistence length. For even larger aspect ratios, the length usually exceeds the persistence length. This is the regime of semi-flexible polymers, of which DNA is an example of tremendous importance. Finally, in the limit of very small persistence lengths, we arrive at the classical, flexible synthetic polymers [2].

Second, mixtures of several components of colloidal, polymeric or amphiphilic character are becoming increasingly important. These mixtures exhibit properties that are not found for each of the "pure systems", and open up the possibility to tune and control material properties [2]. Well-known examples are the depletion interaction between colloidal particles induced by polymers in solution [3–16], the intriguing mesophases in mixtures of spherical and rod-like colloids [17–24], the tuning of membrane properties by anchored polymers [25–29] and amphiphilic block copolymers [30–36], and the modification of the properties of polymer melts by addition of colloidal particles to form nano-composites [4, 37–40] .

Third, biological and biomimetic systems share many macromolecules and properties with *Soft Matter* systems [2]. Indeed, the application of concepts and ideas from physics to biological systems has become one of the most intense activities in *Soft Matter* research in recent years [41–47].

In the present thesis, we focus on the understanding of structural and dynamical properties of colloids, which even when they are one of the "simplest" systems studied by the *Soft Matter* community, there

are still a wide range of questions to be answered. In fact, colloids are difficult to ignore because we are surrounded of and even composed by them. They function in every body cell, in the blood, and in all body fluids, especially the intra- and inter-cellular fluids. All life processes take place in a colloidal system, and that is true both of the normal fluids and secretions of the organism, and of the bacterial toxins, as well as, in large measure of the reactions, which confer immunity and let us live for longer times. Also, we can enjoy little pleasures of life trough their incredible taste, in the milk that we drink, the mayonnaise that we put on the fries and the butter that we spread on our bread. Moreover, our daily life is full of colloids; we can find them in the polluted air, paints, cosmetics, medicines, and inside more complicated devices like the colloidal liquid that is in the plasma televisions.

One of the most simple and common picture of a colloidal system is when one kind of substance (dispersed phase) is suspended in another (continuous phase). Both substances can be gas-, liquid- and solid-like. There is a jungle of colloidal systems that include aerosols (liquid droplets or solid particles in gas), emulsions (liquid droplets in liquid), foams (gas bubbles in a liquid) and suspensions (solid particle in a liquid) [48]. The present thesis focuses on the study of the latter ones.

One of the important historical events about these systems took place in 1827. While examining grains of pollen suspended in water under a microscope, Robert Brown (1773-1858) observed tiny particles ejected from the pollen grains, executing a continuous jittery motion. He then observed the same motion in particles of inorganic matter, enabling him to rule out the hypothesis that the effect was life-related. Although Brown did not provide a theory to explain the motion. Brownian motion was the matter of intense debates for around one century until Albert Einstein (1879-1955) in his work "*On the movement of small particles suspended in a stationary liquid demanded by the molecular kinetic theory of heat*" gave a concrete physical explanation of it [49].

Brownian motion is one of the most important properties of colloidal suspensions because it maintains the particles in dispersed state, fighting against gravity that pulls particles towards earth and attractive interactions derived by the maximization of the entropy that tend to bring particles together. The response of suspensions to applied stress are dramatically altered by Brownian motion. A suspension can flow and can behave like an extremely viscous material upon application of stress. The energy injected to the suspension can be easily dissipated in non-intuitively way if the system exhibits Brownian motion. If the particles are arrested, i. e., Brownian motion is hindered such as in gels or glassy systems, only a fraction of the energy can be dissipated immediately leading to viscoelastic behavior [48].

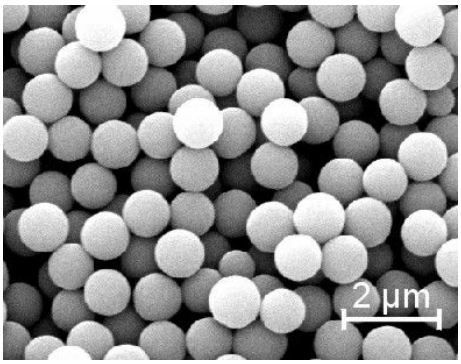

Figure 1.2: Colloidal particles. (Taken from Ref. [50])

The word "colloid" was introduced by Thomas Graham (1805-1869), which is derivated from the Greek word κοιια that means "glue - oid". In his experiments, Graham observed particles that can be distinguished from molecules by their slow diffusion and inability to penetrate through membranes with pore sizes smaller than 10 nm [49]. For instance, there are no restrictions on the shape of the colloids, neither for the composition of the continuous phase. But they have to exhibit Brownian motion, and as a consequence their size is restricted to be in the range between ~ 10 nm and ~ 10 µm, see Fig. 1.2 [51].

In recent years, predominantly in the last three decades, colloids have been exploited to understand the principles of equilibrium many-body transitions such as fluid-solid transitions, fluid-fluid phase separation and freezing. The reason behind the popular use of colloidal suspensions for studying physical phenomena lies in the fact that they can be studied in real-space, that their interactions can be tuned, and that they can be brought into equilibrium with the surrounding molecular solvent [52]. Due to the separation of length scales and times associated with size difference of the colloidal suspensions constituents (i. e. on one hand, the colloidal particles, and on the other hand the solvent molecules), fluctuations of the solvent molecules can be averaged, resulting in a simplification of the system with less degrees of freedom. Furthermore, the interactions between colloidal particles can be tuned to create a rich variety of physical systems [48].

The equilibrium states of colloidal suspensions were the first to be addressed both with simulations and experiments [53–55]. The development of the optical methods, such as Light Scattering [54, 56–59] and Confocal Microscopy [60–64], to mention a few, constitute a breakthrough in Colloidal Science. Such methods were applied to study phase behavior of novel colloidal systems, first the "simple" case of hard-sphere-like interactions between colloids [54, 65], and then later attractive and repulsive colloidal systems were (and have been continued to be) addressed [66–72].

An external field or a carefully chosen boundary condition provides a natural way to control colloidal suspensions [73–75]. Both the dynamics and structure of colloidal suspensions can be controlled by external fields such as light and shear fields or manipulating the boundary conditions as in confinement and directed colloidal epitaxy. An external field or a boundary condition can be imposed on a colloidal suspension and the response of the suspension can be studied [48].

Confinement is, in simplistic terms, limiting the phase space that colloidal particles can explore. Both the dynamics and structure of colloidal suspensions are altered upon confinement. Furthermore, all kinds of phenomena such as layering, wetting, pre-freezing, capillary condensation are introduced when confining a bulk suspension [76]. One may consider confinement as a constriction that modifies the thermodynamic behavior, just like other external fields. Confinement can be achieved by geometric confinement, light or magnetic fields. In this thesis, only geometric confinement is considered where the colloidal suspensions are held under the influence of external fields evoking simple traps and substrates. Geometric confinement can be thought of as controlling the boundary conditions or manipulating the dimensions of colloidal suspensions [48].

Colloidal systems under confinement have been studied early on the context of manipulating the crystalline order. Pieranski looked at colloidal crystals confined in wedge geometry. Varying the confinement gap with respect to position in the wedge, he observed change in ordering of colloidal crystals [77, 78]. The wedge geometry was later evoked for charged colloids. The crystallization behavior and dynamics of charged colloidal particles in a charged wedge of very low opening angles was examined by experiments [78–81], theory and simulations [82–85]. These studies led to the observation of exotic crystalline structures. Wedge geometry and other parallel confinement schemes were used to study dynamics and structure of bidisperse and polydisperse colloidal suspensions [86–90]. In these measurements, the characteristic confinement length is gradually decreased, upon which the dynamics of the suspension is found to slow down with no major change in structure. Recently, studies suggest that the slowing down of dynamics is connected to glass transition and dynamic heterogeneities [86, 91–95]. These studies also point out the similarities between the molecular glass transition [96–100] and the colloidal glass transition [68, 101, 102]. This suggests that intuitions obtained from colloidal suspensions can be transferred to glass transition at molecular level. Recently, mode coupling theory is also adapted for confined systems and confirm the trends observed in experiments. Yet the dynamics and the morphology of dynamic heterogeneities as a function of the characteristic confinement length are still not well understood [48].

The aforementioned paragraphs help us to elucidate the complexity of the main topic to be attacked in the present thesis: the understanding of the dynamical and static properties of colloids under confinement. Even with the scientific work that has already been done, there are plenty of open questions. We would like to highlight those concerning the self-assembly of colloidal suspension by external fields, like the following ones: how is the dynamics of two colloids affected by a third one when there are hydrodynamic interactions? can we control the hydrodynamic coupling? how is the dynamics of a single file of Brownian particles when they are subjected to periodic landscapes? what happens with the structure and the dynamics when the available space is restricted from a plane to a line passing by intermediate dimensions? and, if we put layers of colloids over a substrate, how is their structure? how do the colloids move? This thesis has the answer for the previous questions and some explanations about really interesting structural and dynamic phenomena found during the research development.

So far, we have given some inspiration to the reader. Now, it is time to explain rest of the text. The Thesis is organized as follows, in Chapter 2 we explain some key features in order to give the reader a background, such as direct inter-colloidal interactions, the physical description of external fields -more specifically beams of light- which can interact with colloidal particles. We also give the description of the interference of beams in order to create more complicated potential landscapes like a sinusoidal field in a large planar area. Finally, we give a general idea on computer simulations and its importance, not only for the developing of the present thesis, but for the develop of Science during the last half of century.

In Chapter 3, we focus on the problem of a quasi–zero–dimensional confinement and its consequences on the dynamics of the colloidal particles. Specially, we explore the hydrodynamic coupling between colloids immersed in a low Reynolds number fluid. We consider colloidal arrays composed of two and three particles; each colloid is trapped in a single harmonic potential, which basically restrict each particle in a quasi–zero–dimension, but allows them to interact with the other colloids only via hydrodynamic forces. Here, we face the problem of understanding the role of a third-body on the two-body hydrodynamic correlation functions. Furthermore, we put emphasis on a collinear configuration of particles, although the salient features of an equilateral triangle configuration are outlined. So far, in Chapter 3 we explicitly show that the presence of a third body affects the auto– and cross–correlation functions and their behavior can be different from the one commonly seen in a two–particle system.

The one–dimension problem is studied in Chapter 4, where we report the dynamical properties of interacting colloids confined to one–dimension and subjected to external periodic energy landscapes. We

particularly focus on the influence of the hydrodynamic interactions on the mean–square displacement. We study colloidal systems with two types of repulsive inter–particle interactions, namely, Yukawa and super–paramagnetic potentials. We find that in the homogeneous case, hydrodynamic interactions lead to an enhancement of the particle mobility and the mean–square displacement at long–times scales as t^{α}, with $\alpha = 1/2 + \epsilon$ and ϵ being a small correction. This correction, however, becomes much more important in the presence of an external field, which breaks the homogeneity of the particle distribution along the file. Therefore, the latter promotes a richer dynamical scenario due to the hydrodynamical coupling among particles.

The one–, quasi–one–, quasi–two and two–dimensional cases are analyzed in Chapters 5 and 6. We study the structural properties of interacting colloids confined in a parabolic trap. By changing the trap stiffness, we are able to control the dimension of the system and, thus, we can explore the structural evolution imposed by the geometrical confinement. Although the particles feel the interaction with the parabolic potential, there is no wall–particle contribution to the hydrodynamic interactions. More specifically, in Chapter 5, we focus on the ordering in the perpendicular and parallel directions to the confinement. We also investigate the evolution of the configuration of the first layer of neighbors of the particles. Hence, we find that according to the inter–particle interactions, i. e., short–range and long–range repulsive interaction potentials, the particles exhibit interesting ordering features inside the trap that lead to a rich structural landscape.

The dynamical properties of the system described in Chapter 5 are explored in Chapter 6. Here, we calculate the mean square displacement, which allows us to understand the elf-diffusion of the particles at different temporal regimes: short, intermediate and long (in the colloidal time scale).

The quasi–three–dimensional case is discussed in detail in Chapter 7. We present a study of a model colloidal suspension consisting of Yukawa–like particles distributed on two parallel planar layers. The application of a modulated external potential to the bottom layer breaks the homogeneity and isotropy of the particle distribution and, therefore, introduces a new competing length scale. We explore the way in which the structure and dynamical properties depend on both the strength and the periodicity of the modulated substrate. We find that each monolayer exhibits properties that are dissimilar from those present in the substrate–free case, and can be tuned by changing accordingly the commensurability. Thus, the present model system shows to what extent self–assembly can be directed or controlled by changing the energetic landscapes either using substrates or modifying the geometry of the system.

Finally, in Chapter 8 we give our concluding remarks of the present thesis and expectations in the research line in which the present work

has been fully developed and enriching the understanding of interacting colloids in confinement.

BIBLIOGRAPHY

[1] E. C. Oğuz, *Ph.D. thesis*, Heinrich-Heine-Universität Düseldorf, 2012.

[2] G. Gompper, J. Dhont and D. Richter, *The European Physical Journal E*, 2008, **26**, 1–2.

[3] H. Lekkerkerker, W.-K. Poon, P. Pusey, A. Stroobants and P. Warren, *EPL (Europhysics Letters)*, 1992, **20**, 559.

[4] A. P. Chatterjee and K. S. Schweizer, *The Journal of chemical physics*, 1998, **109**, 10464.

[5] R. Tuinier, G. A. Vliegenthart and H. N. Lekkerkerker, *The Journal of Chemical Physics*, 2000, **113**, 10768.

[6] K. Chen and Y.-q. Ma, *The Journal of Physical Chemistry B*, 2005, **109**, 17617–17622.

[7] A. Louis, P. Bolhuis, E. Meijer and J. Hansen, *The Journal of chemical physics*, 2002, **117**, 1893.

[8] S. Yang, D. Yan, H. Tan and A.-C. Shi, *Physical Review E*, 2006, **74**, 041808.

[9] J. Joanny, L. Leibler and P. De Gennes, *Journal of Polymer Science: Polymer Physics Edition*, 1979, **17**, 1073–1084.

[10] X. Ye, T. Narayanan, P. Tong, J. Huang, M. Lin, B. Carvalho and L. Fetters, *Physical Review E*, 1996, **54**, 6500.

[11] P. González-Mozuelos, J. Méndez-Alcaraz and R. Castañeda-Priego, *The Journal of chemical physics*, 2005, **123**, 214907.

[12] R. Castañeda-Priego, A. Rodríguez-López and J. Méndez-Alcaraz, *Physical Review E*, 2006, **73**, 051404.

[13] A. Louis, P. Bolhuis, J. Hansen and E. Meijer, *Physical review letters*, 2000, **85**, 2522–2525.

[14] S. Ramakrishnan, M. Fuchs, K. S. Schweizer and C. F. Zukoski, *The Journal of chemical physics*, 2002, **116**, 2201.

[15] Y. Mao, M. Cates and H. Lekkerkerker, *Physica A: Statistical Mechanics and its Applications*, 1995, **222**, 10–24.

[16] A. Stradner, H. Sedgwick, F. Cardinaux, W. C. Poon, S. U. Egelhaaf and P. Schurtenberger, *Nature*, 2004, **432**, 492–495.

[17] G. Koenderink, G. Vliegenthart, S. Kluijtmans, A. Van Blaaderen, A. Philipse and H. Lekkerkerker, *Langmuir*, 1999, **15**, 4693–4696.

[18] F. Mantegazza, M. Caggioni, M. Jiménez and T. Bellini, *Nature Physics*, 2005, **1**, 103–106.

[19] P. Bolhuis and D. Frenkel, *The Journal of chemical physics*, 1994, **101**, 9869.

[20] M. Adams, Z. Dogic, S. L. Keller and S. Fraden, *Nature*, 1998, **393**, 349–352.

[21] N. R. Jana, L. Gearheart and C. J. Murphy, *Advanced Materials*, 2001, **13**, 1389.

[22] W. Schärtl, G. Lindenblatt, A. Strack, P. Dziezok and M. Schmidt, in *Trends in Colloid and Interface Science XII*, Springer, 1998, pp. 285–290.

[23] S. Jungblut, R. Tuinier, K. Binder and T. Schilling, *The Journal of chemical physics*, 2007, **127**, 244909.

[24] J. M. Brader, A. Esztermann and M. Schmidt, *Physical Review E*, 2002, **66**, 031401.

[25] C. Hiergeist and R. Lipowsky, *Journal de Physique II*, 1996, **6**, 1465–1481.

[26] V. Frette, I. Tsafrir, M.-A. Guedeau-Boudeville, L. Jullien, D. Kandel and J. Stavans, *Physical review letters*, 1999, **83**, 2465–2468.

[27] C. R. Martin, *Nanomaterials–a membrane-based synthetic approach*, Dtic document technical report, 1994.

[28] C. A. Naumann, O. Prucker, T. Lehmann, J. Rühe, W. Knoll and C. W. Frank, *Biomacromolecules*, 2002, **3**, 27–35.

[29] R. Lipowsky, H.-G. Döbereiner, C. Hiergeist and V. Indrani, *Physica A: Statistical Mechanics and its Applications*, 1998, **249**, 536–543.

[30] B. M. Discher, Y.-Y. Won, D. S. Ege, J. C. Lee, F. S. Bates, D. E. Discher and D. A. Hammer, *Science*, 1999, **284**, 1143–1146.

[31] D. E. Discher and A. Eisenberg, *Science*, 2002, **297**, 967–973.

[32] A. Mecke, C. Dittrich and W. Meier, *Soft Matter*, 2006, **2**, 751–759.

[33] X. Shuai, H. Ai, N. Nasongkla, S. Kim and J. Gao, *Journal of Controlled Release*, 2004, **98**, 415–426.

[34] M. L. Adams, A. Lavasanifar and G. S. Kwon, *Journal of pharmaceutical sciences*, 2003, **92**, 1343–1355.

[35] C. Nardin and W. Meier, *Reviews in Molecular Biotechnology*, 2002, **90**, 17–26.

[36] A. Taubert, A. Napoli and W. Meier, *Current opinion in chemical biology*, 2004, **8**, 598–603.

[37] M. Zapotocky, L. Ramos, P. Poulin, T. Lubensky and D. Weitz, *Science*, 1999, **283**, 209–212.

[38] E. Currie, W. Norde and M. Cohen Stuart, *Advances in colloid and interface science*, 2003, **100**, 205–265.

[39] J. Hooper, K. Schweizer, T. Desai, R. Koshy and P. Keblinski, *The Journal of chemical physics*, 2004, **121**, 6986.

[40] J. Liu, D. Cao and L. Zhang, *The Journal of Physical Chemistry C*, 2008, **112**, 6653–6661.

[41] K. Jacobson, O. G. Mouritsen and R. G. Anderson, *Nature cell biology*, 2007, **9**, 7–14.

[42] A. Katzir-Katchalsky and P. F. Curran, *Nonequilibrium thermodynamics in biophysics*, Harvard University Press Cambridge, 1965, vol. 1.

[43] G. S. Campbell and J. M. Norman, *Introduction to environmental biophysics*, Springer Verlag, 1998.

[44] K. S. Cole, *Membranes, ions, and impulses: a chapter of classical biophysics*, Univ of California Press, 1968, vol. 1.

[45] S. Suresh, *Acta Materialia*, 2007, **55**, 3989–4014.

[46] M. Daune and W. Duffin, *Molecular biophysics: structures in motion*, Oxford University Press Oxford, 1999.

[47] M. V. Volkenstein, *Molecular biophysics*, Academic press New York, 1977.

[48] H. B. Eral, *Ph.D. thesis*, University of Twente, 2011.

[49] B. Duplantier, in *Einstein, 1905–2005*, Springer, 2006, pp. 201–293.

[50] C. Bechinger, *The Bechinger Group web-page*, http://www.pi2.uni-stuttgart.de/contact/index.php?article_id=1.

[51] S. Herrera-Velarde, *Ph.D. thesis*, División de Ciencias en Ingenierías. Campus León. Universidad de Guanajuato, 2008.

[52] A. Yethiraj, *Soft Matter*, 2007, **3**, 1099–1115.

[53] P. Pusey and W. Van Megen, *Nature*, 1986, **320**, 340–342.

[54] W. Van Megen, S. Underwood and P. Pusey, *Physical review letters*, 1991, **67**, 1586–1589.

[55] K. Davis, W. Russel and W. Glantschnig, *Science*, 1989, **245**, 507–510.

[56] A. Vrij, *The Journal of Chemical Physics*, 1979, **71**, 3267.

[57] P. Pusey, H. Fijnaut and A. Vrij, *The Journal of Chemical Physics*, 1982, **77**, 4270.

[58] A. Philipse and A. Vrij, *The Journal of chemical physics*, 1988, **88**, 6459.

[59] A. Philipse and A. Vrij, *Journal of colloid and interface science*, 1989, **128**, 121–136.

[60] A. Van Blaaderen, A. Imhof, W. Hage and A. Vrij, *Langmuir*, 1992, **8**, 1514–1517.

[61] A. Van Blaaderen and P. Wiltzius, *SCIENCE-NEW YORK THEN WASHINGTON-*, 1995, 1177–1177.

[62] J. C. Crocker, D. G. Grier *et al.*, *Journal of colloid and interface science*, 1996, **179**, 298–310.

[63] A. D. Dinsmore, E. R. Weeks, V. Prasad, A. C. Levitt and D. A. Weitz, *Applied Optics*, 2001, **40**, 4152–4159.

[64] V. Prasad, D. Semwogerere and E. R. Weeks, *Journal of Physics: Condensed Matter*, 2007, **19**, 113102.

[65] A. Philipse and A. Vrij, *The Journal of chemical physics*, 1987, **87**, 5634.

[66] C. De Kruif, P. Rouw, W. Briels, M. Duits, A. Vrij and R. May, *Langmuir*, 1989, **5**, 422–428.

[67] P. Rouw and C. De Kruif, *Physical Review A*, 1989, **39**, 5399.

[68] P. N. Pusey, *Journal of Physics: Condensed Matter*, 2008, **20**, 494202.

[69] S. Lai, W. Ma, W. Van Megen and I. Snook, *Physical Review E*, 1997, **56**, 766.

[70] J. Wu, D. Bratko, H. Blanch and J. Prausnitz, *The Journal of Chemical Physics*, 2000, **113**, 3360.

[71] K. Kremer, M. O. Robbins and G. S. Grest, *Physical review letters*, 1986, **57**, 2694–2697.

[72] C. P. Royall, M. E. Leunissen, A.-P. Hynninen, M. Dijkstra and A. van Blaaderen, *The Journal of chemical physics*, 2006, **124**, 244706–244706.

[73] H. Löwen, *Journal of Physics: Condensed Matter*, 2001, **13**, R415.

[74] H. Löwen, *Journal of Physics: Condensed Matter*, 2008, **20**, 404201.

[75] D. Vollmer, *Soft Matter*, 2006, **2**, 445–447.

[76] S. A. Rice, *Chemical Physics Letters*, 2009, **479**, 1–13.

[77] P. Pieranski, L. Strzelecki and B. Pansu, *Physical Review Letters*, 1983, **50**, 900–903.

[78] C. Murray, *Mrs Bulletin*, 1998, **23**, 33–38.

[79] A. B. Fontecha, H. J. Schöpe, H. König, T. Palberg, R. Messina and H. Löwen, *Journal of Physics: Condensed Matter*, 2005, **17**, S2779.

[80] P. Wette, H. J. Schöpe and T. Palberg, *The Journal of chemical physics*, 2005, **122**, 144901–144901.

[81] P. Wette, H. J. Schope and T. Palberg, *The Journal of Chemical Physics*, 2005, **123**, 174902.

[82] Z. Németh and H. Löwen, *Physical Review E*, 1999, **59**, 6824.

[83] T. Fehr and H. Löwen, *Physical Review E*, 1995, **52**, 4016.

[84] P. Scheidler, W. Kob and K. Binder, *EPL (Europhysics Letters)*, 2000, **52**, 277.

[85] P. Scheidler, W. Kob and K. Binder, *EPL (Europhysics Letters)*, 2002, **59**, 701.

[86] C. R. Nugent, K. V. Edmond, H. N. Patel and E. R. Weeks, *Physical review letters*, 2007, **99**, 025702.

[87] P. S. Sarangapani and Y. Zhu, *Physical Review E*, 2008, **77**, 010501.

[88] K. V. Edmond, C. R. Nugent and E. R. Weeks, *Physical Review E*, 2012, **85**, 041401.

[89] K. W. Desmond and E. R. Weeks, *Physical Review E*, 2009, **80**, 051305.

[90] M. Hermes and M. Dijkstra, *EPL (Europhysics Letters)*, 2010, **89**, 38005.

[91] A. H. Marcus, J. Schofield and S. A. Rice, *Phys. Rev. E*, 1999, **60**, 5725–5736.

[92] S. C. Glotzer, *Journal of Non-Crystalline Solids*, 2000, **274**, 342–355.

[93] E. R. Weeks, J. C. Crocker, A. C. Levitt, A. Schofield and D. A. Weitz, *Science*, 2000, **287**, 627–631.

[94] E. R. Weeks and D. Weitz, *Physical review letters*, 2002, **89**, 095704.

[95] E. R. Weeks and D. Weitz, *Chemical physics*, 2002, **284**, 361–367.

[96] C. A. Angell, *Science*, 1995, **267**, 1924–1935.

[97] M. Ediger, *Annual review of physical chemistry*, 2000, **51**, 99–128.

[98] C. Angell, K. Ngai, G. McKenna, P. McMillan and S. Martin, *Journal of Applied Physics*, 2000, **88**, 3113–3157.

[99] M. Alcoutlabi and G. B. McKenna, *Journal of Physics: Condensed Matter*, 2005, **17**, R461.

[100] C. Alba-Simionesco, B. Coasne, G. Dosseh, G. Dudziak, K. Gubbins, R. Radhakrishnan and M. Sliwinska-Bartkowiak, *Journal of Physics: Condensed Matter*, 2006, **18**, R15.

[101] P. Pusey and W. Van Megen, *Physical review letters*, 1987, **59**, 2083–2086.

[102] W. Van Megen, *Journal of Physics: Condensed Matter*, 2002, **14**, 7699.

2

THEORETICAL BACKGROUND

"Whenever a theory appears to you as the only po
one, take this as a sign that you have neither understood the
theory nor the problem which it was intended to solve"
-Karl Po

In the following paragraphs, we give some details about the theoretical background that the reader may need to understand and enjoy the reading of this thesis. Different approaches to describe the Brownian motion are discussed. In a quite general way, we present aspects such as direct inter-colloidal interactions and the interaction of the colloidal particles with some external fields. Also, we explain what is a computer simulation and why its implementation has been a breakthrough for Science during the last half of century.

2.1 BROWNIAN MOTION THEORY

Human lives are full of uncertainties, as with many natural phenomena. No one can precisely foresee what will happen in the next second, minute, ... and so on. Rather than accepting the fact that the future is always uncertain, many models and algorithms have been continuously formulated for the prediction of matters involving uncertain elements. One of them is the Brownian model. Brownian motion is among the simplest of the continuous-time stochastic (or probabilistic) processes, and it is a limit of both simpler and more complicated stochastic processes. This universality is closely related to the universality of the normal distribution. In both cases, it is often mathematical convenient rather than the accuracy of the models that motivates their use. This is because Brownian motion, whose time derivative is everywhere infinite, is an idealized approximation to actual random physical processes, which always have a finite time scale. In the present Section we describe different approaches to model the Brownian motion. If the reader is interested about the incredible history of the first description of the Brownian motion, one can take a look at the Apendix A.

2.1.1 *Einstein Description*

Einstein was interested in proving the existence of atoms since his early days in science. He formulated a theory describing the Brownian motion on theoretical grounds unaware of the existence of phenomenon. Einstein's argument was two fold. First part of the argument is as follows: let $\rho = \rho(x, t)$ be the Probability Density Function (PDF) that a Brownian particle is at x at time t. Then, ρ satisfies the diffusion equation [1]

$$\frac{\partial \rho}{\partial t} = D\Delta\rho \tag{2.1}$$

where D is a positive constant, called the coefficient of diffusion. Assuming that the particle start from the origin at the initial time $t = 0$, so that $\rho(x, 0) = \delta(x)$ then

$$\rho(x, t) = \frac{1}{(4\pi Dt)^{3/2}} exp\left(-\frac{|x|}{4Dt}\right), \tag{2.2}$$

where $|x|$ is the Euclidean distance of x from the origin. In the second part of the argument, Einstein connected the D to other physical measurable quantities. Eisntein considered a colloidal particle in dynamic equilibrium where on one hand, the colloidal osmotic pressure balances the applied force (K) on the particle [1],

$$K = k_B T \frac{\Delta\nu}{\nu}, \tag{2.3}$$

where the number of particles per volume is given by ν, k_B is the Boltzmann constant and T is the temperature. Assuming K as the gravitational force on the particle and integrating Eq. 2.3 Einstein obtained the sedimentation equilibrium connecting the number of particles at a given height [1].

On the other hand, a flux balance is required to explain the phenomena. The Stokesian particle flux produced by the gravitational force is canceled by a diffusive flux of particles. Considering that the Brownian particles moving in the fluid experience a resistance due to the friction, the force (K) imparts to each particle a velocity of the form: $K/m\vartheta$; where ϑ is a constant with the dimension of frequency (inverse-time) and m is the mass of the particle. Therefore, the particles pass a unit area per unit of time due to the action of the force K is given by $\nu K/m\vartheta$. This Stokesian flux is balanced flux induced by random fluctuations, i. e., $\nu K/m\vartheta = D\Delta\nu$ [1].

Einstein thus obtained an expression for the "diffusion coefficient" assuming Stokesian form for the particle velocities imposed by the gravitational force [1],

$$D = \frac{RT}{6N_{av}\pi a\eta} \tag{2.4}$$

containing Avogadros's number (N_{av}), molar gas constant (R), the absolute temperature (T), the particle radius (a), and the solvent viscosity (η).

To predict the time dependence of Brownian motion, Einstein turned to a probabilistic consideration of the diffusive motion, in particular, to obtain the mean squared displacement of a particle [1]

$$\left\langle r(t)^2 \right\rangle = 6Dt. \tag{2.5}$$

Furthermore, assuming a gravitational force, i.e. ($K = mg$) and integrating Eq. 2.3, Einstein obtained the sedimentation equilibrium relation connecting the number of the particles at a given height (N) to thermal energy ($k_B T$) [1],

$$N = N_0 exp\left(-\frac{(m + \breve{m})g(h - h_0)}{k_B T}\right). \tag{2.6}$$

In Eq. 2.6, the number of particles (N) at hight h above a reference height h_0 and $\breve{m}$ is the mass of the fluid displaced by a particle of mass m.

The theoretical derivation of mean square displacement and sedimentation equilibrium was a key step to prove the discontinuous nature of matter. Attempts to measure Brownian particles in experiments had failed due to the non linearity of displacement with time. Einstein's now-familiar expressions provided measurable quantites that were directly compared with theory [1].

2.1.2 *Langevin Equation*

As described before, a colloid exerts the so-called Brownian motion due to thermal collisions with the solvent molecules. This erratic motion can be described on the basis on Newton's equation of motion, where the interactions of the Brownian particle with the solvent molecules are taken into account by a rapidly fluctuating force. The statistics of Brownian motion can be studied in this way when reasonable approximations for the statistical properties of the fluctuating force can be made.

Relaxation times for fluids are known experimentally to be the order 10^{-14}s. As will be established shortly, relevant times scales for Brownian particles are at least 10^{-9} s. This separation in time scales is the consequence of the very large mass of the Brownian particle relative to that of a solvent molecule, and is essential for the validity of the Langevin description [2].

The interaction of the spherical Brownian particle with the solvent molecules is separated into two parts. First of all, there is a rapidly varying force $\mathbf{f}(t)$ with time t as the result of *random* collisions of the solvent molecules with the Browninan particle. This force fluctuates on the aforementioned solvent time scale of 10^{-14}s [2]. Secondly, as

the Brownian particles attains a velocity $\mathbf{v} = \mathbf{p}/M$ ($\mathbf{p}$ is the momentum coordinate of the Brownian particle and M is the mass), there is a friction force due to *systematic* collisions with the solvent molecules [2]. When the volume of the Brownian particles is much larger than that of the solvent molecules, this systematic force equals the hydrodynamic friction force of a macroscopically large sphere. For not too large velocities, that friction force is directly proportional to the velocity of the Brownian particle and the proportionality constant γ is the friction constant: $\texttt{friction force} = \gamma\mathbf{p}/M$. The friction coefficient of a macroscopically large sphere is equal to [2],

$$\gamma = 6\pi\eta_0 a, \tag{2.7}$$

with η_0 the shear viscosity of the solvent and a the radius of the Brownian particle. The friction coefficient in Eq. 2.7 is commonly referred to as Stokes's friction coefficient. Newtons's equation of motion for a spherical Brownian particle is thus written as [2],

$$\frac{d\mathbf{p}}{dt} = -\gamma\frac{\mathbf{p}}{M} + \mathbf{f}(t). \tag{2.8}$$

The position coordinate $\mathbf{r}$ of the Brownian particle is, by definition, related to the momentum coordinate as [2],

$$\frac{d\mathbf{r}}{dt} = \frac{\mathbf{p}}{M}. \tag{2.9}$$

Since the systematic interaction with the solvent molecules is made explicit (the first term on the right-hand side (rhs) of Eq. 2.8), the ensemble average of the fluctuating force $\mathbf{f}$ is equal to zero [2],

$$\langle\mathbf{f}(t)\rangle = 0. \tag{2.10}$$

Due to the aforementioned large separation in time scales, it is sufficient for the calculation of the thermal movement of the Brownian particle to use a delta correlated random force in time, that is [2],

$$\langle\mathbf{f}(t)\mathbf{f}(t')\rangle = \mathbf{G}\delta(t-t'), \tag{2.11}$$

where δ is the delta distribution and $\mathbf{G}$ is a constant 3×3-dimensional matrix, which may be regarded as a measure of the fluctuating force, and is referred to as the *fluctuation strength*. Such a delta correlated random force limits the description to a time resolution which is large with respect to the solvent time scale of 10^{-14}s [2].

Eq. 2.8 is Newton's equation of motion for a macroscopic particle with fluctuating random force added to account for the thermal collisions of the solvent molecules with the Brownian particle. Such an equation of motion in the sense that the momentum coordinate of the Brownian particle as well as its position coordinate, are now stochastic variables. It makes no sense to ask for a deterministic solution of Eqs. 2.8 and 2.9, since only ensemble averaged properties of

the random force $\mathbf{f}$ are specified. The effort should be aimed at the calculation of the conditional probability density function of $\mathbf{p}$ and $\mathbf{r}$ at the time t, given their initial values at time $t = 0$. The solution of the Langevin equation is the specification of the PDF for the stochastic variable $(\mathbf{p}, \mathbf{r})$. Note that Eq. 2.8 is mathematically meaningless as it stands without the specifications given in Eq. 2.10 and 2.11 of the statistical properties of the random force $\mathbf{f}$ [2].

Integration of Eq. 2.8 yields,

$$\mathbf{p}(t) = \mathbf{p}(0)\exp\left[-\frac{\gamma}{M}t\right] + \int_0^t dt'\mathbf{f}(t')\exp\left[-\frac{\gamma}{M}(t-t')\right]. \tag{2.12}$$

Now let τ be a time interval much larger than the solvent time scale of 10^{-14}s. The random force evolves through many independent realizations during that time interval. On the other hand, let τ be so small that $exp\,[-\gamma t/M]$ is almost constant over times of the order of τ, that is, we take $\tau << M/\gamma$. with this choice of τ, Eq. 2.12 can be rewritten as [2],

$$\mathbf{p}(t) = \mathbf{p}(0)\exp\left[-\frac{\gamma}{M}t\right] + \sum_{j=0}^{\aleph-1}\exp\left[-\frac{\gamma}{M}(t-j\tau)\right]\int_{j\tau}^{(j+1)\tau} dt'\mathbf{f}(t'), \tag{2.13}$$

where $\aleph = t/\tau$. Since the random force evolves through many independent realizations during the time interval τ, each integral in Eq. 2.13 is a Gaussian variable with a mean equal to zero. This is a consequence of the central limit theorem as each integral may be regarded as a sum of many statistically equivalent terms [2]. Furthermore, since a sum of independent Gaussian variables is also a Gaussian variable, it follows Eq. 2.13 that [2],

$$\mathbf{x}_1 \equiv \mathbf{p}(t) - \mathbf{p}(0)\exp\left[-\frac{\gamma}{M}t\right], \tag{2.14}$$

is a Gaussian variable.

What about the position coordinate $\mathbf{r}$ of the Brownian particle? The above reasoning is easily extended to include the position coordinate. Using 2.9, integration of Eq. 2.12 yields [2],

$$\begin{aligned}\mathbf{r}(t) = \quad & \mathbf{r}(0) + \tfrac{\mathbf{p}(0)}{\gamma}\left\{1 - \exp\left[-\tfrac{\gamma}{M}t\right]\right\} + \\ & \tfrac{1}{\gamma}\int_0^t dt'\mathbf{f}(t')\left\{1 - \exp\left[-\tfrac{\gamma}{M}(t-t')\right]\right\}.\end{aligned} \tag{2.15}$$

Following the same reasoning as before shows that [2],

$$\mathbf{x}_2 \equiv \mathbf{r}(t) - \mathbf{r}(0) - \frac{\mathbf{p}(0)}{\gamma}\left\{1 - \exp\left[-\frac{\gamma}{M}t\right]\right\}, \tag{2.16}$$

is a Gaussian variable with a mean equals to zero.

Consider the stochastic variable $(\mathbf{p}, \mathbf{r})$. Let us define the variable [2],

$$\mathbf{X} \equiv (\mathbf{x}_1, \mathbf{x}_2) = \begin{cases} \int_0^t dt' \mathbf{f}(t') exp\left[-\frac{\gamma}{M}(t-t')\right], \\ \frac{1}{\gamma}\int_0^t dt' \mathbf{f}(t')\left[1 - exp\left[-\frac{\gamma}{M}(t-t')\right]\right] \end{cases}, \tag{2.17}$$

where Eqs. 2.13 2.15 are used in the second line. According to the above discussion, $\mathbf{X}$ is a Gaussian variable. For given initial values $\mathbf{p}(0)$ and $\mathbf{r}(0)$ of the momentum and position coordinates, the PDF of the variable $\mathbf{X}$ is clearly identical to the PDF of $(\mathbf{p}, \mathbf{r})$. Hence, the PDF of $(\mathbf{p}, \mathbf{r})$ is given by [2],

$$P(\mathbf{p}, \mathbf{r}, t|\mathbf{p}(0), \mathbf{r}(0), t = 0) = \frac{1}{(2\pi)^{n/2}\sqrt{det\mathbf{D}}} exp\left[-\frac{1}{2}\mathbf{X}\cdot\mathbf{D}^{-1}\cdot\mathbf{X}\right], \tag{2.18}$$

with

$$\mathbf{D} = \langle \mathbf{X}\mathbf{X}\rangle \equiv \begin{pmatrix} \langle \mathbf{x}_1\mathbf{x}_1\rangle & \langle \mathbf{x}_1\mathbf{x}_2\rangle \\ \langle \mathbf{x}_2\mathbf{x}_1\rangle & \langle \mathbf{x}_2\mathbf{x}_2\rangle \end{pmatrix}. \tag{2.19}$$

$det\mathbf{D}$ denotes the determinant of $\mathbf{D}$, and $n = 6$ is the dimension of $\mathbf{X}$. Note that each of the matrices $\langle \mathbf{x}_i\mathbf{x}_j\rangle$, $i, j = 1, 2$, is 3×3-dimensional, so that $\mathbf{D}$ is 6×6-dimensional. Using Eqs. 2.10 and 2.11, the ensemble averages $\langle \mathbf{x}_i\mathbf{x}_j\rangle$ are easily calculated [2],

$$\langle \mathbf{x}_1\mathbf{x}_1\rangle = \frac{M\mathbf{G}}{2\gamma}\left\{1 - exp\left[-\frac{2\gamma}{M}t\right]\right\}, \tag{2.20}$$

$$\langle \mathbf{x}_1\mathbf{x}_2\rangle = \langle \mathbf{x}_2\mathbf{x}_1\rangle = \frac{M\mathbf{G}}{2\gamma}\left\{1 - exp\left[-\frac{2\gamma}{M}t\right]\right\}^2, \tag{2.21}$$

$$\tag{2.22}$$

$$\langle \mathbf{x}_2\mathbf{x}_2\rangle = \frac{m\mathbf{G}}{\gamma^3}\left\{\frac{\gamma}{M}t - \frac{1}{2}\left(exp\left[-\frac{2\gamma}{M}t\right] - 1\right) - 2\left(1 - exp\left[-\frac{2\gamma}{M}t\right]\right)\right\}. \tag{2.23}$$

It is now possible to identify the matrix $\mathbf{G}$, using the equipartition theorem, which states that [2],

$$\lim_{t\to\infty}\langle \mathbf{p}(t)\mathbf{p}(t)\rangle = \hat{\mathbf{I}}\frac{M}{\beta}, \tag{2.24}$$

where $\beta = \frac{1}{k_B T}$, with $k_B T$ Boltzmann's constant and T the temperature, and $\hat{\mathbf{I}}$ the unit matrix. The fluctuation strength now follows from the definition of the variable $\mathbf{x}_1$ (Eq. 2.14) and the ensemble average given in Eq. 2.20. For times $t >> M/\gamma$, Eq. 2.20 reduces to [2],

$$\langle \mathbf{p}(t)\mathbf{p}(t)\rangle = \mathbf{G}\frac{M}{2\gamma}. \tag{2.25}$$

Comparison with Eq.2.24 identifies the fluctuation strength [2],

$$\mathbf{G} = \hat{\mathbf{I}}\frac{2\gamma}{\beta}. \tag{2.26}$$

This relation is often referred to as a fluctuation dissipation theorem, because it connects the fluctuation strength with the friction coefficient, which determines the dissipation of kinetic energy into heat. With the identification of the fluctuation strength $\mathbf{G}$, the PDF of the Gaussian variable $(\mathbf{p}, \mathbf{r})$ is completely specified [2].

2.1.3 *Smoluchowski Equation*

We want to apply now our derivation to the case of a Brownian particle in a force field $\mathbf{F}(\mathbf{r})$. The corresponding Langevin equation is [3]

$$\frac{d\dot{\mathbf{p}}}{dt} = -\gamma\dot{\mathbf{r}} + \mathbf{F}(\mathbf{r}) + \sigma\xi(t), \tag{2.27}$$

for scalar friction constant γ and amplitude σ of the fluctuating force. We will assume in this section the *limit of strong friction*. In this limit the magnitude of the frictional force $\gamma\dot{\mathbf{r}}$ is much larger than the magnitude of the force of inertia $d\dot{\mathbf{p}}/dt$, i. e. [3],

$$|\gamma\dot{\mathbf{r}}| >> |\gamma\ddot{\mathbf{r}}|, \tag{2.28}$$

therefore, Eq. 2.27 becomes

$$\gamma\dot{\mathbf{r}} = \mathbf{F}(\mathbf{r}) + \sigma\xi(t) \tag{2.29}$$

where $\eta(t) \equiv \sigma\xi(t)$ is Gaussian white noise characterized through the following statistical moment and correlation function [3]:

$$\langle\eta(t)\rangle = 0, \tag{2.30}$$

$$\langle\eta(t)\eta(t')\rangle = 2\frac{\gamma k_B T}{\sigma^2}\delta(t-t') \tag{2.31}$$

Eq. 2.27 corresponds the Fokker-Planck equation

$$\frac{\partial\wp(\mathbf{r}, t|\mathbf{r}_0, t_0)}{\partial t} = \left(\nabla^2\frac{\sigma^2}{2\gamma^2} - \nabla\cdot\frac{\mathbf{F}(\mathbf{r})}{\gamma}\right)\wp(\mathbf{r}, t|\mathbf{r}_0, t_0). \tag{2.32}$$

In case that the force field can be related to a scalar potential, i. e., $\mathbf{F}(\mathbf{r}) = -\nabla U(\mathbf{r})$, one expects that the Boltzmann distribution $exp[-U(\mathbf{r})/k_B T]$ is stationary, i. e., time-independent [3]. This expectation should be confined to force fields: $\nabla\times\mathbf{F} = 0$ [3].

It turns out that the expectation that the Boltzmann distribution is a stationary solution of the Smoluchowski equation has to be introduced as a postulate rather than a consequence of 2.32. Defining the parameters $D = \sigma^2/2\gamma^2$ and $\beta = 1/k_B T$, the *postulate* of the stationary behavior of the Boltzmann equation is [3]

$$\left(\nabla\cdot\nabla D(\mathbf{r}) - \nabla\cdot\frac{F(\mathbf{r})}{\gamma(\mathbf{r})}\right)exp\left[-\beta U(r)\right] = 0. \tag{2.33}$$

We have included the possibility that the coefficients σ and γ defining the fluctuating and dissipative forces are spatially dependent [2]. In

the rest of the subsection, we will not explicit state the dependence on the spatial coordinates $\mathbf{r}$ anymore .

Actually, the postulate 2.33 of the stationary of the Boltzmann distribution is not sufficient to obtain an equation with the appropriate behavior at thermal equilibrium. In fact, one needs to require the more stringent postulate that at equilibrium does not exist a net flux of particles (or of probability) in the system [3]. This should either hold or destroyed, e. g., through chemical reactions. We need to establish the expression for the flux before we investigate the ramifications of the indicated postulate [3].

An expression for the flux can be obtained in a vein similar to that adopted in the case of free diffusion. We note that 2.32 can be written [3]

$$\frac{\partial \wp(\mathbf{r}, t|\mathbf{r}_0, t_0)}{\partial t} = \nabla \cdot \left(\nabla D - \frac{\mathbf{F}(\mathbf{r})}{\gamma} \right) \wp(\mathbf{r}, t|\mathbf{r}_0, t_0). \tag{2.34}$$

Integrating this equation over some arbitrary volume Ω, with the definition of the particle number in this volume [3]

$$N_\Omega(t|\mathbf{r}_0, t_0) = \int_\Omega d\mathbf{r} \wp(\mathbf{r}, t|\mathbf{r}_0, t_0), \tag{2.35}$$

and using 2.34, yields

$$\frac{\partial N_\Omega(t|\mathbf{r}_0, t_0)}{\partial t} = \int_\Omega \nabla \cdot \left(\lambda D - \frac{\mathbf{F}(\mathbf{r})}{\gamma} \right) \wp(\mathbf{r}, t|\mathbf{r}_0, t_0), \tag{2.36}$$

and after applying Gauss' theorem,

$$\frac{\partial N_\Omega(t|\mathbf{r}_0, t_0)}{\partial t} = \int_{\partial\Omega} d\mathbf{a} \cdot \left(\nabla D - \frac{\mathbf{F}(\mathbf{r})}{\gamma} \right) \wp(\mathbf{r}, t|\mathbf{r}_0, t_0). \tag{2.37}$$

The lhs of this equation describes the rate of change of the particle number, the rhs contains a surface integral summing up scalar products between the vector quantity [3]

$$\mathbf{j}(\mathbf{r}, t|\mathbf{r}_0, t_0) = \left(\nabla D - \frac{\mathbf{F}(\mathbf{r})}{\gamma} \right) \wp(\mathbf{r}, t|\mathbf{r}_0, t_0), \tag{2.38}$$

and the surface elements $d\mathbf{a}$ of $\partial\Omega$. Since particles are neither generated nor destroyed inside the volume Ω, we must interpret $\mathbf{j}(\mathbf{r}, t|\mathbf{r}_0, t_0)$ as a particle flux at the boundary $\partial\Omega$. Since the volume and its boundary are arbitrary, the interpretation of $\mathbf{j}(\mathbf{r}, t|\mathbf{r}_0, t_0)$ as a particle flux at the boundary $\partial\Omega$. Since the volume and its boundary are arbitrary as given by Eq. 2.38 as a flux should hold everywhere in Ω [3].

We can now consider the ramifications of the postulate that at equilibrium the flux vanishes. Applying Eq. 2.38 to the Boltzmann distribution $\wp_0(\mathbf{r}_0) = N \exp[-\beta U(\mathbf{r})]$, for some appropiate normalization factor N, yields the equilibrium flux [3]

$$\mathbf{j}_0(\mathbf{r}) = \left(\nabla D - \frac{\mathbf{F}(\mathbf{r})}{\gamma} \right) N \exp[-\beta U(\mathbf{r})]. \tag{2.39}$$

With this definition the postulate discussed above is

$$\left(\nabla D - \frac{\mathbf{F}(\mathbf{r})}{\gamma}\right) N \exp\left[-\beta U(\mathbf{r})\right] \equiv 0. \tag{2.40}$$

The derivative $\nabla D \exp\left[-\beta U(\mathbf{r})\right] = \exp\left[-\beta U(\mathbf{r})\right](\nabla D + \beta \mathbf{F}(\mathbf{r}))$ allows us to write Eq. 2.40 as,

$$\exp\left[-\beta U(\mathbf{r})\right]\left(D\beta \mathbf{F}(\mathbf{r}) + \nabla D - \frac{\mathbf{F}(\mathbf{r})}{\gamma}\right) \equiv 0. \tag{2.41}$$

From this, it follows

$$\nabla D = \mathbf{F}(\mathbf{r})(\gamma^{-1} - D\beta), \tag{2.42}$$

an identity which is now as the so-called *fluctuation-dissipation theorem* [3].

The fluctuation-dissipation theorem is better known for the case of spatially independent D in which case follows $D\beta\gamma = 1$, i. e., with the definitions above [3]

$$\sigma^2 = 2k_B T\gamma. \tag{2.43}$$

This equation implies a relationship between the amplitude σ of the fluctuating forces and the amplitude γ of the dissipative (frictional) forces in the Langevin equation 2.27, hence, the name *fluctuation-dissipation theorem* needs to obey a temperature-dependent relationship in order for a system to attain thermodynamic equilibrium [3]. There exist more general formulations of this theorem which we will discuss further below in connection with response and correlation functions [3].

In this form, Eq. 2.42 (the fluctuation-dissipation theorem)allows us to formulate the Fokker-Planck equation [3]. For any function $f(\mathbf{r})$ holds with Eq. 2.42

$$\nabla \cdot \nabla D f = \nabla \cdot \nabla f + \nabla \cdot f \nabla D = \nabla \cdot \nabla f + \nabla \cdot \mathbf{F}\left(\frac{1}{\gamma} - D\beta\right) f. \tag{2.44}$$

From this, one finally obtains the Fokker-Plank equation, Eq. 2.32

$$\frac{\partial \wp(\mathbf{r}, t|\mathbf{r}_0, t_0)}{\partial t} = \nabla \cdot D\left(\nabla - \beta \mathbf{F}(\mathbf{r})\right) \wp(\mathbf{r}, t|\mathbf{r}_0, t_0). \tag{2.45}$$

One refers to Eq. 2.45 as the Smoluchowski equation [3].

2.2 INTER-PARTICLE INTERACTION POTENTIALS

Nowadays, it is well-known that the colloids undergo a stochastic movement. Due to this non-stopping movement, we can have an scenario where the particles are so close that they tend to coagulate. The stabilization of colloidal suspensions is a topic of great interest, not just for the scientific community but for the the industry as well, due

to the enormous amount of daily use products where the aggregation is a non-desirable effect. The interaction that leads to the coagulation of the colloidal suspensions are the well-known Van der Waals interaction [4, 5] and they appear due to the fact that one dielectric dipole, spontaneously generated on the surface of one of the molecules, induces another dipole on one neighboring particle; the induced dipole will tend to align itself with the first dipole created.

2.2.1 *Derjaguin-Landau-Verwey-Overbeek (DLVO) potential*

The Van der Waals attraction between microscopic dipoles, which are separated at a distance r, has a dependence of the form r^{-6} and r^{-7} for intermediate and long distances respectively. If we consider two big spheres, each one with a radius a, separated a center-to-center distance r, the attraction energy is given by the expression [6, 7]:

$$U_{vdW}(r) = -\frac{1}{6}A\left[\frac{2a^2}{r^2-4a^2} + \frac{2a^2}{r^2} + \ln\left(\frac{r^2-4a^2}{a^2}\right)\right], \tag{2.46}$$

where A is the Hamaker's constant, which includes the properties of the material and depends on the polarizability of both colloids and the continuous phase. The detailed calculus of the Hamaker's constant is a really challenging task, although, for practical purposes, the following estimation given by Israelachvili [8] is sufficient [6, 7]:

$$A = \frac{3h\nu(n_1+n_2)^2(n_1-n_2)^2}{16\sqrt{2}(n_1^2+n_2^2)^{3/2}}, \tag{2.47}$$

Actually, the strong Born repulsion of the electrons and the forces associated with the finite size of the solvent molecules make the van der Waals potential to have a finite value at the particle contact, but such value is several times larger that the thermal energy k_BT, which induces an irreversible aggregation

where h is the Planck's constant, ν is the characteristic frequency and n_1, n_2 are the refraction indexes of the colloid and the solvent, respectively. From Eq. 2.47 we notice that we can suppress the van der Waals attraction if the refraction indexes of the colloidal particles and the solvent are the same, i.e., if $n_1 = n_2$. For materials where the indexes are different, from Eq. 2.47 one notices that for colloidal distances $r \approx 2a$, the van der Waals interaction diverges negatively as $-(r-2a)^{-1}$ and as a inevitable consequence the system tend to coagulate [6, 7]. On the other hand this overlap between particles is forbidden due to the Bohr's repulsion, this fact is usually modeled with the well-known hard-sphere potential [6],

$$U(r) = \begin{cases} 0 & r \geqslant 2a \\ \infty & r < 2a \end{cases} \tag{2.48}$$

Thus, in order to avoid colloidal aggregation, we need a mechanism to stabilize the colloidal suspension. Now, we will discuss shortly two of the most common mechanisms to reach the colloidal stabilization, which are *charge stabilization* and *steric stabilization*.

To study the charge stabilization we suppose that every colloid has certain amount of electric charge, which is called bare charge $Z|e|$,

where e stands for the elementary charge. Therefore, when colloids are in contact with a polar solvent (like water), there is charge dissociation on the colloidal surface as a consequence of the liberation of the counter-ions (ions with an opposite charge than the colloidal charge), each of them carrying a charge $q|e|$. On the other hand, the granular presence is not considered in an explicit form, the solvent is modeled as a continuous medium characterized by a dielectric constant ϵ_s. The intensity of the electric field generated by a bare charge of the colloidal particles attracts the free counter-ions; one fraction of them are absorbed or strongly bounded to the surface of the colloids [6, 7].

The latter phenomenon is known as counter-ions condensation. This layer of ions is known as *Stern layer*. In some descriptions of the present model is common that the bounded counter-ions and the free counter-ions (not bounded to any colloid) are treated in a separated way. The effect of the bounded counter-ions is to re-normalize the charge of the colloidal particles from their bare charge Z to a new value, which is called *effective charge* Z_{eff}, where $Z_{\text{eff}} < Z$ [6, 7]. The process of replacing the bare charge Z for an effective charge Z_{eff} is the same as replacing a colloidal particle for a similar one, which is significantly bigger, but it has a smaller charge [6, 9]. In general, the effective charge depends on the geometry of the particle, the colloidal concentration and the thermodynamic properties of the electrolyte. Numeric studies show that for low charged colloids, Z_{eff} is proportional to Z, but for highly charged ones such that $Z \to \infty$ the charge Z_{eff} saturates at a certain value $Z_{\text{eff}}^{\text{sat}}$. Even nowadays, the determination of Z_{eff} as a function of Z is a demanding task form the theoretical and from the computational points of view [6, 7, 10–12].

On the other hand, the range of the interaction potential is reduced because the rest of the counter-ions in the solvent screen the Coulombic repulsion between colloids. The charge distribution in the system gives the necessary elements to calculate the electrostatic potential in any point of the space belonging to the colloidal suspension. Such potential is one of the key elements in the Poisson-Boltzmann (PB) mean-field theory due to the fact that it is possible to quantify the micro-ion-colloid correlations and the forces between colloids, in such a way that one can quantify the effective interaction potential and the thermodynamics of the system [6, 7].

The PB equation describes the electric potential around a colloidal particle [6, 7],

$$\nabla^2\Phi = -\frac{e}{\epsilon_0\epsilon_s}\sum_i z_i c_{i0} \exp\left(-\frac{z_i e\Phi}{k_B T}\right), \tag{2.49}$$

where $\epsilon_0 = 8.85 \times 10^{-12}$ As/Vm is the vacuum permitivity, ϵ_s is the solvent relative permitivity ($\epsilon_s = 81$ for water), $e = 1.6 \times 10^{-19}$C is the elemental charge, z_i is the valence of the i-th species of ion, and

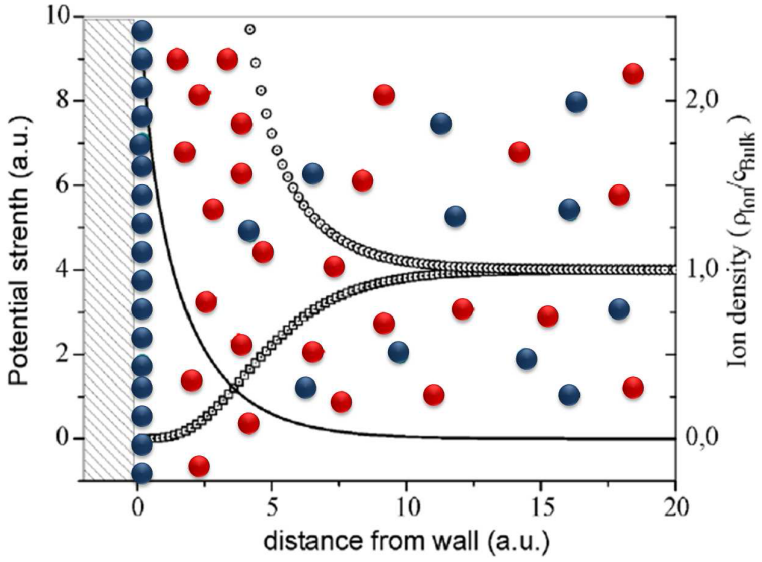

Figure 2.1: Schematic plot of an infinite wall with negative (blue points) charges on the surface and in the positive (red points) counter-ions and salt ions in solution. The solid line corresponding to the left scale shows the electrostatic potential Φ as a function of the distance from the wall. The two scatter plots, corresponding to the left scale, show the distribution of the positive (top curve) and negative (bottom curve) in front of the wall in units of the bulk ion density. (Taken and adapted from Refs. [6, 9])

c_{i0} is the concentration of the i-th species of ion in the bulk (away from the particle surface). The negative superficial charge of a colloid is taken into account by considering the correct boundary conditions. The PB equation can be visualized as the well-known Poisson equation, where the charge density ρ is proportional to a Boltzmann distribution [6, 7]. This kind of distribution is originated from the entropic and energetic competition, the electrostatic part favors an ordered and localized array of the ions while the entropic factors are competing to generate a random and uniform distribution of ions. The PB description offers reliable results but unfortunately it is a non-linear differential equation that cannot be solved analytically, except for certain kind of geometries such as the Gouy-Chapman geometry, which is shown in Fg. 2.1 [6, 9, 13] and consist on an infinite wall; this physical picture corresponds to the limit in which the colloid diameter is much bigger than the diameter of the ions [6, 7].

Linearisation of the PB equation, Eq. 2.49 ,yields an approximate solution which is valid for small potentials, i. e., $e\Phi << k_B T$, or large colloid-colloid separations [6, 7]

$$\Phi(r) = \frac{Ze}{4\pi\epsilon_0\epsilon_W}\frac{\exp(\kappa\sigma/2)}{1+\kappa\sigma/2}\frac{\exp(-\kappa r)}{r}, \tag{2.50}$$

with r the instance fro the center of the colloidal particle. The potential 2.50 constitutes the well-known repulsive part of the DLVO

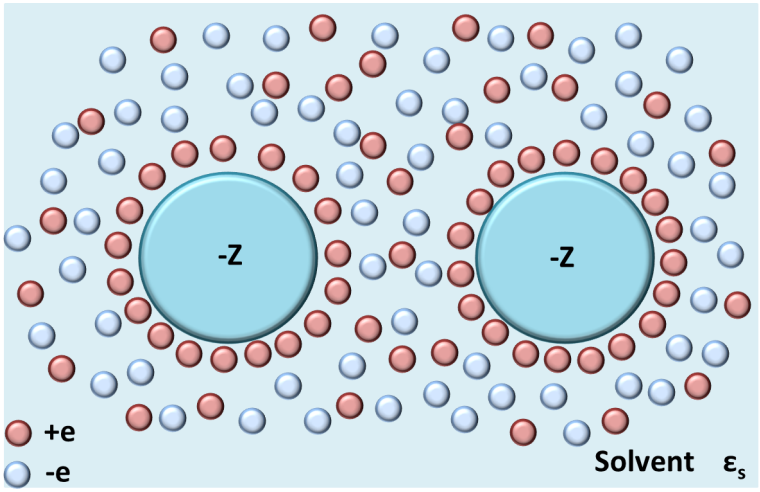

Figure 2.2: Schematic picture of two colloids with their corresponding clouds of micro-ions (Adapted from Ref. [6]).

potential. Note that the finite geometry of the colloid is taken into account by the second factor which matches unity for point-like particles ($a = 0$). The inverse screening length κ is [6, 7]

$$\kappa = \sqrt{\frac{\epsilon_0 \epsilon_W k_B T}{\sum_i (e z_i^2) c_{i0}}}. \tag{2.51}$$

The pair interaction between colloids is obtained by integrating the normal component of the Maxwell's stress tensor os the surface of the colloid yielding,

$$u(r) = \frac{(Ze)^2}{4\pi\epsilon_0\epsilon_W} \left(\frac{\exp(\kappa\sigma/2)}{1+\kappa\sigma/2} \right)^2 \frac{\exp(-\kappa r)}{r}, \tag{2.52}$$

with r now the center-to-center distance between colloidal particles. The pair interaction is proportional to the number of surface charges Z squared and decreases by a factor of ϵ_W^{-1} due to the polarization of the water molecules. The last factor reflects the fast decay of the pair interaction with respect to the distance r originating from screening effects as follows: according to Eq. 2.51, the screening length is diminished by all ions present in the solvent. It is already known that the cloud of positive counter-ions screens the negative surface charge of the colloids which will be screened even stronger in the presence of further positive charged ions [6, 7]. Also, if the solvent contains negative ions the clouds of counter-ions will be themselves screened as is sketched in Fig 2.2 [6, 7].

Another technique used in these days to suppress the colloidal attraction is the steric stabilization. In this alternative method, each colloid is covered by small polymeric wires, see Fig. 2.3. According to the solvent properties, the polymers repel each other, this gives rise

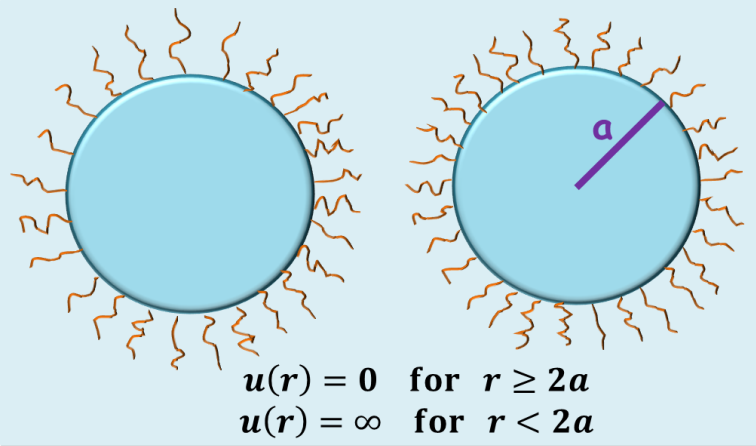

Figure 2.3: Schematic picture of two colloids, each with polymeric hairs that avoid that the particles touch each other giving rise to short range repulsive potentials (adapted from Ref. [6]).

to an excluded-volume interaction between colloids avoiding aggregation. In several systems the polymeric layer can be designed really thin and in such way that the interaction potential among colloids is highly repulsive within a short range. Thus, this potential can be approximated in a good way as the hard-sphere potential. This scheme can also be used to induce thermal-reversible attractions [14, 15].

2.2.2 *Super-paramagnetic potential*

In recent years, the paramagnetic potential has been used in a successful way to study the dynamic and structural properties in colloidal suspensions. This is due to the possibility of defining an effective temperature, also, the interaction magnitude among colloids is the only parameter that controls the phase behavior of the system. These factors have led to the performing of interesting experiments with really high accuracy [6, 16–20].

The magnetic field due to a magnetic dipole $\mathbf{m}$ at a distance $\mathbf{r}$ is given by [21],

$$\mathbf{B}(\mathbf{r}) = \frac{\mu_0}{4\pi}\left[\frac{3\mathbf{r}(\mathbf{r}\cdot\mathbf{m}) - \mathbf{m}}{|\mathbf{r}|^3}\right]. \tag{2.53}$$

The interaction due to the presence of another dipole at the position $\mathbf{r}_j$ is given by [6],

$$U(r_{ij}) = \mathbf{m}_j \cdot \mathbf{B}(r_i), U(r_{ij}) = \frac{\mu_0}{4\pi}\left[\frac{\mathbf{m}_i \cdot \mathbf{m}_j}{|\mathbf{r}|^3} - 3\frac{(\mathbf{m}_i \cdot \mathbf{r}_{ij})(\mathbf{m}_j \cdot \mathbf{r}_{ij})}{|\mathbf{r}|^5}\right] \tag{2.54}$$

where r_{ij} is the relative distance between the center of the particles. If te particles are located in a plane and there is an external magnetic field $\mathbf{H}$ applied perpendicularly to that plane, the dipole moments will align in the direction of the field $(\mathbf{m}\cdot\mathbf{r}_{ij})$ and the interaction can be described just as a dipole-dipole interaction. Also, if we define the

magnetization of a particle as $\mathbf{M} = \langle \mathbf{m} \rangle$ which, for low intensity fields, is related with the applied field by the relation $\mathbf{M} = \chi_m \mathbf{H}$, where χ_m is the magnetic susceptibility of the particle. Thus, the colloidal interaction is given by [6],

$$U(r_{ij}) = \frac{\mu_0}{4\pi} \frac{M^2}{r_{ij}^3} = \frac{\mu_0}{4\pi} \frac{\chi^2 H^2}{r_{ij}^3}. \tag{2.55}$$

From Eq. 2.55, we can define the parameter Γ, which determines the magnitude of the interaction between the colloidal particles [6],

$$\Gamma = \frac{\mu_0}{4\pi} \frac{\chi^2 H^2 \rho^{3/2}}{k_B T} \propto \frac{1}{T_{eff}}, \tag{2.56}$$

where ρ is the density of the colloidal particles, related with the mean distance among particles (d), which for the two-dimensional case is $d \equiv \rho^{-1/2}$. From Eq. 2.56 we notice that the value of Γ can be interpreted as the inverse of an *effective* temperature and can be easily controlled by changing the external magnetic field $\mathbf{H}$. Now, expressing the colloid-colloid interaction in terms of Γ, we obtain the super-paramagnetic potential as [6]

$$\beta U(r_{ij}) = \frac{\Gamma}{(r_{ij}/d)^3}. \tag{2.57}$$

It is important to notice that the latter expression is expressed in terms of the mean particle distance, which is the natural scaling parameter for the present super-paramagnetic system [6].

2.3 INTERACTION OF COLLOIDAL PARTICLES WITH STRONG EXTERNAL FIELDS

In the following, we provide a brief description to the basic interactions between colloidal particles and external substrate potentials generated by laser light [6, 7]. First, we explain the origin of the gradient force and then turn to the radiation pressure. The two forces are illustrated in Fig. 2.4 [6, 7].

An intuitive explanation of the gradient force can be summarized as follows: colloidal particles are dielectric objects and therefore experience a force in an homogeneous light field towards the maximum intensity value. However, this requires that [6, 7]

$$\epsilon_K(\lambda) > \epsilon_W(\lambda), \tag{2.58}$$

with $\epsilon_K(\lambda)$ and $\epsilon_W(\lambda)$ being the dielectric constants of the colloidal particles and water, respectively, and λ the wave length of the light. To prove Eq. 2.58, let E_K and E_W denote the electric field strengths induced by a light beam in a colloidal particle and water respectively.

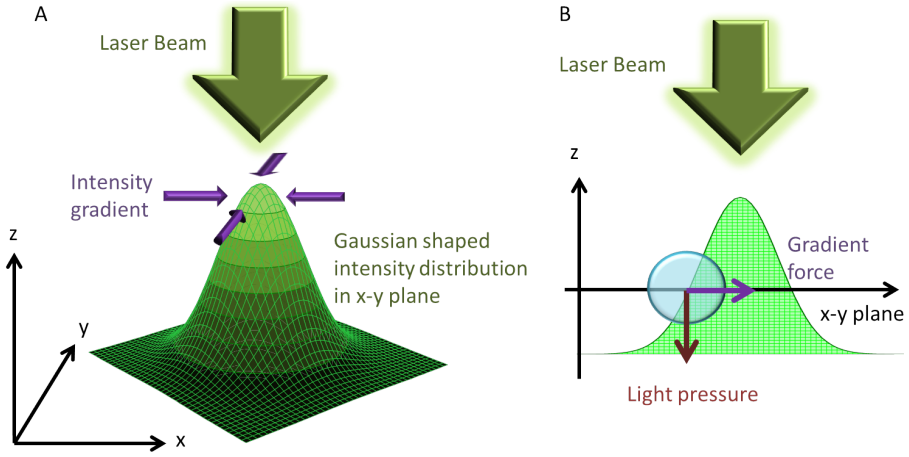

Figure 2.4: A) Gaussian-shaped intensity profile in x-y-plane created by a laser beam which propagates in the z-direction. As indicated by the purple arrows, the intensity gradient radially points to the center of the beam where the intensity is the greatest. B) Cross section of the intensity profile. The colloidal particle is sketched as a blue sphere. The two forces acting on the particle are indicated by the cherry –light pressure– and the purple arrows –gradient force– (adapted from Ref. [7]).

According to [22], those two field strengths are related to each other via [6, 7]

$$E_K = \frac{3\epsilon_W(\lambda)}{\epsilon_K(\lambda) + 2\epsilon_W(\lambda)} E_W. \tag{2.59}$$

If $\epsilon_K(\lambda) \neq \epsilon_W(\lambda)$, the colloidal particle appears as a dipole,

$$d = (\epsilon_K(\lambda) - \epsilon_W(\lambda)) V_K E_K, \tag{2.60}$$

with $V_K = 4/3\pi r_K^3$ the volume and r_K the radius of the colloidal particle. Since the dipole moment interacts with the light electric field, the interaction energy becomes [6, 7]

$$U_{grad} = -\frac{1}{2} d \cdot E_K = -2\pi\epsilon_W \epsilon_K r_K^3 \left(\frac{\epsilon_K(\lambda) - \epsilon_W(\lambda)}{\epsilon_K(\lambda) + 2\epsilon_W(\lambda)} \right) E_W^2. \tag{2.61}$$

To trap the colloidal particle in the center of a laser beam, $U_{grad} < 0$ is required,a condition fulfilled if Eq. 2.58 is valid [6, 7].

The light pressure of a laser beam exerts a second force on a colloidal particle; because of scattering, momentum is transferred from the laser beam to the particle. According to [21], the momentum density of an electromagnetic wave is given by [6, 7]

$$\mathbf{g} = \frac{\mathbf{S}}{c^2} = \epsilon_0 (\mathbf{E} \times \mathbf{B}), \tag{2.62}$$

with $\mathbf{S}$ the Poynting vector and $\mathbf{B}$ the magnetic field. The momentum transferred to the colloidal particle point in the direction of $\mathbf{g}$ provided that the laser beams acts on the particle symmetrically [6, 7].

The light pressure in then given by the momentum transferred per unit area and time,

$$p = c|\mathbf{g}| = c\epsilon_0\epsilon_W E_0 B_0 = \frac{\epsilon_W(\lambda)}{c} I_{scat}. \tag{2.63}$$

Here, E_0 and B_0 denote the amplitudes of the electric and the magnetic field respectively, and I_{scat} refers to the intensity scattered at the surface of the colloidal particle. In the case of a small sphere in an oscillating electromagnetic field, the scattering is mostly caused by dipole scattering. According to Rayleigh, an analytical expression can be derived [6, 7, 23],

$$I_{scat} = \frac{8\pi}{3}\frac{\sigma^6}{\lambda^4}\left(\frac{\epsilon_K(\lambda) - \epsilon_W(\lambda)}{\epsilon_K(\lambda) + 2\epsilon_W(\lambda)}\right) I_{Laser}, \tag{2.64}$$

with σ the diamater of the sphere and I_{Laser} the intensity of the incident laser beam. The light pressure is then obtained by dividing the scattered intensity by the speed of light in water $c/\epsilon_W(\lambda)$ [6, 7],

$$p_{scat} = \frac{8\pi}{3c}\frac{\sigma^6}{\lambda^4}\epsilon_W(\lambda)\left(\frac{\epsilon_K(\lambda) - \epsilon_{W(\lambda)}}{\epsilon_K(\lambda) + 2\epsilon_W(\lambda)}\right) I_{Laser}. \tag{2.65}$$

2.3.1 *Creation of 1D periodic potentials*

A 1D periodic light potential is created through the use of two overlapping expanded laser beams having the same intensity (see Fig 2.5.A). Fig 2.5.B shows an intensity cross section along the x-axis to visualize the intensity distribution in the $x-y$-plane. The wave vectors $\mathbf{K}_1$ and $\mathbf{K}_2$ have the same modulus, i. e. $|\mathbf{K}_1| = |\mathbf{K}_2| = 2\pi/\lambda$, and the same angle φ in the x-direction with respect to the $x-y$-plane are

$$K_{1,x} = |\mathbf{K}_1|\cos\varphi = \frac{2\pi}{\lambda}\sin\left(\frac{\theta}{2}\right), \tag{2.66}$$

$$K_{2,x} = -|\mathbf{K}_1| = -\frac{2\pi}{\lambda}\sin\left(\frac{\theta}{2}\right). \tag{2.67}$$

Describing the two laser beams as planar waves in the x−direction, i. e. $E_1(x) = A\exp(iK_{1,x}x)$ and $E_1(x) = A\exp(iK_{2,x}x)$, the total amplitude can be written as

$$E(x) = E_1(x) + E_2(x) = 2A\cos(K_{1,x}x). \tag{2.68}$$

According to Eq. 2.61, the gradient potential U_{grad} is proportional to E^2 and the 1D periodic potential U_{el} therefore becomes

$$U_{el} = -U_0\left[1 + \cos(2K_{1,x}x)\right] = -U_0\left[1 + \cos\left(\frac{2\pi}{d}x\right)\right], \tag{2.69}$$

with d the period of the potential,

$$d = \frac{\pi}{K_{1,x}} = \frac{\lambda}{2\cos\varphi} = \frac{\lambda}{2\sin(\theta/2)}. \tag{2.70}$$

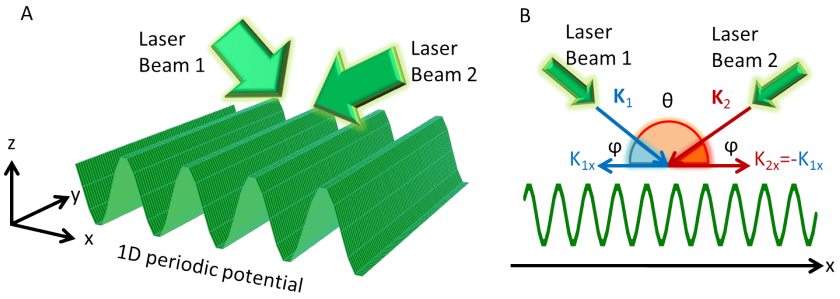

Figure 2.5: 1D periodic light potential created with two interfering laser beams. A) three-dimensional illustration. B) Cross section along the x-axis. $K_{\alpha,x}$ ($\alpha = 1, 2$) are the laser beam wave vectors and the projections into the $x-y$-plane, respectively. φ denotes the incidental angle and θ the angle between the two beams (adapted from Ref. [7]).

θ denotes the angle between the two laser beams. Loudiyi et. al.[24] have evaluated the potential strength U_0 through integration over spherical particle volume,

$$V_0 = \underbrace{2\epsilon_W(\lambda)\sigma^3\left(\frac{\epsilon_K(\lambda)-\epsilon_W(\lambda)}{\epsilon_K(\lambda)+2\epsilon_W(\lambda)}\right)}_{=:A}\underbrace{\frac{4P}{cr_0^2}}_{=:B}\underbrace{\frac{j_1(\pi\sigma/d)}{2\pi\sigma/d}}_{=:C}. \tag{2.71}$$

The factor A is known from the gradient potential, Eq. 2.61. The factor B depends on the laser power P and on the beam radius r_0 in the $x-y$-plane. $c = 3\times10^8 m/s$ denotes the speed of light. The factor C incorporates the finite particle size with j_1 the first order spherical Bessel function. Since $C \to 0$ for $\sigma \to \infty$, large colloids less feel light potentials than small ones. The linear dependence of U_0 on the laser power P has been verified experimentally in [25, 26]

Due to the easy-handling of the magnitude of interaction V_0 and the angle θ in experiential conditions, the use of light fields on colloidal suspensions has found a big variety of applications, some of the most striking ones are,

- Not long ago, the hydrodynamic coupling on the dynamics of two particles held in potential wells could be directly measured, such wells were experimentally created by laser beams [27]. Lately, the laser tweezers have served to develop a huge amount of experimental setups (see Fig. 2.6) that can trap one of few colloidal particles in order to study basic physical properties of the colloidal systems [28–36].

- It is of great importance to study colloidal suspensions with external fields with well defined geometries; the latter can be created by the interference of laser beams. The depth of the minima and the periodicity of the light field can be experimentally controlled, see Fig. 2.7 [37–40].

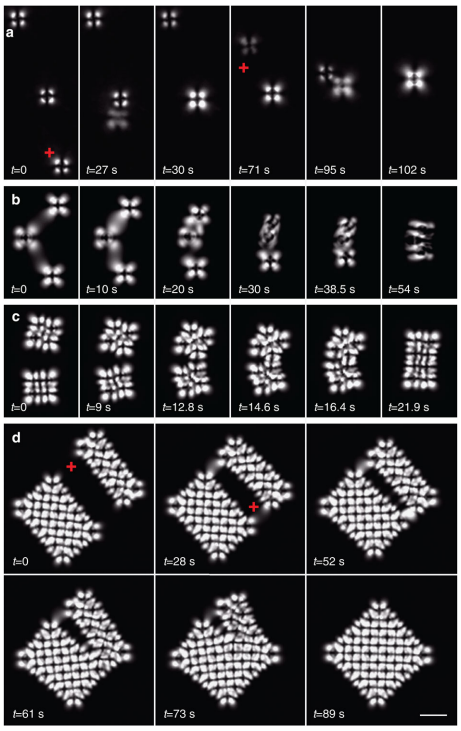

Figure 2.6: Laser-tweezers assembly of a 3D dipolar colloidal crystal observed under crossed polarizers. (a) Three isolated colloidal particles of 4μm diameter in the ZLI-2806-filled homeotropic cell of ~ 25μm thickness appear as bright objects with a dark cross in the centre. Using laser tweezers, one particle is brought close to the other and they spontaneously form a chain of two particles in a direction perpendicular to the plane of the image. The pair appears like a single but larger and brighter particle (third image from the left). The third particle is brought to the couple and it spontaneously forms a dipolar colloidal chain of three particles on top of each other. (b) Three chains, each made of three dipolar particles, are brought close to each other and they start to assemble into a frustrated colloidal trio. Note the tilting of the chains. (c) Two colloidal blocks of $2 \times 2 \times 3$ particles self-assemble into $2 \times 4 \times 3$ blocks. (d) Colloidal blocks of $2 \times 6 \times 3$ and $4 \times 6 \times 3$ particles assemble into the final $6 \times 6 \times 3$ dipolar colloidal crystal. The assembly at the initial stage was guided by the laser tweezers until blocks started to attract themselves. Scale bar, 10μm. In all images, the small red cross is the optical trap, used to direct the colloidal assembly (taken from Ref. [36]).

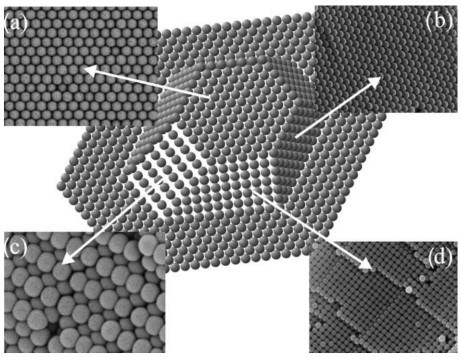

Figure 2.7: Scanning electron microscopy (SEM) images of four facets of a face-centred cubic (fcc) structure compared with a model crystal (center): (a) outer (111), (b) inner (111), (c) inner (110), (d) inner (100) (taken from Ref. [39], which was originally published in Ref.[40] copyright (2003) Wiley-VCH).

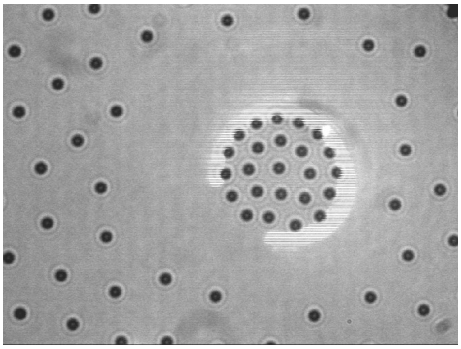

Figure 2.8: Some particles are trapped inside a circular wall that is formed with the laser tweezer (taken from Ref. [41]).

- Fields created by laser beams are also implemented to confine particles in regions of the space, this is possible due to the radiation pressure which basically pulls the particles in the direction of the beam. The latter mechanism allows to control the thermal fluctuations perpendicular to a surface, in such way, that the fluctuations are just around 3% of the diameter of the colloids, see Fig. 2.8. 2D colloidal fluctuations exhibit quite interesting behaviors different form those in three-dimensional ones.

- One of the most difficult experimental tasks is to study the colloidal suspensions at very high or very low densities. Due to the Brownian motion it is difficult to maintain, experimentally, constant densities, also, for dense systems some particles can coagulate due to the van der Waals forces. With laser beams certain impurities can be removed from the system, but one of the highlights of using laser traps is that they can be used to make "*stockyards*" of colloids, see Fig. 2.9. The colloids are trapped with no possibility of going out from the stockyard, also the particles that are outside from it can not penetrate it, in this

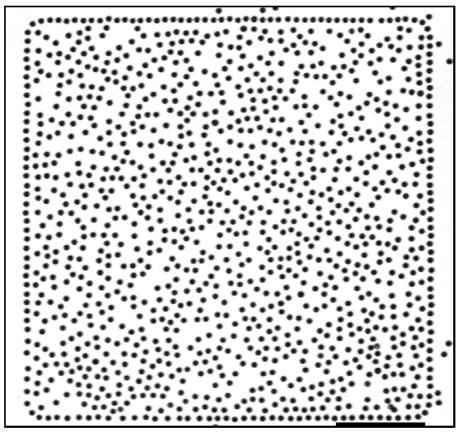

Figure 2.9: Snapshot of a colloidal liquid monolayer at medium density. The length of the black bar equals 50μm. The density of the system is distributed homogeneously. The effect of the scanned laser tweezers can be seen, as the particles on the laser trap align like a pearlnecklace, creating an impenetrable barrier for the particles inside (taken from Ref. [26]).

way the density is held constant and can be easily varied by changing the size of the stockyard.

2.4 COMPUTER SIMULATIONS

In its narrowest sense, a computer simulation is a program that runs on a computer and that uses step-by-step methods to explore the approximate behavior of a mathematical model. Usually this is a model of a real-world system (although the system in question might be an imaginary or hypothetical one). Such a computer program is a computer simulation model. One run of the program on the computer is a computer simulation of the system. The algorithm takes as its input a specification of the system's state (the value of all of its variables) at some time t. It then calculates the system's state at time $t + 1$. From the values characterizing the second state, it then calculates the system's state at time $t + 2$, and so on. When it runs on a computer, the algorithm thus produces a numerical picture of the evolution of the system's state, as it is conceptualized in the model [42].

This sequence of values for the model variables can be saved as a large collection of "data" and is often viewed on a computer screen using methods of visualization. Often, but certainly not always, the methods of visualization are designed to mimic the output of some scientific instruments that the simulation appears to be measuring a system of interest [42].

Sometimes the step-by-step methods of computer simulation are used because the model of interest contains continuous (differential) equations (which specify continuous rates of change in time) that cannot be solved analytically -either in principle or perhaps only in

practice. This underwrites the spirit of the following definition given by Paul Humphreys: *"any computer-implemented method for exploring the properties of mathematical models where analytic methods are not available"* [42]. But even as a narrow definition, this one should be read carefully, and not be taken to suggest that simulations are only used when there are analytically unsolvable equations in the model. Computer simulations are often used either because the original model itself contains discrete equations-which can be directly implemented in an algorithm suitable for simulation-or because the original model consists of something better described as rules of evolution than as equations [42].

In the former case, when equations are being "discretized" (the turning of equations that describe continuous rates of change into discrete equations), it should be emphasized that, although it is common to speak of simulations "solving" those equations, a discretization can at best only find something which approximates the solution of continuous equations, to some desired degree of accuracy. Finally, when speaking of "a computer simulation" in the narrowest sense, we should be speaking of a particular implementation of the algorithm on a particular digital computer, written in a particular language, using a particular compiler, etc. There are cases in which different results can be obtained as a result of variations in any of these particulars [42].

More broadly, we can think of computer simulation as a comprehensive method for studying systems. In this broader sense of the term, it refers to an entire process. This process includes choosing a model; finding a way of implementing that model in a form that can be run on a computer; calculating the output of the algorithm; and visualizing and studying the resultant data. The method includes this entire process-used to make inferences about the target system that one tries to model-as well as the procedures used to sanction those inferences. This is more or less the definition of computer simulation studies in Winsberg 2003 [43].

> "*Successful simulation studies do more than compute numbers. They make use of a variety of techniques to draw inferences from these numbers. Simulations make creative use of calculational techniques that can only be motivated extra-mathematically and extra-theoretically. As such, unlike simple computations that can be carried out on a computer, the results of simulations are not automatically reliable. Much effort and expertise goes into deciding which simulation results are reliable and which are not*" [42].

In the last half of century, the computer simulation techniques have become an important tool in Natural Sciences, since together with the experimental and theoretical techniques constitute, nowadays, one of the most striking keys for the developing of the modern science.

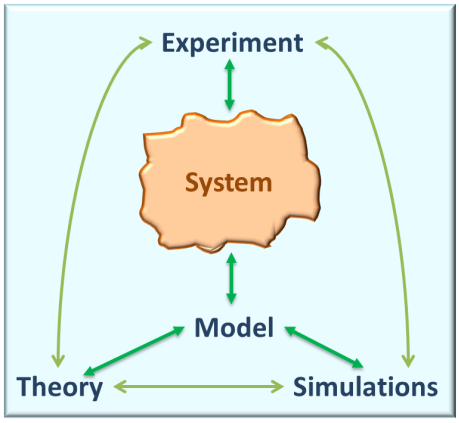

Figure 2.10: Schematic cartoon of the relation between experiment, theory and computer simulations (Adapted from reference [6]).

In fact, these three ways of studying the Nature are closely related. With the time, the computers have become more powerful, in such way that new computational techniques have been developed in order to perform more accurate and faster calculations, which allow us to perform deep studies that are a complement of the theory and experiments. These methods are powerful in the sense that, in the conventional theoretical treatments, a lot of approximations have to be performed which are not required in the computer simulations. In fact, the complexity and detailed level in which a problem is attecked with is a personal choice of the person who is simulating, though limited by the computational power and time, also by the finite precision by which the real system is transferred in an abstract model. In this way, the calculated predictions by the simulation allow the feedback with hypothesis [6], theories and experiments as it is shown in Fig. 2.10

To mention some of the advantages of the computer simulations, we have to refer that they can be used to study properties that are really difficult to be experimentally measured, e. g., the free energy or the chemical potential. Also, some of the control parameters which can be easily handled in the simulations could be really expensive or difficult to be performed in the lab, e. g., really high or low temperatures. It is important to highlight that the computer simulations offer the possibility to perform systematic studies of the control parameters simply by altering them [6].

The details of simulations techniques implemented in the present Thesis can be found in an extense set of publications, for more details see Refs. [6, 44–54].

BIBLIOGRAPHY

[1] B. Duplantier, in *Einstein, 1905–2005*, Springer, 2006, pp. 201–293.

[2] J. K. Dhont, *An introduction to dynamics of colloids*, Elsevier Science, 1996, vol. 2.

[3] I. Kosztin, *Lecture Notes*, 2000, http://www.ks.uiuc.edu/~kosztin/PHYCS498NSM/LectureNotes/.

[4] J. T. G. Overbeek and M. Sparnaay, *Discussions of the Faraday Society*, 1954, **18**, 12–24.

[5] R. Hogg, T. Healy and D. Fuerstenau, *Trans. Faraday Soc.*, 1966, **62**, 1638–1651.

[6] S. Herrera-Velarde, *Ph.D. thesis*, División de Ciencias en Ingenierías. Campus León. Universidad de Guanajuato, 2008.

[7] J. Baumgartl, *Ph.D. thesis*, Physikalisches Institut der Universität Stuttgart, 2007.

[8] J. N. Israelachvili, *Intermolecular and surface forces: revised third edition*, Academic press, 2011.

[9] M. Brunner, *Ph.D. thesis*, Universität Konstanz, 2003.

[10] R. Castañeda-Priego, L. F. Rojas-Ochoa, V. Lobaskin and J. Mixteco-Sánchez, *Physical Review E*, 2006, **74**, 051408.

[11] L. F. Rojas-Ochoa, R. Castañeda-Priego, V. Lobaskin, A. Stradner, F. Scheffold and P. Schurtenberger, *Physical review letters*, 2008, **100**, 178304.

[12] J. C. Mixteco-Sánchez, *Ph.D. thesis*, División de Ciencias en Ingenierías. Campus León. Universidad de Guanajuato, 2011.

[13] D. F. Evans and H. Wennerström, *The colloidal domain: where physics, chemistry, and biology meet*, Wiley-vch New York, 1999.

[14] A. P. Eberle, N. J. Wagner, B. Akgun and S. K. Satija, *Langmuir*, 2010, **26**, 3003–3007.

[15] A. P. Eberle, N. J. Wagner and R. Castañeda-Priego, *Physical Review Letters*, 2011, **106**, 105704.

[16] S. Lin, B. Zheng and S. Trimper, *Physical Review E*, 2006, **73**, 066106.

[17] K. Zahn, J. M. Méndez-Alcaraz and G. Maret, *Physical review letters*, 1997, **79**, 175–178.

[18] P. Castañeda, *Ph.D. thesis*, CINVESTAV-IPN, 2003.

[19] K. Zahn, R. Lenke and G. Maret, *Physical review letters*, 1999, **82**, 2721–2724.

[20] G. Gompper and M. Schick, *Soft Matter: Colloidal order: entropic and surface forces*, Vch Verlagsgesellschaft Mbh, 2007, vol. 3.

[21] J. D. Jackson and R. F. Fox, *American Journal of Physics*, 1999, **67**, 841.

[22] J. A. Stratton, *Electromagnetic theory*, Wiley-IEEE Press, 2007, vol. 33.

[23] M. Kerker, 1969.

[24] K. Loudiyi and B. J. Ackerson, *Physica A: Statistical Mechanics and its Applications*, 1992, **184**, 26–41.

[25] C. Bechinger, M. Brunner and P. Leiderer, *Physical review letters*, 2001, **86**, 930–933.

[26] M. Brunner, *Ph.D. thesis*, Dissertation, Universität Konstanz, 2003.

[27] J.-C. Meiners and S. R. Quake, *Physical review letters*, 1999, **82**, 2211–2214.

[28] J. Crocker, J. Matteo, A. Dinsmore and A. Yodh, *Physical review letters*, 1999, **82**, 4352–4355.

[29] E. R. Dufresne and D. G. Grier, *Review of scientific instruments*, 1998, **69**, 1974–1977.

[30] P. T. Korda, M. B. Taylor and D. G. Grier, *Physical review letters*, 2002, **89**, 128301.

[31] K. Kegler, M. Salomo and F. Kremer, *Physical review letters*, 2007, **98**, 058304.

[32] D. G. Grier, *Nature*, 2003, **424**, 810–816.

[33] A. Meyer, A. Marshall, B. G. Bush and E. M. Furst, *Journal of rheology*, 2006, **50**, 77.

[34] Y. Roichman, V. Wong and D. G. Grier, *Physical Review E*, 2007, **75**, 011407.

[35] J. Hoogenboom, D. Vossen, C. Faivre-Moskalenko, M. Dogterom and A. Van Blaaderen, *Applied Physics Letters*, 2002, **80**, 4828–4830.

[36] A. Nych, U. Ognysta, M. Škarabot, M. Ravnik, S. Žumer and I. Muševič, *Nature communications*, 2013, **4**, 1489.

[37] C. Bechinger, *Current opinion in colloid & interface science*, 2002, **7**, 204–209.

[38] H. Löwen, *Journal of Physics: Condensed Matter*, 2001, **13**, R415.

[39] N. V. Dziomkina and G. J. Vancso, *Soft Matter*, 2005, **1**, 265–279.

[40] C. López, *Advanced Materials*, 2003, **15**, 1679–1704.

[41] G. Maret, *The Maret Group web-page*, http://hera.physik.uni-konstanz.de/oldmaret/research/colloids/index.htm.

[42] E. Winsberg, in *The Stanford Encyclopedia of Philosophy*, ed. E. N. Zalta, Summer 2013 edn., 2013.

[43] E. Winsberg, *Philosophy of science*, 2003, **70**, 105–125.

[44] D. Frenkel, B. Smit and M. A. Ratner, *Physics Today*, 1997, **50**, 66.

[45] D. Fincham, *Molecular Simulation*, 1987, **1**, 1–45.

[46] M. P. Allen and D. J. Tildesley, *Computer simulation of liquids*, Oxford university press, 1989.

[47] D. L. Ermak, *The Journal of Chemical Physics*, 1975, **62**, 4189.

[48] D. L. Ermak and H. Buckholz, *Journal of Computational Physics*, 1980, **35**, 169–182.

[49] A. Iniesta and J. G. de la Torre, *The Journal of Chemical Physics*, 1990, **92**, 2015.

[50] D. L. Ermak and J. McCammon, *The Journal of chemical physics*, 1978, **69**, 1352.

[51] G. Piacente, *Ph.D. thesis*, Universiteit Antwerpen, 2005.

[52] K. Nelissen, *Ph.D. thesis*, Universiteit Antwerpen, 2008.

[53] H. Zhao, *Ph.D. thesis*, Universiteit Antwerpen, 2012.

[54] F. Córdoba Valdés, *Ph.D. thesis*, Universidad de Guanajuato, 2012.

3

HYDRODYNAMIC CORRELATIONS IN THREE-PARTICLE COLLOIDAL SYSTEMS IN HARMONIC TRAPS

"The most exciting phrase to hear in science, the one that heralds new discoveries, is not 'Eureka!' but rather «hmm... that's funny...»"
– I. Asimov

Colloidal suspensions are composed of particles that are dispersed in a continuum medium usually called solvent [1]. They constitute an essential part in life, for instance, the great majority of the processes in the human body take place on (or are supported) by colloidal suspensions. Additionally, colloids have a considerable significance in many industrial and technological applications, such as paints, foods, medicines, just to mention a few [1]. From a physical point of view, colloids serve as model systems to understand, for example, the effective interactions in many-body systems [2–6], the rheology of suspensions [7] and both the phase behaviour and some arrested states of matter, such as gels and glasses, see, e. g., [8, 9] and references therein.

Although colloidal suspensions are commonly used as models of some atomic systems, in a liquid-like environment colloidal particles exhibit indirect interactions mediated by the solvent which, to a great extent, differentiate them from atoms, namely, HI [10]. Contrary to direct interactions, such as Coulomb and excluded-volume interactions [5, 6], HI can be tuned, but never completely screened or switched off [11, 12]. Using a simple physical picture, one can understand HI in the following way. The motion of a given colloidal particle induces a flow field in the solvent, which is felt by the surrounding colloids, i. e., when a colloid moves, it displaces the fluid in its immediate vicinity [13], then, the motion of one particle causes a solvent-mediated force on the neighbouring particles. Thus, HI are indirect interactions that affect the dynamical behaviour of colloids [14]. Such interactions lead to non-trivial complex hydrodynamic coupling between colloids that extends over many mean-interparticle distances [15]. The understanding of HI in complex fluids is of particular relevance in several

branches of science [16], since phenomena like hydrodynamic synchronisation in either biological systems (sperm, cilia, flagella) [17, 18] or active colloidal arrays [19], and the dynamics of microswimmers [20–23] can only be explained in terms of hydrodynamic coupling.

The effects of HI on the coupling between two colloids or a colloid near a wall have been the subject of intense research during the last few decades [24–27]. Experiments in such a direction have been made possible thanks to the use of video microscopy techniques and the optical control of colloids [28]. Optical traps use the forces exerted by strongly focused beams of light to move and trap micron-sized objects [29]. The development of optical tweezers has been essential in the manipulation of colloids [13, 29–31]. The salient features of optical manipulation have been widely exploited to trap colloids in harmonic potentials and use them as model systems to understand the slow dynamics of a large variety of complex systems [32–53].

Over the last two decades, it has been clear that HI play a crucial role in the dynamics of suspended bodies [54, 55]. However, due to their long-range nature, HI represent a difficult problem to be tackled with both experimental and theoretical tools [15]. The pioneering work of Meiners and Quake [56] opened up the possibility of understanding two-body hydrodynamic coupling through the measurement of the auto- and cross-correlation hydrodynamic functions. After the work of Meiners and Quake [56], several research groups studied the hydrodynamic coupling in systems composed of two equal-sized colloidal particles trapped in harmonic potentials [15, 17, 55, 57–61] and under the action of linear shear flows [62, 63]. Recently, the tilting, rotational and translational dynamics of two colloids in a single optical potential were reported by Tränkle et al. [64].

In contrast to the two-particle system, hydrodynamic correlation between three or more particles is a topic that remained unexplored during the last decade. However, recent experimental and theoretical works have pointed out toward our understanding of several interesting phenomena, such as particle synchronisation, in few-body systems driven by hydrodynamic coupling [19, 65–68].

The aim of this Chapter is to study the effect of a third particle on the two-body hydrodynamic correlation function. We particularly focus on the dynamical modes that allow us to define the degree of hydrodynamic correlation between particles. As a suitable model, we choose a system composed of three particles suspended in a low Reynolds number fluid. Every colloid is highly confined in a single harmonic potential and particles interact only via hydrodynamic forces. The correlations are obtained by solving the Langevin equation of motion assuming that the diffusion tensor is constant. It is noteworthy to mention that it is a hard task to find a general analytical solution even for a few-body configuration; analytical solutions are here achieved in some symmetric particle configurations (see also

Ref. [11]). To overcome such limitation, we have developed an algorithm which allows us to obtain numerically the correlation functions for an arbitrary configuration of particles. We validate our approximation by comparing our results with Brownian Dynamics (BD) simulations, which are carried out with the explicit inclusion of HI and without any further assumption, i. e., the Rotne-Prager diffusion tensor [10, 69] is not considered constant during the simulations. We also revisit the two-particle system. The collective and relative hydrodynamic modes in three-particle systems are explicitly described. We put special attention to the particular case of a collinear configuration but an equilateral triangle configuration is also considered. The particular details of the numerical algorithm and other particle configurations will be presented elsewhere [70].

After above paragraphs, the Chapter is organized as follows. In Section 3.1, we introduce the BD simulation technique [69] employed to compute the hydrodynamic correlation functions. We also discuss the main physical assumptions that allows us to solve either analytically or numerically the equations of motion. In 3.2 we present the full theoretical derivation and results of the two-body hydrodynamic correlation functions in two- and three-particle colloidal systems. For the sake of the discussion, we first revisit the hydrodynamic correlations in a two-particle system, where the analytical solution is tested against simulations and numerical results. We also show our findings for a three-particle collinear configuration. In this particular case, the cross-correlation function exhibits positive values; this unexpected behaviour dominates at both intermediate- and long-times and, to the best of our knowledge, it has not been observed in a two-particle configuration. In the same section, we briefly discuss the main characteristics of the correlation functions for an equilateral triangle configuration. Finally, the some concluding remarks about the Chapter are presented in 3.3.

3.1 COMPUTER SIMULATIONS AND PHYSICAL ASSUMPTIONS

3.1.1 *Brownian dynamics simulations*

Brownian motion theory was developed to describe the dynamics of particles whose mass and size are much larger than the solvent particles where they are suspended. The equation for the discrete trajectory, $\mathbf{r}_i(t)$, of a colloidal particle i obeying Brownian motion with HI, after a finite time step Δt, reads as [69]

$$\mathbf{r}_i = \mathbf{r}_i^0 + \sum_j^N \frac{\partial D_{ij}^0}{\partial r_j}\Delta t + \sum_j^N \beta D_{ij}^0 \mathbf{F}_j^0 \Delta t + r_i(\Delta t), \tag{3.1}$$

where N is the number of particles, $\beta = (k_B T)^{-1}$ is the inverse of the thermal energy; k_B is the Boltzmann constant and T the abso-

lute temperature; D^0_{ij} is the $3N \times 3N$ diffusion tensor; $\mathbf{F}^0_j$ is the total force acting on the j-th particle and the index "o" indicates that the variable must be calculated at the beginning of the time step [69]. The term r_i represents a random displacement with a Gaussian distribution function whose mean value is zero and a covariance matrix given by $\langle r_i(\Delta t) r_j(\Delta t) \rangle = 2D^0_{ij}\Delta t$; these conditions fulfill the fluctuation-dissipation theorem [69]. The HI are taken into account by means of the Rotne-Prager tensor [10]. This tensor satisfies the relation $\sum_j \frac{\partial D_{ij}}{\partial r_j} = 0$, hence, this term does not appear in our simulation algorithm. The values for the set of 3N displacements $\{r_i\}$ can be obtained from either a multivariate normal deviate generator or a weighted sum of normal random deviates [69, 71].

In this Chapter we use the same set of parameters as the one in the experiments of Meiners and Quake [56], i. e., latex spheres with a diameter, $2a$, of 1.0 ± 0.025 μm and trap stiffness, k, of 18.5 pN/μm. We choose as the unit of length the particle radius, therefore, the value of the reduced trap stiffness, $k^* \equiv ka^2/k_BT$, at standard room temperature is $k^*_{x,y,z} \approx 1117$. We use the same reduced trap stiffness in all directions for all the particle distributions here studied; anisotropic traps are not considered. Besides, equal-sized spheres with stick surface hydrodynamic boundary conditions are assumed and the reduced time step is $\Delta t^* = 5 \times 10^{-5}$, where $t^* = tD_0/a^2$ is the reduced time. We use 10^6 time steps, which lead to a maximum simulation time of $t^*_{max} = 50$. This time window allows us to reduce the statistic uncertainties in such a way that error bars are smaller than the symbol size used in the plots.

Equation (3.1) provides the translational motion of particle i, which is then used to evaluate the translational-translation correlation with itself and the other particles. However, it is well-known that there exists rotational-translational hydrodynamic coupling between colloids [57, 58]. The spheres will, in general, rotate while translating (as described by the rotational-translational diffusion tensors) but for torque-free spheres this coupling should not influence on their translational velocities, i. e., the translational motion of hydrodynamically interacting spheres to which no external torques are applied must be decoupled from their rotational motion (but not viceversa). Thus, provided the harmonic traps (which are the external fields) do not exert torques on the spheres (a reasonable assumption), the linear relation between applied forces and translational sphere velocities are fully described by the translational-translational hydrodynamic diffusion tensors only, and this even when the spheres are mutually close to each other. To better clarify this point, the rotational coupling can be easily estimated according to the work of H. Stark and co-workers, see, e. g., Refs. [57, 58]. To estimate the rotational contribution we consider similar particle separations of around $3a$. Besides, in the aforementioned work, the system parameters, reduced trap stiffness and particle ra-

dius, are rather similar to the ones used in this Chapter. Furthermore, we use the same value of the angular spring constant, ζ, as the one experimentally reported in [58]. Thus, the rotation-translation coupling becomes one order of magnitude smaller than the translational hydrodynamic coupling obtained from the particle positions provided by equation (3.1). Thus, since the rotation-translation coupling represents less than the 10% of the whole hydrodynamic coupling, we can safely disregard it from our present analysis, although its effects will be considered elsewhere [70].

3.1.2 *Constant diffusion tensor approximation*

Our physical model consists of particles highly confined in their corresponding harmonic traps. To obtain a good estimation of the maximum particle displacement around each potential minimum, one can consider that a particle performs displacements in all directions that are bounded by the fact that the particle cannot overcome a potential barrier, created by the harmonic trap, greater than its own mean kinetic energy. Thus, the maximum displacement reached by the particle in, for example, the x-direction must satisfy the following condition: $\frac{1}{2}k\delta x_{max}^2 = \frac{1}{2}k_B T$. This leads to the relation: $\delta x_{max} = \sqrt{\frac{1}{k^*}}a$. Using the experimental parameters of Meiners and Quake [56], one finds that $\delta x_{max} \approx 0.03a = 15nm$. Then, the time needed to diffuse such a distance is $\tau = \delta x_{max}^2/D_0 \approx 2 \times 10^{-4}s$. According to Tränkle et al. [64], their tracking technique has a temporal resolution of $10^{-4}s$ and a precision of $5nm$. Thus, our predictions could be experimentally corroborated.

From our previous analysis, it is evident that particles will perform small, but experimentally measurable, displacements around the trap minima. Then, the relative distance between particles does not vary significantly. Hence, one can assume that the diffusion tensor remains constant at all times. This assumption, as we will see further below, allows us to linearise the equations of motion, and, therefore, to facilitate the mathematical procedure, either analytic or numeric, to solve the equations for the particles trajectories. So, the expressions for the correlation functions will be compared with BD simulation results. This comparison is twofold. First, it allows to elucidate the accuracy of the constant diffusion tensor approximation and, second, it gives us the opportunity to analyse differences and similarities between the numerical and BD methodologies.

The lack of symmetry in some of the particle configurations here considered does not allow us to find, in general, an analytical solution. However, it is still possible to solve numerically the set of coupled equations. Besides, a numerical procedure has the advantage that can be easily extended to particle configurations with more than three particles [70]. Then, a numerical route is, on one hand, useful

to studying the hydrodynamic coupling of spheres distributed in diverse configurations and, on the other hand, it allows us a direct and fast evaluation of the dynamical modes.

3.2 TWO- AND THREE-PARTICLE SYSTEMS

The results shown in the present Chapter differ from previous works [11, 56] in what regards the use of the Rotne-Prager tensor, which provides a description of the particle dynamics beyond the Oseen tensor. The selection of the Rotne-Prager tensor resides in the fact that it is a more accurate diffusion tensor at shorter separations. This is an important issue since it has been recently shown that there exist differences in the correlation functions in two-particle systems when particles are very close [72]. Then, one can expect that those particle configurations with small gap sizes, which might lie out of the Oseen description, could be better described within the Rotne-Prager formalism. In the following, we outline the main steps to obtain the temporal correlation functions.

3.2.1 *Two-particle configuration*

We now present the full theoretical description that accounts for the analytical expressions of the auto- and cross-correlation functions in a system composed of two particles. The analysis of the two-particle system will serve as the basis for the more complex problem of adding a third particle or even more. Furthermore, this case will be considered as a reference system when comparing with the expressions of the three-particle system.

We follow the Langevin dynamics framework presented by Meiners and Quake [56]. For the sake of clarity and comparative purposes, we try to preserve the notation used in [56]. Hence, because beads are thermally excited and they interact only trough their influence on the surrounding medium, the corresponding equation of motion for one particle can be written as

$$\frac{d\mathbf{r}_n}{dt} = \sum_{m=1}^{N} D_{nm}\left[-k(\mathbf{r}_m - \mathbf{r}_m^0) + \mathbf{f}_m(t)\right], \tag{3.2}$$

where $n, m = 1, 2$, $\mathbf{r}_n = (r_{n,x}, r_{n,y}, r_{n,z})$ is the vector position of the n-particle; N is the number of the particles in the system ($N = 2$); D_{nm} is the diffusion tensor and the term $-k(\mathbf{r}_m - \mathbf{r}_m^0)$ is the interaction of the beads with the harmonic trap, where $\mathbf{r}_m^0$ is the position vector of the potential minimum and k is the trap stiffness. In equation (3.2) it is assumed that k has the same value in all directions, but, in general, it can be represented as a diagonal matrix whose entries could possess different values. This corresponds to the case of an anisotropic

trap, which is not considered in this Chapter, but having k expressed in a matrix form allows us to mathematically generalise the equations of motion, as it is shown further below. Additionally, in the BD simulations and subsequent calculations the correlation functions are always defined relative to the (mean) trapping positions, however, for simplicity, from now on $\mathbf{r}_n$ stands for $\mathbf{r}_n - \mathbf{r}_n^0$. The stochastic force, $\mathbf{f}_m(t)$, satisfies the following relations,

$$\begin{aligned} \langle \mathbf{f}_m(t) \rangle &= 0, \\ \langle \mathbf{f}_n(t)\mathbf{f}_m(t') \rangle &= 2D_{nm}^{-1} k_B T \delta(t-t'), \end{aligned} \tag{3.3}$$

where the brackets $\langle \ldots \rangle$ stand for an ensemble average. HI are included through the Rotne-Prager diffusion tensor, D_{nm}, which reads as [10]

$$\begin{aligned} D_{nn} &= \frac{\hat{I}}{\zeta}, \\ D_{nm} &= \frac{1}{\zeta}\left\{ \frac{3a}{4r_{nm}} \left[\hat{I} + \hat{\mathbf{r}}_{nm}\hat{\mathbf{r}}_{nm}\right] + \right. \\ &\quad \left. \frac{1}{2}\left(\frac{a}{r_{nm}}\right)^3 \left[\hat{I} - 3\hat{\mathbf{r}}_{nm}\hat{\mathbf{r}}_{nm}\right] \right\}, \end{aligned} \tag{3.4}$$

where $\zeta = 6\pi\eta a$ is the friction coefficient of a sphere of radius a in a solvent with viscosity η, $\hat{I}$ denotes the unitary matrix, and $\hat{\mathbf{r}}_{nm}$ is the unit vector parallel to $\mathbf{r}_{nm} = \mathbf{r}_m - \mathbf{r}_n$.

The distance between beads can be considered constant [11, 56]. Then, one can assume that $\mathbf{r}_2 - \mathbf{r}_1 \approx E\hat{\mathbf{x}}$ [11, 15, 56, 66], where E is the distance between the harmonic potential minima and, hence, we define it as the mean distance between colloidal particles, while the unit vector $\hat{\mathbf{x}}$ provides the direction of the relative vector connecting the center of particles. A cartoon of the system is displayed in figure 3.1(a). The assumption of constant particle separation allows us to consider D_{nm} as a constant tensor [56], and, therefore, equation (3.2) becomes linear. Then, the diffusion tensor can be rewritten as,

$$\begin{aligned} D_{11} = D_{22} &= \begin{pmatrix} \alpha & 0 & 0 \\ 0 & \alpha & 0 \\ 0 & 0 & \alpha \end{pmatrix}, \\ D_{12} = D_{21} &= \begin{pmatrix} \gamma & 0 & 0 \\ 0 & \beta & 0 \\ 0 & 0 & \beta \end{pmatrix}, \end{aligned} \tag{3.5}$$

where we have introduced the following definitions,

$$\begin{aligned} \alpha &= \frac{1}{\zeta}, \\ \gamma &= \frac{1}{6\pi\eta E}\left[\frac{3}{2} - \nu^2\right], \\ \beta &= \frac{1}{12\pi\eta E}\left[\frac{3}{2} + \nu^2\right]. \end{aligned} \tag{3.6}$$

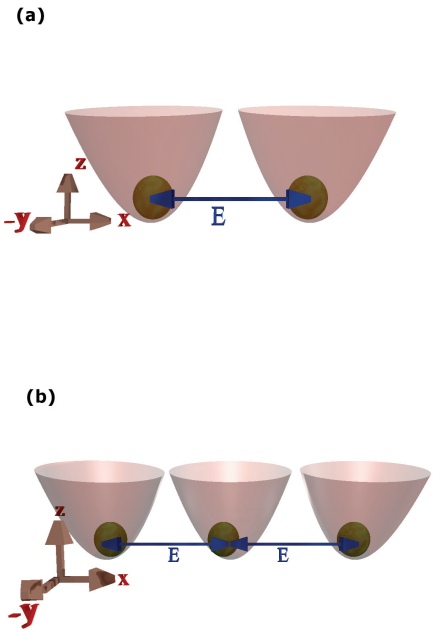

Figure 3.1: Schematic representation of the particles confined in the harmonic traps. **(a)** Two-particle system, and **(b)** three-particle system in a collinear array. E denotes the mean distance between two adjacent particle centers.

Both γ and β depend on $\nu \equiv \frac{a}{E}$ and are independent of it in the limit $\nu \to 0$, which corresponds to the constant Oseen tensor approach addressed by Meiners and Quake [56]. The term ν becomes more important when particles are close to each other, however, at very short distances, when the gap between particles is of the order of $0.1a$, lubrication forces have to be taken into account explicitly [7, 73]. Nevertheless, the latter ones are disregarded in our description, however we consider a few cases -just for illustration purposes- where the mean separation between particles is too short that lubrication forces are expected to play a prominent role. Although the Rotne-Prager approximation works well for particle distances larger than $E \approx 3a$ [16], it has the virtue of preserving the positive definiteness (and hence the physically required decay of all correlation functions) for all non-overlap configurations. In addition, it has the simplifying feature of being pairwise additive.

Then, for the sake of generality, one can assume that the spring constant, k, has different values in each direction [64]. The equation of motion (see (3.2)) can then be written in a compact way using the following matrix notation,

$$\frac{d}{dt}\mathbf{R} = \mathcal{M}\mathbf{R} + \mathbf{v}, \tag{3.7}$$

where

$$\begin{aligned} \mathbf{R} &= \begin{pmatrix} \mathbf{r}_1 \\ \mathbf{r}_2 \end{pmatrix}, \\ \mathbf{v} &= \begin{pmatrix} \mathbf{v}_1 \\ \mathbf{v}_2 \end{pmatrix} = \begin{pmatrix} [D_{11}] & [D_{12}] \\ [D_{21}] & [D_{22}] \end{pmatrix} \begin{pmatrix} \mathbf{f}_1 \\ \mathbf{f}_2 \end{pmatrix}, \end{aligned} \tag{3.8}$$

and $\mathcal{M}$ is a $3N \times 3N$ matrix. The general solution of (3.7) is given by,

$$\mathbf{R}(t) = \psi(t) \cdot \int_{t_0}^{t} \psi^{-1}(t') \cdot \mathbf{v}(t')dt' + \psi(t) \cdot \mathbf{c}, \tag{3.9}$$

where $\psi(t)$ is the matrix composed by the solutions of the homogeneous solution of (3.7); the constant $\mathbf{c}$ can be calculated by setting the initial conditions, $\mathbf{c} = \psi^{-1}(t_0) \cdot \mathbf{R}(t = 0)$. One can evaluate straightforwardly the eigenvalues and the corresponding eigenvectors of the matrix $\mathcal{M}$. Thus, the matrix $\psi(t)$ is computed when the eigenvalues of $\mathcal{M}$ and the corresponding normalised eigenvectors are explicitly known.

Using (3.3), one can prove that $\langle \mathbf{v}_m(t)\mathbf{v}_n(t')\rangle = 2k_B T D_{mn}\delta(t-t')$, so we can obtain analytic expressions for the auto-correlation and cross-correlation functions in any direction. The auto-correlation functions can be expressed, in general, as

$$\langle r_{n,i}(t) r_{n,i}(0)\rangle = \frac{k_B T}{2k_i}\left(e^{-t\frac{1+\varepsilon_i'}{\tau_i}} + e^{-t\frac{1-\varepsilon_i'}{\tau_i}}\right), \tag{3.10}$$

with $n = 1, 2$ and $i = x, y, z$; while the cross-correlation functions take the following functional form

$$\langle r_{n,i}(t) r_{m,j}(0)\rangle = \delta_{ij}\frac{k_B T}{2k_i}\left(e^{-t\frac{1+\varepsilon_i'}{\tau_i}} - e^{-t\frac{1-\varepsilon_j'}{\tau_j}}\right), \tag{3.11}$$

with $n \neq m = 1, 2$ and $i, j = x, y, z$, and $\tau_i = \frac{\zeta}{k_i}$ is the fundamental relaxation time determined by the trap strength k_i and the friction coefficient of the sphere ζ. The dimensionless parameter ε_i' describes the ratio between the mobility of a single bead and the strength of the hydrodynamic coupling between particles [56]. In particular, along the longitudinal direction $\varepsilon_x' \equiv \varepsilon_x - \nu^3$, with $\varepsilon_x = \frac{3}{2}\nu$, while in the transversal direction $\varepsilon_{y,z}' \equiv \varepsilon_{y,z} - \nu^3$ with $\varepsilon_{y,z} = \frac{3}{4}\nu$.

Equations (3.10) and (3.11) exhibit the same functional form as those obtained by Meiners and Quake (see equations (4) and (5) in [56]). However, the arguments are slightly different because we use a different diffusion tensor. Nevertheless, one can easily recover the expressions derived within the Oseen tensor approximation by simply taking the limit $\nu \to 0$ and preserving the linear terms in ν. As we can appreciate, the auto-correlation is a positive-definite quantity since (3.10) is expressed in terms of positive quantities. This means that the presence of more particles in the system is equivalent to adding more positive terms in the auto-correlation function. Then, the self-diffusion of one particle is affected because the strength of the net hydrodynamic force depends on the number of colloids; hence, when more that one neighbour is present it is expected to observe a different dynamical behaviour for each particle. As we will see below, the auto-correlation function for the two- and three-particle systems exhibits a different decay. In contrast, the cross-correlation is composed by the difference of two positive quantities. Therefore, there exists a competition between the dynamics of both particles that lead to anti-correlated motion. In fact, several theoretical and experimental reports have shown that the cross-correlation function in a two-particle system is always negative for all particle separations [55–57]. As we will show below, a different behaviour is observed in the case of a linear array of three particles.

To elucidate the degree of accuracy of the constant diffusion tensor approximation, we compare equations (3.10) and (3.11) with those results obtained from BD simulations. Additionally, we evaluate the correlation functions through the numerical solution of the set of coupled equations of motion (3.7). The auto- and cross-correlation functions are depicted in figures 3.2(a) and 3.2(b), respectively, when the distance between the harmonic traps is $E = 4a$. From both figures, one can observe that the numerical procedure perfectly agrees with

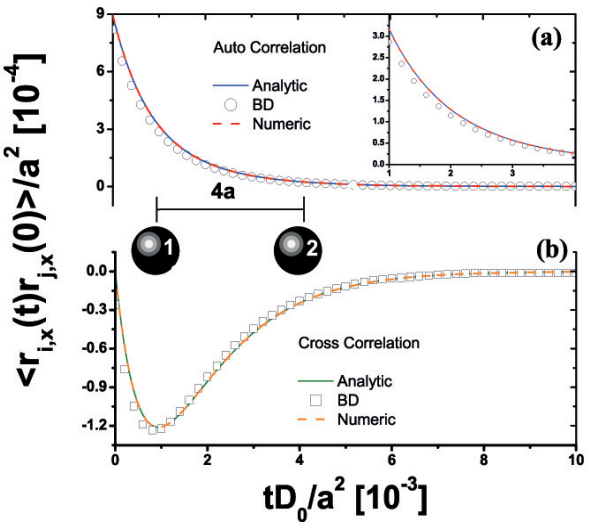

Figure 3.2: **(a)** Auto-correlation and **(b)** cross-correlation functions in the x-direction for a two-particle system. Solid lines correspond to the theoretical solution given by equations (3.10) and (3.11), symbols to BD simulations and dashed lines to the numerical solution of the set of differential equations. Inset shows the short-time behaviour of the auto-correlation function. Snapshot shows the particle configuration and indicates the separation between particles.

the analytical expressions. Furthermore, both calculations are in good agreement with the BD computer simulations. Hence, our simulation results confirm that the assumption of a constant diffusion tensor is a very good approximation to study the hydrodynamic correlation for particles highly confined in harmonic potentials. We also find that the correlation functions in the y and z directions show a good agreement between different procedures (data not shown).

3.2.2 *Three-particle configuration*

We now obtain the analytical solution of a collinear array composed of three particles making use of the procedure discussed above. We should anticipate that, as might be expected, there is no general analytical solution to the case of a three-particle system, since the solution depends on the specific configuration of all particles. The motion of each particle is described by equation (3.2) with $N = 3$ and $n, m = 1, 2, 3$. The stochastic force satisfies the same relationships given explicitly in equation (3.3).

For simplicity, we consider that all particles lie in the same plane, i.e., $z = 0$. This allows us to drastically simplify the entries of the diffusion tensor [70]. Despite this particular selection for the location of the colloids, it is still a laborious task to find the analytical solution for the resulting set of coupled linear differential equations. The prob-

lem resides in the fact that to calculate any observable one has to deal with polynomials of sixth grade to obtain the eigenvalues of the 9×9 matrix $\mathcal{M}$. However, it is possible to obtain the analytical solution for those configurations in which the matrix $\mathcal{M}$ becomes sparse, i. e., $\mathcal{M}$ has many entries equal to zero. The sparse matrix representation corresponds to particle distributions such as a collinear and equilateral particle configurations. Here, we study in detail the analytical solution of a collinear configuration of three particles. However, we have implemented a simple numerical diagonalisation method to evaluate the two-body hydrodynamic correlation functions for any particular three-particle configuration [70]. The explicit details, the functional form of the diffusion tensors, D_{nm}, and the matrix $\mathcal{M}$ for different particle distributions of systems composed of 3 particles will be discussed and presented elsewhere [70].

To solve the set of coupled equations analytically we choose the simplest case, i. e., a collinear configuration. Exploiting the symmetries of this particular choice, it is possible to provide an analytical and exact diagonalisation of the matrix $\mathcal{M}$. In particular, colloids are located at the positions $\{(-E/q, 0, 0), (0, 0, 0), (E, 0, 0)\}$, with particle 3 placed at the origin (see figure 3.1(b)). The parameter q has no fundamental physical significance; it has been introduced to facilitate the algebraic manipulation and to be used as a control parameter of the position of particle 1 with respect to particles 2 and 3. In the limit $q \to 0$, particle 1 is no longer correlated with the others and the correlation functions between particles 2 and 3 have to reduce to the ones obtained in the two-particle system, see (3.10) and (3.11). According to the previous assumptions, many elements of the diffusion tensors are zero and the non-zero entries are easy to evaluate [70]. To simplify the notation, from now on, all quantities are expressed in reduced units.

In principle, the corresponding eigenvalues of matrix $\mathcal{M}$ can be straightforwardly calculated. However, even for this simple particle configuration, a general analytical expression for any value of q cannot be easily obtained since the eigenvalues are the roots of cubic polynomials. Hence, it is not possible to find a simple exact analytical solution. We then decide to expand the roots around $q \approx 0$ in order to obtain an approximate solution. For illustration purposes and the sake of the discussion, we write down the analytical expressions for the first two eigenvalues, λ_1 and λ_2, however, as we will show later, even when a general solution exists, one more assumption has to be made in order to find analytical expressions. Then,

$$\begin{pmatrix} \lambda_1 \\ \lambda_2 \end{pmatrix} = \begin{pmatrix} -k_x \left(1 + \frac{3\nu}{2} - \nu^3 + \frac{9\nu}{2\nu^2-3} q^2 + O(q^3)\right) \\ -k_x \left(1 - \frac{3\nu}{2} + \nu^3 + O(q^4)\right) \end{pmatrix}. \tag{3.12}$$

From the previous expression, we can observe that by taking the limit $q \to 0$, one recovers the expressions for the eigenvalues of the two-

particle system. Furthermore, by considering $\nu^3 \approx 0$, the solution reduces to the one obtained through the Oseen tensor approximation [56].

In the particular case in which the mean distance between particle 1 and 3 is the same as the one between particles 2 and 3, i. e., $q = 1$, the eigenvalues take the following explicit form [70]

$$\boldsymbol{\lambda} = \begin{pmatrix} -k_x\left(1-\frac{3}{4}\nu+\frac{1}{8}\nu^3\right) \\ -k_x\left(1+\frac{3}{16}\left(2+p_1\right)\nu-\frac{1}{16}\nu^3\right) \\ -k_x\left(1+\frac{3}{16}\left(2-p_1\right)\nu-\frac{1}{16}\nu^3\right) \\ -k_y\left(1-\frac{3}{8}\nu-\frac{1}{16}\nu^3\right) \\ -k_y\left(1+\frac{3}{32}\left(2+p_2\right)\nu+\frac{1}{32}\nu^3\right) \\ -k_y\left(1+\frac{3}{32}\left(2-p_2\right)\nu+\frac{1}{32}\nu^3\right) \\ -k_z\left(1-\frac{3}{8}\nu-\frac{1}{16}\nu^3\right) \\ -k_z\left(1+\frac{3}{32}\left(2+p_2\right)\nu+\frac{1}{32}\nu^3\right) \\ -k_z\left(1+\frac{3}{32}\left(2-p_2\right)\nu+\frac{1}{32}\nu^3\right) \end{pmatrix}, \tag{3.13}$$

where $p_1 = \sqrt{132-172\nu^2+57\nu^4}$ and $p_2 = \sqrt{132+172\nu^2+57\nu^4}$. Then, following the same procedure as the one in the two-particle system, we can obtain the analytic expressions for the auto- and cross-correlation functions. We only show the expressions in the x-direction; the expressions for both y- and z-directions have a similar functional form and can be obtained in a similar way [70].

Thus, the auto-correlation functions are given by

$$\begin{aligned} \langle r_{1,x}(t)r_{1,x}(0)\rangle &= \tfrac{1}{2k_x p_1}\left(p_1 e^{\lambda_1 t}+a_1 e^{\lambda_2 t}-a_2 e^{\lambda_3 t}\right), \\ \langle r_{3,x}(t)r_{3,x}(0)\rangle &= \tfrac{1}{k_x p_1}\left(a_1 e^{\lambda_3 t}-a_2 e^{\lambda_2 t}\right), \end{aligned} \tag{3.14}$$

with $a_1 = \left(1+\frac{p_1}{2}-\frac{\nu^2}{6}\right)$ and $a_2 = \left(1-\frac{p_1}{2}-\frac{\nu^2}{6}\right)$. In addition, due to the inherent particle distribution symmetry we obtain that $\langle r_{1,x}(t)r_{1,x}(0)\rangle = \langle r_{2,x}(t)r_{2,x}(0)\rangle$. The cross-correlation functions take the form,

$$\begin{aligned} \langle r_{1,x}(t)r_{2,x}(0)\rangle &= \tfrac{1}{2k_x p_1}\left(-p_1 e^{\lambda_1 t}+a_1 e^{\lambda_2 t}-a_2 e^{\lambda_3 t}\right), \\ \langle r_{n,x}(t)r_{3,x}(0)\rangle &= \langle r_{3,x}(t)r_{n,x}(0)\rangle = \tfrac{12-8\nu^2}{3k_x p_1}\left(e^{\lambda_2 t}-e^{\lambda_3 t}\right). \end{aligned} \tag{3.15}$$

with $n = 1, 2$ and $\langle r_{1,x}(t)r_{2,x}(0)\rangle = \langle r_{2,x}(t)r_{1,x}(0)\rangle$ because the symmetry of the chosen configuration.

Since we constantly use the concept of correlation functions, it is better to use a compact notation. Then, from here on we use the symbol $C_{ij}^{\alpha\beta} \equiv \langle r_{i,\alpha}(t)r_{j,\beta}(0)\rangle$ (temporal-dependence is assumed implicitly) to represent the translational-translational correlation functions between spheres i and j with respect to the Cartesian axes α and β.

Thus, $i, j \in \{1, 2, 3\}$ and $\alpha, \beta \in \{x, y, z\}$. Auto-correlation functions are special cases when $i = j$.

The effect of the third particle on the C_{ij}^{xx} when neighbouring particles are separated by a distance $E = 3.1a$ can be appreciated in figure 3.3. Similar to the results of the two-particle system (figure 3.2), our BD data for both two- and three-particle systems are in good agreement with the analytical results for the auto-correlation (data no shown) and cross-correlation functions (symbols). In particular, the C_{ii}^{xx} of the two- and three-particle systems, i. e., equations (3.10) and (3.14), respectively, are shown in figure 3.3(a). As it has already been observed in previous works [11, 56, 57, 72], the C_{ii}^{xx} for the two-particle system displays the typical monotonous decay. Similarly, in the three-particle system the C_{11}^{xx} and C_{22}^{xx} have exactly the same decay rate; it happens when the closer neighbour is at the same mean distance in both systems. Hence, one can deduce that the presence of particle 3 does not affect the behaviour of the auto-correlation of particles 1 and 2. This observation agrees with the reported experimental data of two particles, where the change in the auto-correlation functions due the presence of a second bead turns out to be so small that is not noticeable in the measurements [56]. However, the decay of C_{33}^{xx} is slightly slower than the rest of the auto-correlation functions. This behaviour is associated with the hydrodynamic force that adjacent particles exert on particle 3, which could result from a more complex fluid velocity field reaching particle 3 that, in consequence, promotes a self-interaction for a longer time than the other two particles.

The cross-correlation functions of both configurations are shown in figure 3.3(b). In this figure we also present our BD simulations to compare with the analytic expressions given by equations (3.11)and (3.15), solid and dashed lines, respectively. Note that because of the symmetry in the collinear configuration $C_{13}^{xx} = C_{23}^{xx}$. As can be noticed from the figure, at short times, $t^* < 10^{-3}$, C_{12}^{xx} in the two-particle system and C_{13}^{xx} for the three-particle system are almost identical, but for longer times a clear separation is distinguishable. However, beyond the similarities and evident differences displayed in figure 3.3(b), we observe that the cross-correlation function of each system exhibits only negative values; the same behaviour is always obtained for all values of E (data not shown). The anti-correlation effect and, mainly, the time delay -related with the so-called "memory effect"- are striking features that have been pointed out in previous works with two-particle systems [17, 56, 57, 64, 72]. Although HI act instantaneously and an instantaneous propagation of the forces through the fluid is expected, there exists an anti-correlation because the relative modes dominate at longer times over the collective ones. The former are present when spheres translate in opposite directions and some fluid has to be pulled into or squeezed out of the region between the two particles leading to a slower decay. When the spheres translate collec-

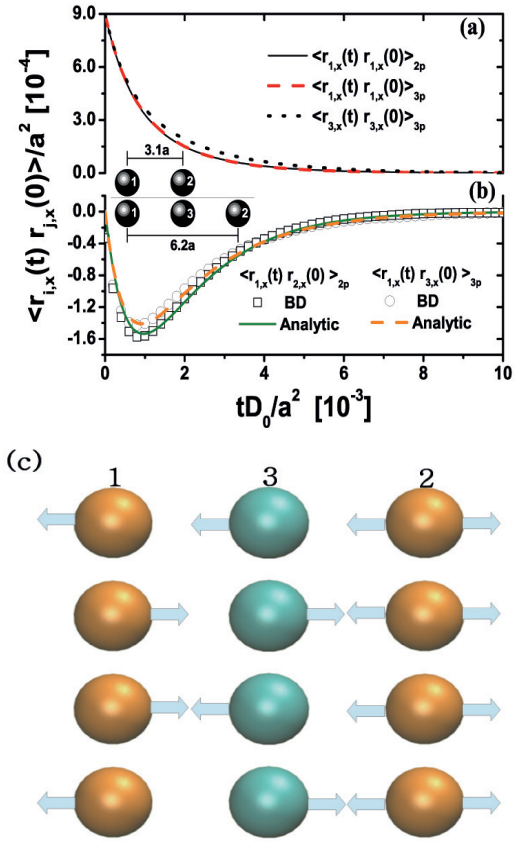

Figure 3.3: **(a)** Auto-correlation functions of the two-particle (solid line) and three-particle (dashed and dotted lines) systems. **(b)** Cross-correlation functions of the two-particle (solid line) and three-particle (dashed line) systems. Lines correspond to the theoretical solution and symbols to BD simulations. Snapshot displays the kind of particle configuration and indicates the distance between particles in both systems. (c) Schematic representation of the coupled motions in the three particle system. For this configuration the system has three dynamical relaxation modes. The superposition of these modes leads to positive contributions to the cross-correlation that dominate at intermediate-times between particles 1 and 2 (see text for the explanation).

tively in coordinated motion the fluid surrounding them is just displaced as a whole. So, the collective mode relax faster than the relative one [57]. Experiments with driven particles exhibit similar dynamical behaviour, where the main properties of the stable synchronised state are determined by the normal mode with the longest relaxation time [74]. On the other hand, although the motion of one particle creates a flow field that instantaneously reaches the neighbouring particle, due to the trapping, the second particle that is receiving the disturbing wave "reacts" only after a finite time. Hence, the correlation evolves on a characteristic time scale, which is related to the natural relaxation time of the harmonic well and is determined by both the trap strength and the friction that the bead experiences [56, 57].

The above explanation is certainly valid for the hydrodynamic coupling of systems composed of two-particles, however, we argue that the same physical picture remains valid for two close neighbouring particles in any three-particle system. For a two-particle system, particle dynamics exhibits two dynamical modes, while in the three-particle collinear array there are eight possible coupled directions of motion (see figure 3.3(c)) that correspond to three dynamical relaxation modes. In this scenario, we have one collective mode where all particles move in the same direction (left or right), and two relative motions: *i)* a pair of adjacent particles, (1,3) or (2,3), moves in the same direction and the other particle 2 (1) moves in the opposite direction, and, *ii)* the middle particle 3 moves in the opposite direction to the collective motion of the outermost particles 1 and 2. Then, the relative motions dominate the dynamics of a pair of close neighbouring particles; also, they relax slower and, as a consequence, the corresponding cross-correlation function exhibits only negative values.

According to the behaviour of C_{13}^{xx} shown in figure 3.3(b), we have deduced that collective modes relax faster than the relative ones, at least for this pair of particles. We infer that the presence of particle 2 only modifies slightly the position and depth of the minimum in the cross-correlation. This means that for particle 1 (or 3), the anti-correlation is not as strong as the negative correlation present in the two-particle system. A more surprising outcome is related with the position of the minimum, which is different than that of the corresponding minimum in the two-particle system. This effect indicates that particle 1 (or 3) reacts in a shorter time. We will return to this point in the next paragraph, but, for now, we claim that the observed behaviour is due to emerging positive correlation effects in the collinear array of particles. Finally, we should point out that the C_{ij}^{xx} between the pairs of particles $(1,3)$, $(3,1)$, $(3,2)$ and $(2,3)$ share the same analytical solution given by (3.15).

We have also found that positive correlation effects in the three particle system are more evident in the C_{12}^{xx}. In figure 3.4(a) we plot the C_{12}^{xx} when the mean separation between particles 1 and 2 is $E_{12} =$

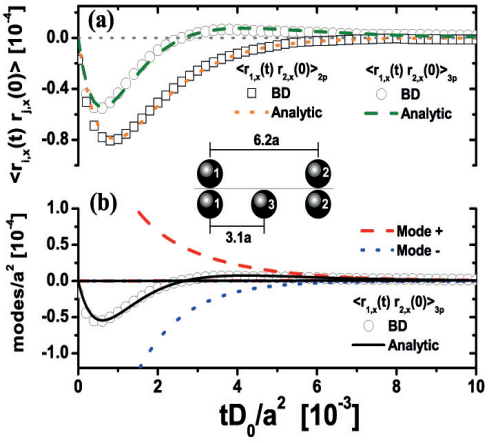

Figure 3.4: **(a)** Cross-correlation functions of the two-particle (dotted line) and the three-particle (dashed line) systems. **(b)** Individual dynamical modes and total cross correlation function (solid line) between particles 1 and 2 in the three-particle system. Dashed and dotted lines denote the positive and negative modes, respectively, given by (3.15). In both figures, symbols correspond to BD simulations and the horizontal dotted line is just a guide to the eye. Snapshot displays the kind of particle configuration and indicates the distance between particles in both systems.

6.2a. For the sake of the discussion, we also plot the cross-correlation of a two-particle system (solid line) at the same separation. As can be observed, there is a very good agreement between the analytical expressions and the BD simulations. From figure 3.4(a) it is clear that the presence of particle 3 affects dramatically the hydrodynamic coupling between the outermost particles. We observe the following interesting features: *i*) the depth of the minimum is smaller, indicating a loss of anti-correlation, *ii*) the position of the minimum has moved to the left, which gives evidence that particle 1 (or 2) reacts in a shorter time than its counterpart in the two-particle system and *iii*) the appearance of a positive maximum at intermediate times that dominates the long-time behaviour of the correlation between particles 1 and 2. We should stress that the last two features do not appear in the two-particle system. Moreover, we might associate the shift of the minimum with the exhibited coordinated motion due to a dragging effect [16]. Then, particles 1 and 2 experience a reduction of the effective friction (drag) due to the presence of 3.

To gain a deeper understanding of the positive hydrodynamic correlation effects between particles 1 and 2 (see snapshot in figure 3.4), we plot separately the different contributions of (3.15) in figure 3.4(b). One can see that at short times the negative mode dominates leading to negative values of the total cross-correlation function, but, at intermediate-times the positive mode becomes the dominant contribution. This means that the collective modes relax slower giving rise

to an unexpected positive hydrodynamic coupling between particles 1 and 2 mediated by the presence of the third one.

A systematic analysis of the position of the time-delayed anti-correlation and the position of the maximum positive correlation as a function of the mean distance between particles is presented in figure 3.5(a). At small particle separations, particle 1 reacts at shorter times, while at large separations the minimum position reaches the value found in the case of the two-particle system. When particle 2 is far away from particle 1, the positive correlation effect disappears, i. e., the amplitude of the maximum goes to zero, although its position moves toward very long-times. Moreover, the full behaviour of C_{12}^{xx} as a function of the particle separation, E, is displayed in figure 3.5(b). The observed decay at different separations corroborates that the positive modes dominate at intermediate-times and they relax slowly in contrast to the negative modes which relax faster. For the sake of completeness, an analogous analysis, as the one presented in 3.5(b), has been performed by means of BD simulations using the Oseen tensor. The simulation results show that the Oseen tensor reproduces the same physical picture as the one provided by the Rotne-Prager tensor, however, it predicts significant differences in the amplitude of both maximum negative and positive cross-correlation in the whole time window (data not shown).

To further understand the unexpected positive cross-correlation mechanisms, we now analyse C_{12}^{xx} in two slightly different scenarios. First, we fix the distance between particle 1 and 2 to $E = 8.4a$ and let the position of particle 3 vary along the line that connects the three particles (see snapshot in figure 3.6(a)). Thus, E_{13} varies from left to right, i. e., from short separations ($E_{13} = 2.2a$) until reaching the middle position ($E = 4.2a$). A second scenario involves the change in the position of particle 3 perpendicular to the line that connects particles 1 and 2 centers (see snapshot in figure 3.6(b)). Interestingly, from the cross-correlations functions depicted in figure 3.6, we can observe that the positive correlation between particle 1 and 2 depends strongly of the relative position of particle 3. For the situation shown in the snapshot of figure 3.6(a), when particle 3 is too close to particle 1 (2), the cross-correlation function shows only negative values (see square symbols for $E_{13} = 2.2$ in figure 3.6(a)). However, when the position of particle 3 is near the half of E_{12} we again see positive values in the cross-correlation function (see dotted line in figure 3.6(a) for $E_{13} = 3.4$). Then, when particle 3 reaches the middle position between particles 1 and 2, the maximum positive correlation is observed. A similar behaviour is seen in the cross-correlation functions for the scenario illustrated in the snapshot of figure 3.6(b). When particle 3 is exactly at the half-separation between particles 1 and 2, the cross-correlation function presents the maximum positive correlation value. However, the positive correlation effects begin to decrease

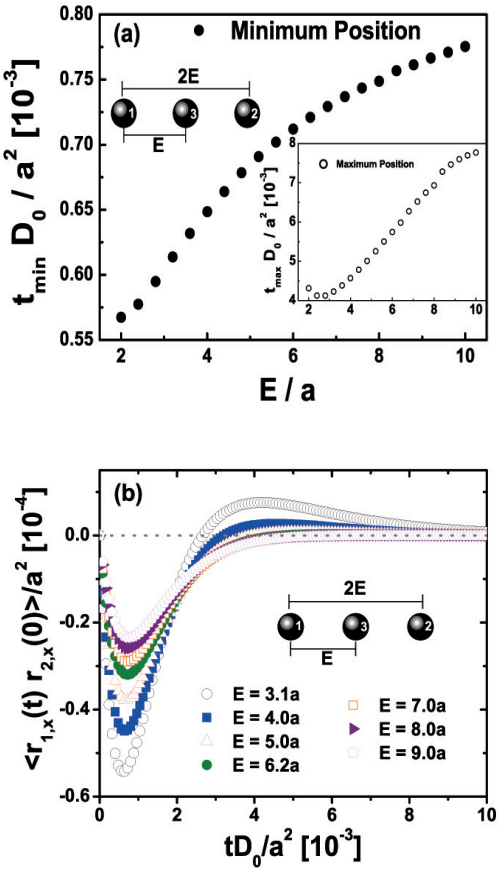

Figure 3.5: **(a)** Minimum position of the cross-correlation function (see (3.15)) between particles 1 and 2 as a function of the mean particle separation for the three-particle collinear array (see figure 3.1(b)). Inset shows the position of maximum positive correlation as a function of the particle separation. **(b)** Cross-correlation function between particles 1 and 2 as a function of time for different inter-particle distance E in the three-particle collinear system. The horizontal dotted line is just a guide to the eye. Snapshot shows the particle configuration and the separation among particles.

when E_y increases, where E_y is the perpendicular distance measured from the horizontal line that connects particles 1 and 2. Thus, increasing E_y results in particle configurations where the cross-correlation function exhibits only negative values (see curves for $E_y \geqslant 1.153$ in figure 3.6(b)). At this point, it is remarkable that the presence of the middle particle not only promote positive correlations, but also its relative position. The observed behaviour greatly supports and encourages the idea of tuning the degree of hydrodynamic correlation between particles by controlling the relative position between them.

The collinear scenario might help to elucidate hydrodynamic correlations in highly confined systems, where it is not uncommon to find small regions with only two or three particles interacting via both direct and indirect forces. However, a natural question that arises is whether similar effects are present in different particle distributions. Recently, it has been enlightened that the analytical diagonalisation of the Oseen matrix is possible in the case of highly symmetric particle configurations; the symmetry of a regular polygon ensures the straightforward evaluation of the two-body correlations [11]. Unfortunately, the analytical procedure for an arbitrary particle configuration rapidly becomes unmanageable. Nonetheless, although it is possible to find an analytic solution for the case of an equilateral triangular configuration, we would like to discuss the hydrodynamic coupling for this configuration within the context of the numerical evaluation of the correlation functions and BD simulations. Thus, in the following, we exploit the advantages of our numerical algorithm and compare its results with BD simulation data. Although in the present Chapter we focus our analysis in colloidal systems composed by only three particles, the inclusion of more particles will elucidate mechanisms of coupled motion that will lead to information about the way in which one is able of controlling the flow field [74]. Numerical and BD preliminary results show that in an hexagonal particle distribution some pairs of particles exhibit the same positive cross-correlation mechanisms as in the collinear array. However, a systematic study on this direction is in progress and will be published elsewhere [70].

3.2.3 *Equilateral triangle configuration*

The effect that a third particle has on the motion of two beads has been recently explored in experiments using driven colloids [74]. Authors of [74] studied the hydrodynamic behaviour of two beads in a condition of no coupling when a third bead is introduced into the system. The two spheres become coupled through the third bead and their synchronisation state is tuned by the position and orientation of the third bead, which acts as a control or "master" bead [74].

We here study the main features of an equilateral triangular configuration. We mainly focus our discussion on the hydrodynamic corre-

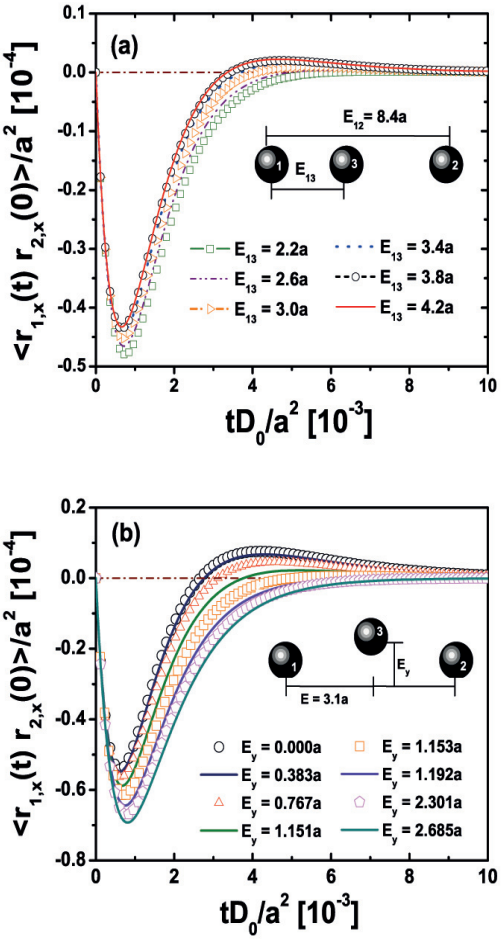

Figure 3.6: Cross-correlation functions between particles 1 and 2 as a function of time for different inter-particle distances in the three-particle collinear system. **(a)** The distance between particles 1 and 3 (E_{13}) is varied, while $E_{12} = 8.4a$ is kept constant. **(b)** The position of particle 3 (E_y), perpendicular to the line that connects particle 1 and 2 is varied, while $E_{12} = 6.2a$ is kept constant. The horizontal line is just a guide to the eye. Snapshot in each figure shows the particle configuration and the separation between particles.

lation functions in the x-direction. However, we briefly examine the behaviour of the correlations in the other directions although the data is not shown.

Figure 3.7(a) shows simultaneously a snapshot of the system when the mean inter-particle separation is $E = 4a$ and the corresponding hydrodynamic correlation functions in the x-direction. In general, we observe a good agreement between simulations and the numerical solution. In this particular configuration, the three particles should feel, on average, the same hydrodynamic force coming from neighbouring particles. From figure 3.7(a) we can observe that the differences between the C_{11}^{xx} and C_{33}^{xx} are practically unnoticeable. However, as can be seen from the inset, the decay of C_{33}^{xx} is slightly faster. This means that the "memory" of particle 3 is lost at shorter times. The fact that C_{33}^{xx} has a slightly faster decay than the corresponding $C_{11}^{xx} = C_{22}^{xx}$ is solely due to the anisotropy of the hydrodynamic interaction; this so-called anisotropy is enforced by the particular selection of the particles distribution. Thus, the C_{11}^{xx} (connecting particles 1 and 2) should be identical with $C_{33}^{\alpha\alpha}$ in the direction connecting particles 3 and 2 (1). In addition, if we compare C_{11}^{xx} in figure 3.7(a) with the C_{11}^{xx} of figure 3.2(a), we can notice that the correlation function for the three-particle system has a slightly different decay than the analogous correlation function in the two-particle system. Taking into account that in both configurations the inter-particle separation is the same ($E = 4a$), the observed difference should be related to the effect of the third body on the auto-correlation functions, which is absent in the two-particle system. Thus, particle 3 induces correlations on the self-motion of particles 1 and 2; a rather similar behaviour was observed in the collinear array.

Let us now focus on the cross-correlation functions displayed in figure 3.7(b). First, we note that C_{12}^{xx} and C_{13}^{xx} ($= C_{23}^{xx}$) show an anti-correlation (negative values) in the whole time window, which means that in both functions the relative modes decay slower than the collective ones and, thus, the slow mode dominates leading to the observed anti-correlation behaviour.

The fact that C_{12}^{xx} exhibits a deeper minimum than the one reported in C_{13}^{xx} is exclusively due to the hydrodynamic anisotropies introduced by the particular choice of the particle distribution. Then, C_{12}^{xx} should be equal to C_{13} in the direction connecting particles $(1, 3)$. According to this picture, the total hydrodynamic force acting on any particle comes from the different flows originated by the neighbouring particles, then, the three particles are physically equivalent.

Concerning the cross-correlation functions in the y-direction (data not shown), we find that C_{ij}^{yy} also exhibits pure negative values in the time window. Besides, in this direction, again due to the selection of the reference frame, we observe that the C_{12}^{yy} has a lower anti-correlation than the $C_{13}^{yy} = C_{23}^{yy}$. In general, the strongest anti-

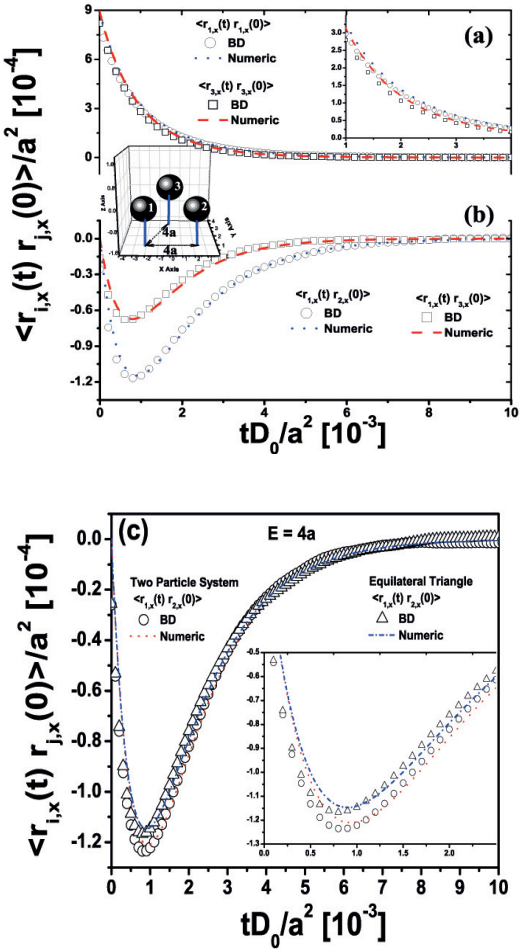

Figure 3.7: **(a)** Auto-correlation functions C_{11}^{xx} and C_{33}^{xx} and **(b)** Cross-correlation functions, C_{12}^{xx} and C_{13}^{xx}, of an equilateral triangle configuration. Inset displays the short time behaviour of the auto-correlation functions. Snapshot shows the inter-particle distance as well as the particle configuration. **(c)** Cross-correlation functions C_{12}^{xx} in the two-particle system and the equilateral triangle configuration when $E_{12} = 4a$. Inset shows their short-time behaviour. In all figures, open symbols denote BD simulations, and dotted and dashed lines the numerical solution of equation (3.2) assuming a constant diffusion tensor.

correlation is observed between particles 1 and 2 along the x-direction, C_{12}^{xx}, and the lowest anti-correlation is between the same pair of particles, but in the y-direction, C_{12}^{yy}.

Figure 3.7(b) shows that in an equilateral configuration the minima of the cross-correlation functions are not located at the same point. A slightly larger time-delay is observed in the reacting time of particles 1 and 2 than the corresponding to particles 1 and 3. A similar effect is observed in the cross-correlation functions in the y-direction, i. e.a larger time-delay is observed for the function with larger anti-correlation (C_{13}^{yy}). In general, we have found that the cross-correlation functions with larger negative values (anti-correlation), C_{12}^{xx} and C_{13}^{yy}, show a larger time-delay compared with the correlation functions with lower negative values, C_{12}^{yy} and C_{13}^{xx}.

In order to elucidate the extent to which the cross-correlation is modified when a third particle is added in the system, in figure 3.7(c) we compare C_{12}^{xx} of the two-particle system (figure 3.2(b)) with the corresponding C_{12}^{xx} in the equilateral configuration (figure 3.7(b)); the separation between particles 1 and 2 is the same in both scenarios. Taking into account the numerical values of these functions, we note that there is a small but still quantifiable difference in the position and depth of the minimum of the correlation functions. From the inset of figure 3.7(c), it is possible to observe that around the minimum, the cross-correlation function for the two-particle system shows slightly larger values in both the reaction time and the anti-correlation than the cross-correlation function in the three-particle system. We argue that the observed "loss" of anti-correlation and the shorter reaction time exhibited in C_{12}^{xx} for the three-particle system proves once again that the presence of the third particle hydrodynamically contributes to the two-body cross-correlation functions. In fact, a similar behaviour is observed in the y-direction, where C_{12}^{yy} for the two-particle system shows a larger anti-correlation than the one in C_{12}^{yy} for the three-particle system (data not shown).

Thus, our results suggest that the presence of particle 3 promotes positive correlation effects in x- and y-directions among particles 1 and 2. This is a relevant and unexpected result since it has been reported that correlations evolve in a characteristic time scale that is only a function of the relaxation time; the latter is only a function of the trap stiffness [57]. Then, the third particle seems to modify the "reacting" time. We could argue that, in analogy to the collinear configuration, the shift to the left in the minimum may be associated to the flow field that induces a kind of dragging effect and allows the particles to experience a smaller "effective" friction.

3.3 CONCLUDING REMARKS

We have studied the hydrodynamic correlation in systems consisting of two and three colloidal particles. They are embedded in a low Reynolds number fluid and interact only through hydrodynamic forces. The correlations were analysed by means of BD simulations, and solving (numerically and analytically) the equations of motion. We have particularly addressed the question of the importance of a third body on the two-body correlation functions for different particle configurations, namely, collinear and triangle particle distributions. To elucidate the relevance of the hydrodynamic tensor, in contrast to previous works [11, 56], we included the HI at the level of the Rotne-Prage diffusion tensor.

We have explicitly shown that a third particle influences the self-motion of the two other particles, as well as the two-body cross-correlation functions, leading to very interesting and non-trivial dynamical phenomena. In particular, we observed the appearance of positive hydrodynamic correlated motion mediated by the presence of a third body. We also found that the type of configuration, the distance between particle centres, and the number of particles play a significant role in the description of the hydrodynamic correlation functions and, therefore, the dynamical modes of the system.

We should remark that in the two- and three-particle systems studied in the present Chapter, we always observed a small discrepancy between the BD simulations and either the numeric or analytic results; the deviations were below the 5%. The differences reported here must be associated with the fact that in the simulations the diffusion tensor is not assumed to be constant, which is the condition we enforced to linearise the set of non-linear equations of motion. Additionally, we must recall that at very small particle separations lubrication forces can dominate the particle dynamics and, in consequence, could have a strong influence on the dynamical modes, however, lubrication forces were not considered in our description.

Similar to recent experiments on driven colloids [74], we found that the dynamical behaviour induced by the presence of the third particle can be used as a novel way to tune the hydrodynamic correlation between particles. According to the relative position of the third particle, the coupled motion of the first two beads may be affected and even positive or negative correlation effects could be promoted. In fact, the presence of more than two particles typically decrease the particle diffusion, but in driven motion, however, the particle mobility can be enhanced by the neighbours. Hence, a full understanding of the previous simple particle distributions (collinear and triangle configurations) might be helpful to create different arrays of particles that promote more complex hydrodynamic correlations, in such way that the net flow field could be efficiently tuned.

The analytical methodology employed in the configurations we studied is hard to extend to more complex particle distributions. As an alternative route, we developed a numerical procedure, which can be used straightforwardly to study the dynamical modes in arrays composed of three or more particles. Our numerical methodology can also be extended to explore other interesting scenarios, e. g., larger collinear arrays of particles or a particle in a cage to gain insight into caging phenomena and elucidate caging mechanisms. Results along such directions will be reported elsewhere.

Last, but not least, we should mention that further theoretical and experimental work is needed to explore the many-body forces on the hydrodynamic coupling in few-particle colloidal systems.

BIBLIOGRAPHY

[1] R. J. Hunter, *Foundations of Colloid Science*, Oxford University Press, Inc., 2nd edn., 2001.

[2] L. F. Rojas-Ochoa, R. Castañeda-Priego, V. Lobaskin, A. Stradner, F. Scheffold and P. Schurtenberger, *Phys. Rev. Lett.*, 2008, **100**, 178304.

[3] C. Haro-Pérez, L. F. Rojas-Ochoa, R. Castañeda-Priego, M. Quesada-Pérez, J. Callejas-Fernández, R. Hidalgo-Alvarez and V. Trappe, *Phys. Rev. Lett.*, 2009, **102**, 018301.

[4] R. Castañeda-Priego, A. Rodríguez-López and J. M. Méndez-Alcaraz, *Phys. Rev. E*, 2006, **73**, 051404.

[5] L. Belloni, *J. Phys.: Cond. Matt.*, 2000, **12**, R549.

[6] C. Likos, *Phys. Rep.*, 2001, **348**, 267.

[7] N. J. Wagner and J. F. Brady, *Physics Today*, 2009, **62**, 27.

[8] A. P. R. Eberle, N. J. Wagner and R. Castañeda-Priego, *Phys. Rev. Lett.*, 2011, **106**, 105704.

[9] A. P. R. Eberle, R. Castañeda-Priego, J. M. Kim and N. J. Wagner., *Langmuir*, 2012, **28**, 1866.

[10] J. K. G. Dhont, *An Introduction to Dynamics of Colloids*, Elsevier, 1996.

[11] G. M. Cicuta, J. Kotar, A. T. Brown, J. H. Noh and P. Cicuta, *Phys. Rev. E*, 2010, **81**, 051403.

[12] P. P. Lele, J. W. Swan, J. F. Brady, N. J. Wagner and E. M. Furst, *Soft Matter*, 2011, **7**, 6844.

[13] T. Franosch, M. Grimm, M. Belushkin, F. M. Mor, G. Foffi, L. Forró and S. Jeney, *Nature*, 2011, **478**, 85.

[14] G. Nägele, *Phys. Rep.*, 1996, **272**, 215.

[15] S. Henderson, S. Mitchell and P. Bartlett, *Phys. Rev. Lett.*, 2002, **88**, 088302.

[16] M. Reichert, *Hydrodynamic Interactions in Colloidal and Biological Systems*, PhD Thesis, 2006.

[17] J. Kotar, M. Leoni, B. Bassetti, M. C. Lagomarsino and P. Cicuta, *Proc. Nat. Acad. Sci.*, 2010, **107**, 7669.

[18] R. Golestanian, J. M. Yeomans and N. Uchida, *Soft Matter*, 2011, **7**, 3074.

[19] L. Damet, G. M. Cicuta, J. Kotar, M. C. Lagomarsino and P. Cicuta, *Soft Matter*, 2012, **8**, 8672.

[20] V. Lobaskin, D. Lobaskin and I. M. Kulic, *Eur. Phys. J. Special Topics*, 2008, **157**, 149.

[21] M. T. Downton and H. Stark, *J. Phys.: Cond. Matt.*, 2009, **21**, 204101.

[22] A. Vifan and H. Stark, *Phys. Rev. Lett.*, 2009, **103**, 199801.

[23] W. Yang, V. R. Misko, K. Nelissen, M. Kong and F. M. Peeters, *Soft Matter*, 2012, **8**, 5175.

[24] G. K. Batchelor, *J. Fluid Mech.*, 1976, **74**, 1.

[25] J. C. Crocker, *J. Chem. Phys.*, 1996, **106**, 2837.

[26] E. R. Dufresne, T. M. Squires, M. P. Brenner and D. G. Grier, *Phys. Rev. Lett.*, 2000, **85**, 3317.

[27] M. D. Carbajal-Tinoco, R. Lopez-Fernandez and J. L. Arauz-Lara, *Phys. Rev. Lett.*, 2007, **99**, 138303.

[28] A. Ashkin, *Proc. Nat. Acad. Sci.*, 1997, **94**, 4853.

[29] D. G. Grier, *Nature*, 2003, **424**, 810.

[30] E. M. Furst, *Curr. Opin. Coll. Surf. Sci.*, 2005, **10**, 79.

[31] A. V. Arzola, K. Volke-Sepúlveda and J. L. Mateos, *Phys. Rev. Lett.*, 2011, **106**, 168104.

[32] C. Bechinger and E. Frey, *Soft Matter, edited by G. Gompper and M. Schick (Wiley-VCH)*, 2007, **3**, 87.

[33] V. Blickle, T. Speck, U. Seifert and C. Bechinger, *Phys. Rev. E*, 2007, **75**, 060101(R).

[34] M. Evstigneev, O. Zvyagolskaya, S. Bleil, R. Eichhorn, C. Bechinger and P. Reimann, *Phys. Rev. E*, 2008, **77**, 041107.

[35] A. V. Arzola, K. Volke-Sepulveda and J. L. Mateos, *Opt. Exp.*, 2009, **17**, 3429.

[36] S. Herrera-Velarde and R. Castañeda-Priego, *J. Phys.: Cond. Matt.*, 2007, **19**, 226215.

[37] S. Herrera-Velarde and R. Castañeda-Priego, *Phys. Rev. E*, 2008, **77**, 041407.

[38] D. V. Tkachenko, V. R. Misko and F. M. Peeters, *Phys. Rev. E*, 2010, **82**, 051102.

[39] C. Coste, J. B. Delfau, C. Even and M. Saint-Jean, *Phys. Rev. E*, 2010, **81**, 051201.

[40] J. B. Delfau, C. Coste, C. Even and M. Saint-Jean, *Phys. Rev. E*, 2010, **82**, 031201.

[41] E. C. Euán-Díaz, V. R. Misko, F. M. Peeters, S. Herrera-Velarde and R. Castañeda-Priego, *Physical Review E*, 2012, **86**, 031123.

[42] J. Mikhael, J. Roth, L. Helden and C. Bechinger, *Nature*, 2008, **454**, 501.

[43] S. E. Shawish, J. Dobnikar and E. Trizac, *Soft Matter*, 2008, **4**, 191.

[44] M. C. Jenkis and S. U. Egelhaaf, *J. Phys.: Cond. Matt.*, 2008, **20**, 404220.

[45] M. Schmiedeberg, J. Mikhael, S. Rausch, J. Roth, L. Helden, C. Bechinger and H. Stark, *Eur. Phys. J. E*, 2010, **32**, 25.

[46] J. Mikhael, M. Schmiedeberg, S. Rausch, J. Roth, H. Stark and C. Bechinger, *Proc. Nat. Acad. Sci.*, 2010, **107**, 7216.

[47] J. Mikhael, G. Gera, T. Bohlein and C. Bechinger, *Soft Matter*, 2011, **7**, 1352.

[48] T. Bohlein, J. Mikhael and C. Bechinger, *Nature Materials*, 2012, **11**, 126.

[49] J. C. N. Carvalho, W. P. Ferreira, G. A. Farias and F. M. Peeters, *Phys. Rev. B*, 2011, **83**, 094109.

[50] S. Herrera-Velarde and R. Castañeda-Priego, *Phys. Rev. E*, 2009, **79**, 041407.

[51] C. Reichhardt and C. J. Olson-Reichhardt, *Proc. of SPIE*, 2009, **7400**, 74000J.

[52] C. Dalle-Ferrier, M. Krüger, R. D. L. Hanes, S. Walta, M. C. Jenkins and S. U. Egelhaaf, *Soft Matter*, 2011, **7**, 2064.

[53] R. D. L. Hanes, C. Dalle-Ferrier, M. Schmiedeberg, M. C. Jenkins and S. U. Egelhaaf, *Soft Matter*, 2012, **8**, 2714.

[54] J. Mewis and N. J. Wagner, *Colloidal Suspension Rheology*, Cambridge University Press, 1st edn., 2012.

[55] S. Henderson, S. Mitchell and P. Bartlett, *Phys. Rev. E*, 2001, **64**, 061403.

[56] J. C. Meiners and S. R. Quake, *Phys. Rev. Lett.*, 1999, **82**, 2211.

[57] M. Reichert and H. Stark, *Phys. Rev. E*, 2004, **69**, 031407.

[58] S. Martin, M. Reichert, H. Stark and T. Gisler, *Phys. Rev. Lett.*, 2006, **97**, 248301.

[59] A. Ziehl, J. Bammert, L. Holzer, C. Wagner and W. Zimmerman, *Phys. Rev. Lett.*, 2009, **103**, 230602.

[60] L. A. Hough and H. D. Ou-Yang, *Phys. Rev. E*, 2002, **65**, 021906.

[61] E. R. Dufresne, T. M. Squires, M. P. Brenner and D. Grier, *Phys. Rev. Lett.*, 2000, **85**, 3317.

[62] J. Bammert, L. Holzer and W. Zimmermann, *Eur. Phys. J. E*, 2010, **33**, 313.

[63] R. M. and S. T., *arXiv preprint arXiv:1203.3441*, 2012.

[64] B. Tränkle, M. Speidel and A. Rohrbach, *Physical Review E*, 2012, **86**, 021401.

[65] M. P. Polin and D. G. Grier, *Phys. Rev. Lett.*, 2006, **96**, 088101.

[66] R. Leonardo, S. Keen, J. Leach, C. D. Saunter, G. Love, G. Ruocco and M. J. Padgett, *Phys. Rev. E*, 2007, **76**, 061402.

[67] G. M. Cicuta, E. Onofri, M. C. Lagomarsino and P. Cicuta, *Phys. Rev. E*, 2012, **85**, 016203.

[68] M. Leoni and T. B. Liverpool, *Phys. Rev. E*, 2012, **85**, 040901.

[69] D. L. Ermak and J. A. McCammon, *J. Chem. Phys.*, 1978, **69**, 1352.

[70] F. Córdoba-Valdés, E. C. Euán-Díaz, S. Herrera-Velarde and R. Castañeda-Priego, *To be submitted*, 2013.

[71] M. P. Allen and D. J. Tildesley, *Computer Simulation of Liquids*, Oxford University Press, 1st edn., 1989.

[72] H. Dong-Hui, Y. Tao and L. Wei-Hua, *Chin. Phys. Soc.*, 2007, **16**, 3138.

[73] B. Dünweg and A. J. C. Ladd, *Adv. Polym. Sci.*, 2009, **221**, 89.

[74] R. Lhermerout, N. Bruot, G. M. C. J. Kotar and P. Cicuta, *New Journal of Physics*, 2012, **14**, 105023.

4

SINGLE-FILE DIFFUSION IN PERIODIC ENERGY LANDSCAPES: THE ROLE OF HYDRODYNAMIC INTERACTIONS

"A thinker sees

his

own

failure are for him answers above all."

– Friedrich Nietzsche

Colloidal suspensions are made of mesoscopic objects, i. e., colloids, that even in the absence of any kind of external perturbation exhibit interesting static and dynamical properties [1]. Furthermore, when the suspension is confined, it shows new features that are not found at the bulk. For instance, in highly restricted geometries, such as q1D and 1D systems, the long-time Mean-Square Displacement (MSD) follows a sub-diffusive non-Fickian behavior, i. e., $W(t) \propto t^{\alpha}$, with $\alpha < 1$ [2–17].

Single-file Diffusion (SFD) is the diffusion of particles in q1D geometries where the particles exhibit random-walk movements in channels so narrow that no mutual passage is possible [18]. Rigorous theoretical results for SFD have been derived in detail for the simple case of hard-rods [19–22]. It was predicted that the $W(t)$, for times much longer that the direct interaction time τ, i. e., the time that a particle needs to move a significant fraction of the mean particle distance is given by the relation [23, 24],

$$\lim_{t \gg \tau} W(t) = F\sqrt{t}, \tag{4.1}$$

where F is the so-called SFD mobility factor. Recently, Kollmann [25] reported a theoretical study on the long-time behavior of SFD that is valid for atomic and colloidal systems as long as the interaction is the same and of finite range. For overdamped systems, i. e., colloidal suspensions, Kollmann also showed that the mobility factor can be expressed as [25],

$$F^{q} = \frac{S(q)}{\rho}\sqrt{\frac{D_c(q)}{\pi}}\Big|_{q<<2\pi/\sigma}, \tag{4.2}$$

where ρ is the number particle density, σ is the particle diameter, and q, $S(q)$ and $D_c(q)$ are the magnitude of the wavevector, the static structure factor, and the short time *collective*-diffusion coefficient, respectively, in q-space [1].

According to Eq. (4.2), the long-time character of SFD is thus determined by the short-time *collective* dynamics at long wavelengths; $q \to 0$. In such a limit, $S(q) \to S(0)$, where $S(0)$ of monodisperse systems corresponds to the normalized isothermal compressibility [1] that can be measured by using either experiments [4] or computer simulations [16]. Furthermore, $D_c(q)$ can be rewritten as $D_c(q) = D_0 H(q)/S(q)$ [1], with D_0 and $H(q)$ as the free-particle diffusion coefficient and the hydrodynamic factor, respectively. Using previous expressions in Eq. (4.2), it reads now as,

$$F^q = \frac{1}{\rho}\sqrt{\frac{D_0 S(q) H(q)}{\pi}}|_{q\to 0}. \tag{4.3}$$

Eqs. (4.1) and (4.3) draw a remarkably simple picture of 1D diffusion at long-times: the self-diffusion process, determined by the width of the self-PDF, is proportional to $t^{1/2}$ and the proportionality constant is determined by the short-time individual particle dynamics, which is a function of the interparticle interactions and density through the $S(q)$ and the hydrodynamic coupling given by $H(q)$. If one assumes that HI can be neglected, i. e., $H(q) = 1$, one finds that the mobility factor reduces to $F^q = \frac{1}{\rho}\sqrt{\frac{D_0 S(0)}{\pi}}$. Lin *et al.* showed that this expression accurately reproduces the mobility factor of hard-rods, F^{HR} [4]. Additionally, using hybrid molecular dynamics and stochastic rotations dynamics computer simulation method, Sané *et al.* corroborated the $\sqrt{t}$-dependence of the MSD of hard-rods and found that the particle mobility factor, with the explicit inclusion of hydrodynamic interactions, is given by F^{HR} [26].

Recent experiments of charged macroscopic particles (millimetric steel balls) confined in circular channels [27] and a linear channel of finite length [28] exhibited a particle diffusion slower than the $t^{1/2}$ behavior. Delfau et al. [28] experimentally identified three different dynamical regimes, which have been recently studied theoretically [29, 30], and found that the particle response to thermal fluctuations strongly depends either on the particle position in the channel or the local potential it experiences. The slower diffusion found in the previous experiments can be explained in terms of the lack of an overdamped dynamics in the system composed of steel particles [31].

During the last decade, the influence of the inter-particle interactions on the SFD of 1D colloidal suspensions has been discussed extensively using experiments, simulations and theory [2–9, 11, 13–17, 26–42]. However, as far as we know, the effects of HI on the SFD have been seldom studied [26]. Furthermore, to the best of our knowledge, numerical simulations for high densities or large potential strengths are

not available for the case in which HI are explicitly included. Thus, a natural question that arises is whether SFD of colloidal systems with different interaction ranges is affected by the HI. This question has been experimentally addressed using 2D colloidal systems composed of superparamagnetic colloidal particles on the air-water interface and exposed to external magnetic fields [43, 44]. Authors reported experimental [43] and computer simulation [44] evidence for an enhancement, due to the HI, of the self-diffusion function, $D_s(t)$, of colloids at intermediate and long times.

Moreover, the action that both external fields and HI exert on colloidal particles results in interesting hydrodynamic behaviors [45–48]. For example, the motion of a colloidal particle in a strong optical trap reveals that at short time-scales resonances in the Brownian motion exists in contrast to overdamped systems [45]. Besides, the influence of external fields in 1D colloidal systems has been studied [14, 15, 37, 49] without taking into account HI or in dilute samples [50], where HI can be simply ignored. In addition, we have to point out that the coupling of external fields with HI gives rise to a rich dynamical scenario that has not been studied in detail yet.

Thus, the main goal of this Chapter is to understand the effects of HI on the SFD of repulsively interacting colloidal particles subjected to spatially periodic energy landscapes. We provide the full dynamical description in terms of the external potential parameters, namely, strength and commensurability. We particularly demonstrate that the mean-square displacement at long-times undergoes a subdiffusive behavior of the form $W(t) = Ft^{\alpha}$, with $\alpha = \frac{1}{2} + \epsilon$, and ϵ being a correction that together with the particle mobility factor, F, are sensitive to the potential parameters and the HI.

After the previous words, the Chapter is organized as follows. In Sec. 4.1 we briefly explain the Brownian dynamics simulation. We also introduce the interaction potentials and the expressions of the physical quantities to be measured during the simulations. In section 4.2 we present a detailed analysis and discussion of our results. Finally, the Chapter ends with a section of concluding remarks shown in section 4.3.

4.1 BROWNIAN DYNAMICS SIMULATION AND INTERACTION POTENTIALS

Diffusion in 1D channels is studied by means of Brownian dynamics (BD) computer simulations. We apply the same simulation methodology described in Refs. [14–16], but, we include now HI by using the Rotne-Prager mobility tensor [51]. We typically consider N particles, $N \approx 400$ with HI and $N \approx 1000$ without HI. Particles move in a line of length L, which is linked to the number particle density according to the expression $\rho = N/L$; L has to be chosen to guarantee the conti-

nuity of the external potential on the borders of the line, this point is discussed further below. Since particles are restricted to diffuse on the line, we only use periodic boundary conditions in the x-direction in order to simulate an infinite system. The packing fraction is $\varphi = \sigma\rho$ and the mean particle distance is defined as $d \equiv \rho^{-1}$ [14–16].

The time step used in the BD simulations is $\Delta t = 2 \times 10^{-4} \, (\rho^2 D_0)^{-1}$, with $D_0 = \frac{k_B T}{6\pi\eta a}$ the free-particle diffusion coefficient of particles of radius a immersed in a solvent of viscosity η, k_B the Boltzmann constant and T the absolute temperature. The maximum time window reached in the simulations is $t_{max} = 500\,(\rho^2 D_0)^{-1}$, i. e., 2.5×10^6 time steps. To facilitate the analysis and reduce the set of parameters in our study, we use the following scaling factors: d for the distance; d^2/D_0 for the time; and $k_B T$ for the energy.

4.1.1 *Brownian dynamics*

We now point out some details of the Brownian dynamics: i) the mesoscopic size of the colloids ($\sigma \sim$ some nanometers to few micrometers) ensures the validity of Langevin dynamics [51]. Solvent molecules are treated as variables having *fast* dynamics and they are integrated out in the dynamics of colloids, whereas the latter ones follow a *slow* dynamics and are treated explicitly; ii) we assume *local thermodynamic equilibrium*, i. e., particle velocities obey fast dynamics which implies that the memory of velocities is lost much faster than the time scales of interest. We are thus interested in time scales longer than the momentum relaxation time, $t >> \tau_m = \frac{m}{6\pi\eta a}$; this is known as the diffusive temporal regime [52] with m being the mass of the colloid.

We express the discrete position Langevin equation for particle i as [52],

$$\begin{aligned} \mathbf{r}_i(t+\Delta t) = \; & \mathbf{r}_i(t) + \{\beta \sum_{j=1}^{N} \mathbf{D}_{ij} \cdot [-\nabla_{\mathbf{r}_j} U(\mathbf{r}^{\{N\}}) + \mathbf{F}_j^{ext}] \\ & + \sum_{j=1}^{N} \nabla_{\mathbf{r}_j} \cdot \mathbf{D}_{ij}\}\Delta t + \xi_i(t), \end{aligned} \tag{4.4}$$

which gives us the new position of particle i at time $t + \Delta t$. Eq. (4.4) depends on the particle position at a previous time, $\mathbf{r}_i(t)$, the net force acting on the particle and the stochastic force due to the collisions with the solvent molecules. The net force on particle i has two contributions: the force due to the particle-particle interaction; U is the total pair potential energy, and its coupling with the external-field, $\mathbf{F}_i^{ext}$. HI are also included through the Rotner-Prager mobility tensor [51, 52],

$$\begin{aligned} \mathbf{D}_{ii} &= D_0 \mathbf{I} = \tfrac{k_B T}{6\pi\eta a}\mathbf{I}, \\ \mathbf{D}_{ij} &= \left(\tfrac{k_B T}{8\pi\eta r_{ij}}\right)\left(\mathbf{I} + \tfrac{\mathbf{r}\otimes\mathbf{r}}{r_{ij}^2}\right) + k_B T \left(a^2/4\pi\eta r_{ij}^3\right)\left(\tfrac{\mathbf{I}}{3} - \tfrac{\mathbf{r}\otimes\mathbf{r}}{r_{ij}^2}\right), \end{aligned} \tag{4.5}$$

where $\mathbf{I}$ is a 3×3 unit matrix (in the 3D case) and the symbol $\otimes$ denotes a dyadic product. One notes that this mobility tensor includes the lowest corrections of particle size over the Oseen tensor description [51], and corresponds to the case of an unbounded fluid. One thus should keep in mind that our treatment of HI is only approximate for particles which are separated by a distance on the order of a. One notes that the mobility tensor introduces long-range interactions and couples distant particles. Eq. (4.4) reduces to the standard Langevin equation without HI when $\mathbf{D}_{ij} \to D_0\mathbf{I}$ [14–16].

The stochastic term, $\xi(t)$, mimics the action of a thermal heat bath and obeys the fluctuation-dissipation relation [51],

$$\langle \xi_i(\Delta t)\xi_j(\Delta t)\rangle = 2\mathbf{D}_{ij}\Delta t, \tag{4.6}$$

which is numerically implemented by a Cholesky decomposition [52, 53]. We deal with the dynamics of non-deformable particles in an unbounded fluid. One can then check that $\nabla_{\mathbf{r}_j} \cdot \mathbf{D}_{ij} = 0$ for the Rotner-Prager mobility tensor. This is different when we deal with a non-slip surface, where this term is non-zero and therefore should be taken into account explicitly [51, 52].

4.1.2 *Pair distribution function and mean-square displacement*

To obtain structural information of the particle ordering along the channel, we calculate the pair distribution function, $g(x)$. The function $g(x)$ is the probability of finding a particle at a distance x from a particle located at the origin. It can be measurable in both experiments and computer simulations according to the definition [14–16],

$$g(x) = \frac{1}{N\rho}\langle \sum_{i=1}^{N-1}\sum_{j>i}^{N} \delta(x - x_{ij})\rangle, \tag{4.7}$$

where the angular brackets $\langle \cdots \rangle$ denote a statistical (temporal or ensemble) average.

The mean-square displacement is computed by using the expression [14–16],

$$W_x(t) = \langle \Delta x(t)^2\rangle = \frac{1}{N}\sum_{i=1}^{N}\langle [x_i(t) - x_i(0)]^2\rangle. \tag{4.8}$$

As we will see further below, at short-times the MSD behaves as $W_x(t) \propto t$, i. e., normal diffusion, whereas at long-times it shows a much slower power-law dependence. Then, for the sake of the discussion, at long-times we fit our simulation data according to the relation,

$$W_x(t) = Ft^{\alpha}. \tag{4.9}$$

Thus, all the effects associated to the HI can be described in terms of α and the particle mobility factor F.

During our simulations, the averages are taken over at least ten different independent stochastic realizations to reduce the statistical uncertainties. Error bars in the plots are smaller than the symbol size. For the MSD , the associated errors are statistical significant only at reduced times $tD_0/d^2 > 350$, but still, there is a clear separation between the MSD curves and no overlap between error bars is observed during the time window used in this Chapter.

4.1.3 *Interaction potentials*

We consider a system of charged colloidal particles with radius a interacting *via* a repulsive screened-Coulomb potential. For distances $r < \sigma = 2a$, the interaction is hard-core, but for $r > \sigma$, two colloidal particles separated by a distance r interact *via* the repulsive part of the Derjaguin-Landau-Verwey-Overbeek (DLVO) pair potential [14, 16, 54, 55],

$$\beta u(r) = Z_{eff}^2 \lambda_B \left[\frac{e^{\kappa a}}{1+\kappa a}\right]^2 \frac{e^{-\kappa r}}{r}, \tag{4.10}$$

where $\beta \equiv (k_B T)^{-1}$ is the inverse of the thermal energy, Z_{eff} is the effective charge, $\lambda_B = e^2/4\pi\epsilon k_B T$ is the Bjerrum length (in international units) [56], with e the proton charge and ϵ the solvent dielectric permittivity, and κ is the Debye screening parameter [54, 55]. We have used the same set of parameters as those in Ref. [14]. In our study, the packing fraction, $\varphi = \sigma\rho$, is a control parameter for Yukawa systems.

Additionally, paramagnetic colloids have served as excellent models to investigate fundamental properties that are related to the role of hydrodynamics, melting transitions, order-disordered transitions and the elastic behavior in two-dimensional crystals [44, 57]. In the experiments, an external and constant magnetic field is applied in the perpendicular direction of the air-water interface [43]. This leads to a tunable quasi long-range magnetic dipole-dipole interaction between colloids. Such an interaction can be described by the potential [44, 57],

$$\beta u(r) = \frac{\Gamma}{r^3}, \tag{4.11}$$

where r is the reduced separation (in units of the mean particle distance) between two colloids and $\Gamma \equiv \beta(\frac{\mu_0}{4\pi})\chi_{eff}^2 B^2 d^{-3}$ is the mean interaction energy in units of the thermal energy, μ_0 is the vacuum susceptibility, B is the applied magnetic field, and χ_{eff} is the magnetic susceptibility of the particles. For paramagnetic colloids the potential strength, Γ, is the relevant parameter to be varied, which is equivalent to changing the particle number density because an increase in Γ results in an increase of collision rates between particles [12, 44, 57].

Among important experimental tools that help us to understand complex fluids are optical traps created by the interference of two laser beams [58]. In experiments, the interaction between laser beams

and the colloids induces potentials with an incredibly precision which permits one to create precise and strong confinement and, as a consequence, a reliable control of the colloidal motion [59, 60]. In the last years, optical traps have also been implemented in colloidal systems to induce an optical substrate [61], i. e., periodic or random energy landscape. Its effect on the dynamics and the structure turned out to be fascinating [62, 63].

The total external energy can then be written as $U^{ext} = \sum_{i=1}^{N} u^{ext}(\mathbf{r}_i)$, where $u^{ext}(\mathbf{r}_i)$ is the external potential, usually referred as the substrate, acting on particle i, which here is given by the expression [14, 15, 63],

$$u^{ext}(\mathbf{r}_i) = V_0 \sin\left(\frac{2\pi x_i}{a_L}\right), \tag{4.12}$$

where V_0 is the amplitude or strength of the external potential and a_L its periodicity. Now, it is appropriate to define the commensurability factor as [14, 15]

$$p \equiv \frac{d}{a_L} = \frac{N}{n_{a_L}}, \tag{4.13}$$

where n_{a_L} is the number of sinusoidal potential periods within the channel of length L. The commensurability factor is an important control parameter in our further analysis. In our simulations, L is also chosen to guarantee the continuity of the external potential on the borders of the channel.

Thus, a systematic variation of all parameters allows us to investigate the diffusive behavior of particles along the channel. We have performed a detailed analysis and here present only representative results.

4.2 RESULTS AND DISCUSSIONS

Our results cover a wide range of homogeneous and heterogeneous systems, which are characterized by the set of parameters displayed in Fig. 4.1. The formers are represented by a commensurability factor $p = 0$ and the later ones are explicitly described in the inset with $\varphi = 0.43$ for charged colloids and $\Gamma = 4.67$ for superparamagnetic particles.

4.2.1 *Homogeneous systems;* $V_0 = 0$

It is well-known that, in the absence of external fields, the static properties of any complex fluid do not depend explicitly on the HI. This simply means that in homogeneous systems the HI effects always average to zero. This provides us a benchmark to test the Brownian dynamics methods that explicitly include HI. We then test the reliability of our simulation method by looking at the structure of the

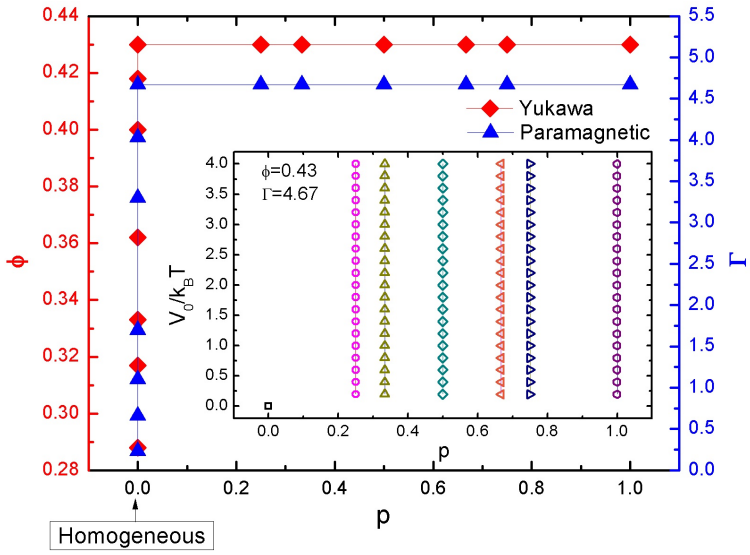

Figure 4.1: (Color online) Parameters space used in the present Chapter. The homogeneous cases correspond to $p = 0$. The heterogeneous cases are those with $p \neq 0$. Inset shows the values of the substrate strength, V_0, for each value of the commensurability factor, p.

colloids along the channel. In Fig. 4.2 we show the pair distribution functions, $g(x)$, of both Yukawa and superparamagnetic particles. We explicitly provide results with and without HI and for different particle densities (low and high) and potential parameters (weak and strong couplings). We observe that the $g(x)$ exhibits the typical behavior found in homogeneous fluids and recently discussed in Ref. [16]. More important is the fact that the $g(x)$ does not depend on the HI. This confirms that even in 1D fluids the HI do not affect the equilibrium structure. It also guarantees that our Brownian dynamics method with the HI at the level of the Rotner-Prager mobility tensor is correctly implemented.

We turn now to the mean-square displacement. We first study the case reported by Sané *et al.*, where a very short-range Weeks-Chandler-Andersen potential is used to mimic the properties of a hard-rod system [26]. Our simulation results are in good agreement with those predicted by the authors [26] (data not shown), although we do not consider the influence of walls, and find that the MSD at long-times is given by Eq. (4.1) and the mobility factor is completely described by F^{HR} [26]. Thus, we might conclude that for overdamped systems with hard-core-like interactions, SFD is accurately determined by the theoretical approximation proposed by Kollmann [4, 25].

The MSD of the systems above discussed are displayed in Fig. 4.3. The physical behavior of the MSD , without HI, has also been studied in detail in Ref. [16], where it is shown that Eq. (4.1) describes the long-time behavior of the particle diffusion along the channel

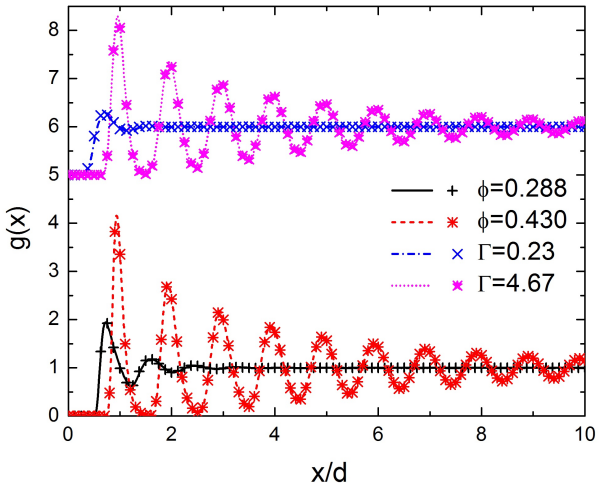

Figure 4.2: (Color online) Pair distribution functions of 1D colloidal homogeneous systems. Curves are shifted for clarity. The upper curves represent the superparamagnetic particles, whereas the lower curves the charged (Yukawa) colloids. Results with HI are indicated with symbols and without HI with lines.

and the mobility factor depends on the particle-particle interaction (see also Eq. (4.2)) until it reaches almost the same value at high-densities (Yukawa) or strong couplings (superparamagnetic). However, we also plot those cases obtained with the explicit inclusion of HI, which were not considered in Ref. [16]. We interestingly observe that for the time window indicated as "the region of interest", i. e., long-times, the MSD's with HI are larger than the MSD's in the absence of the HI. The reason of this behavior can be understood in terms of the long-range hydrodynamic coupling between particles, see, e. g., Refs. [43, 44]. This coupling also enhances the diffusion due to the *collective diffusion* induced and mediated by the HI. Collective diffusion is a dynamic process related with the cooperative movements of many particles that lead and promote a collective and faster diffusion of the particles in the file. We should note, interestingly, that a similar collective diffusion is observed at long times in finite-size systems i. e., circular channels, composed of particles interacting with long-range potentials and where the HI are not present [17, 37].

To better understand the effects of the HI on the diffusion of the particles along the file, we also compute the exponent α and the mobility factor F, where the MSD can be approximated, with high accuracy, by the power-law relation given by Eq. (4.9). Both parameters are depicted in Fig. 4.4. In general, we find that the values of the parameters predicted with the inclusion of HI are larger than those where HI are disregarded, but they behave in a similar way. In particular, α is 0.5 for the case without HI, in excellent agreement with the theoretical

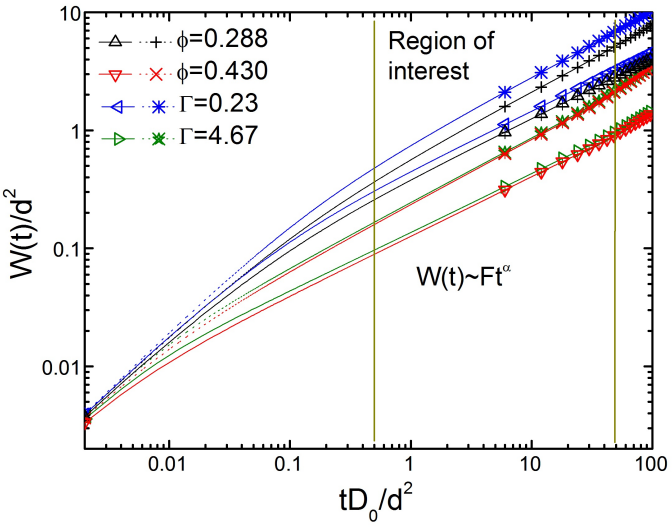

Figure 4.3: (Color online) Mean-square displacements of 1D colloidal homogeneous systems; Yukawa particles and superparamagnetic colloids. Results with HI are indicated with stars and without HI with triables. The time window where the dynamic factors, α and F, are calculated, is indicated between vertical lines.

predictions of Kollmann [25] (see Eq. (4.1)), and it takes the value of 0.56 with HI and independently of the interaction potential between particles; the inclusion of HI results in an increase of around 12% in α, which means a faster, but still, subdiffusive behavior. We also find that F decreases (in an exponential-like fashion) with increasing either the density (Yukawa) or the inter-particle coupling (superparamagnetic). This phenomenon is explained in Ref. [16] as follows: as the density (or potential strength) is increased, the colloids are more localized and just oscillate around their equilibrium positions; at this point, the highly packed fluid consists of a quasi-regularly spaced sequence of particles where the relative distance is represented to within a few percent by $1/\rho$.

4.2.2 *Heterogeneous systems;* $V_0 \neq 0$

1D colloidal systems under periodic energy landscapes have shown interesting structural and dynamic properties. For example, it is observed that the competition between both particle-particle and particle-field interactions gives rise to a rich variety of adsorbate phases [14]. It has also been demonstrated that the action of the external field leads to very interesting phenomena, such as the localization of the particles and, in special conditions, to depinning-like effects, which are observed in an enhancement of the mobility factor and a loss of spatial correlation along the file [14, 15]. Thus, the study of the par-

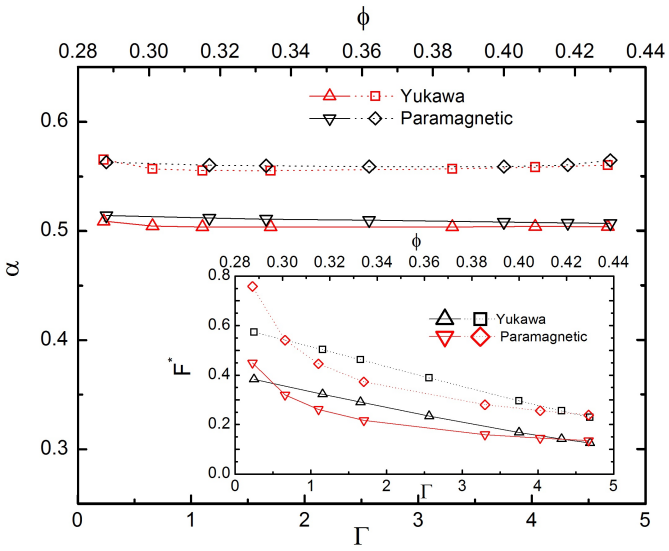

Figure 4.4: (Color online) Dynamic factors, α and F, of 1D colloidal homogeneous systems as a function of the density (Yukawa particles) and coupling strengths (superparamagnetic colloids). Results with HI are indicated with squares and without HI with triangles. They are obtained by fitting the mean-square displacement with Eq. (4.9). The lines are guides to the eye.

ticle diffusion in energy landscapes turns out to be fascinating and, even more, complex when HI are taken into account explicitly.

Before we discuss in detail our results, we should point out that in previous works S. Herrera-Velarde and R. Castañeda-Priego studied the MSD for $p \gtrsim 1$ and found that its long-time behavior follows the power-law given by Eq. (4.1). Hence, in the present section we explore the influence of the external sinusoidal potential (see Eq. (4.12)) in an extended regime of commensurabilities, i. e., $0 < p \leqslant 1$, and its consequences on the dynamical properties of particles moving in periodic energy landscapes. The potential parameters are displayed in Fig. 4.1.

Yukawa particles

For the sake of the discussion and for illustrative purposes, we show in Fig. 4.5 the equilibrium positions of the Yukawa particles along the file. The energy landscape imposed by the external field is depicted by the sinusoidal curves that are shifted in the vertical direction for clarity. One can notice the variation of the number of particles per potential minima is dictated by the commensurability factor p. Regarding the structure, we do not observe considerable differences when HI are explicitly included (data not shown). Thus, from now on, we focus our attention on the dynamical properties.

We start analyzing the behavior of α, which is displayed in Fig. 4.6. Upper figure shows the cases $p \leqslant 1/2$ and the lower one $1/2 < p \leqslant 1$.

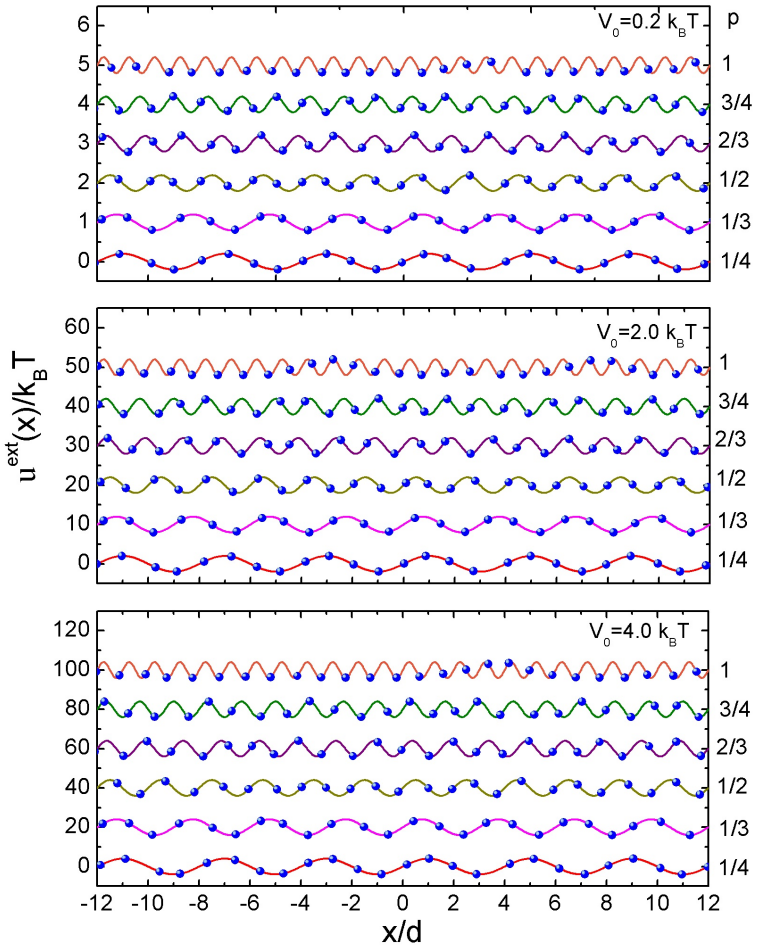

Figure 4.5: (Color online) Blue dots: Equilibrium positions of Yukawa particles along the file for different values of the commensurability factor $p(= 1/4, 1/3, 1/2, 2/3, 3/4, 1)$. Three values of the external coupling strength, V_0, are displayed. Solid lines: Sinusoidal contribution of the external potential (see equation (4.12)). Curves are shifted in the vertical direction for clarity. The packing fraction is $\varphi = 0.43$ and the parameters of the external field are indicated in the inset of Fig. 4.1.

In the former cases, we observe that, except for $p = 1/2$, $\alpha = 0.5$ and $\alpha \approx 0.6$ without and with HI, respectively. This behavior is independent of the coupling parameter V_0. This means that the particles experience faster diffusion due to their hydrodynamical coupling with the external potential. However, for $p = 1/2$ particles will diffuse slower for $V_0 \gtrsim 1.8 k_B T$, even without considering HI explicitly; this slow decay should be associated with the distribution of particle along the sinusoidal field. This point will be discussed in more detail below.

For $p > 1/2$ (see Fig. 4.6(b)) the following interesting features are noticed: *i*) for $p = 2/3$ and $p = 3/4$ diffusive behavior occurs with the characteristic exponent $\alpha = 0.5$, i. e., normal SFD, when HI are neglected, however, with the inclusion of HI the diffusive behavior is $\alpha \approx 0.6$, but it decreases with V_0 reaching a saturation value of $\alpha \approx 0.55$ for $p = 2/3$ and $\alpha \approx 0.5$ for $p = 3/4$. The latter is in good agreement with Ref. [14] where the commensurability factor $p \approx 0.82$ was investigated. *ii*) $p = 1$ exhibits a non-monotonic behavior with a minimum located at $V_0 \approx 0.4 k_B T$. After this point, the diffusion becomes faster until it reaches a plateau of around $\alpha \approx 0.55$. However, contrary to the other previous cases, the inclusion of HI lead to a complete unexpected slower diffusion when $V_0 \gtrsim 0.6 k_B T$. This behavior is explained below.

So far we have found that, except for $p = 1$, HI promote a faster particle diffusion as compared with the case without HI, but the exponent α depends on the coupling with the external potential. Then, to understand the dynamical scenario discussed above, we now use simple physical arguments to better appreciate the competition between the particle-particle potential and the accommodation of the particles on the potential minima along the file. The way in which particles are accommodated in the channel depends on the particular choice of p. For example, the difference between $p = 1/4$ and $p = 3/4$ resides in the fact that for the former there are 4 particles per potential minimum, and for the latter 4 particles are distributed over 3 potential minima. This can be best seen in Fig. 4.5.

Then, for $p = 1/2$ both F and α show a decay starting at around $V_0/k_B T = 2.0$. This case corresponds to two particles per minimum. Thus, from an energetic point of view, the pair of particles is competing for their localization at the minimum (see Fig. 4.5 for $p = 1/2$), but due to their repulsive interaction (see Eq. (4.10)), they will never be in contact and, as a consequence, they cannot be located at the minimum. However, the pair behaves like an effective *dimer* whose center of mass is, on average, at the position of the potential minimum. When $V_0 (< 2 k_B T)$ is small, due to thermal fluctuations, the *dimers* overcome the well depth and also the energetic barrier induced by the surrounding *dimers*, i. e., weak localization. Thus, normal SFD is found without including HI and $\alpha = 0.6$ with HI. For larger $V_0 (> 2 k_B T)$, the *dimers* turn out to be more strongly localized around the minimum with

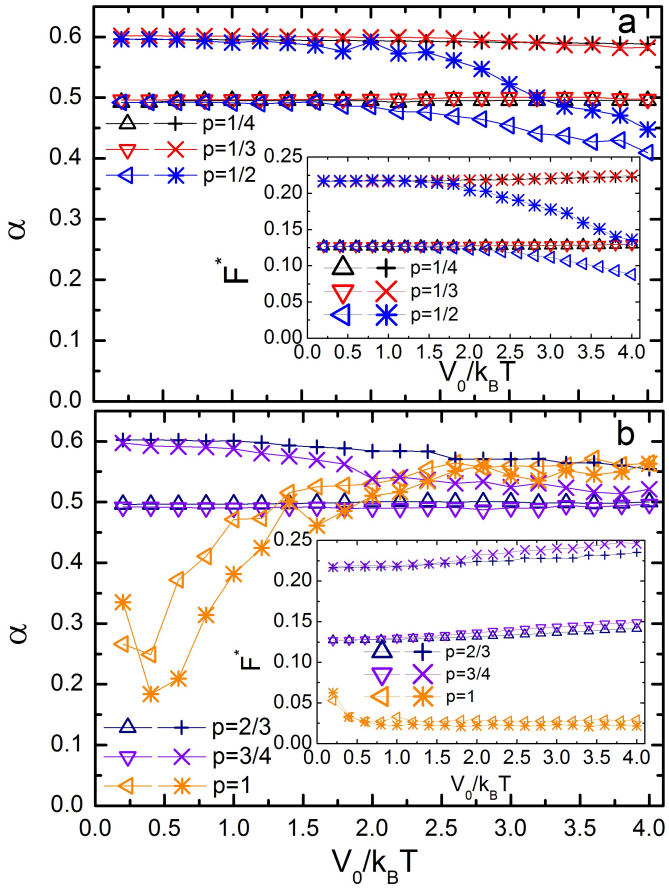

Figure 4.6: Dynamic factors, α and F, that characterize the diffusion of Yukawa particles as a function of the coupling strength, V_0, for different commensurability scenarios. The packing fraction is $\phi = 0.43$. We show results with (stars) and without (open triangles) HI. The lines are guides to the eye.

each particle of the effective *dimer* trying to occupy the potential minimum. This competition makes the collective diffusion harder and the diffusion of the entire file becomes slower even in the presence of hydrodynamical coupling.

In contrast to $p = 1/2$, the dynamical behavior for the case $p = 1$ is more complex and less intuitive. First of all, this case corresponds to one particle per minimum (see Fig. 4.5 for $p = 1$). Our results reveal three different dynamical regimes: 1) very weak coupling ($V_0 < 0.6 k_B T$); shows a decrease in the diffusion, 2) weak coupling ($0.6 k_B T \lesssim V_0 \lesssim 1.6 k_B T$); exhibits an increase in the diffusion, and 3) strong coupling ($V_0 > 1.6 k_B T$); almost normal SFD is observed. The latter regime is consistent with the results presented in Ref. [14]. In all the regimes, the diffusion is sub-diffusive, i. e., $\alpha < 1$. However, it is important to stress that for very weak couplings, as expected, HI describe a faster diffusion than in the situation without HI; in the limit $V_0 << k_B T$, the value 0.6 is recovered (data not shown). Nonetheless, at weak and strong couplings the opposite scenario is found: hydrodynamical coupling among particles leads to a slower diffusion. This behavior is completely unexpected, since for the other commensurability factors HI promoted a faster diffusion. Thus, in these regimes HI give rise to an *anti-cooperative* dynamics, which can be associated with a possible increase of the energy dissipation due to friction with the solvent. Moreover, for $p = 1$ every colloid could be, on average, located at the potential minimum. When this condition is satisfied, a collective dynamics along the file emerges and the diffusion is given by the normal SFD; this scenario is observed at strong couplings, where the external field enforces the particles to occupy the potential minima. This is the same mechanism that allows us to observe the exponential decay of the corresponding reduced mobility factor displayed in the inset of Fig. 4.6 [16]. Unfortunately, the complexity of the dynamics at weak couplings cannot be entirely explained in terms of the competition to occupy the potential minimum of the external field.

To visualize in a better way the non-monotonic dependence of the particle dynamics for $p = 1$, we show in Fig. 4.7 the mean-square displacement for different values of V_0, which are chosen according to the dynamical regimes discussed above. At short-times, the diffusion is normal and independent of both the inter-particle interaction and the external potential. At intermediate times the dynamics becomes sub-diffusive (in all cases) with an almost well-defined plateau, which indicates that the particle spends a considerable time on the potential minimum. However, the long-time behavior shows an unexpected non-monotonic variation that strongly depends on the external potential strength V_0. This is the evidence of the non-trivial and complex competition between the particle-particle and the particle-substrate interactions that leads to the dynamical factors displayed in Fig. 4.6.

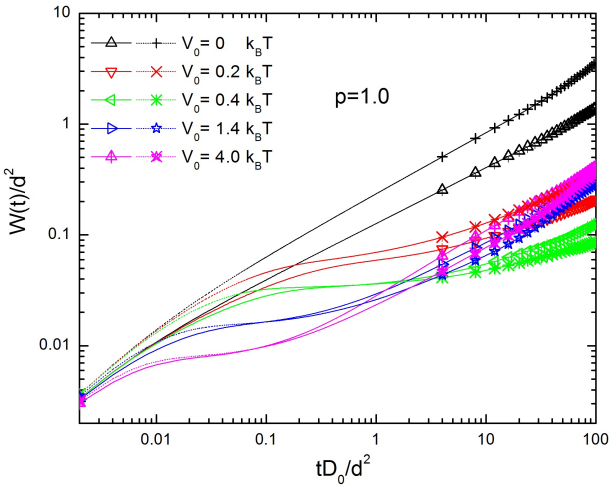

Figure 4.7: (Color online) Mean-square displacements of 1D Yukawa particles on a sinusoidal potential given by Eq. (4.12) with a commensurability factor $p = 1$ and different values of the external potential strength V_0. Results with HI are indicated with stars and without HI with triangles.

The behavior of the reduced mobility factor, F^*, is also depicted in Fig. 4.6. The mobilities calculated with inclusion of the HI for $p \neq 1$ are larger than those obtained without them, as in the homogeneous case. Thus, HI allow a faster motion and strong dynamic couplings that lead to collective motions that result in an enhancement of particle mobility. For $p = 1/4,\ 1/3,\ 2/3$, and $3/4$ (see Fig. 4.5), F shows a slow increase with V_0, being more noticeable when $p = 3/4$. The latter effect has been investigated in Ref. [14]. The increase of the mobility factor, even larger than the homogeneous case, see inset of Fig. 4.4, is due to the noise-assisted effect, in which thermal fluctuations act cooperatively leading to higher particle mobility [14]. The enhancement of F also reveals a depining of the file from its sinusoidal substrate. Then, the HI contribute to this noise-assisted effect due to the fact that they promote the diffusion of the particles and give the opportunity to the particles to be less pinned to the external field.

Paramagnetic colloids

In order to answer the question whether the previous dynamical scenario depends on the kind of interaction potential, we turn now to the case of superparamagnetic colloids, where particles interact with a long-range potential given by Eq. (4.11). In the following paragraphs we will focus on the similarities and differences among the dynamical properties exhibited by both superparamagnetic and Yukawa particles. We should mention that in previous Yukawa many-particle

system, the screening parameter κ was chosen in the intermediate range such that nearest neighbor particles are correlated but the interparticle interaction is completely screened for larger distances.

Due to the strong repulsion, the paramagnetic colloids show similar particle configurations along the file as the Yukawa particles, see Fig. 4.8. In this case, we consider that the long-time behavior of the MSD scales as $\propto t^{\alpha}$ and can be fitted according to Eq. (4.9). The external potential parameters are depicted in Fig. 4.1 and the corresponding dynamic factors, α and F, are displayed in Fig. 4.9.

For $p < 1/2$ we find that α is independent of the nature of the repulsive interaction potential among the particles and the inclusion of HI promotes a faster diffusion. For $1/2 < p < 1$ we observe that α decays slowly when $V_0 \gtrsim 1.0 k_B T$; it decreases reaching a saturation value of $\alpha \approx 0.54$ for $p = 2/3$ and $\alpha \approx 0.52$ for $p = 3/4$. The latter is in good agreement with Ref. [15] for $p \approx 0.82$. In the particular case $p = 1/2$, it decays at smaller values of V_0 and its magnitude is also smaller than the one obtained for Yukawa particles. This means that the dynamics of superparamagnetic particles is slightly slower. This can also be associated with the accommodation of the particles on the potential minima. From Fig. 4.8, we still see the effective *dimers* around some minima, however, we can also appreciate that some particles are located on the maxima (in this case the probability is higher) due to the stronger repulsion at short-distances and the long-range spatial correlation between particles. This increases the contribution of the interparticle potential to the particle distribution along the sinusoidal substrate. In fact, we can argue that particles find meta-stable equilibrium positions that are not frequently observed when the interaction potential is of short-range and as a consequence making it more difficult the collective diffusion in the channel.

For $p = 1$ we have similar dynamical regimes: 1) very weak coupling ($V_0 < 0.4 k_B T$); shows a decrease in the diffusion, 2) weak coupling ($0.4 k_B T \lesssim V_0 \lesssim 2.0 k_B T$); exhibits an increase in the diffusion, 3) strong coupling ($V_0 > 2.0 k_B T$). The transition from weak to strong coupling is located at larger $V_0 (> 2 k_B T)$ than the Yukawa particles. Interestingly, this strong coupling dynamical region seems to be, in both cases, almost independent of the HI and the kind of interaction between particles ($\alpha \approx 0.55$).

Insets of Fig. 4.9 show the behavior of F for the different values of p and V_0. Specifically for $p < 1/2$ and $1/2 < p < 1$ there is an increase in the mobility factor, being more dramatic for $V_0/k_B T \geqslant 2.0$ and similar to the Yukawa particles. For $p = 1/2$, the decrement of the mobility factor for $V_0/k_B T \geqslant 2.0$ is larger than the decay of F shown by the Yukawa particles (see inset of Fig. 4.9(a)). Thus, superparamagnetic colloids exhibit a stronger *non-cooperative* behavior than the Yukawa particles. Moreover, as in the case of the Yukawa particles, for $p = 1$ we find that F decays exponentially (see inset of Fig. 4.9(b)).

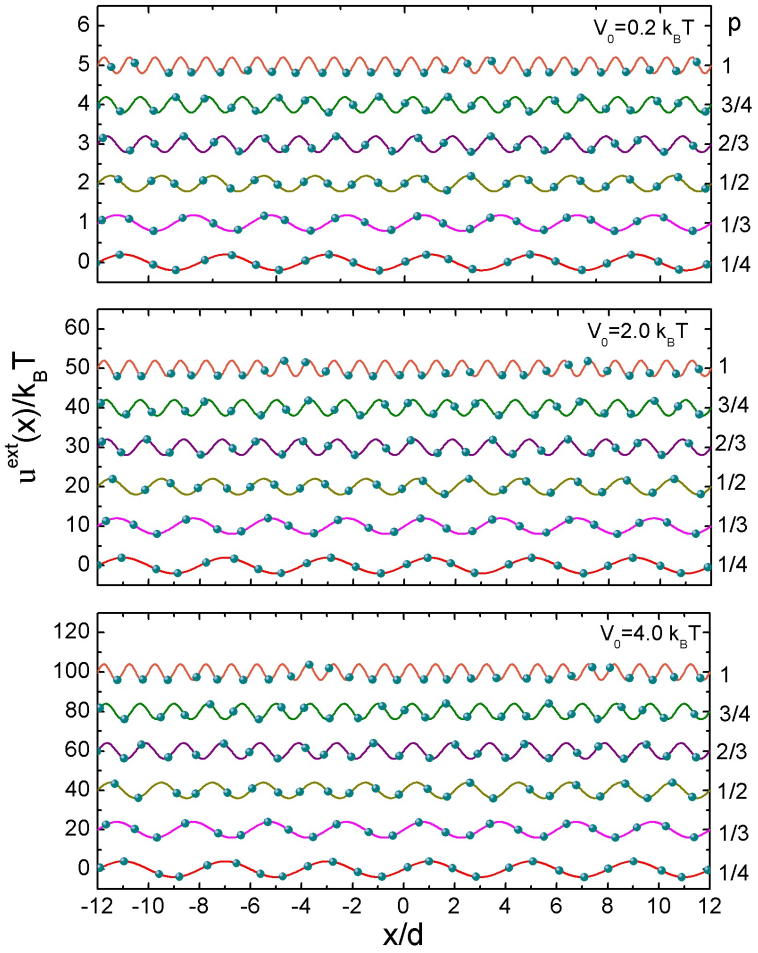

Figure 4.8: (Color online) Blue dots: Equilibrium positions of the superparamagnetic colloids along the file for different values of the commensurability factor $p(= 1/4, 1/3, 1/2, 2/3, 3/4, 1)$. Three values of the external coupling strength, V_0, are displayed. Solid lines: Sinusoidal contribution of the external potential (see equation (4.12)). Curves are shifted in the vertical direction for clarity. The coupling parameters is $\Gamma = 4.67$ and the parameters of the external field are indicated in the inset of Fig. 4.1

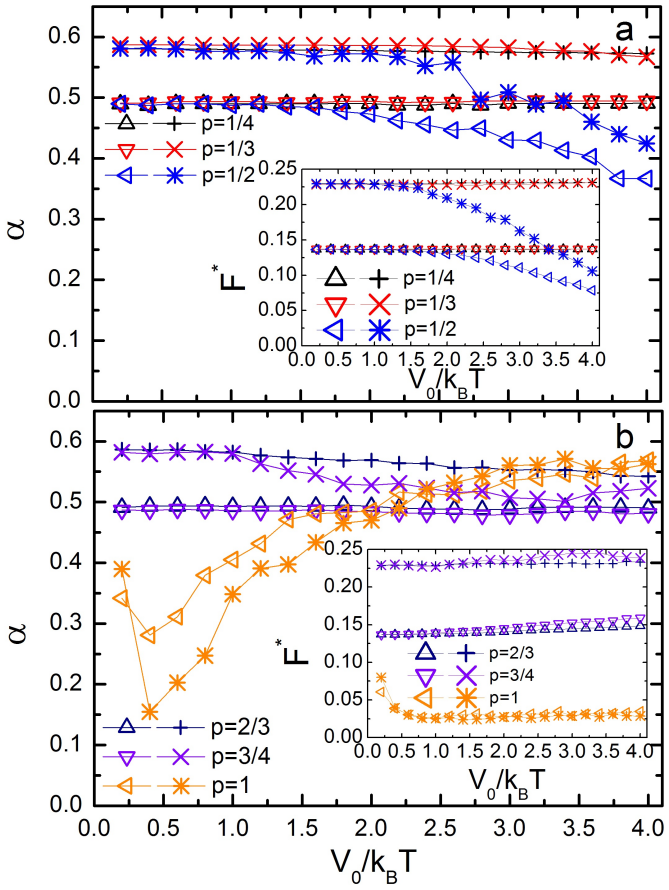

Figure 4.9: Dynamic factors, α and Γ, that characterize the diffusion of the superparamagnetic colloids as a function of the coupling strength, V_0, for different commensurability scenarios. The coupling parameter is $\Gamma = 4.67$. We show results with (stars) and without (open triangles) HI. The lines are guides to the eye.

This confirms that the behavior of F imposed by the external field is present regardless the kind of repulsive interaction potential between particles [16].

4.3 CONCLUDING REMARKS OF CHAPTER 4

We have theoretically investigated the effects due to HI on the diffusive properties of repulsively interacting colloids confined in a 1D channel and subjected to a periodic external potential in the present Chapter. We considered two types of interparticle interactions, namely, Yukawa and super-paramagnetic potentials. We performed an extensive study covering an extended parameter space that includes weak and strong couplings among particles and different values of the external potential strength. We found that, in general, the complex dynamical scenario of both systems is basically the same because both potentials led to a correlation of the particles at long interparticle separations. A different behavior is thus expected with attractive and repulsive short-range potentials.

We also found that HI led to an enhancement of the particle mobility. In particular, the mean-square displacement exhibits a subdiffusive behavior at long-times and it scales as a power-law $W(t) \propto t^{\alpha}$, with $\alpha < 1$. In homogeneous systems, we found that α deviates from the normal SFD and takes the value of $\alpha \approx 0.6$. When the external potential is switched on, the particle diffusion became sensitive to the strength and commensurability of the sinusoidal potential with the inter-particle spacing. Most of the dynamical properties can be explained in terms of collective diffusion, due to the long-range nature of the HI, and the competition between particle-particle and particle-substrate interactions. The latter ones are responsible for the particles accommodation on the minima of the external potential. However, the case $p = 1$ is particular due to the fact that the system exhibits three dynamical regimes that still need to be explored in detail in order to understand the dynamical anti-cooperative behavior imposed, in this case, by the HI.

Last, but not least, we have to point out that our simulations have allowed us to extend the understanding of the SFD in systems composed of interacting Brownian particles under one-dimensional modulated energy landscapes and the action of HI. These results could be corroborated in experiments with light force fields.

BIBLIOGRAPHY

[1] G. Nägele, *Phys. Rep.*, 1996, **272**, 215.

[2] C. Lutz, M. Kollmann and C. Bechinger, *Phys. Rev. Lett.*, 2004, **93**, 026001.

[3] C. Lutz, M. Kollmann, P. Leiderer and C. Bechinger, *Journal of Physics: Condensed Matter*, 2004, **16**, S4075.

[4] B. Lin, M. Meron, B. Cui, S. A. Rice and H. Diamant, *Phys. Rev. Lett.*, 2005, **94**, 216001.

[5] B. Lin, B. Cui, J.-H. Lee and J. Yu, *EPL (Europhysics Letters)*, 2002, **57**, 724.

[6] X. Xu, B. Lin, B. Cui, A. R. Dinner and S. A. Rice, *The Journal of Chemical Physics*, 2010, **132**, 084902.

[7] D. T. Valley, S. A. Rice, B. Cui, H. M. Ho, H. Diamant and B. Lin, *The Journal of Chemical Physics*, 2007, **126**, 134908.

[8] X. Xu and S. A. Rice, *The Journal of Chemical Physics*, 2005, **122**, 024907.

[9] X. Xu, S. A. Rice, B. Lin and H. Diamant, *Phys. Rev. Lett.*, 2005, **95**, 158301.

[10] A. Taloni and F. Marchesoni, *Phys. Rev. Lett.*, 2006, **96**, 020601.

[11] B. Cui, B. Lin, S. Sharma and S. A. Rice, *The Journal of Chemical Physics*, 2002, **116**, 3119–3127.

[12] Q.-H. Wei, C. Bechinger and P. Leiderer, *Science*, 2000, **287**, 625–627.

[13] K. Nelissen, V. R. Misko and F. M. Peeters, *EPL (Europhysics Letters)*, 2007, **80**, 56004.

[14] S. Herrera-Velarde and R. Castañeda-Priego, *J. Phys.: Cond. Matt.*, 2007, **19**, 226215.

[15] S. Herrera-Velarde and R. Castañeda-Priego, *Phys. Rev. E*, 2008, **77**, 041407.

[16] S. Herrera-Velarde, A. Zamudio-Ojeda and R. Castaneda-Priego, *The Journal of Chemical Physics*, 2010, **133**, 114902.

[17] D. V. Tkachenko, V. R. Misko and F. M. Peeters, *Phys. Rev. E*, 2009, **80**, 051401.

[18] P. Hänggi and F. Marchesoni, *Reviews of Modern Physics*, 2009, **81**, 387–442.

[19] T. Harris, *Diffusion with "collisions" between particles*, Rand Corporation, 1965.

[20] R. Arratia, *The Annals of Probability*, 1983, **11**, pp. 362–373.

[21] D. G. Levitt, *Phys. Rev. A*, 1973, **8**, 3050–3054.

[22] J. K. Percus, *Phys. Rev. A*, 1974, **9**, 557–559.

[23] J. Kärger, *Phys. Rev. A*, 1992, **45**, 4173–4174.

[24] K. Hahn, J. Kärger and V. Kukla, *Phys. Rev. Lett.*, 1996, **76**, 2762–2765.

[25] M. Kollmann, *Phys. Rev. Lett.*, 2003, **90**, 180602.

[26] J. Sane, J. T. Padding and A. A. Louis, *Faraday Discuss.*, 2010, **144**, 285–299.

[27] G. Coupier, M. Saint Jean and C. Guthmann, *Phys. Rev. E*, 2006, **73**, 031112.

[28] J. B. Delfau, C. Coste, C. Even and M. Saint Jean, *Phys. Rev. E*, 2010, **82**, 031201.

[29] J. B. Delfau, C. Coste and M. Saint Jean, *Phys. Rev. E*, 2012, **85**, 041137.

[30] J. B. Delfau, C. Coste and M. Saint Jean, *Phys. Rev. E*, 2012, **85**, 061111.

[31] C. Coste, J.-B. Delfau, C. Even and M. Saint Jean, *Phys. Rev. E*, 2010, **81**, 051201.

[32] G. Piacente, I. V. Schweigert, J. J. Betouras and F. M. Peeters, *Phys. Rev. B*, 2004, **69**, 045324.

[33] L. Lizana and T. Ambjörnsson, *Phys. Rev. Lett.*, 2008, **100**, 200601.

[34] T. Ambjörnsson, L. Lizana, M. A. Lomholt and R. J. Silbey, *J. Chem. Phys.*, 2008, **129**, 185106.

[35] T. Ambjörnsson and R. J. Silbey, *J. Chem. Phys.*, 2008, **129**, 165103.

[36] L. Lizana and T. Ambjörnsson, *Phys. Rev. E*, 2009, **80**, 051103.

[37] D. Lucena, D. V. Tkachenko, K. Nelissen, V. R. Misko, W. P. Ferreira, G. A. Farias and F. M. Peeters, *Phys. Rev. E*, 2012, **85**, 031147.

[38] D. V. Tkachenko, V. R. Misko and F. M. Peeters, *Phys. Rev. E*, 2010, **82**, 051102.

[39] S. Varga, G. Ballo and P. Gurin, *J. Stat. Mech.: The. Exp.*, 2011, P11006.

[40] S. J. Manzi, J. J. Torrez-Herrera and V. D. Pereyra, *Phys. Rev. E*, 2012, **86**, 021129.

[41] Q.-H. Wei, C. Bechinger and P. Leiderer, in *Trends in Colloid and Interface Science XIII*, ed. D. TeÅŸak and M. Martinis, Springer Berlin / Heidelberg, 1999, vol. 112, pp. 227–230.

[42] T. R. Stratton, S. Novikov, R. Qato, S. Villarreal, B. Cui, S. A. Rice and B. Lin, *Phys. Rev. E*, 2009, **79**, 031406.

[43] K. Zahn, J. M. Méndez-Alcaraz and G. Maret, *Phys. Rev. Lett.*, 1997, **79**, 175–178.

[44] B. Rinn, K. Zahn, P. Maass and G. Maret, *EPL (Europhysics Letters)*, 1999, **46**, 537.

[45] T. Franosch, M. Grimm, M. Belushkin, F. M. Mor, G. Foffi, L. Forron and S. Jeney, *Nature (London)*, 2011, **478**, 85– 88.

[46] J. C. Meiners and S. R. Quake, *Phys. Rev. Lett.*, 1999, **82**, 2211.

[47] M. Reichert and H. Stark, *Phys. Rev. E*, 2004, **69**, 031407.

[48] R. Fitzgerald, *Physics Today*, 2001, **54**, 18–20.

[49] A. Ryabov and P. Chvosta, *Phys. Rev. E*, 2011, **83**, 020106(R).

[50] R. D. L. Hanes, C. Dalle-Ferrier, M. Schmiedeberg, M. C. Jenkins, M. and S. U. Egelhaaf, *Soft Matter*, 2012, **8**, 2714.

[51] J. K. G. Dhont, *An Introduction to Dynamics of Colloids*, Elsevier, 1996.

[52] M. Manghi, X. Schlagberger, Y.-W. Kim and R. R. Netz, *Soft Matter*, 2006, **2**, 653–668.

[53] M. P. Allen and D. J. Tildesley, *Computer simulation of liquids*, Clarendon Press, New York, NY, USA, 1989.

[54] P. Debye and E. Hückel, *Physikalische Zeitschrift*, 1923, **24**, 185.

[55] E. J. W. Verwey and Overbeek, *Theory of the Stability of Lyophobic Colloids*, Elsevier Publishing Company Inc., Amsterdam, 1948.

[56] L. F. Rojas-Ochoa, R. Castañeda-Priego, V. Lobaskin, A. Stradner, F. Scheffold and P. Schurtenberger, *Phys. Rev. Lett.*, 2008, **100**, 178304.

[57] S. Herrera-Velarde and H. H. von Grunberg, *Soft Matter*, 2009, **5**, 391–399.

[58] A. Ashkin, *Proc. Nat. Acad. Sci.*, 1997, **94**, 4853.

[59] E. M. Furst, *Curr. Opin. Coll. Surf. Sci.*, 2005, **10**, 79.

[60] M. C. Jenkins and S. U. Egelhaaf, *J. Phys.: Cond. Matt.*, 2008, **20**, 404220.

[61] C. Bechinger and E. Frey, *Soft Matter, edited by G. Gompper and M. Schick (Wiley-VCH)*, 2007, **3**, 87.

[62] K. Dholakia and T. Čižmár, *Nat. Photon.*, 2011, **5**, 335–342.

[63] S. Herrera-Velarde and R. Castañeda-Priego, *Phys. Rev. E*, 2009, **79**, 041407.

5

STRUCTURAL PHASES AND DIMENSIONAL VARIATIONS INDUCED BY A PARABOLIC POTENTIAL IN COLLOIDAL SYSTEMS

"Change happens very slow and very sudden."
–Dorothy Bryant, The Kin of Ata Are Waiting for You

During the last two decades, there has been a growing interest in describing both the structure and diffusion of particles in cavities or geometrically restricted environments. This interest is motivated by everyday problems, such as the temporal behavior of the moisture expansion and mass gain of freshly fired bricks that behaves as $\sim t^{\frac{1}{4}}$; this non-Fickian diffusion behavior is due confinement effects [1]. Biological phenomena have also caught the attention, since the quality of the performance of our vital organs is closely related with the transport of particles in narrow compartments. For example, there are studies of renal water re-adsorption; a striking point discussed is the way in which the pores of the kidney are able to discriminate between water and urea as a function of the pore width [2]. At the molecular level, the degree of confinement is a key factor for the understanding of the clustering and alignment of vesicles and red blood cells in micro-capillaries [3], and also the slow dynamics shown by catalyzers involved in genetic recombination [4]. Moreover, the fact that DNA molecules can be transported and counted in surfactant nanotubes is another issue related with geometrical constraints [5]. Furthermore, the ion transport through the cell membrane is a vital problem as well [6]. In addition, the diffusion in crowded biological environments is relevant in many branches of science [7], such as biophysics and medicine, just to mention a few. Hence, the effects due to particle confinement are of interest for a broader area of the soft matter community.

From experimental point of view, it is difficult to study *in situ* the effects of geometrical constraints in biological systems. However, the zeolites constitute one of the experimental model systems that have provided information of the transport of biomolecules in geometrically restricted environments. In fact, the diffusion in zeolites has been intensively studied [8] until the point that the molecular path through their membranes has been highly controlled [9]. This has

also led to questions on how a liquid is ordered in nanopores [10], how to manipulate the structure and diffusion of molecules through nanopores or capillaries [11–20] and how substances diffuse through carbon nanotubes [21–23].

On the other hand, the use of colloidal particles as model systems has provided an excellent benchmark system to study structural and dynamical properties under strong confinement [24]. Colloidal systems offer many advantages over atomic and molecular fluids [25]; this is due to the tunability of the inter-particle potential and the slower dynamics [26]. Colloids have served as ideal models to address several complex problems, ranging from the ones on the atomistic scale [27, 28] to the mesoscopic scale, particle separation [29], ratcheting and pumping [30], and even for non-equilibrium systems such as driven granular media [31].

A distinctive characteristic of a huge amount of colloidal suspensions appears when the colloids are immersed in a liquid-like environment. Thus, the colloidal dynamics is influenced by the indirect interactions mediated by the solvent, typically known as HI [32–34]. In strong confinement conditions, HI could lead to interesting and non-trivial dynamical behaviors [35, 36].

Nowadays, there is an enormous interest in the ordering and diffusion of colloids under confinement. From experimental point of view, Rice *et al.* have extensively studied the phase behavior of confined colloidal suspensions in narrow channels [37–47] . The width of the channel serves as the control parameter to change the system dimensionality. This has allowed reliable quantification of the structural and dynamical properties when the system goes from a one-dimensional, 1D, behavior to a 2D phase (or vice versa) passing through q1D- or 2D-scenarios.

In a number of recent experimental studies [38–61] the walls of the channel play an important role, since they contribute to the wall-particle HI that affect the diffusion of colloids [48]. However, it is possible to avoid the hydrodynamic effects of the walls by using optical traps that allow us to create optical channels [51, 53, 55–57, 59, 60, 62–66] that mimic the geometrical confinement, thus, affecting only the direct interaction with the colloids. In our model system, there is no wall-particle HI because the parabolic potential acts only on the colloids without affecting the solvent distribution. Hence, the HI between colloids are taken into account in the same way as in an unbounded fluid. In particular, the Rotner-Prager diffusion tensor [32] is used explicitly in the calculations.

A parabolic potential, which can be experimentally created by the interference of highly focused laser beams [67], is typically used to avoid the incorporation of physical boundaries that introduce additional effects, as mentioned previously. The effects of the application of a parabolic potential that confines interacting particles have been

theoretically studied by two of us [27, 68–78]. Specifically, structural and dynamic transitions as a function of the inter-particle interaction, the trap amplitude, the temperature (even at $T = 0$, where a large variety of ground states are observed), the density and the coupling with periodic external fields have been studied.

The aim of this Chapter is to understand the ordering of colloidal particles subjected to a parabolic confinement. Then, by varying the trap stiffness, it is possible to change the available space to the colloids and, in consequence, to control the dimensionality of the system. This allows us to fully study the distribution of particles inside the parabolic trap. Particularly, the particle density is kept constant in order to, on the one hand, reduce the number of physical variables in our model and, on the other hand, to highlight the effects of the confinement and the inter-particle interaction on the structural properties. The dynamical properties will be reported elsewhere [36]. Two types of inter-particle interactions, namely, superparamagnetic and Yukawa [35], are considered. We perform BD simulations including HI at the level of the Rotne-Prager diffusion tensor [79, 80]. Our findings are summarized in a structural phase diagram.

The manuscript is organized as follows. In Section 6.1 we give some details about the model system; inter-particle interaction potentials and the external parabolic potential. The standard Ermak-McCammon algorithm to carry out BD simulations is presented in Sec. 6.1.5. Our main results and discussions are included in Sec. 6.2. Finally, a summary of the main results is stated in Sec. 5.4.

5.1 MODEL SYSTEM

Colloidal phase behavior shows a rich diversity of self-assembled mesophases, which can be either fluid or solid [81]. This diversity together with the ability to control the inter-particle interaction among colloids allow us to study directly the relationship between interactions and phase behavior [81]. Tunability is a characteristic of colloids that became possible some years ago with the development of different control techniques, such as the optical tweezers [81]. The tunability also allows the tweaking of colloidal interactions on the fly, making thus achievable the transition through different states of the whole phase diagram. This has potentially-important applications in designing advanced materials of paramount importance for the condensed matter community.

5.1.1 *Equations of motion*

The description of Brownian motion for time scales $t \gg \tau_B$ (overdamped limit), where τ_B is the relaxation time of the particle momenta, is given by the Langevin equation [32]

$$\frac{d\mathbf{r}_i}{dt} = \beta \sum_{j=1}^{N} [-\nabla_{\mathbf{r}_j} U(\mathbf{r}^N, t) + \mathbf{F}_j^{ext}(\mathbf{r}^N, t)] \cdot \mathbf{D}_{ij} + \sum_{j=1}^{N} \nabla_{\mathbf{r}_j} \cdot \mathbf{D}_{ij} + v_i(t), \tag{5.1}$$

where $\beta \equiv (k_B T)^{-1}$ is the inverse thermal energy, with k_B and T being the Boltzmann constant and absolute temperature, respectively, $U(\mathbf{r}^N, t)$ is the total potential energy for the given particle configuration and the external force on the particle j is given by $\mathbf{F}_j^{ext}(\mathbf{r}^N, t) = -\nabla_{\mathbf{r}_j} U^{ext}(\mathbf{r}^N, t)$, where $U^{ext}(\mathbf{r}^N, t)$ is the external energy potential. $\mathbf{D}_{ij}$ is the diffusion tensor and $v(t)$ is the Langevin random velocity that contains the action of a thermal bath and obeys the fluctuation-dissipation relationship,

$$\langle v_i(t) v_j(t') \rangle = 2\mathbf{D}_{ij}\delta(t - t'), \tag{5.2}$$

where $\delta(t - t')$ is the Kronecker delta.

5.1.2 *Superparamagnetic and Yukawa potentials*

From a scientific point of view, colloidal dispersions can be used as model systems for soft condensed matter. This is due to the fact that their physical properties can be studied simultaneously, i.e., in real time, by using three different complementary methods; namely, experiment, theory, and computer simulations. The specific details of both superparamagnetic and Yukawa colloidal systems studied in this Chapter have been reported elsewhere [34, 35, 82–85], thus, we briefly discuss their main features.

Superparamagnetic colloids at the air-water interface have served as excellent models to investigate fundamental properties that are related to the role of hydrodynamics and melting transition, as well as the elastic behaviour and the phonon band structure in two-dimensional crystals [34, 82, 86–88]. In such an experimental model, an external and constant magnetic field is applied in the perpendicular direction of the interface. This leads to a long-range magnetic dipole-dipole interaction between colloids of the form [34, 82, 85]

$$\beta u(r) = \frac{\Gamma(\frac{d}{a})^3}{r^3}, \tag{5.3}$$

where r is the separation between two colloids in units of the particle radius, $a = 2.35\mu m$ [82]. $\Gamma = \beta(\frac{\cdot\cdot 0}{4\pi})\rho^{(3/2)}\chi_{eff}^2 B^2$ is the mean

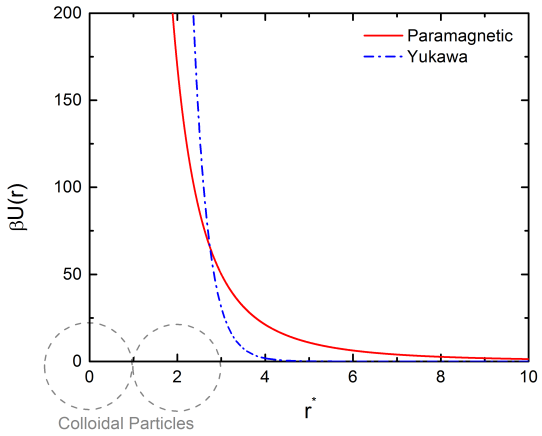

Figure 5.1: Superparamagnetic (solid line) and Yukawa (dashed line) pair potentials given by equations (6.4) and (7.1), respectively.

interaction energy or inter-particle strength normalized with the thermal energy, B is the magnitude of the applied magnetic field, $--_0$ is the magnetic constant and χ_{eff} is the effective magnetic susceptibility of the particles. The units of $\beta(\frac{--_0}{4\pi})\chi_{eff}^2 B^2$ are length to the cube, although the term $\rho^{(3/2)}$ makes it non-dimensional scaled with the mean inter-particle distance, $d = 1/\sqrt{\rho}$, where ρ is the particle number density. A variation in Γ can be related with a change in B, T, and/or ρ [34, 85]. In particular, for the superparamagnetic system, the average packing fraction of colloids is $\phi = 0.1205$, defined as $\phi = \pi a^2 \rho$, and the inter-particle strength is $\Gamma(\frac{d}{a})^3 = 1353.59$. The use of superparamagnetic colloids makes possible a straightforward comparison between theoretical predictions and experiments.

We also consider colloids interacting with a repulsive screened Coulomb potential (Yukawa). For distances $r < \sigma (= 2a)$, the interaction is hard-core. For $r \geqslant \sigma$, two colloidal particles interact via the repulsive part of the DLVO pair potential, see, e.g., Refs. [84, 89, 90],

$$\beta u(r) = Z_{eff}^2 \lambda_B \left[\frac{e^{\kappa a}}{1+\kappa a}\right]^2 \frac{e^{-\kappa r}}{r}, \tag{5.4}$$

where Z_{eff} is the effective charge, κ is the Debye screening parameter and λ_B is the Bjerrum length [89, 90]. The potential parameters used in equation (7.1) were taken from [83]; $a = 1.4\mu m$, $Z_{eff} = 5400$, $\lambda_B = 0.72$, and $\kappa^{-1} = 550$ nm. For charged colloids, the average packing fraction used in our calculations is $\phi = 0.1766$.

The potentials (see Fig. 5.1) were chosen because they correspond to two different limits: long-range interaction (superparamagnetic particles) and short-range interaction (Yukawa particles). The range of the latter is tunable through the value of the inverse screening length κ.

5.1.3 *External fields*

During the last decade, optical traps have been widely used in colloidal systems as a tunable substrate. Scientists have found that their effect on the dynamics and the structural configuration is fascinating [24, 91, 92]. The advantage of optical trapping is two-fold: first, it allows us to confine particles in small regions of space, and second, it also serves to control the position of colloids with high precision. Thus, it can be considered as a well-controlled particle-substrate potential. Then, if one is able to understand the interaction between the laser fields and the colloids [24], its incorporation in the theoretical models and computer simulations facilitates the study of the physical properties of the system, see, e.g., Refs. [24, 92] and references therein.

The simplest potential trap can be modeled as a harmonic potential. In this Chapter, we introduce an external potential to confine the particles in one direction. Mathematically, this potential takes the following functional form,

$$u^{ext}(\mathbf{r}_i) = \frac{1}{2} k y_i^2, \tag{5.5}$$

with k being the trap stiffness [72]. To have a visual representation of the full system, Fig. 5.2 shows a cartoon of the parabolic potential and a configuration of superparamagnetic particles (distributed in the plane) for the reduced trap stiffness $k^* \equiv k a^2/k_B T = 2$.

5.2 bd! SIMULATIONS AND OBSERVABLES

We use the algorithm proposed by Ermak and McCammon for solving the Langevin equation (6.1) [80] together with the fluctuation-dissipation relationship given by equation (6.2). Both equations constitute the standard Brownian dynamics method [80]. HI are explicitly included at the level of the Rotner-Prager (RP) diffusion tensor [32, 34, 79],

$$\begin{aligned} \mathbf{D}_{ii} &= D_0 \mathbf{I} = \tfrac{k_B T}{6\pi\eta a}\mathbf{I}, \\ \mathbf{D}_{ij} &= (k_B T/8\pi\eta r_{ij})(\mathbf{I} + \tfrac{\mathbf{r}\otimes\mathbf{r}}{r_{ij}^2}) + \\ &\quad k_B T(a^2/4\pi\eta r_{ij}^3)(\tfrac{\mathbf{I}}{3} - \tfrac{\mathbf{r}\otimes\mathbf{r}}{r_{ij}^2}), \end{aligned} \tag{5.6}$$

where η is the solvent viscosity, $\mathbf{I}$ is the unitary matrix and D_0 stands for the diffusion constant of a single isolated particle in an unbounded fluid. One notes that the RP diffusion tensor includes the lowest corrections of particle size over the Oseen tensor description [32]. The diffusion tensor $\mathbf{D}_{ij}$ introduces long-ranged interactions and couples distant particles. The stochastic term, equation (6.2), is numerically implemented by a Cholesky decomposition[79, 93]. We are dealing with the dynamics of non-deformable particles in an unbounded fluid. In this case, one can straightforwardly check that $\nabla_{\mathbf{r}_j} \cdot \mathbf{D}_{ij} = 0$.

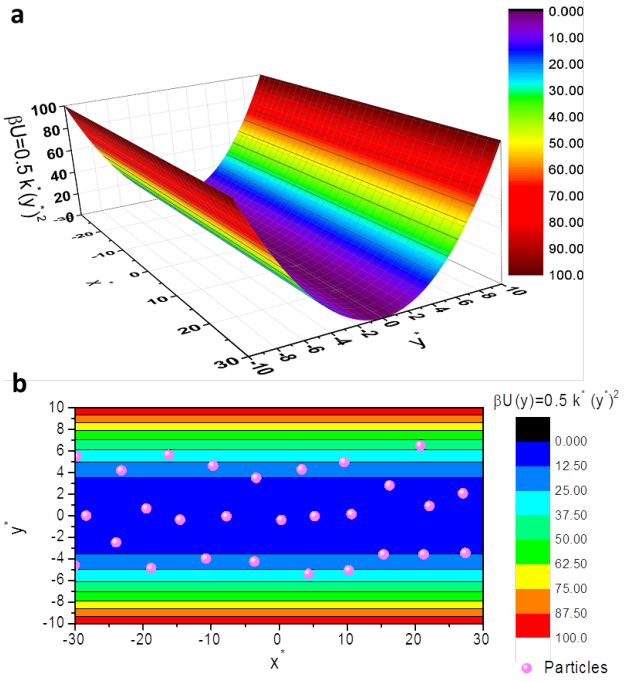

Figure 5.2: a) Cartoon of the parabolic potential and b) configuration of superparamagnetic particles (distributed in the plane) for the reduced trap stiffness $k^* = 2$.

The parabolic potential (5.5) confines the colloidal particles along the y-direction, thus, periodic boundary conditions are applied only in the x-direction. However, since we keep the particle density constant, ρ, we have to find the appropriate box length in the x-direction, L_x, for each value of k; the latter determines the length of confinement in the y-direction. Technically, this is done by monitoring the average maximum displacement, L_y^{max}, allowed by the external potential. Thus, $L_x = N/(\rho L_y^{max})$, where N is the number of particles used in the simulations. We demonstrate further below that L_x can be roughly estimated using an energetic criterion.

Once the value of L_y^{max} is calculated for a given trap stiffness, k, we let the system evolve during 1.5×10^6 time steps before averages are computed. The number of time steps of the average loop is 1.5×10^7. We save the configurations every 10 time steps. Thus, 1.5×10^6 configurations are used to measure the observables. The radius of the particles, a, and the thermal energy, $k_B T$, are taken as the scaling factor for all units of distance and energy, respectively. From now on, all quantities are expressed in reduced units. Due to the explicit incorporation of HI, $N = 800$ particles are used in the simulation. The reduced time step, Δt, is chosen as $\Delta t D_0/a^2 = 0.0002$, where t is the time.

One of the computed observables is the so-called structure factor, $S(q_x)$, which characterises the variations in the local density at the

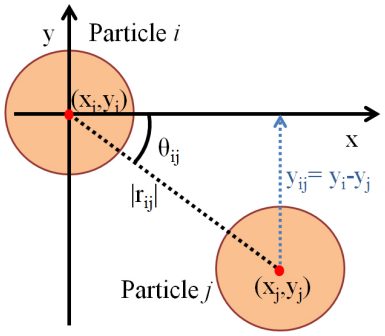

Figure 5.3: Angle, θ_{ij}, formed by the center-to-center line between particles i and j and the x-axis.

spatial frequency $q \equiv 2\pi/\lambda$, where λ is the wavelength [94]. Then, the static structure factor is obtained by using the relation [84],

$$S(q_x) = \frac{1}{N}\left\langle \left(\sum_{i=1}^{N} \cos(q_x \cdot x_i)\right)^2 + \left(\sum_{i=1}^{N} \sin(q_x \cdot x_i)\right)^2 \right\rangle, \qquad (5.7)$$

where the angular brackets $\langle \cdots \rangle$ denote an ensemble average and q_x is the magnitude of the wavevector in the x-direction.

We also compute the probability of finding a particle along the y-direction through the expression,

$$P(y) = \left\langle \frac{1}{N}\sum_{i=1}^{N} \delta(y - y_i) \right\rangle. \qquad (5.8)$$

This is a normalised distribution, $\int_{-\infty}^{\infty} P(y)dy = 1$.

Equations (5.7) and (5.8) describe the spatial distribution of particles in the parabolic potential. However, the angular distribution, i.e., the probability of two neighbouring particles whose center-to-center distance forms an angle θ with respect to the x-axis, provides a full description of the local distribution of the first neighbours layer. This distribution is evaluated through the following expression,

$$P(\theta) = \left\langle \frac{1}{N}\sum_{i=1}^{N}\sum_{j=1}^{M_i} \frac{1}{M_i}\delta(\theta - \theta_{ij}) \right\rangle, \qquad (5.9)$$

where θ_{ij}, as shown in Fig. 5.3, is the angle formed by the center-center line between particles i and j, and the x-axis; M_i is the number of the particles within the first layer of neighbours around the particle i. This is also a normalised distribution, $\int_{-\pi/2}^{\pi/2} P(\theta)d\theta = 1$.

5.3 RESULTS AND DISCUSSION

5.3.1 *Dimensionality*

We restrict ourselves to colloidal systems with the same packing fraction; this avoids effects associated to density variations. Then, the set of physical parameters is reduced and only determined by the parameters that define the inter-particle potential and the external field. Fig. 5.4a shows the mean packing fraction and mean inter-particle distance as a function of the trap stiffness. In each case, the relative error is less than 5%.

The average maximum distance, $|L_y^{max}|$, that particles can reach in the y direction due to the confinement is presented in Fig. 5.4b. We also plot the function: $L_y^{max}/a \propto \sqrt{\frac{2}{k^*}}$, that comes from the relation $u^{ext}(\pm L_y^{max}) = k_B T$, i.e., it corresponds to the maximum distance at which a Brownian particle cannot cross the energetic barrier imposed by the external potential. The constant of proportionality, C, should be equal to 1 in the case of a free particle, however, since particles interact via a pair potential, one could expect that the previous expression would be able of capturing the dependence of L_y^{max} with k using an appropriate value for C. In fact, C has to take into account the energetic contribution of the inter-particle potential. Solid lines in Fig. 5.4b also display the best estimation for C. For the Yukawa colloidal system $C \approx 9$, whereas for superparamagnetic colloids we find that $C \approx 12$. We observe that the analytical expression describes correctly the dependence of L_y^{max} with k, nonetheless, the differences between the simulations and the analytical expression are larger for the superparamagnetic particles. This could be due to the long-range behaviour of the interaction between superparamagnetic colloids, see Fig. 5.1, i.e., long-range potential contributions play a role in the total potential energy.

Having computed the maximum displacement along the y-direction and considering periodic boundary conditions in the x-direction. we propose the following definition of dimensionality in terms of L_y^{max}. A 1D system is thus defined for separations $|L_y^{max}| < 3a$, i.e., a single-file of particles. A q1D system is then reached at separations where there exist finite, but small, fluctuations in the y-direction; $|L_y^{max}| < 8a$. A q2D system is such that mutual passage is allowed, however, the movement along the y-direction is limited by a quantity R_c, which is smaller but of the order of the inter-particle interaction range. Finally, we recover the properties of a 2D system when $|L_y^{max}| > R_c$. In table 5.1 we summarise this particular classification, which will allow us to associate the structural ordering with the system dimensionality.

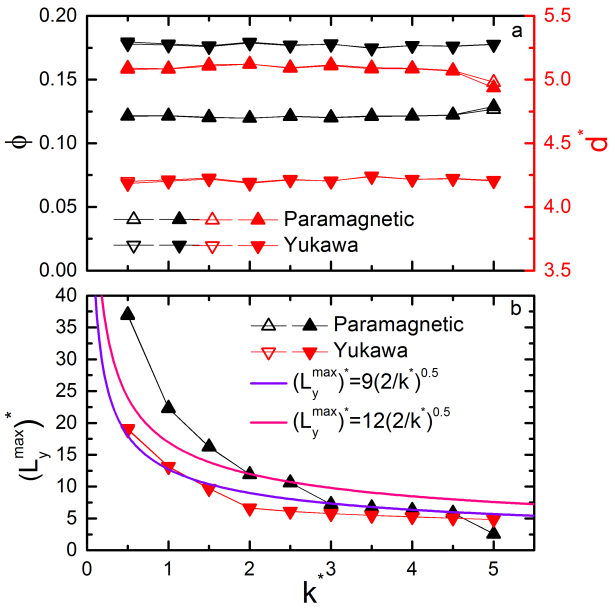

Figure 5.4: (a) Average packing fractions ϕ (left y-axis) and mean interparticle distance (right y-axis), $d/a = \sqrt{\pi/\phi}$, as a function of the trap stiffness, k; lines just guide the eye. (b) Average maximum distance along the y-direction. Symbols correspond to Brownian dynamics simulations with (closed symbols) and without (open symbols) HI, and solid lines to the expression $L_y^{max}/a = C\sqrt{\frac{2}{k^*}}$.

5.3.2 *Superparamagnetic colloids*

To elucidate the changes in the spatial distribution of particles along the parabolic channel, equilibrium configurations for superparamagnetic colloids as a function of the trap stiffness are shown in Fig. 5.5; such particle configurations are obtained using BD simulations without HI. From the figure, it is easy to note that k^* allows one to tune the system dimensionality; from q2D (small values k^*) to 1D (high values k^*). Furthermore, the resulting structure exhibits a well-defined number of strata, which can be controlled by varying the strength of the external potential, k^*. We should point out that the variety of structures is similar to the ones reported in the experiments performed in the group of Rice, where the degree of confinement or dimensionality is provided through the width of the ribbon channel, see, e.g., Ref. [37]. In the latter case, a wall-particle hydrodynamic coupling should be taken into account to explain the diffusion properties of colloids. However, this point will be addressed elsewhere [36].

The probability distribution of finding a particle along the y-axis, $P(y)$, is shown in Figs. 5.6 and 5.7. In both figures, one observes that the distribution exhibits several well-defined peaks. The maxima indicate the most likely regions occupied by the particles. These peaks are separated by minima; they represent regions where particles are

Dimensionality	Interval in the y-direction
1D	$\lvert L_y^{max}\rvert \leqslant 3a$
q1D	$3a < \lvert L_y^{max}\rvert \leqslant 8a$
q2D	$8a < \lvert L_y^{max}\rvert \leqslant R_c$
2D	$\lvert L_y^{max}\rvert > R_c$

Table 5.1: Definition of the system dimensionality in terms of the maximum available displacement, $|L_y^{max}|$, of the particles along the y-direction. R_c is a cutoff distance that is of the order of the interparticle interaction range.

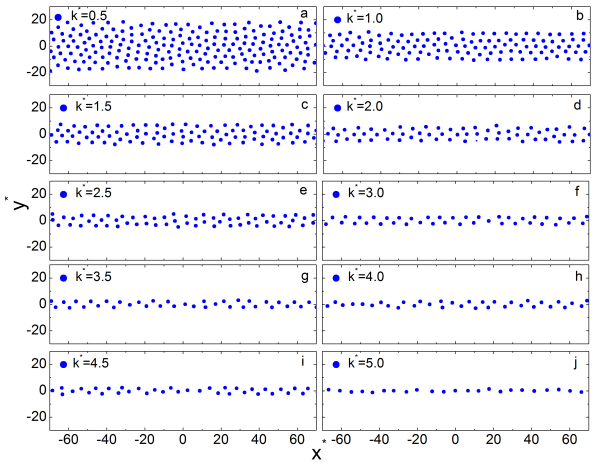

Figure 5.5: Equilibrium configurations of superparamagnetic particles as a function of the reduced trap stiffness, k^*. One observes that particles self-assembly in strata.

basically absent. This feature manifests the fact that particles are distributed in strata along the direction of confinement. As mentioned above, similar structures were observed experimentally in confined interacting colloids [37] and in simulations [95]. Each peak can be well-approximated by a distribution of the form: $p(y) \approx \exp[-\beta E(y)]$, where $E(y)$ is the energy at a given position. In the case of a maximum, it should be the energy of localisation. Thus, the difference between consecutive maxima and minima will give us an estimation of the energetic barrier, ΔE, that a particle has to overcome in order to move through different strata. At weak couplings, Fig. 5.6a, mutual passage is allowed and particles can move almost freely between different strata. As k^* increases, the number of peaks decreases, in fact, each peak is associated with a line of particles at a certain y-distance. From the figure, one can also obtain the value of the aforementioned energetic barrier. For example, in the case $k^* = 0.5$ we have $\Delta E \approx 1.4 k_B T$; this value is slightly higher than the average kinetic energy per particle. Thus, particle exchange between consecutive strata may seem possible. However, for $k^* = 1.0$ one has that

$\Delta E \approx 2.2 k_B T$ and, hence, particle exchange becomes more difficult, however, we should mention that the energetic barrier is not a monotonic function that increases with trap stiffness. Then, it is clear that even at weak couplings particles cannot entirely move freely along the y-direction and they become highly localised in small regions. This degree of confinement is consistent with a q2D system.

The results for $P(y)$ at moderate confinements are shown in Fig. 5.6b. There, one can observe a transition from q2D to q1D when the trap stiffness increases from $k^* = 2$ to $k^* = 3$. This transition is well-represented by the change in the number of strata described by the peaks of the distribution; it changes from 3 to 2 strata, respectively. Interestingly, when $k^* = 2.5$, the resolution of the third stratus is very low. In fact, the central peak has a height similar to the two minima of the distribution. Furthermore, the energetic barrier in this case is $\Delta E \approx 0.7 k_B T$, which allows to exchange particles between different strata. This picture is different in the other two accompanying cases, where the energetic barrier is clearly larger than the average kinetic energy per particle.

We further increase the values of the trap stiffness to move toward the set of parameters that correspond to strong couplings. The results are shown in Figs. 5.7a and 5.7b. The features seen in Fig. 5.7a describe a system that will undergo a structural transition from q1D to 1D; the height of the maxima and the energetic barriers decrease with increasing k^*. In consequence, one can control continuously the probability of particle exchange among the strata. On the other hand, Fig. 5.7b shows a probability distribution that represents a system where particles are extremely localised in the y-direction; the peak height is close to the unity value, $P(y_{max}) \approx 0.85$, and its width (related with the standard deviation of the distribution), is slightly larger than the particle diameter, $\approx 3.0a$. These features are a clear indication that the system has reached the so-called single-file configuration [35, 76], see Fig. 5.5j.

We should mention that, as might be expected, the distribution of particles along the y-direction is not affected by the HI. In all cases, i.e., from weak to strong confinement, the probability distribution $P(y)$ does not change whether or not HI is taken into account.

Empirical criteria have been developed to identify the freezing transition in both 2D and 3D [96, 97]. One of them is the 2D version of the Hansen-Verlet freezing rule, which states that a 2D liquid freezes when the amplitude of the highest peak in the structure factor, $S(q_x^{max})$, exceeds a critical value of ≈ 5.5 [98]. Also, two of us proposed a liquid-solid structural freezing rule (not in the thermodynamic sense) for 1D systems [99] similar to the Hansen-Verlet criterion. In this case, the height of the peak has to be $S(q_x^{max}) \sim 7$. Thus, following a similar analogy, we define a structural phase in interacting colloidal systems in a parabolic potential in terms of the height of the main peak of the

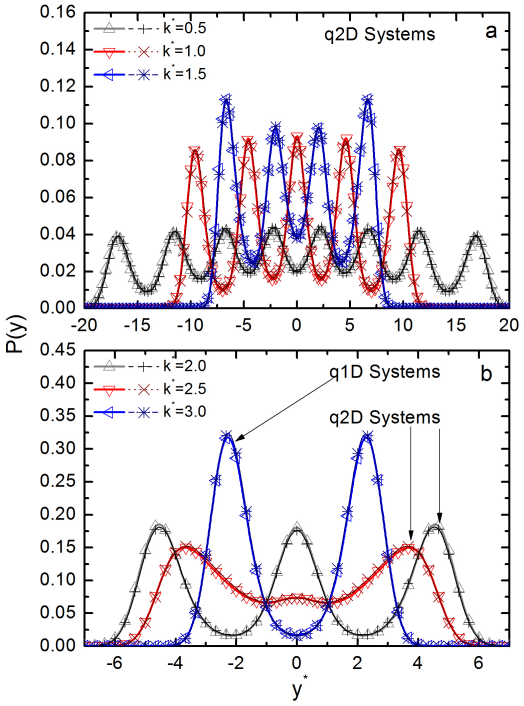

Figure 5.6: Probability distribution, $P(y)$, of finding a particle along the y-direction for superparamagnetic colloids in the weak and intermediate confinement regime. Triangles: without HI, stars: with HI.

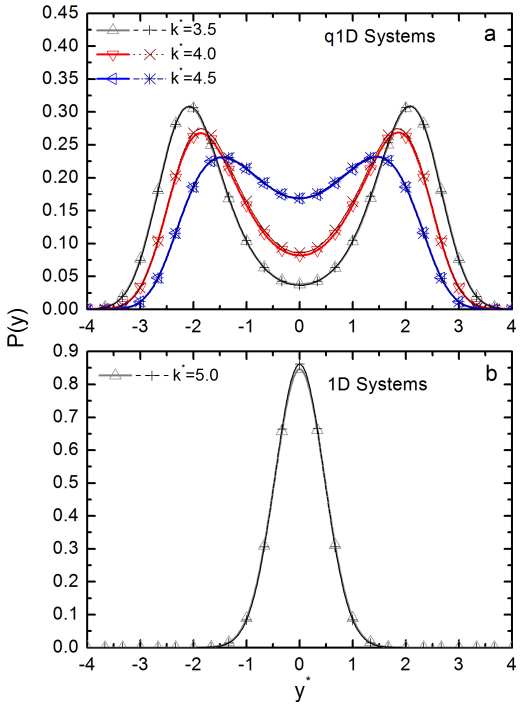

Figure 5.7: Probability distribution, $P(y)$, of finding a particle along the y-direction for superparamagnetic colloids in strong confinement regime. Triangles: without HI, stars: with HI.

Structural state	$S(q_x^{max})$
Liquid	$\leqslant 2.5$
Cooled Liquid	$2.5 < S(q_x^{max}) < 3.0$
Super-Cooled Liquid	$3.0 \leqslant S(q_x^{max}) \leqslant 5.5$ (2D) $3.0 \leqslant S(q_x^{max}) \leqslant 7.0$ (1D)

Table 5.2: Definition of the structural phases in terms of the amplitude or height of the $S(q_x^{max})$.

structure factor. This information is summarised in Table 5.2, which will serve as a guide for classifying the structural re-ordering, from a regular liquid to a super-cooled liquid structural phase. A variation in the height of $S(q_x^{max})$ is associated with a spatial frequency or length correlation that starts to be dominant in the system. Thus, a super-cooled liquid state can be understood as a liquid-like state with a well-defined length scale.

Figures 5.8 and 5.9 show the $S(q_x)$ for a homogeneous 2D super-paramagnetic colloidal system as well as the $S(q_x)$ for the weak and intermediate confinement regimes; the characteristic spatial frequency of the homogeneous system has the value $q_{1stP}a \equiv 1.3$, where 1stP stands for first-peak, which corresponds to the mean particle distance. According to the definition given in Table 5.2, the system structural phase corresponds to a super-cooled liquid state.

The structure factors for weak confinement are shown in Fig. 5.8a. For $k^* = 0.5$, the system exhibits a typical liquid phase; the first peak of $S(q_x)$ is located at $q_{1stP}a$ and the height of the peak is below 2.5. When the spring constant is increased to $k^* = 1.0$, there is an interesting phenomenon: the first and the second peaks have similar heights and are located around $q_{1stP}a$ and $2q_{1stP}a$. This means that the ordering of particles is either at a distance d or $d/2$; this can be interpreted as a coexistence of two structural domains with different lattice constants. By increasing k^* to $k^* = 1.5$, it is found that the first peak is at $q_{1stP}a$. Comparing with the previous case, the second peak, that was located around $2q_{1stP}a$, now splits in two peaks, one at $q_xa \approx d/\sqrt{2}$ and the other one at a q similar to the second peak of the 2D reference system.

The $S(q_x)$ for moderate confinement is shown in Fig. 5.8b. Specifically, for $k^* = 2$ the $S(q_x^{max})$ is at $q_xa = 1.9$, which indicates that the particles are closer to each other than in the 2D case thus forming more compact structures. In this case, the $S(q_x^{max})$ is slightly smaller when the HI are considered. This means that the HI allow the system to fluidize. We should mention that the coupling of the external field with the HI is not trivial (see first term in equation (6.1)). The former breaks the homogeneity in the particle distribution, giving rise to a heterogeneous system where the HI can play an important role

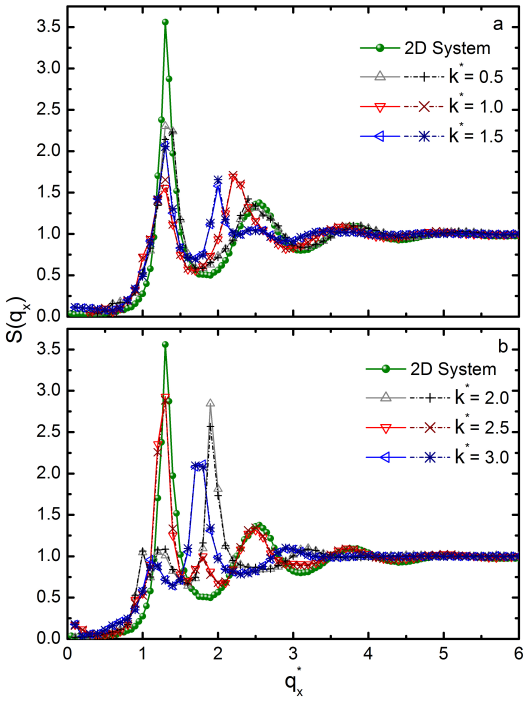

Figure 5.8: Structure factor, $S(q_x)$, along the x-direction for superparamagnetic colloids for weak and intermediate confinement. Triangles: without HI, stars: with HI.

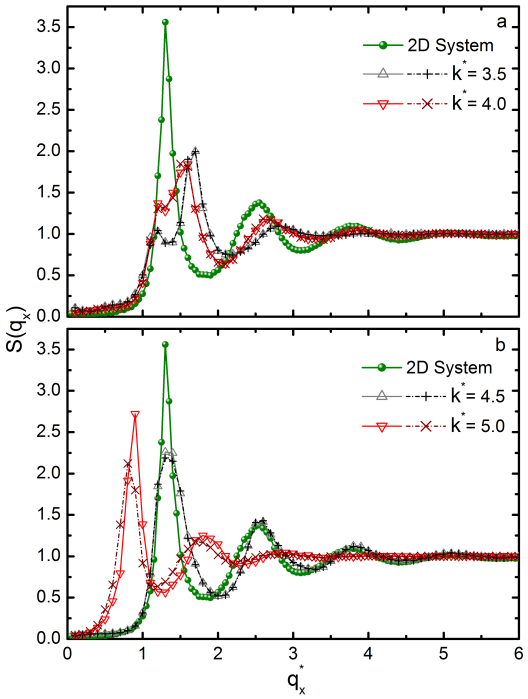

Figure 5.9: Structure factor, $S(q_x)$, along the x-direction for superparamagnetic colloids for strong confinement. Triangles: without HI, stars: with HI. Triangles: without HI, stars: with HI.

in determining both the structure and the dynamics. This feature has been recently highlighted in the SFD of interacting colloids in periodic energy landscapes [35, 69].

For $k^* = 2.5$, the system is in a cooled liquid state, but it can be still classified as a q2D system; the particles are separated from each other by distance $\sim d$ similar to 2D. However, there is some reminiscent from the previous structure ($k^* = 2.0$), which is indicated by a small peak at $q_x a \approx 1.8$. When k^* takes the value $k^* = 3.0$, the system undergoes a dimensional transition from q2D to q1D (see Fig. 5.6b). This clearly affects the ordering along the x-direction. The $S(q_x^{max})$ is located at $q_x a \sim 1.74$ and its height is around 2. This means that the prevailing distance among the particles in the x-direction is $\approx d/\sqrt{2}$; we also find a small peak at the q_x that corresponds to the mean interparticle distance d. Thus, the dimensional transition is correlated with a change in the structural state since the system goes from a cooled-liquid state to a liquid state. This is related with a loss of correlation along the x-direction.

The effects of increasing the strength of the parabolic potential in the probability of particle exchange among two rows, discussed previously in the parameter $P(y)$, are also reflected in the structure factor $S(q_x)$. As one increases the spring constant until $k^* = 4.0$, see Fig. 5.9a, the system dimensionality is q1D and always exhibits a liquid phase with a competition among two characteristic lengths: $\approx d/\sqrt{2}$ and d. For the spring constant $k^* = 4.5$, shown in Fig. 5.9b, the system undergoes a structural re-ordering compared with $k^* = 4.0$. This system is also prior to the transition 1D→1D found through the analysis of $P(y)$ (see Fig. 5.7). Furthermore, particles are preferentially distributed with an interparticle distance d and the structure is similar to the one found for the 2D system. This is an interesting effect because the same behavior is found for the system at $k^* = 2.5$, which is right before the q2D→q1D transition. Thus, it seems that any system that is going to experience a dimensionality variation shows a structure, in the x-direction, similar to the 2D case, although the structural state is below the previous one.

The structure factor for the case $k* = 5.0$, shown in Fig. 5.9b corresponds to a 1D system according to the probability distribution $P(y)$ shown in Fig. 5.7b. The $S(q_x)$ shows a peak that corresponds to a mean distance among particles of $\approx \sqrt{2}d$, longer than all the previous cases. Thus, particles are forming more open structures. However, the structural state without HI corresponds to a cooled liquid, but when HI are considered explicitly the corresponding state becomes of a liquid. As it was explained before, the HI promote the fluidization of the system in the x-direction.

So far we have studied the particle correlations in the directions perpendicular and parallel to the confinement. We have seen that a change in the system dimensionality is correlated with a variation in

the structural phase. The external imposed confinement breaks the homogeneity of the particle distribution and the analysis of the correlations in two particular directions might not be sufficient to understand the ordering in the system. Thus, we now analyze the angular probability distribution of the first layer of neighbors around a central particle. The distributions are shown in Figs. 5.10 and 5.11 and allow us to better understand the distribution of the particles not just in one preferable direction, but in the plane where they are confined. In the 2D reference system, the system is in a super-cooled liquid state and the probability of finding a neighbor is the same at any given angle. For this particular superparamagnetic fluid, it is still below the 2D freezing and no hexagonal phases occur. When $k^* = 0.5$ (see Fig. 5.10a), the system exhibits an hexagonal-like structure, as can be seen in the three well defined peaks; one at $\theta = 0°$ (aligned along the x-axis) and the others at $\theta = \pm 60°$ (not aligned along the x-axis), which are further referred as the main peak and secondary peaks, respectively. The main peak is slightly larger than the secondary peaks, this is linked with $P(y)$: particles tend to be stratified, although the possibility of particle exchange is finite.

As k increases within the interval $1.0 \leqslant k^* \leqslant 1.5$, the peaks tend to be more localized. Actually, the main peak grows and the secondary peaks are located at $|\theta| < 60°$. The former is related with the stratification process because the particles self-assembly in strata; the latter ones are connected with changes of the second peak of the $S(q_x)$ discussed above. Neighboring particles that belong to the different strata show configurations of deformed hexagons and the particles tend to be at distances smaller than d. The particles are even more localized for $k^* = 2.0$ (see Fig. 5.10b), the main peak is almost twice as large as the secondary peaks. The latter ones are now at $\theta \approx \pm 50°$. This configuration corresponds to three well defined rows found by the $P(y)$ and the $S(q_x)$ whose highest peak is located at $q_x a = 1.9$. The complete picture is the signature of a zig-zag configuration (see Fig. 5.5d).

For $k^* = 2.5$, the angular distribution suffers an abrupt change, the central peak is significantly smaller than the one exhibited by the previous spring constant. Moreover, the secondary peaks at $\theta \approx \pm 45°$ practically do not exist. This change should be associated with the change in the system dimensionality. Thus, the angular distribution also gives a clear indication that the system will undergo a transition from 2D to q1D. While k increases within the interval $3.0 \leqslant k^* \leqslant 4.5$, the main peak of $P(\theta)$ also increases (see Figs. 5.10b and 5.11a). Besides, the secondary peaks are located at smaller angles and they become broader as a consequence of the particle exchange among strata as it was discussed above (see Figs. 5.6b and 5.7a). When $k^* = 5.0$, colloidal particles exhibit a single-file configuration (see Figs. 5.5j and 5.7a). This leads to the formation of only one and well-defined

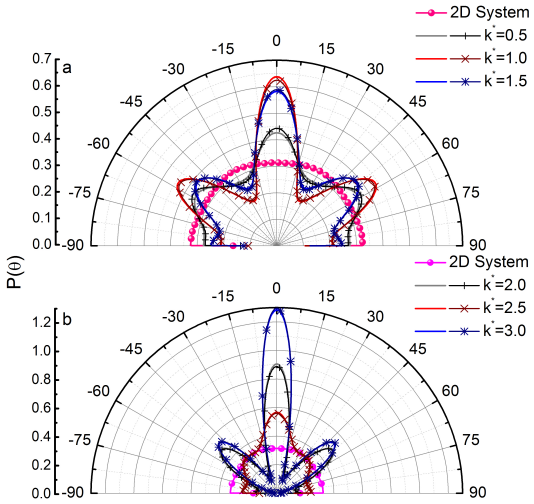

Figure 5.10: Angular probability, $P(\theta)$, of the first layer of neighbors for superparamagnetic colloids in the weak and intermediate confinement regimes. Triangles: without HI, stars: with HI.

peak at $\theta = 0°$. The peak found including HI is slightly larger than the one without HI, which is a counter-intuitive behavior; the HI allow the particles to be more aligned in one file but they also allow them to be in a more fluid-like state as it was previously pointed out in the $S(q_x)$ (see Fig. 5.9b).

We have seen that a rich scenario of structural phases and dimensional variations can be induced by a parabolic potential. The latter reproduces similar effects to rigid walls, but avoids the HI between the walls and the particles and, in addition, possible capillarity contributions. Thus, the ordering of particles is just given by the strength of the coupling with the confining potential and the (direct and indirect) inter-particle interactions. Hence, the absence of physical walls makes possible a better understanding of the structure inside the parabolic potential.

Finally, in an effort to summarize the results obtained through the probability distribution, the structure factor and the angular distribution, the structural phase diagram of superparamagnetic colloids subjected to a parabolic potential is displayed in Fig. 5.12. In this phase diagram, we explicitly indicate those states when the system undergoes a kind of freezing (increase of $S(q_x^{max})$) or melting (decrease of $S(q_x^{max})$) together with a re-ordering in the first-neighbor layer. The most interesting result shown in the phase diagram is the impossibility of the system, within the window of trap stiffness values, to reach again the super-cooled liquid state that is only present in the absence of the parabolic confinement, i.e., $k = 0$.

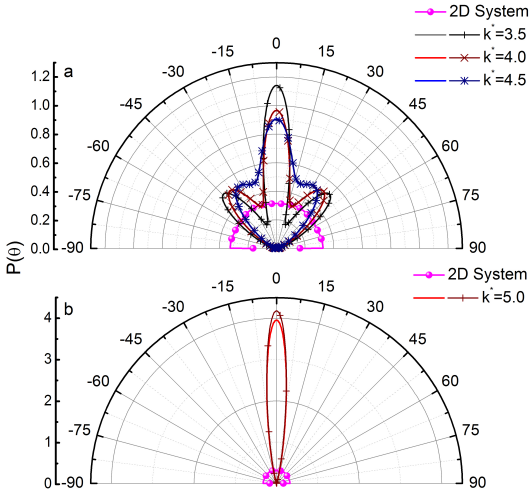

Figure 5.11: Angular probability, $P(\theta)$, of the first layer of neighbors for superparamagnetic colloids in the strong confinement regime. Triangles: without HI, stars: with HI.

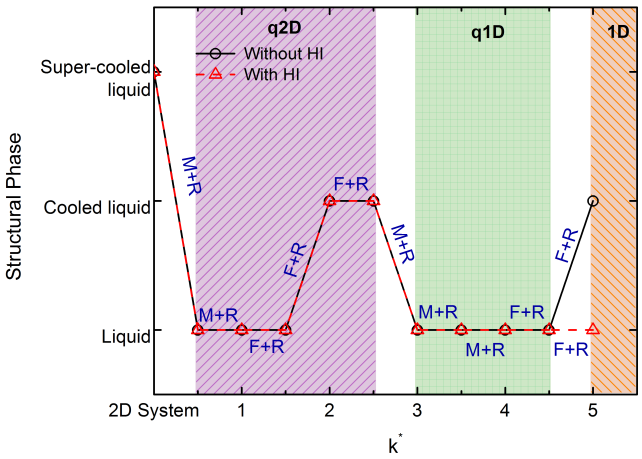

Figure 5.12: Structural phase diagram of the superparamagnetic colloidal system. Horizontal axis denotes the value of the reduced trap stiffness, $k\alpha^2/k_BT$. Vertical axis indicates the structural phase transition found through the analysis of the $S(q_x^{max})$. The letters M and F stand for a *melting*- and *freezing*-like transitions, respectively. The letter R indicates that there is a re-ordering in the angular probability of the first layer of neighbors. The regions 2D, q2D, q1D and 1D were found by calculating L_y^{max} (see Fig. 5.4) and taking into account the definition introduced in Table 5.1. Symbols correspond to Brownian dynamics simulations with (open triangles) and without (open circles) HI.

5.3.3 *Yukawa particles*

The phase behaviour and dynamical properties of a 2D highly charged colloidal suspension in a periodic energy landscape has been recently studied by two of us [100]. In the absence of a substrate, i.e., no external-field, we found that spontaneous crystallisation occurs at $\phi \approx 0.196$. In this Chapter, we have chosen a packing fraction 10% below such a density of crystallisation. Thus, in contrast to superparamagnetic colloids, the charged colloidal suspension is close to the freezing transition. This behaviour is confirmed through the observables. For example, the structure factor exhibits a peak near to the one predicted by the Hansen-Verlet criterion [96]. Besides, the angular distribution of the first layer is described by a nearly hexagonal distribution (data not shown).

To avoid presenting many figures with similar results as the ones obtained for the superparamagnetic system, we here only summarise the main differences between both colloidal systems. First of all, the probability distribution $P(y)$ at strong confinement certainly exhibits q1D behaviour (see Fig. 5.13). This means that at the same confinement strength, the distribution shows three peaks. This might be related with the fact that for high values of k^* particles become closer to each other, however, as mentioned above, at short separations, the amplitude of the Yukawa potential is larger than the superparamagnetic one, see Fig. 5.1. Thus, to reach the single-file behaviour, one needs to further increase the value of the trap stiffness. Then, charged colloids undergo only a transition from 2D to q1D within the values of k^* here explored. We should mention that this system also organizes in strata (data not shown).

On the other hand, the order along the x-direction shows a richer structural phase. First, note that the structure factor for the homogeneous case shows two peaks; this is a fingerprint that the system is close to a freezing transition. At weak confinement, the signature of the freezing disappears, but, in some cases the $S(q_x^{max})$ reaches the same amplitude as in the homogeneous-2D reference system (see Fig. 5.14a), which means that even in this regime the system experiences a kind of re-entrant freezing. A further increase in the confinement strength leads to a non-monotonic variation in the amplitude of the structure factor peaks (see Fig. 5.14b). Nonetheless, their locations are quite similar to the ones in the purely 2D case. In the strong coupling regime, shown in Fig. 5.15, the system undergoes a monotonic increase in the height of the main peak, however, there is no further evidence of a liquid-solid transition, since the second peak does not exhibit the typical shoulder associated with such a transition. This behaviour is fully consistent with the one observed for repulsive 1D colloidal systems as a function of the potential strength or packing fraction [100].

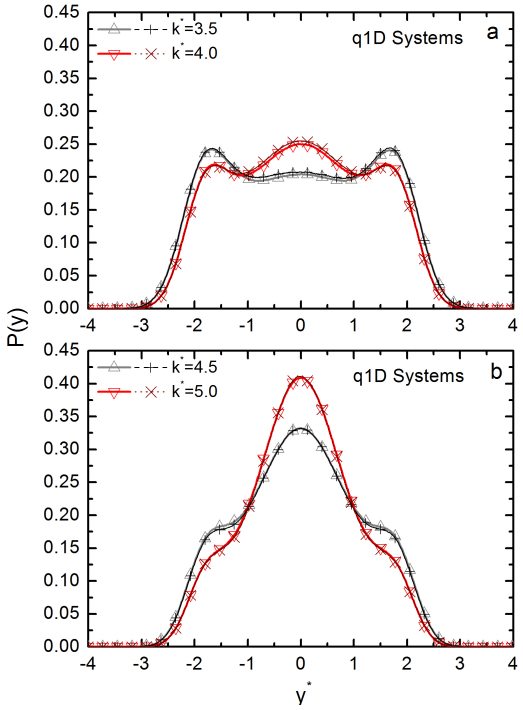

Figure 5.13: Probability distribution, $P(y)$, of finding a particle along the y-direction for charged colloids at the strong coupling regime. Triangles: without HI, stars: with HI.

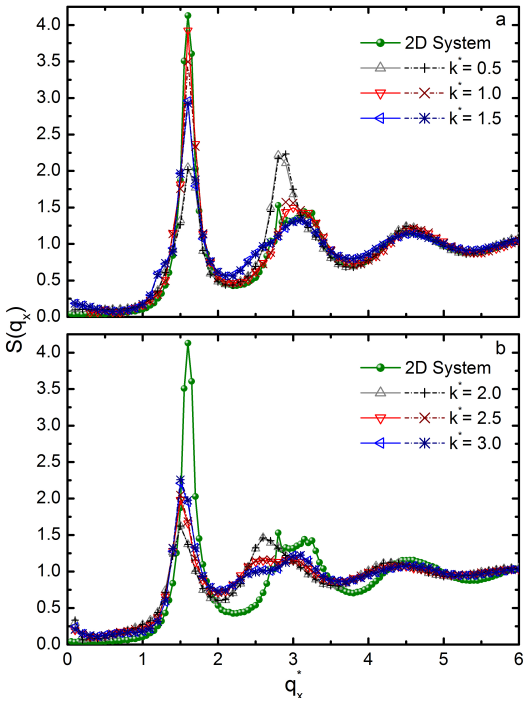

Figure 5.14: Structure factor, $S(q_x)$, along the x-direction for charged colloids in the weak and intermediate confinement regimes. Triangles: without HI, stars: with HI.

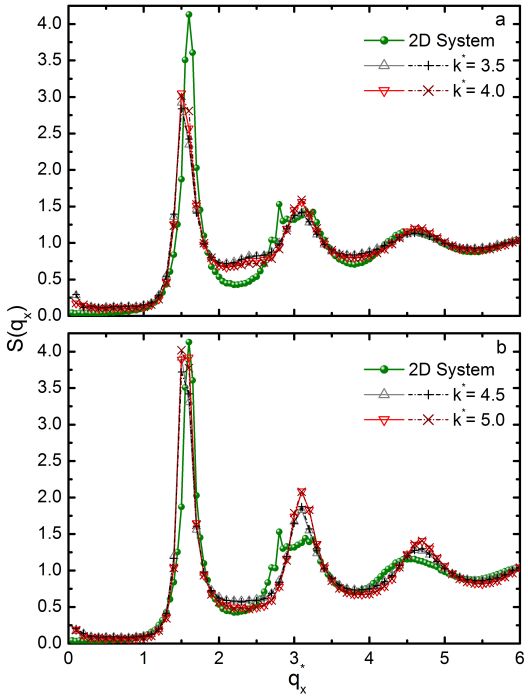

Figure 5.15: Structure factor, $S(q_x)$, along the x-direction for charged colloids in the strong confinement regime. Triangles: without HI, stars: with HI.

The angular distribution of the first-neighbor layer, for weak and moderate confinement, is shown in Fig. 5.16. Here, one starts from a clear hexagonal-like distribution to a more disordered structure characterized by a loss in the angular localization; the change in the peaks in Fig. 5.16a shows that the hexagonal phase is lost when k^* increases. In Fig. 5.16b the peaks become sharper, reflecting that particles are more localized. Besides, the peaks are rotated with respect to the 2D homogeneous reference system and show almost the same distribution as in the superparamagnetic case. At strong confinement, the layer behaves in a similar fashion as the distribution seen in Fig. 5.11 (data not shown).

The structural phase diagram for the charged colloidal system is explicitly shown in Fig. 5.17. There, we summarize the dimensional variations and the structural phases observed as a function of the degree of confinement. We should emphasize that, in comparison to the superparamagnetic system, the q2D window is characterized with a re-entrant freezing, the transition from q2D to q1D is described by a re-entrant melting effect, whereas the q1D window is wider with a continuous freezing. Additionally, in contrast with the superparamagnetic suspension, charged colloids inside a parabolic potential can reach the super-cooled liquid state. Thus, an important conclusion is that the structural phases depend on the details of the inter-particle potential.

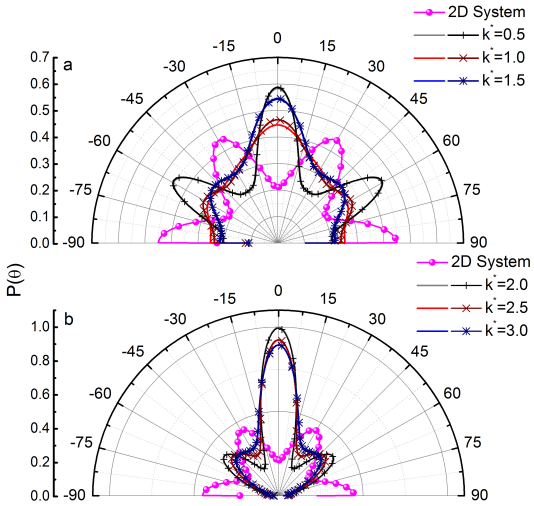

Figure 5.16: Angular probability, $P(\theta)$, of the first layer of neighbors for charged colloids in the weak and intermediate confinement regimes. Triangles: without HI, stars: with HI.

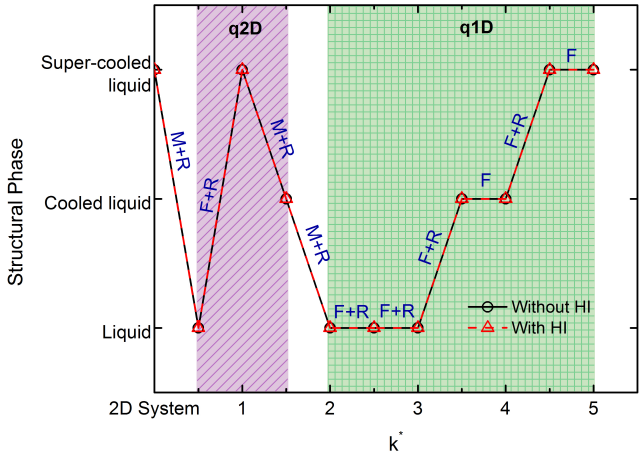

Figure 5.17: Structural phase diagram of the charged colloidal system. Horizontal axis denotes the value of the reduced trap stiffness, $k\alpha^2/k_BT$. Vertical axis indicates the structural phase transitions found through the analysis of the $S(q_x^{max})$. The letters M and F stand for a *melting*- and *freezing*-like transitions, respectively. The letter R indicates that there is a re-ordering in the angular probability of the first layer of neighbors. The regions 2D, q2D, q1D and 1D were found by calculating L_y^{max} (see Fig. 5.4) and taking into account the definition introduced in Table 5.1. Symbols correspond to Brownian dynamics simulations with (open triangles) and without (open circles) HI.

5.4 CONCLUDING REMARKS OF CHAPTER 5

In the present Chapter, we have explicitly shown that structural transitions occur in interacting colloidal systems subjected to a parabolic external field. By increasing the trap stiffness, we found a loss (gain) of structural ordering classified as *melting*-like (*freezing*-like). These findings open up the possibility of experimentally exploring the rich scenario of structural phases by confining the suspension in, for example, optically created energy landscapes.

In particular, we analyzed the angular ordering of the first layer of neighbors, which helped us in the characterization of the structural phase transitions. Superparamagnetic particles showed smooth transitions between super-cooled liquid, cooled-liquid and liquid structural phases, while the system of Yukawa particles suddenly jumped from super-cooled liquid to liquid (and viceversa) with a small increase of the trap stiffness. We also found that, independently of the interparticle potential, the HI are totally dissipated in the y-direction but in the x-direction allow the particles to be less localized in a given configuration and, consequently, keeps the system in a more liquid-like state as shown by the behavior of $S(q_x)$.

Last, but not least, we should emphasize that our study can give a better understanding of the structural signatures of interacting particles in either thin cavities or geometrically restricted environments, such as blood in veins, flows of substances through organs, particles located in zeolites, just to mention a few. In the aforementioned systems, the dynamical behaviour clearly deserves a special attention; results in this direction will be published elsewhere. The complete dynamical state diagram of the colloidal systems analyzed here would shed light on the structure and dynamical behavior of more complex systems under crowded or highly confined conditions. This information is of particular interest for a broad community of soft condensed matter.

BIBLIOGRAPHY

[1] S. D. Savage, M. A. Wilson, M. A. Carter, W. D. Hoff, C. Hall and B. McKay, *Journal of Physics D: Applied Physics*, 2008, **41**, 055402.

[2] J. A. Schafer, *Kidney International*, 2004, **66**, S20 – S27.

[3] J. L. McWhirter, H. Noguchi and G. Gompper, *PNAS*, 2009, **106**, 6039–6043.

[4] A. Granéli, C. C. Yeykal, R. B. Robertson and E. C. Greene, *PNAS*, 2006, **103**, 1221–1226.

[5] M. Tokarz, B. Åkerman, J. Olofsson, J.-F. Joanny, P. Dommersnes and O. Orwar, *PNAS*, 2005, **102**, 9127–9132.

[6] C. Dellago and G. Hummer, *Phys. Rev. Lett.*, 2006, **97**, 245901.

[7] M. Długosz and J. Trylska, *BMC Biophysics*, 2011, **4**, 3.

[8] J. Kärger, *Adsorption*, 2003, **9**, 29–35.

[9] D. Dubbeldam, E. Beerdsen, S. Calero and B. Smit, *PNAS*, 2005, **102**, 12317–12320.

[10] J. Köfinger, G. Hummer and C. Dellago, *PNAS*, 2008, **105**, 13218–13222.

[11] K. K. Mon and J. K. Percus, *J. Chem. Phys.*, 2002, **117**, 2289–2292.

[12] A. Das, S. Jayanthi, H. S. M. V. Deepak, K. V. Ramanathan, A. Kumar, C. Dasgupta and A. K. Sood, *ACS Nano*, 2010, **4**, 1687–1695.

[13] D. Chaudhuri and S. Sengupta, *J. Chem. Phys.*, 2008, **128**, 194702_1–194702_12.

[14] M. Chávez-Páez, M. Medina-Noyola and M. Valdez-Covarrubias, *Phys. Rev. E*, 2000, **62**, 5179.

[15] K. Binder, Y. Chui, P. Nielaba, A. Ricci and S. Sengupta, *Nanophenomena at Surfaces*, 2011, 1–18.

[16] A. Imperio, J. Padding and W. Briels, *arXiv preprint arXiv:1103.4939*, 2011.

[17] M. Gordillo, B. Martínez-Haya and J. Romero-Enrique, *J. Chem. Phys.*, 2006, **125**, 144702.

[18] W. Irvine and V. Vitelli, *Soft Matter*, 2012.

[19] E. Oğuz, R. Messina and H. Löwen, *EPL (Europhysics Letters)*, 2011, **94**, 28005.

[20] N. Saklayen, G. Hunter, K. Edmond and E. Weeks, *arXiv preprint arXiv:1209.1108*, 2012.

[21] J.-A. Garate, N. J. English and J. M. D. MacElroy, *J. Chem. Phys.*, 2009, **131**, 114508.

[22] J. Palmer, J. Moore, J. Brennan and K. Gubbins, *Adsorption*, 2011, **17**, 189–199.

[23] T. Mutat, J. Adler and M. Sheintuch, *J. Chem. Phys.*, 2012, **136**, 234902.

[24] F. Eever, *Europhys. Journal E*, 2013, **X**, X.

[25] S. Ross and E. Morrison, *Colloidal systems and interfaces*, John Wiley and Sons, New York, NY (US), 1988.

[26] A. Yethiraj, *Soft Matter*, 2007, **3**, 1099–1115.

[27] G. Piacente, I. V. Schweigert, J. J. Betouras and F. M. Peeters, *Solid state communications*, 2003, **128**, 57–61.

[28] G. Piacente, I. V. Schweigert, J. J. Betouras and F. M. Peeters, *Physical Review B*, 2004, **69**, 045324.

[29] W. Yang, V. Misko, K. Nelissen, M. Kong and F. Peeters, *Soft Matter*, 2012, **8**, 5175–5179.

[30] P. K. Ghosh, V. R. Misko, F. Marchesoni and F. Nori, *Physical review letters*, 2013, **110**, 268301.

[31] M. Clerc, P. Cordero, J. Dunstan, K. Huff, N. Mujica, D. Risso and G. Varas, *Nature physics*, 2008, **4**, 249–254.

[32] J. K. G. Dhont, *An Introduction to Dynamics of Colloids*, Elsevier, 1996.

[33] G. Nägele, *Phys. Rep.*, 1996, **272**, 215.

[34] B. Rinn, K. Zahn, P. Maass and G. Maret, *EPL (Europhysics Letters)*, 1999, **46**, 537.

[35] E. C. Euán-Díaz, V. R. Misko, F. M. Peeters, S. Herrera-Velarde and R. Castañeda-Priego, *Physical Review E*, 2012, **86**, 031123.

[36] E. C. Euán-Díaz, V. R. Misko, F. M. Peeters, S. Herrera-Velarde and R. Castañeda-Priego, *submitted (2013)*.

[37] S. A. Rice, *Chemical Physics Letters*, 2009, **479**, 1 – 13.

[38] B. Cui, B. Lin, S. Sharma and S. Rice, *J. Chem. Phys.*, 2002, **116**, 3119–3127.

[39] B. Lin, M. Meron, B. Cui, S. Rice and H. Diamant, *Phys. Rev. Lett.*, 2005, **94**, 216001.

[40] B. Cui, B. Lin and S. A. Rice, *J. Chem. Phys.*, 2001, **114**, 9142–9155.

[41] S. Novikov, S. Rice, B. Cui, H. Diamant and B. Lin, *Phys. Rev. E*, 2010, **82**, 031403.

[42] X. Xu, S. Rice, B. Lin and H. Diamant, *Phys. Rev. Lett.*, 2005, **95**, 158301.

[43] D. Valley, S. Rice, B. Cui, H. Ho, H. Diamant and B. Lin, *J. Chem. Phys.*, 2007, **126**, 134908.

[44] E. Wonder, B. Lin and S. Rice, *Phys. Rev. E*, 2011, **84**, 041403.

[45] X. Xu, B. Lin, B. Cui, A. Dinner and S. Rice, *J. Chem. Phys.*, 2010, **132**, 084902.

[46] T. Stratton, S. Novikov, R. Qato, S. Villarreal, B. Cui, S. Rice and B. Lin, *Phys. Rev. E*, 2009, **79**, 031406.

[47] B. Lin, D. Valley, M. Meron, B. Cui, H. Ho and S. Rice, *The Journal of Physical Chemistry B*, 2009, **113**, 13742–13751.

[48] M. D. Carbajal-Tinoco, R. Lopez-Fernandez and J. L. Arauz-Lara, *Physical review letters*, 2007, **99**, 138303.

[49] J. Baumgartl, J. L. Arauz-Lara and C. Bechinger, *Soft Matter*, 2006, **2**, 631–635.

[50] J. Santana-Solano and J. L. Arauz-Lara, *Physical review letters*, 2001, **87**, 038302.

[51] R. Bubeck, C. Bechinger, S. Neser and P. Leiderer, *Physical review letters*, 1999, **82**, 3364.

[52] S. Neser, C. Bechinger, P. Leiderer and T. Palberg, *Physical review letters*, 1997, **79**, 2348.

[53] Q.-H. Wei, C. Bechinger, D. Rudhardt and P. Leiderer, *Physical review letters*, 1998, **81**, 2606.

[54] Q.-H. Wei, C. Bechinger and P. Leiderer, *Science Signaling*, 2000, **287**, 625.

[55] D. G. Grier, *Nature*, 2003, **424**, 810–816.

[56] J. E. Curtis, B. A. Koss and D. G. Grier, *Optics Communications*, 2002, **207**, 169–175.

[57] E. R. Dufresne and D. G. Grier, *Review of scientific instruments*, 1998, **69**, 1974–1977.

[58] J. C. Crocker and D. G. Grier, *Physical review letters*, 1996, **77**, 1897.

[59] M. C. Jenkins and S. U. Egelhaaf, *Journal of Physics: Condensed Matter*, 2008, **20**, 404220.

[60] M. C. Jenkins and S. U. Egelhaaf, *Advances in colloid and interface science*, 2008, **136**, 65–92.

[61] K. Sandomirski, E. Allahyarov, H. Löwen and S. U. Egelhaaf, *Soft Matter*, 2011, **7**, 8050–8055.

[62] E. M. Furst, *Current opinion in colloid & interface science*, 2005, **10**, 79–86.

[63] G. Milne, K. Dholakia, D. McGloin, K. Volke-Sepulveda and P. Zemánek, *Optics express*, 2007, **15**, 13972–13987.

[64] K. Volke-Sepúlveda, S. Chávez-Cerda, V. Garcés-Chávez and K. Dholakia, *JOSA B*, 2004, **21**, 1749–1757.

[65] A. V. Arzola, K. Volke-Sepúlveda and J. L. Mateos, *Physical review letters*, 2011, **106**, 168104.

[66] A. V. Arzola, K. Volke-Sepúlveda and J. L. Mateos, *Opt. Express17*, 2009, 3429–3440.

[67] J. C. Meiners and S. R. Quake, *Phys. Rev. Lett.*, 1999, **82**, 2211.

[68] W. P. Ferreira, G. A. Farias and F. M. Peeters, *Journal of Physics: Condensed Matter*, 2010, **22**, 285103.

[69] J. C. N. Carvalho, K. Nelissen, W. P. Ferreira, G. A. Farias and F. M. Peeters, *Phys. Rev. E*, 2012, **85**, 021136.

[70] F. F. Munarin, W. P. Ferreira, G. A. Farias and F. M. Peeters, *Phys. Rev. E*, 2008, **78**, 031405.

[71] W. Yang, K. Nelissen, M. Kong, Y. Li and Y. Tian, *The European Physical Journal B-Condensed Matter and Complex Systems*, 2011, 1–7.

[72] W. P. Ferreira, F. F. Munarin, G. A. Farias and F. M. Peeters, *Journal of Physics: Condensed Matter*, 2006, **18**, 9385.

[73] W. P. Ferreira, J. C. N. Carvalho, P. W. S. Oliveira, G. A. Farias and F. M. Peeters, *Phys. Rev. B*, 2008, **77**, 014112.

[74] J. E. Galván-Moya, K. Nelissen and F. M. Peeters, *Phys. Rev. B*, 2012, **86**, 184102.

[75] W. Yang, K. Nelissen, M. Kong, Z. Zeng and F. M. Peeters, *Phys. Rev. E*, 2009, **79**, 041406.

[76] D. Lucena, D. V. Tkachenko, K. Nelissen, V. R. Misko, W. P. Ferreira, G. A. Farias and F. M. Peeters, *Phys. Rev. E*, 2012, **85**, 031147.

[77] D. Lucena, W. P. Ferreira, F. F. Munarin, G. A. Farias and F. M. Peeters, *arXiv preprint arXiv:1209.6472*, 2012.

[78] J. C. N. Carvalho, W. P. Ferreira, G. A. Farias and F. M. Peeters, *Phys. Rev. B*, 2011, **83**, 094109.

[79] M. Manghi, X. Schlagberger, Y.-W. Kim and R. R. Netz, *Soft Matter*, 2006, **2**, 653–668.

[80] D. L. Ermak and J. A. McCammon, *J. Chem. Phys.*, 1978, **69**, 1352.

[81] A. Yethiraj, *Soft Matter*, 2007, **3**, 1099–1115.

[82] K. Zahn, J. M. Méndez-Alcaraz and G. Maret, *Phys. Rev. Lett.*, 1997, **79**, 175–178.

[83] S. Bleil, H. H. von Grünberg, J. Dobnikar, R. Castañeda-Priego and C. Bechinger, *EPL (Europhysics Letters)*, 2006, **73**, 450.

[84] S. Herrera-Velarde and R. Castañeda-Priego, *J. Phys.: Cond. Matt.*, 2007, **19**, 226215.

[85] S. Herrera-Velarde and R. Castañeda-Priego, *Phys. Rev. E*, 2008, **77**, 041407.

[86] K. Zahn, R. Lenke and G. Maret, *Phys. Rev. Lett.*, 1999, **82**, 2721–2724.

[87] N. Hoffmann, F. Ebert, C. N. Likos, H. Löwen and G. Maret, *Phys. Rev. Lett.*, 2006, **97**, 078301.

[88] P. Keim, G. Maret and H. H. von Grünberg, *Phys. Rev. E*, 2007, **75**, 031402.

[89] P. Debye and E. Hückel, *Physikalische Zeitschrift*, 1923, **24**, 185.

[90] E. J. W. Verwey and Overbeek, *Theory of the Stability of Lyophobic Colloids*, Elsevier Publishing Company Inc., Amsterdam, 1948.

[91] K. Dholakia and T. Čižmár, *Nat Photon*, 2011, **5**, 335–342.

[92] S. Herrera-Velarde, E. C. Euán-Díaz, F. Córdoba-Valdés and R. Castañeda-Priego, *Journal of Physics: Condensed Matter*, 2013, **25**, 325102.

[93] M. P. Allen and D. J. Tildesley, *Computer simulation of liquids*, Clarendon Press, New York, NY, USA, 1989.

[94] J. P. Hansen and I. R. McDonald, *Theory of Simple Liquids*, Academic Press, 1986.

[95] D. Tkachenko, V. Misko and F. Peeters, *Physical Review E*, 2009, **80**, 051401.

[96] J.-P. Hansen and L. Verlet, *Phys. Rev.*, 1969, **184**, 151–161.

[97] H. Löwen, T. Palberg and R. Simon, *Phys. Rev. Lett.*, 1993, **70**, 1557–1560.

[98] J. Q. Broughton, G. H. Gilmer and J. D. Weeks, *Phys. Rev. B*, 1982, **25**, 4651–4669.

[99] S. Herrera-Velarde, A. Zamudio-Ojeda and R. Castañeda-Priego, *The Journal of Chemical Physics*, 2010, **133**, 114902.

[100] S. Herrera-Velarde and R. Castañeda-Priego, *Phys. Rev. E*, 2009, **79**, 041407.

6

SELF-DIFFUSION OF INTERACTING COLLOIDS IN A PARABOLIC POTENTIAL

"Re

doing."
-Wernher von Braun

The diffusion of colloids in geometrically restricted environments has been widely studied and the interest on it has grown during the last few decades. From technological point of view, it is crucial to understand the rate and extent of transport of macro-molecules and other solutes into porous environments like the fibers and cellulosic materials due to their importance for the industry of paper-making, textiles, and chromatography [1]. Nowadays, it is known that factors that limit the particle transport into pores can involve both thermodynamics and kinetics processes, and physical barriers [1].

Natural environments also offer the opportunity to study transport of particles through restricted paths, which usually lead to anomalous diffusion. For example, the formation of river networks, frost on glass or geological veins are processes whose diffusion is dominated by the transport of particles rather than convection [2], just to mention a few. Some patterns occurring in these systems can be modeled as a diffusion-limited aggregation process [2]. Moreover, conservation of clean underground river banks is now a top priority. Recently, complex theoretical dynamical models based on the mass balance equation [3] have been developed to describe the contaminant transport in the presence of dissolved organic matter and bacterial particles in physically heterogeneous aquifers during riverbank filtration [3].

On the other hand, colloids have been used to understand both biophysical and physicochemical processes carried out by our body. For instance, biochemical reactions in living systems occur in complex heterogeneous media in highly crowded conditions that non-specific interactions between macromolecules may hider diffusion. This is a major process that determines metabolism, transport, and signaling between cells [4]. Furthermore, the interaction with the small cages formed by the neighboring particles increases the stability of proteins [5]. Moreover, in medicine, the degree of confinement is one of

the keys to understand the structure and dynamics of the red-blood cells [6]. Understanding the diffusion of cerebrospinal fluid in our brain has been extremely important due to the fact that it can shed some light on the mechanisms of neurological diseases like vanishing white matter [7], which develops when restricted and anomalous diffusion is found in relatively spared regions with high cellularity [8, 9]. Hence, transport of particles in highly confinement conditions is a topic of broad interest for the Soft Matter community.

Colloidal particles exhibit solvent-mediated indirect interactions typically called hydrodynamic interactions (HI). Specifically, under restricted geometries, it has been found that the dependence of the self-diffusion coefficient on the HI is much stronger than in unbounded fluid [10, 11]. However, strong charged particles behave qualitatively differently: far field HI, prevailing on systems of strongly repulsive interactions, support the diffusion of a particle out of its dynamic cage created by its neighboring particles. This process leads to a hydrodynamic enhancement of the mean square displacement (MSD) [12–15]. Although, the complexity of the HI has, so far, partially precluded the full understanding of the long-time dynamics of concentrated interacting colloidal suspensions [16–18].

One special concern is the effect that confining mechanisms, which restrict the accessible space of the particles, has a on the colloidal dynamics [19–21]. Confinement allows to probe order-disorder phenomena via the sensibility to boundary conditions [21]. For highly confined systems, like circular or cylindrical cavities, it has shown that such systems exhibit slow dynamics (single-file diffusion) and even freezing-like transitions occur [22–26]. One question that rises naturally is related with effects associated with the degree of confinement, i.e.,, when it becomes either less or more severe. If the confinement is relaxed, it is expected that at some point the system should cross over to ordinary Fickian diffusion at long time scales [27–29]. Rice *et. al.* [30] found that when the accessible space is changed, certain properties of the 2D confined suspensions exhibit 2D features, whereas others deviate from the 2D and the 1D descriptions [27, 30].

From experimental point of view, confined colloidal systems have been extensively studied two decades ago [31–49]. Part of the experimental work has been focused on the self-assembly structures [50, 51] and also on the understanding of hydrodynamic interactions of the particles in channels where their accessible space ranges from q1D to q2D [30, 37, 38, 40, 52–57]. In most cases, the wall-particle hydrodynamic interactions play an important role on the particle transport and hide the effects associated only to the particle-particle interactions [58].

One way to avoid the complex hydrodynamic contribution due to the wall is by using an energetic trap that only interacts with the colloids. This kind of external field is experimentally achievable through

the interference of laser beams [59, 60]. The same model has been theoretically used by some of us to explore the structural properties and the external field leads to phase transitions in systems composed of interacting particles [59, 61–71].

Recently, we studied the structural properties of interacting colloids confined in a parabolic trap [72]. We found that by changing the trap stiffness, one is able to control the dimensionality of the system and in consequence, a rich scenario of structural phases appears. Now, we focus on the effect of the confinement on the dynamics of the same systems that undergo structural phase transitions. It is important to mention that, even when the structure is the same, the HI could modify the dynamical scenario of colloidal systems[73, 74]. We report the dynamics at short, intermediate and long-times through the analysis of the mean square displacement (MSD).

The manuscript is organized as follows. The colloidal model is briefly mentioned in Section 6.1. We also describe the equations of motion, the inter-particle potential and the functional form of the parabolic trap. The physical quantities are described in Section 6.1.5. We discuss the dynamics of the system at different temporal regions in Section 6.2. Finally, we give our concluding remarks in Section 6.3.

6.1 THEORETICAL BACKGROUND

6.1.1 *Equations of motion and Brownian dynamics simulations*

The description of Brownian motion for time scales $t \gg \tau_B$ (overdamped limit), where τ_B is the relaxation time of the particle momenta, is given by the Langevin equation [75]

$$\frac{d\mathbf{r}_i}{dt} = \beta \sum_{j=1}^{N} [-\nabla_{\mathbf{r}_j} U(\mathbf{r}^N, t) + \mathbf{F}_j^{ext}(\mathbf{r}^N, t)] \cdot \mathbf{D}_{ij} + \sum_{j=1}^{N} \nabla_{\mathbf{r}_j} \cdot \mathbf{D}_{ij} + v_i(t), \tag{6.1}$$

where $\beta \equiv (k_B T)^{-1}$ is the inverse thermal energy, with k_B and T being the Boltzmann constant and absolute temperature, respectively, $U(\mathbf{r}^N, t)$ is the total potential energy for the given particle configuration and the external force on the particle j is given by $\mathbf{F}_j^{ext}(\mathbf{r}^N, t) = -\nabla_{\mathbf{r}_j} U^{ext}(\mathbf{r}^N, t)$, where $U^{ext}(\mathbf{r}^N, t)$ is the external energy potential. $\mathbf{D}_{ij}$ is the diffusion tensor and $v(t)$ is the Langevin random velocity that contains the action of a thermal bath and obeys the fluctuation-dissipation relationship,

$$\langle v_i(t) v_j(t') \rangle = 2\mathbf{D}_{ij}\delta(t - t'), \tag{6.2}$$

where $\delta(t - t')$ is the Kronecker delta.

The algorithm proposed by Ermak and McCammon for solving the Langevin equation (6.1) [76] together with the fluctuation-dissipation

relationship given by equation (6.2) are used to sample the trajectory of any colloidal particle. Both equations constitute the standard Brownian dynamics method [76]. HI are explicitly included at the level of the Rotner-Prager (RP) diffusion tensor [74, 75, 77],

$$\begin{aligned} \mathbf{D}_{ii} &= D_0\mathbf{I} = \tfrac{k_B T}{6\pi\eta a}\mathbf{I}, \\ \mathbf{D}_{ij} &= (k_B T/8\pi\eta r_{ij})(\mathbf{I} + \tfrac{\mathbf{r}\otimes\mathbf{r}}{r_{ij}^2}) + \\ &\quad k_B T(a^2/4\pi\eta r_{ij}^3)(\tfrac{\mathbf{I}}{3} - \tfrac{\mathbf{r}\otimes\mathbf{r}}{r_{ij}^2}), \end{aligned} \tag{6.3}$$

where η is the solvent viscosity, $\mathbf{I}$ is the unitary matrix and D_0 stands for the diffusion constant of a single isolated particle in an unbounded fluid. One notes that the RP diffusion tensor includes the lowest corrections of particle size over the Oseen tensor description [75]. The diffusion tensor $\mathbf{D}_{ij}$ introduces long-ranged interactions and couples distant particles. The stochastic term, equation (6.2), is numerically implemented by a Cholesky decomposition[77, 78]. We are dealing with the dynamics of non-deformable particles in an unbounded fluid. In this case, one can straightforwardly check that $\nabla_{\mathbf{r}_j} \cdot \mathbf{D}_{ij} = 0$.

6.1.2 *Superparamagnetic and Yukawa potentials*

From a scientific point of view, colloidal dispersions can be used as model systems for soft condensed matter. This is due to the fact that their physical properties can be studied simultaneously, i.e., in real time, by using three different complementary methods; namely, experiment, theory, and computer simulations. The specific details of both superparamagnetic and Yukawa colloidal systems studied in this work have been reported elsewhere [73, 74, 79–82], thus, we briefly discuss their main features.

Superparamagnetic colloids at the air-water interface have served as excellent models to investigate fundamental properties that are related to the role of hydrodynamics and melting transition, as well as the elastic behaviour and the phonon band structure in two-dimensional crystals [73, 74, 83–85]. In such an experimental model, an external and constant magnetic field is applied in the perpendicular direction of the interface. This leads to a long-range magnetic dipole-dipole interaction between colloids of the form [73, 74, 81]

$$\beta u(r) = \frac{\Gamma(\frac{d}{a})^3}{r^3}, \tag{6.4}$$

where r is the separation between two colloids in units of the particle radius, $a = 2.35\mu m$ [73]. $\Gamma = \beta(\frac{--_0}{4\pi})\rho^{(3/2)}\chi_{eff}^2 B^2$ is the mean interaction energy or inter-particle strength normalized with the thermal energy, B is the magnitude of the applied magnetic field, $--_0$ is the magnetic constant and χ_{eff} is the effective magnetic susceptibility of the particles. The units of $\beta(\frac{--_0}{4\pi})\chi_{eff}^2 B^2$ are length to the cube,

although the term $\rho^{(3/2)}$ makes it non-dimensional scaled with the mean inter-particle distance, $d = 1/\sqrt{\rho}$, where ρ is the particle number density. A variation in Γ can be related with a change in B, T, and/or ρ [74, 81]. In particular, for the superparamagnetic system, the average packing fraction of colloids is $\phi = 0.1205$, defined as $\phi = \pi a^2 \rho$, and the inter-particle strength is $\Gamma(\frac{d}{a})^3 = 1353.59$. The use of superparamagnetic colloids makes possible a straightforward comparison between theoretical predictions and experiments.

We also consider colloids interacting with a repulsive screened Coulomb potential (Yukawa). For distances $r < \sigma (= 2a)$, the interaction is hard-core. For $r \geqslant \sigma$, two colloidal particles interact via the repulsive part of the DLVO pair potential, see, e.g., Refs. [80, 86, 87],

$$\beta u(r) = Z_{\text{eff}}^2 \lambda_B \left[\frac{e^{\kappa a}}{1+\kappa a}\right]^2 \frac{e^{-\kappa r}}{r}, \tag{6.5}$$

where Z_{eff} is the effective charge, κ is the Debye screening parameter and λ_B is the Bjerrum length [86, 87]. The potential parameters used in equation (7.1) were taken from [79]; $a = 1.4\mu m$, $Z_{\text{eff}} = 5400$, $\lambda_B = 0.72$, and $\kappa^{-1} = 550$ nm. For charged colloids, the average packing fraction used in our calculations is $\phi = 0.1766$.

6.1.3 *External fields*

During the last decade, optical traps have been widely used in colloidal systems as a tunable substrate. Scientists have found that their effect on the dynamics and the structural configuration is fascinating [88–90]. The advantage of optical trapping is two-fold: first, it allows us to confine particles in small regions of space, and second, it also serves to control the position of colloids with high precision. Thus, it can be considered as a well-controlled particle-substrate potential. Then, if one is able to understand the interaction between the laser fields and the colloids [90], its incorporation in the theoretical models and computer simulations facilitates the study of the physical properties of the system, see, e.g., Refs. [89, 90] and references therein.

The simplest potential trap can be modeled as a harmonic potential. In this work, we introduce an external potential to confine the particles in one direction. Mathematically, this potential takes the following functional form,

$$u^{ext}(\mathbf{r}_i) = \frac{1}{2} k y_i^2, \tag{6.6}$$

with k being the trap stiffness [91].

6.1.4 *Constant density*

The parabolic potential (6.6) confines the colloidal particles along the y-direction, thus, periodic boundary conditions are applied only in

the x-direction. However, since we keep the particle density constant, ρ, we have to find the appropriate box length in the x-direction, L_x, for each value of k; the latter determines the length of confinement in the y-direction. Technically, this is done by monitoring the average maximum displacement, L_y^{max}, allowed by the external potential. Thus, $L_x = N/(\rho L_y^{max})$, where N is the number of particles used in the simulations. We have demonstrated that L_x can be roughly estimated using an energetic criterion [72].

Once the value of L_y^{max} is calculated for a given trap stiffness, k, we let the system evolve during 1.5×10^6 time steps before averages are computed. The number of time steps of the average loop is 1.5×10^7. We save the configurations every 10 time steps. Thus, 1.5×10^6 configurations are used to measure the observables. The radius of the particles, a, and the thermal energy, $k_B T$, are taken as the scaling factor for all units of distance and energy, respectively. From now on, all quantities are expressed in reduced units. Due to the explicit incorporation of HI, $N = 800$ particles are used in the simulation. The reduced time step, Δt, is chosen as $\Delta t D_0/a^2 = 0.0002$, where t is the time.

6.1.5 *Dynamical observables*

Due to the fact that the mobility of a colloidal particle reflects the mechanical and dynamical properties of the micro– and macro–environment (dynamical cages formed by the first layer of neighbors and the bulk, respectively) where it is embedded, we calculate the mean-square displacement (MSD) [80]

$$W_{r_i}(t) = \langle \Delta r_i(t)^2 \rangle = \frac{1}{N} \sum_{i=1}^{N} \langle [r_i(t) - r_i(0)]^2 \rangle, \tag{6.7}$$

where $r_i = x, y$ and $\langle \cdots \rangle$ denotes an ensemble average. The long-time regime of the MSD for a 2D colloidal system can be described through the relation $W(t) = F^{(2D)} \cdot t$, where $F^{(2D)}$ is the mobility factor; it is directly connected with the long-time self diffusion coefficient $F^{(2D)} = D_L$ [75]. When one is considering a pure 1D system the dynamics is slower, thus, the relation becomes $W(t) = F^{(1D)} \cdot \sqrt{t}$; the mobility factor is $F^{(1D)} = \rho^{-1} \sqrt{D_0 S(q) H(q)/\pi}|_{q \to 0}$, where D_0, $S(q)$ and $H(q)$ are the free-particle diffusion coefficient, the structure factor and the hydrodynamic factor, respectively [92]. When the system is held in an external field which induces a geometrical restriction the relation could take the form $W(t) = F \cdot t^{\alpha}$ [93].

6.2 MEAN-SQUARE DISPLACEMENT

Our attention is mainly focused on the changes of the dynamical behavior caused by the confinement; the latter imposed by a parabolic

trap. By keeping the density constant, we reduce the parameter spectrum that could lead to a reacher scenario. Moreover, the effects associated to density changes are avoided. The results of a reference 2D system are shown for each inter–particle potential; *i.e.*, the system consists of interacting particles without external field and with periodic boundary conditions in both directions.

For the sake of the discussion, from now on, we use the following reduced units: $r^* \equiv r/a$, $k^* \equiv ka^2/k_BT$, $t^* \equiv tD_0/a^2$, $W^*(t) \equiv W(t)/a^2$.

6.2.1 *Superparamagnetic colloids*

It is important to point out that the particle dynamics is analyzed through different conditions imposed by the external field, whereas the structure has been reported elsewhere [72]. One may think that when colloids are highly ordered in rows, the particle diffusion behaves as in a typical single-file dynamics or 1D file-server-like character, as it was called by Cui *et. al.* [94]. These authors pointed out that for dense q2D colloidal systems, by virtue of exchanges of particles between the ordered domains, the time dependence has mixed character [94]. This can be better described in Fig. 6.1, which shows the MSD in the x-direction of a 2D colloidal superparamagnetic system in a log-log scale. In most cases, the MSD as a function of time can be characterized in three regions. A *linear region* in which the MSD is proportional to the time; this behavior results from particle displacements within a cage of fluctuating neighbors. Then, one can find the *transient region*, where the system goes from a normal diffusion behavior to the collective behavior, the present region is characterized by a not easy dependence of MSD on the time. Finally, at somewhat longer time, the MSD has a sublinear dependence on time and for most of the cases with a decreased mobility factor. This temporal behavior has been associated with a single-file-like contribution to MSD arising from correlated motion in the more disordered regions which is the *long-time region* [95].

The MSD curves for $k^* = 0.5,\ 3.0,\ 5.0$ in the x–direction is shown in Fig. 6.1. In absence of HI, the dynamics at low trap stiffness values, along the x-direction, is similar to the 2D-case. However, for larger values of k^*, the MSD changes its functional form, being less diffusive in the same time interval for $k^* = 3.0$ and more diffusive for $k^* = 5.0$ when compared with the 2D case. Fig. 6.1 also shows the results including HI, which are indicated with open squares. The results qualitatively present similar behaviors to those described before. Quantitatively, the MSDs are larger when HI are included; the enhancement in the particle diffusion has been discussed a few years ago by some authors [10, 73, 74, 82, 96] We will discuss in detail the role of HI in the following paragraphs. The inset of Fig. 6.1 shows the

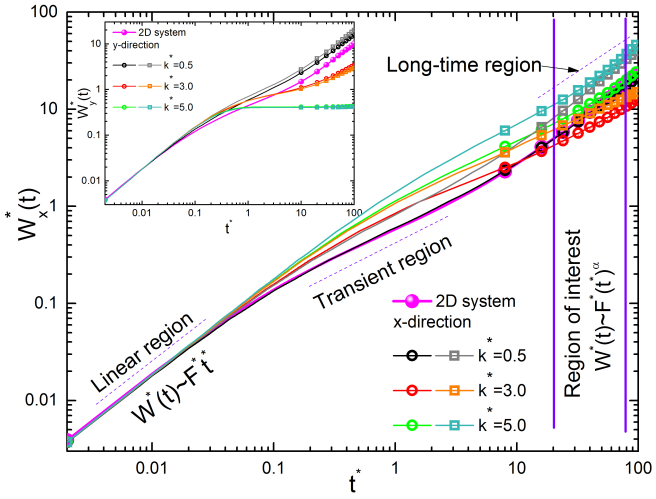

Figure 6.1: Mean-square displacement of superparamagnetic colloids in the x-direction for the 2D system ($k^* = 0$) and for $k^* = 0.5, 2.5$ and 5.0. Beads: 2D system, open circles: results without HI, open squares: results with HI. Inset: MSD in the y-direction for the 2D system and for $k^* = 0.5, 2.5$ and 5.0. Solid beads: 2D system without HI, open circles: results without HI, open squares: results with HI.

MSD in the y-direction. For $k^* = 0.5$, without HI, the particles diffuse faster compared with the 2D case. However, for $k^* = 3.0$ the diffusion is suppressed; smaller slopes than the previous case are found in the transient region. When $k^* = 5.0$, the case corresponds structurally to a 1D system, as was discussed in Ref. [72], the MSD curve shows at the beginning normal diffusion but after a given time the particles have reached their maximum displacement and, as a consequence, after a longer time the MSD curve shows a plateau. When HI are included, the most significant contribution in the y-direction is found when the system is less confined $k^* = 0.5$. Thus, when the degree of confinement grows, the contribution of the HI can be neglected at long-times in the direction of the confinement.

The subdiffusive character of the MSD at long-times (indicated in Fig. 6.1 as "region of interest") is given by the parameter α, which is computed by fitting the MSD curve to the expression $W(t) = Ft^{\alpha}$. Fig. 6.2 shows the values of α in both x and y directions as a function of k^*. In the 2D case ($k^* = 0$), normal diffusion is basically seen in both directions. We first discuss the cases without HI along the x-direction. For $k^* = 0.5$ the value of α_x is, as expected, similar to the 2D system, thus, particles perform normal diffusion. When k^* is increased, α_x shows a non-monotonic behavior. For $k^* = 1.0$, it has a value slightly smaller than in the 2D case, however, for $k^* = 1.5$ it takes a value similar to the one observed for $k^* = 0.5$. When $k^* = 2.0$, the single-file-like behavior starts to appear although the proper value of 0.5 is never reached. In this case, the distribution of the particles along

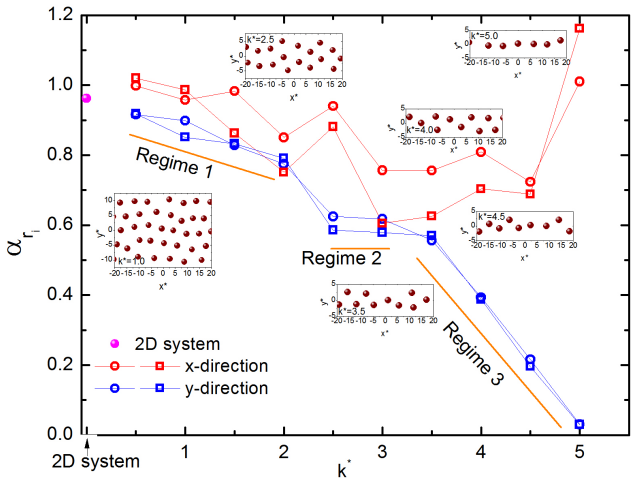

Figure 6.2: α_x and α_y for the superparamagnetic colloids described in Fig. 6.1. α is calculated from the long-time regime of the MSD: $W(t) = Ft^{\alpha}$. Solid beads: 2D system without HI, open circles: results without HI, open squares: results with HI. The solid lines are a guide to the eye. Insets: Equilibrium particle configurations of the system in a fraction of the space, specifically, for $k^* = 1.0, 2.5, 3.5, 4.0, 4.5, 5.0$.

the y-direction corresponds to three well-localized rows [72], whose energetic barriers imposed by the inter-particle interaction make hard the particle exchange among arrows. For $k^* = 2.5$, $\alpha_x = 0.947$ and the single-file-like dynamics is relaxed due to the fact that there are three rows but with a big probability of particle exchange. At higher trap stiffness values, in particular for $k^* = 3.0, 3.5$, the structure of the system is given by two well-defined rows (see Ref. [72]) and, thus, its contribution to the dynamics results in similar values for α_x. When $k^* = 4.0$ the particles can move from one to another file giving rise to an slightly increment of $\alpha_x \approx 0.8$. α_x shows its lowest value along the x-direction when $k^* = 4.5$ ($\alpha_x \approx 0.72$). When $k^* = 5.0$ the particles exhibit, again, normal diffusion due to the fact that the system is not highly structured and the accessible space in x–direction is larger compared with the previous cases

When HI are included, one finds that α_x follows the same functional dependence as in the case without HI. However, the values of k^* when HI are taken into account are smaller and, in consequence, the particle transport becomes considerably slower. This contra-intuitive behavior has also been found in 1D systems when they are coupled to sinusoidal external fields [82]. For the largest k^* analyzed, in contrast with the other values, we find evidence of super-diffusion, since $\alpha_x \approx 1.2$.

On the other hand, the value of the parameter α_y decreases due to the spatial restriction imposed by the external filed. This systematic reduction of the available space is reflected on the dynamics manly in

in three stages. At the first stage, that corresponds to $0.5 \leqslant k^* \leqslant 2.0$, the decay is almost linear in function of k^*. The second stage corresponds to $2.5 \leqslant k^* \leqslant 3.0$, where $\alpha_y \approx 0.6$. At this state, the system undergoes a structural transition from q2D to q1D [72]. The third stage takes place for $k^* > 3.0$, where the decay of α_y is again linear as k^* increases; the reduction of the available space in the y-direction thus induces a structural transition from two rows to one row. This affects the diffusion along the direction of confinement leading to value close to zero for α_y.

6.2.2 *Yukawa*

We also study the case of a system composed of Yulawa particles held in a parabolic trap. Fig. 6.3 shows the corresponding MSD in the x-direction. We notice that, within the temporal window explored, the diffusion at intermediate and long-times is larger than that for the full 2D case, although its dependence with k^* is certainly non-trivial. On the other hand, in the y-direction (see inset), the MSD at the same conditions of confinement is not strongly suppressed as in the case of superparamagnetic particles; the transition region takes place at longer times and higher values of the trap stiffness. This should be associated to the fact that at short-interparticle separations, the interaction among charged particles is stronger than the one for the superparamagnetic colloids [72]. Thus, larger values of the trap stiffness are needed to suppress the diffusion along the y-direction.

Fig. 6.4 shows the kind of sub-diffusion exhibited by the MSD within the region on interest indicated in Fig. 6.3. The point shown for the 2D system indicates that the system shows a slow dynamics $\alpha = 0.87 < 1$ because it is highly packed and close to the freezing point [95]. Comparing the evolution of the parameter α_x with the 2D in the case of neglecting HI, one finds that the system has two clear regimes. These regimes make a perfect correspondence with the structural evolution of the system presented in Ref. [72]. When the system is structurally in a q1D phase, $0.5 \leqslant k^* \leqslant 2.0$, $\alpha_x = 0.95$, which means that particles diffuse faster than in the 2D case. When k^* increases within the interval $2.5 \leqslant k^* \leqslant 5.0$, the system shows a q1D structure and this increases the single-file-like contribution to the MSD resulting in a non-monotonic reduction of α. When HI are taken into account, one finds that the stages previously discussed are not well-defined, although they preserve qualitatively the same behavior.

We turn out to analyze the behavior in the y-direction. First, there are no important differences at long-times between the approaches with and without HI. The parameter α_y decays as a function of k^*; diffusion is reduced by the confinement mechanism. Empirically, we find that α obeys a third-grade polynomial functional form. The evolution of the parameter α_y is smoother for the Yukawa particles

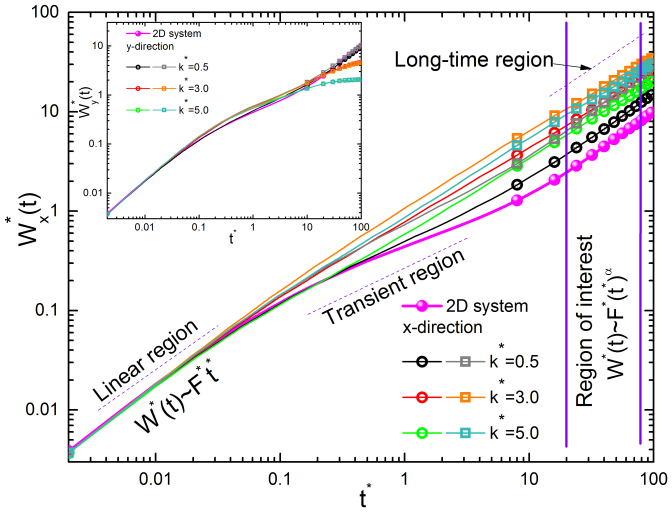

Figure 6.3: Mean-square displacement of Yukawa particle in the x-direction for the 2D system ($k^* = 0$) and $k^* = 0.5, 2.5$ and 5.0. Beads: 2D system, open circles: results without HI, open squares: results with HI. Inset: MSD in the y-direction for the 2D system ($k^* = 0$) and for $k^* = 0.5, 2.5$ and 5.0. Solid beads: 2D system without HI, open circles: results without HI, open squares: results with HI.

than the one for the superparamagnetic particles. One can relate this smoothness with the evolution of the energetic barriers that are created by the formation of the strata [72]. As k^* increases there is a smooth evolution of the energetic barriers imposed by the particle configurations, although for the superparamagnetic case the evolution of the barriers is dramatic, specially around the region where the q2D–q1D takes place [72].. For the Yukawa case, the possibility of particle exchange among the strata is larger than in the superparamagnetic case, which means that the diffusion along the y-direction is not as restricted as the previous case.

6.3 CONCLUDING REMARKS

We have theoretically studied the diffusive behavior of interacting colloids, at a constant density, confined in a external parabolic field. We found that when the degree of confinement is varied through the trap stiffness parameter, the system presents dynamical transitions at long times that exhibit normal, sub- and super-diffusive features. Most of these transitions are strongly associated with the structural variations undergone by the suspension.

Although we found that the HI are mainly dissipated in the y-direction, we observed that HI allow to fluidize the system, but, interestingly, we found a counter-intuitive behavior in the case of superparamagnetic particles, where HI are the responsible of the slowing

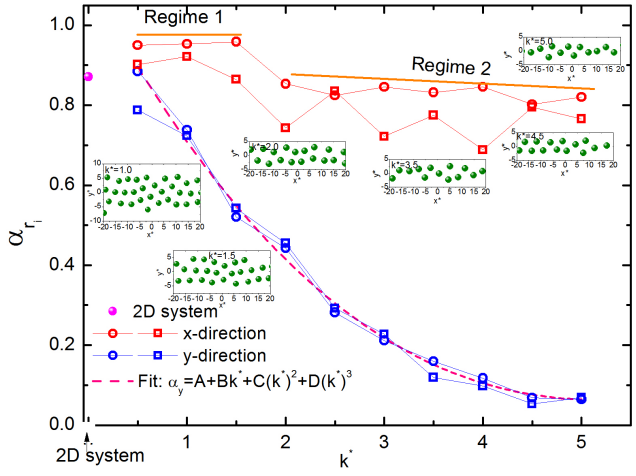

Figure 6.4: α_x and α_y for the Yukawa particles described in Fig. 6.3. α is calculated from the long-time regime of the MSD: $W(t) = Ft^{\alpha}$. Solid beads: 2D system without HI, open circles: results without HI, open squares: results with HI. Dashed line: Fit of the form $\alpha_y = A + Bk^* + C(k^*)^2 + D(k^*)^3$ with $A = 1.11$, $B = -0.463$, $C = 0.061$ and $D = -0.002$. The solid lines only guide the eye. Insets: Equilibrium particle configurations of the system in a fraction of the space, specifically, for $k^* = 1.0, 1.5, 2.0, 3.5, 4.5, 5.0$.

down in the particle diffusion. This mechanism clearly deserves a further investigation.

Finally, we should point out that our study is interesting from many points of view. For example, the discussion can be relevant to find an appropriate approach to much complex problems that involve dynamic heterogeneity induced by the confinement and, in a more general way, can be used to improve models of colloids adsorbed in porous media. A complete dynamical phase diagram will shed light on the complex dynamical behavior of colloidal systems under confinement.

BIBLIOGRAPHY

[1] N. Wu, M. A. Hubbe, O. J. Rojas, S. Park *et al.*, *BioResources*, 2009, **4**, 1222–1262.

[2] T. C. Halsey, *Physics Today*, 2000, **53**, 36–41.

[3] S.-B. Kim and M. Y. Corapcioglu, *Journal of contaminant hydrology*, 2002, **59**, 267–289.

[4] M. Długosz and J. Trylska, *BMC biophysics*, 2011, **4**, 3.

[5] H.-X. Zhou and K. A. Dill, *Biochemistry*, 2001, **40**, 11289–11293.

[6] J. L. McWhirter, H. Noguchi and G. Gompper, *PNAS*, 2009, **106**, 6039–6043.

[7] M. S. van der Knaap, J. C. Pronk and G. C. Scheper, *The Lancet Neurology*, 2006, **5**, 413–423.

[8] H. D. van der Lei, M. E. Steenweg, M. Bugiani, P. J. Pouwels, I. M. Vent, F. Barkhof, W. N. van Wieringen and M. S. van der Knaap, *Archives of neurology*, 2012, archneurol–2011.

[9] D. G. Norris, T. Niendorf and D. Leibfritz, *NMR in Biomedicine*, 2005, **7**, 304–310.

[10] B. Lin, B. Cui, J.-H. Lee and J. Yu, *EPL (Europhysics Letters)*, 2007, **57**, 724.

[11] N. Desreumaux, N. Florent, E. Lauga and D. Bartolo, *The European Physical Journal E: Soft Matter and Biological Physics*, 2012, **35**, 1–11.

[12] R. Pesché and G. Nägele, *EPL (Europhysics Letters)*, 2007, **51**, 584.

[13] G. Petekidis, J. Gapinski, P. Seymour, J. van Duijneveldt, D. Vlassopoulos and G. Fytas, *Physical Review E*, 2004, **69**, 042401.

[14] G. Romeo, L. Imperiali, J.-W. Kim, A. Fernández-Nieves and D. A. Weitz, *The Journal of Chemical Physics*, 2012, **136**, 124905.

[15] R. Pesché, M. Kollmann and G. Nägele, *The Journal of Chemical Physics*, 2001, **114**, 8701.

[16] P. Segre and P. Pusey, *Physical review letters*, 1996, **77**, 771–774.

[17] G. D. Phillies, 1983.

[18] L. Cipelletti, L. Ramos, S. Manley, E. Pitard, D. A. Weitz, E. E. Pashkovski and M. Johansson, *Faraday Discuss.*, 2003, **123**, 237–251.

[19] I. Kretzschmar and J. H. K. Song, *Current Opinion in Colloid & Interface Science*, 2011, **16**, 84–95.

[20] D. Chaudhuri and S. Sengupta, *The Journal of chemical physics*, 2008, **128**, 194702_1–194702_12.

[21] K. Binder, Y. Chui, P. Nielaba, A. Ricci and S. Sengupta, *Nanophenomena at Surfaces*, 2011, 1–18.

[22] Z. Németh and H. Löwen, *Journal of Physics: Condensed Matter*, 1999, **10**, 6189.

[23] E. Oğuz, R. Messina and H. Löwen, *EPL (Europhysics Letters)*, 2011, **94**, 28005.

[24] M. C. Gordillo, B. Martinez-Haya and J. M. Romero-Enrique, *The Journal of Chemical Physics*, 2006, **125**, 144702.

[25] N. Saklayen, G. L. Hunter, K. V. Edmond and E. R. Weeks, *arXiv preprint arXiv:1209.1108*, 2012.

[26] M. Chávez-Páez, M. Medina-Noyola and M. Valdez-Covarrubias, *Physical Review E*, 2000, **62**, 5179.

[27] J. Sané, J. T. Padding and A. A. Louis, *Faraday Discussions*, 2010, **144**, 285–299.

[28] R. Bowles, K. Mon and J. Percus, *The Journal of chemical physics*, 2004, **121**, 10668.

[29] B. Lin, M. Meron, B. Cui, S. A. Rice and H. Diamant, *Physical review letters*, 2005, **94**, 216001.

[30] S. Novikov, S. A. Rice, B. Cui, H. Diamant and B. Lin, *Physical Review E*, 2010, **82**, 031403.

[31] S. A. Rice, *Chemical Physics Letters*, 2009, **479**, 1–13.

[32] Q.-H. Wei, C. Bechinger and P. Leiderer, *Science Signaling*, 2000, **287**, 625.

[33] Q.-H. Wei, C. Bechinger, D. Rudhardt and P. Leiderer, *Physical review letters*, 1998, **81**, 2606.

[34] M. C. Jenkins and S. U. Egelhaaf, *Journal of Physics: Condensed Matter*, 2008, **20**, 404220.

[35] C. Dalle-Ferrier, M. Krüger, R. D. Hanes, S. Walta, M. C. Jenkins and S. U. Egelhaaf, *Soft Matter*, 2011, **7**, 2064–2075.

[36] S. van Teeffelen, C. N. Likos and H. Löwen, *Physical review letters*, 2008, **100**, 108302.

[37] M. D. Carbajal-Tinoco, F. Castro-Román and J. L. Arauz-Lara, *Physical Review E*, 1996, **53**, 3745.

[38] M. D. Carbajal-Tinoco, G. Cruz de León and J. L. Arauz-Lara, *Phys. Rev. E*, 1997, **56**, 6962–6969.

[39] H. Acuna-Campa, M. Carbajal-Tinoco, J. Arauz-Lara and M. Medina-Noyola, *Physical review letters*, 1998, **80**, 5802.

[40] A. Ramírez-Saito, M. Chávez-Páez, J. Santana-Solano and J. L. Arauz-Lara, *Physical Review E*, 2003, **67**, 050403.

[41] J. C. Crocker and D. G. Grier, *Physical review letters*, 1996, **77**, 1897.

[42] Y. Han and D. G. Grier, *Physical review letters*, 2003, **91**, 038302.

[43] S. H. Behrens and D. G. Grier, *Physical Review E*, 2001, **64**, 050401.

[44] E. R. Dufresne, T. M. Squires, M. P. Brenner and D. G. Grier, *Physical review letters*, 2000, **85**, 3317.

[45] R. Bubeck, C. Bechinger, S. Neser and P. Leiderer, *Physical review letters*, 1999, **82**, 3364.

[46] K. Mangold, P. Leiderer and C. Bechinger, *Physical review letters*, 2003, **90**, 158302.

[47] S. Neser, C. Bechinger, P. Leiderer and T. Palberg, *Physical review letters*, 1997, **79**, 2348.

[48] M. Brunner and C. Bechinger, *Physical review letters*, 2002, **88**, 248302.

[49] C. Bechinger and E. Frey, *Journal of Physics: Condensed Matter*, 2001, **13**, R321.

[50] T. R. Stratton, S. Novikov, R. Qato, S. Villarreal, B. Cui, S. A. Rice and B. Lin, *Physical Review E*, 2009, **79**, 031406.

[51] B. Cui, B. Lin, S. Sharma and S. A. Rice, *The Journal of chemical physics*, 2002, **116**, 3119–3127.

[52] B. Cui, H. Diamant and B. Lin, *Physical review letters*, 2002, **89**, 188302.

[53] E. Wonder, B. Lin and S. A. Rice, *Physical Review E*, 2011, **84**, 041403.

[54] B. Lin, D. Valley, M. Meron, B. Cui, H. M. Ho and S. A. Rice, *The Journal of Physical Chemistry B*, 2009, **113**, 13742–13751.

[55] X. Xu, B. Lin, B. Cui, A. R. Dinner and S. A. Rice, *The Journal of chemical physics*, 2010, **132**, 084902.

[56] D. T. Valley, S. A. Rice, B. Cui, H. M. Ho, H. Diamant and B. Lin, *The Journal of chemical physics*, 2007, **126**, 134908.

[57] X. Xu, S. A. Rice, B. Lin and H. Diamant, *Physical review letters*, 2005, **95**, 158301.

[58] M. D. Carbajal-Tinoco, R. Lopez-Fernandez and J. L. Arauz-Lara, *Physical review letters*, 2007, **99**, 138303.

[59] G. Piacente, I. Schweigert, J. Betouras and F. Peeters, *Solid state communications*, 2003, **128**, 57–61.

[60] M. Rex and H. Löwen, *The European Physical Journal E*, 2009, **28**, 139–146.

[61] J. Galván-Moya, K. Nelissen and F. Peeters, *arXiv preprint arXiv:1207.4315*, 2012.

[62] D. Lucena, D. V. Tkachenko, K. Nelissen, V. R. Misko, W. P. Ferreira, G. A. Farias and F. M. Peeters, *Phys. Rev. E*, 2012, **85**, 031147.

[63] D. Lucena, W. Ferreira, F. Munarin, G. Farias and F. Peeters, *Physical Review E*, 2013, **87**, 012307.

[64] J. Carvalho, W. Ferreira, G. Farias and F. Peeters, *Physical Review B*, 2011, **83**, 094109.

[65] F. Munarin, W. Ferreira, G. Farias and F. Peeters, *Physical Review E*, 2008, **78**, 031405.

[66] W. Ferreira, G. Farias and F. Peeters, *Journal of Physics: Condensed Matter*, 2010, **22**, 285103.

[67] W. Yang, K. Nelissen, M. Kong, Z. Zeng and F. Peeters, *Physical Review E*, 2009, **79**, 041406.

[68] D. Tkachenko, V. Misko and F. Peeters, *Physical Review E*, 2009, **80**, 051401.

[69] D. Tkachenko, V. Misko and F. Peeters, *Physical Review E*, 2010, **82**, 051102.

[70] W. Yang, V. Misko, K. Nelissen, M. Kong and F. Peeters, *Soft Matter*, 2012, **8**, 5175–5179.

[71] K. Nelissen, V. Misko and F. Peeters, *EPL (Europhysics Letters)*, 2007, **80**, 56004.

[72] E. C. Euán-Díaz, V. R. Misko, F. M. Peeters, S. Herrera-Velarde and R. Castañeda-Priego, *To be submitted*, 2013, **-**, –.

[73] K. Zahn, J. M. Méndez-Alcaraz and G. Maret, *Phys. Rev. Lett.*, 1997, **79**, 175–178.

[74] B. Rinn, K. Zahn, P. Maass and G. Maret, *EPL (Europhysics Letters)*, 1999, **46**, 537.

[75] J. K. G. Dhont, *An Introduction to Dynamics of Colloids*, Elsevier, 1996.

[76] D. L. Ermak and J. McCammon, *The Journal of chemical physics*, 1978, **69**, 1352.

[77] M. Manghi, X. Schlagberger, Y.-W. Kim and R. R. Netz, *Soft Matter*, 2006, **2**, 653–668.

[78] M. P. Allen and D. J. Tildesley, *Computer simulation of liquids*, Clarendon Press, New York, NY, USA, 1989.

[79] S. Bleil, H. H. von Grünberg, J. Dobnikar, R. Castañeda-Priego and C. Bechinger, *EPL (Europhysics Letters)*, 2006, **73**, 450.

[80] S. Herrera-Velarde and R. Castañeda-Priego, *J. Phys.: Cond. Matt.*, 2007, **19**, 226215.

[81] S. Herrera-Velarde and R. Castañeda-Priego, *Phys. Rev. E*, 2008, **77**, 041407.

[82] E. Euán-Díaz, V. Misko, F. Peeters, S. Herrera-Velarde and R. Castañeda-Priego, *Physical Review E*, 2012, **86**, 031123.

[83] K. Zahn, R. Lenke and G. Maret, *Physical review letters*, 1999, **82**, 2721.

[84] N. Hoffmann, F. Ebert, C. N. Likos, H. Löwen and G. Maret, *Physical review letters*, 2006, **97**, 078301.

[85] P. Keim, G. Maret and H.-H. von Grünberg, *Physical Review E*, 2007, **75**, 031402.

[86] P. Debye and E. Hückel, *Physikalische Zeitschrift*, 1923, **24**, 185.

[87] E. J. W. Verwey and Overbeek, *Theory of the Stability of Lyophobic Colloids*, Elsevier Publishing Company Inc., Amsterdam, 1948.

[88] K. Dholakia and T. Čižmár, *Nat Photon*, 2011, **5**, 335–342.

[89] S. Herrera-Velarde, E. C. Euán-Díaz, F. Córdoba-Valdés and R. Castañeda-Priego, *Journal of Physics: Condensed Matter*, 2013, **25**, 325102.

[90] F. Eever, *Europhys. Journal E*, 2013, **X**, X.

[91] W. P. Ferreira, F. F. Munarin, G. A. Farias and F. M. Peeters, *Journal of Physics: Condensed Matter*, 2006, **18**, 9385.

[92] M. Kollmann, *Phys. Rev. Lett.*, 2003, **90**, 180602.

[93] S. Herrera-Velarde and R. Castañeda-Priego, *Physical Review E*, 2009, **79**, 041407.

[94] B. Cui, B. Lin and S. A. Rice, *The Journal of Chemical Physics*, 2001, **114**, 9142–9155.

[95] E. R. Weeks and D. Weitz, *Physical review letters*, 2002, **89**, 095704.

[96] S. Martens, A. Straube, G. Schmid, L. Schimansky-Geier and P. Hänggi, *arXiv preprint arXiv:1209.5646*, 2012.

7

DIRECTED SELF-ASSEMBLY OF COLLOIDS ON PARALLEL LAYERS BY A ONE-DIMENSIONAL MODULATED SUBSTRATE

"Chaos

—Henry Adams, The Education of Henry Adams

There are certain topics in science that always attract the attention of the research community. Control and manipulation of the physical properties of a system are some of them. For example, the ability to control the structure, size, and orientation in colloidal crystals is an exciting topic in basic science as well as relevant for its considerable technological importance [1]. Furthermore, the ability to manipulate and control colloidal structures at different length scales is one of the ultimate goals in materials science. Recent challenges of colloidal crystallization focus on the preparation of complex two-dimensional colloid arrangements of nanometric dimensions [2]. Furthermore, directed self-assembly of nano-particle systems by external fields has been identified as an important way of control to successfully develop technological applications, see, e. g., Ref. [3], and references therein.

Nowadays, colloidal systems have a place as an important research platform for the understanding of static and dynamical properties in more complex systems. For instance, colloidal suspensions are well suited to study crystal nucleation with an accuracy and depth on a microscopic scale that is hard to reach in atomic or molecular systems [4]. Using experiments, theory and computer simulations one is able to obtain a deeper understanding of crystal nucleation in two- and three dimensions. In particular, colloidal nano-crystals represent an attractive and promising building blocks for advanced materials and devices [5]. However, for a precise control of crystal formation, specialized experimental methods still need to be applied. For example, manipulation of colloidal particles trough optical tweezers are an ideal method for this purpose, since particles can be positioned selectively and one can tune both the phase behavior and the dynamics of colloidal systems [4] .

Soft materials, such as colloidal dispersions, are very susceptible to external forces [6]. Colloidal manipulation by different external fields has witnessed an enormous increase in applications in the last

two decades [1, 6–9]. One simple and effective way to control the colloidal material properties is by the use of geometrical confinement. Walls or confining boundaries act as an external field modifying the thermodynamic behavior of the colloidal suspension [8]. For example, colloids between two parallel plates [7], circular cavities [10], parallel colloidal layers [11] and even one dimensional systems [12] have been extensively investigated because structural and diffusive properties are strongly influenced by the confinement effects [4, 7]. Thus, confinement is an important mechanism in many different areas of physics and technology. Recent reviews that highlight the use and understanding of colloids under confinement can be found in Refs. [6, 13] and references therein.

Colloidal particles can also be manipulated using light [13]. Optical tweezers inspired by the pioneering work of Ashkin [14] are now a widely-used tool in physics and biology [13]. Light fields have been recently used to induce structural changes and to explore the influence of external potentials on the diffusion of colloidal particles [15]. In fact, optical patterns can by now be prepared in reality almost in an arbitrary way by a suitable interference of several laser beams [7].

A 2D colloidal suspension exposed to the interference pattern of two overlapping laser beams shows a phase and diffusive behavior totally different from that of 2D systems on homogeneous substrates. Furthermore, the depth and periodicity of such a light potential can be easily controlled in situ, allowing a systematic investigation of the influence of the corrugated substrate [16]. Since the first report by Chowdhury and co-workers [17], monodisperse 2D colloidal systems interacting with a substrate potential have been studied extensively in experiments, computer simulations and theory over the last few decades [18]. More recent studies concern 2D binary hard-disk mixtures subjected to an spatially periodic potential [19] and the phenomenon of laser-induced condensation [20–22]. In addition, it has been extensively reported that the phase behavior of the 2D colloidal suspension depends on the value of the commensurability ratio p [16, 23–25]. Thus, different phases that were predicted theoretically [23], later on, were corroborated experimentally [24] and by Monte Carlo computer simulations [25].

In the present work we combine the action of an external modulated field and spatial confinement. We investigate the effects that a corrugated substrate has on the properties of two-parallel colloidal monolayers (see Fig. 7.1 for a schematic representation of the system). The parallel equally spaced monolayers model has been recently introduced by Contreras-Aburto *et al.* [11] to study both the microstructure and the effective interactions of Yukawa colloidal suspensions. Here we go one step further and explore the effect that a 1D periodic potential applied exclusively to the bottom layer might have on the structure and dynamics in both monolayers. In the case of

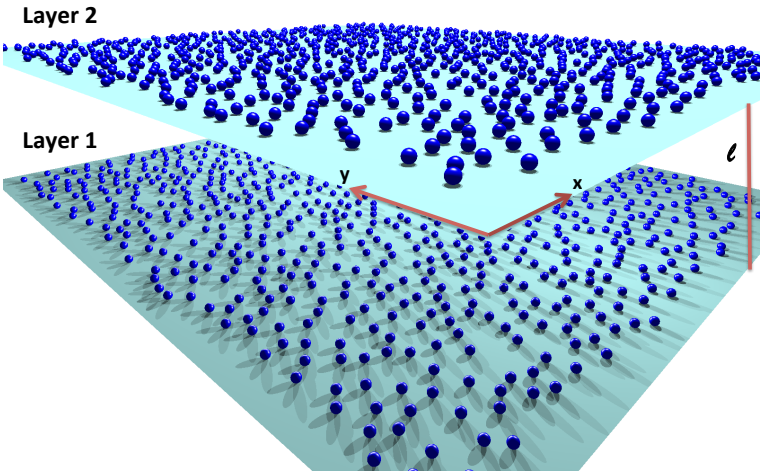

Figure 7.1: Schematic representation of the dual-layer system. The separation between layers is constant, $l = \sigma$, and has been increased for effects of visualization. The modulated potential is applied to layer 1 (bottom layer), whereas layer 2 (top layer) is a substrate-free layer and it is correlated with the bottom layer through the direct interactions between particles. Particle exchange between layers is not allowed. All snapshots were produced using the *POV-Ray* ray tracing program, www. povray. org.

single monolayers, the final equilibrium state is determined by the commensurability scenario and the energetic landscape, that is, the particle-particle and particle-substrate interactions [15, 16, 23–27]. We are interested in determining whether similar structural and dynamic transitions can be induced in the dual-layer system as a function of the substrate strength for two different commensurability ratios $p = 1$ and $p = 2$. Obvious questions deal with: a) the competition among direct interactions between particles of the same layer, b) the extent of changes in layer 1 as a result of the particle reordering on the substrate minima and c) the amount of change in the properties of the top layer due to the proximity of the bottom layer.

The aim of this work is to provide a simple but effective system model where the effects induced by the substrate can be systematically studied by means of molecular simulations. This model could be useful to enhance our ability to manipulate colloidal structures and in some extent might be helpful to elucidate the differences between both supported and unsupported lipid bilayer membranes [28–30].

The remainder of this paper is organized as follows. In section 7.1 we describe in detail the dual-layer model system, the particle interaction potential as well as the external potential. In section 7.2 we discuss salient aspects of the BD methodology and details of the physical observables reported in this work. In section 7.3 we first discuss

the static properties of each layer for both commensurability scenarios. After the statics is investigated, we focus on the dynamical behavior of the colloidal particles in each monolayer. We study the way in which the MSD parallel and perpendicular to the fringes is affected by the strength and periodicity of the external potential. In general, we show that the induced structural behavior has a strong effect on the diffusive behavior of the colloidal particles in both monolayers. Finally, section 7.4 contains our concluding remarks, and some perspectives of future work are briefly mentioned.

7.1 MODEL SYSTEM

Our dual-layer model system is depicted in Fig. 7.1 and consist of two parallel monolayers separated by a fixed distance $l = \sigma$, with σ being the particle diameter; each layer is composed of repulsive interacting colloidal particles and particle exchange between monolayers is not allowed. Each monolayer can be considered as a two-dimensional system consisting of N particles and a particle number density $\rho = N/A$, with A being the total area of the monolayer. For a single monolayer system, the characteristic length scale within the fluid phase, and in absence of any external perturbation, is the mean inter-particle distance d [11, 27]. However, as pointed out in Ref. [11], at intermediate distances between layers ($l > 0$), there is no unique characteristic length for the static structure. The parallel layers model was originally proposed by Contreras-Aburto *et al.* [11] to investigate the static structural behavior as a function of the interlayer spacing and to understand the geometrical effects on the effective interactions among particles of the same layer.

In each monolayer we randomly distributed N colloidal particles; all particles have the same diameter $\sigma = 2a$, where a is the particle radius. We assume that after the hard-core interaction, $r > \sigma$, two colloidal particles separated by a distance r interact via the repulsive part of the DLVO-type potential [31–33],

$$\beta u(r) = Z_{\text{eff}}^2 \lambda_B \left[\frac{e^{\kappa a}}{1+\kappa a}\right]^2 \frac{e^{-\kappa r}}{r}, \tag{7.1}$$

where $\beta \equiv (k_B T)^{-1}$ is the inverse of thermal energy with k_B as the Boltzmann's constant and T being the absolute temperature, Z_{eff} is the effective charge, λ_B is the Bjerrum length and κ^{-1} being the Debye screening length. The potential parameters used in equation (7.1) were taken from the experimental work reported in Ref. [34]. Then, $a = 1.4$ μm, $Z_{\text{eff}} = 5400$, $\lambda_B = 0.72$ nm, and $\kappa^{-1} = 550$ nm. Experimental determination of both the Debye screening length and the effective charge, among other details, can be found in Ref. [34] and references therein. The same set of parameters has been used by two of us to study the ordering and dynamics in one-dimensional systems

[12] and the diffusion of colloidal systems for a single 2D monolayer subjected to a sinusoidal substrate [27].

We apply a 1D periodic potential to the layer 1 shown in Fig. 7.1. A standard practice in computer simulations to introduce a modulated potential is using a cosine or sinusoidal function [15, 25, 27, 35–37]. This kind of function mimics the presence of a corrugated surface where particles will be attracted to the potential minima. Then, the substrate acting on particles lying on the layer 1 is given by [27, 35]

$$u^{ext}(x_i) = V_0 \sin\left(\frac{2\pi x_i}{a_L}\right), \tag{7.2}$$

with V_0 and a_L being the strength and lattice spacing of the external potential, respectively. The relation between the mean inter-particle distance and the potential periodicity defines the commensurability factor $p = \sqrt{3}d/2a_L$. This factor determines the number of potential fringes and consequently the underlying substrate corrugation; it also helps in the description of a large variety of phases in systems under influence of periodic substrates. We here choose d as the unit length. Then, $a_L/d = \sqrt{3}/2$ and $a_L/d = \sqrt{3}/4$ for $p = 1$ and $p = 2$, respectively. Most of the current work in single monolayers has been reported for $p = 1$, however, there exist a few works that have been focused in the next difficult level $p = 2$ [15, 23–25].

7.2 BROWNIAN DYNAMICS SIMULATION AND PHYSICAL OBSERVABLES

Colloidal particles perform an overdamped dynamics due to they are embedded in a viscous solvent. The trajectory that any colloidal particle follows is named Brownian due to the stochastic collisions with the solvent molecules, however, it is also influenced by all the direct interactions present in the system: colloid-colloid and colloid-substrate interactions. In this contribution all calculations have been carried out by means of BD computer simulations. We consider that each particle is effectively confined to one of the monolayers, and the trajectory of particle i that obeys Brownian motion, neglecting HI, reads [38, 39],

$$\vec{r}_i(t + \Delta t) = \vec{r}_i(t) + \beta D_0 \vec{f}_i(t)\Delta t + \delta\vec{r}_i(\Delta t), \tag{7.3}$$

where $\vec{r}_i(t)$ denotes the position of particle i at time t, Δt is the time step and $\vec{f}_i(t) = -\vec{\nabla}_i U$ is the total force acting on particle i due to the interaction with all particles of the same layer as well as particles in the other monolayer, and, in the case of the bottom layer, with the coupling with the external field. For layer 2, the external energy contribution is always zero. $D_0 = k_B T/6\pi\eta a$ is the free-particle diffusion of a sphere of radius a in a solvent of viscosity η. Finally, the random displacement $\delta\vec{r}_i(\Delta t)$ is sampled from a Gaussian distribution with

zero mean and variance $< \delta\vec{r}_i(\Delta t)^2 >= 2D_0\Delta t$ (for each cartesian component) fixed by the fluctuation-dissipation relation[38, 39].

Equation (7.3) gives the trajectory of each colloidal particle. The dynamics of the system is then simulated considering a random initial configuration of $N = 900$ colloidal particles for each monolayer. Due to the presence of the corrugated substrate in the lower monolayer, we choose a rectangular box of lateral dimensions $L_x \times L_y$ with $L_x = \frac{\sqrt{3}}{2}L_y$ ($L_y/d = \sqrt{N}$) and periodic boundary conditions on each direction [27, 37]. After reaching an equilibrium state, we turn on the external potential and increase the values of $V_0^* = V_0/k_BT$ in steps of 0.1. We begin with a homogeneous suspension $V_0^* = 0.0$ until reach a strength of $V_0^* = 8.0$; at each stage we spend, at least, 1×10^5 time steps to reach an equilibrium state for a given value of V_0. This methodology allows a slow relaxation and particles do not get artificially trapped by the sudden exposition of the external potential. A typical time step used in the BD simulations is $\Delta t = 2 \times 10^{-4}(\rho D_0)^{-1}$. The maximum time reached in the BD simulations is $t_{max} = 100(\rho D_0)^{-1}$, i. e., 1.5×10^6 time steps. Finally, it is noteworthy to mention that the packing fraction $\phi = \pi a^2\rho$, is the same in each layer and has been chosen in such way that monolayers exhibit a fluid-like order in absence of the external potential $V_0^* = 0.0$.

From the generated set of equilibrium configurations, we calculate the static structure for both monolayers. In particular, we compute the pair distributions functions perpendicular to the fringes, $g(x)$, and along the fringes, $g(y)$. Such distributions allow us to quantify the inhomogeneities induced in the structure due the presence of the periodic substrate. In addition, they can be measured experimentally by different techniques, allowing a direct comparison between simulation and experimental data. The $g(x)$ is the probability of finding a particle at a distance x given that a particle is located at the origin. It is obtained for each monolayer by averaging over each 20 equilibrium configurations through the relation

$$g(x) = \frac{1}{N\rho}\left\langle \sum_{i=1}^{N-1}\sum_{j>i}^{N}\delta(x - x_{ij})\right\rangle, \tag{7.4}$$

where the angular brackets $\langle\cdots\rangle$ denote a temporal or ensemble average and x_{ij} is the relative distance between particles i and j along x-direction. A similar interpretation and correspondingly equation are valid in the y-direction.

Based on the trajectories of the particles, we calculate dynamical properties such as the MSD. The total MSD is obtained according to the relation [15, 27]

$$W(t) \equiv \langle \Delta r(t)^2\rangle = N^{-1}\sum_{i=1}^{N}\left\langle [\vec{r}_i(t) - \vec{r}_i(0)]^2\right\rangle. \tag{7.5}$$

As the system is highly anisotropic, besides the total MSD, we also study the diffusion across (x-direction) and along (y-direction) the fringes. Thus, equation (7.5) can be rewritten as $W(t) = W_x(t) + W_y(t)$, where $W_x(t)$ and $W_y(t)$ denote the MSD perpendicular and parallel to the fringes, respectively.

Having determined the particle coordinates using equation (7.3), we systematically explored the way in which the corrugated substrate modifies the particle distribution and diffusive behavior in both monolayers. In our study we have fixed the monolayer packing fraction ϕ, the interlayer separation σ and the set of potential parameters $(a, \kappa, Z_{eff}, \lambda_B)$. Then, we focus our analysis on varying the external potential strength V_0^* under two commensurability scenarios: $p = 1$ and $p = 2$. Although we have performed a detailed study for both layers, in next section we present representative results.

7.3 RESULTS AND DISCUSSION

At a packing fraction of $\phi \approx 0.16$ and the same set of experimental parameters that we use in this work, a substrate-free single monolayer is close to a spontaneous freezing transition but still remains in the fluid-phase [27]. In our dual-layer model due to strong correlation between monolayers, even with identical parameters we can not use the same value of ϕ. We perform a systematic study as a function of ϕ in absence of the substrate. Based on pure empirical structural and dynamical criteria [27], we analyzed the transition from liquid-like to solid like order (data not shown). We then choose $\phi = 0.086$ as our packing fraction in each layer when they are separated by a distance σ. We limit our study to the value of $l = \sigma$. This separation leads to strong correlations between monolayers that allows us to elucidate in a better way the effects of the corrugated substrate on both monolayers. Furthermore, for very large layer separations $l \to \infty$, particles on different layers are not longer correlated due to the finite range of the potential between particles and, in consequence, the layers behave as independent 2D systems with a density $\rho = N/A$. Thus, there is not effect of the layer in contact with the substrate on the properties of the upper layer. In contrast, when the layers overlap ($l = 0$) we recover the case of a single monolayer with density $\rho = 2N/A$. Thus, these two limiting cases do not represent the physical situation that we want to emphasize in this work. A systematic study of the structure and dynamics of a multilayer system in presence of a modulated potential as a function of V_0 and intermediates values of l, is still in progress and will be published elsewhere [40].

The intricate competition between colloid-colloid and colloid-substrate interactions plus the commensurability factor p are the origin of the complex structural and dynamical behavior observed in monolayers composed of monodisperse systems [15, 17, 26, 27] and binary mix-

tures [18, 19] on spatially modulated substrates. Despite of this considerable knowledge, up to now, there are neither experiments nor computational studies that probe the effect of a patterned substrate in a system of parallel monolayers.

7.3.1 *Static structure*

Experimentally, a set of crossed laser beams leads to an interference pattern in a colloidal sample [15–17]. This modulated light field affects the positions of the particles, especially at large potential amplitudes. Due to attractive interactions, the particles stay preferentially in the bright parts of the fringes [15]. In our model, particles in layer 1 feel directly the effect of the external modulated potential. Thus, for this layer, one can expect a similar behavior as that observed in single monolayers subjected to corrugated substrates [27]. By varying the substrate strength, we monitor the colloidal structural evolution in both monolayers trough the one-dimensional pair distribution functions. As we mentioned earlier, both $g(x)$ and $g(y)$ quantify the order across and along the fringes, respectively, and make evident the inhomogeneities induced by the external field.

The $g(x)$ and $g(y)$ for the bottom layer as a function of V_0^* are shown in Fig. 7.2. Two commensurability scenarios are displayed, $p = 1$ (left-column) and $p = 2$ (right-column). In absence of substrate, i. e., $V_0^* = 0.0$, we have corroborated that the $g(x)$ and $g(y)$ are equal to each other. Furthermore, both distribution functions exhibit the typical features of repulsive interacting systems: (i) particles do not feel the hard-core interaction, (ii) show a typical fluid like order, i. e., after a few mean inter particles distances they decay to its corresponding ideal-gas value ≈ 1. However, when the external potential is turned on, one clearly observes that, independently of the chosen value for p, the substrate induces changes in the local structure of the suspension.

In the particular case of $p = 1$, one immediately observes the dramatic structural change perpendicular to the fringes (Fig. 7.2a). As V_0^* increases, the $g(x)$ becomes more structured, showing a periodicity imposed by the fringe spacing and is highly correlated at very long distances. Additionally, the peaks in the $g(x)$ become sharper reflecting that particles are more localized and prefer to reside in the minima of the external potential, leading to only one characteristic length scale associated with the substrate periodicity a_L. These features clearly show that in x-direction, the external potential determines the structure perpendicular to the fringes. The behavior here observed can be associated to a crystal-like order (Fig. 7.3a).

Two distinct situations can be distinguished for the $g(y)$ with $p = 1$. Figure 7.2c shows that for small potential strengths, $V_0 \leqslant 2.0 k_B T$, the $g(y)$ exhibits a typical order of a high density fluid. Particles are lo-

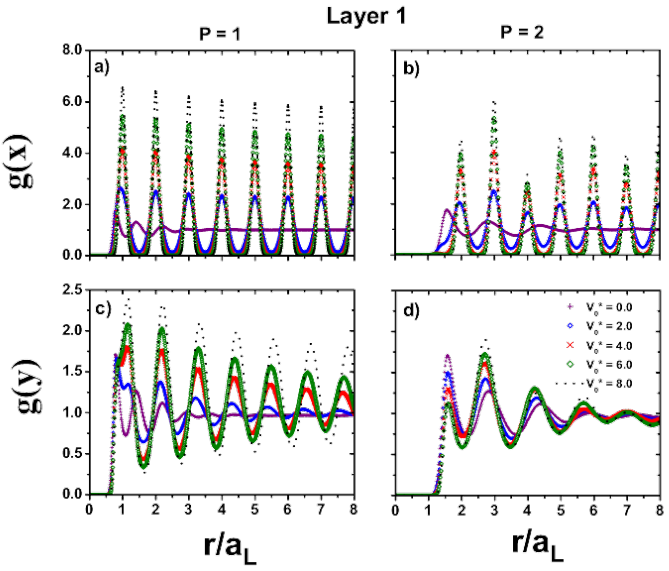

Figure 7.2: Pair distribution functions in the x- and y-directions of layer 1 as a function of $V_0^* = V_0/k_BT$. Two commensurability scenarios are analyzed, $p = 1$ (left-column) and $p = 2$ (right-column). Variable r stands for x- or y- direction, accordingly.

cated at the average-distance and correlations extends over several particle diameters but still the $g(y)$ decays to the expected value of 1. However, for higher strengths, it begins to be more structured and long correlations are clearly visible at long particle separations. Note that in contrast to the $g(x)$, the distribution of the peaks does not correspond with the substrate periodicity. A natural question that arises is why particles re-arrange their configuration in a highly-structured pattern, even if there is not an external potential acting along the y-direction. To answer the question, we should recall that particles are able to move freely along the y-direction, but they are effectively confined in the fringe pattern. In fact, when $p = 1$, the periodicity of the substrate $a_L = \sqrt{3}d/2$ yields an integer number of 30 fringes (channels), where there are, in average, 30 particles in each channel. This situation is nicely depicted in Fig. 7.3a where each fringe corresponds to a q1D channel. This confinement leads to stronger correlations and subsequent ordering along the fringes [12].

We turn now to the evolution of the pair distribution functions $g(x)$ and $g(y)$ in layer 1 for $p = 2$ shown in Fig. 7.2 (right-column). In this case, the number of fringes is twice compared with $p = 1$. Due to the attractive interaction of the substrate, particles will try to be accommodated in all the available fringes. Then, while the external potential attempts to insert particles into the potential minima, the repulsive interaction between particles will try to push them away. The competition colloid-colloid and colloid-substrate interactions then leads to

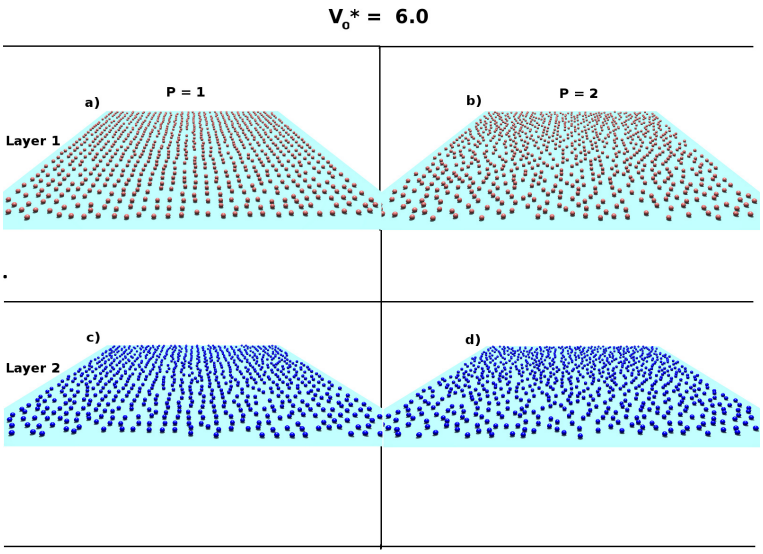

Figure 7.3: Snapshots of both monolayers for the two commensurability factors $p = 1$ (left-column) and $p = 2$ (right-column). The strength of the external potential is $V_0^* = 6.0$.

a loss of ordering (see snapshot in Fig.7.3), where the stronger effects are reflected in the $g(y)$ (Fig. 7.2d).

We can also observe in Fig. 7.2b that the $g(x)$ has once again a periodicity imposed by the external potential but now with $a_L = \sqrt{3}d/4$. Although the peaks are located in positions that are multiples of a_L, it is noteworthy that there is no peak at a distance $r = 1a_L$. Thus, the closest neighbor is located at a distance $r = 2a_L$, which is in contrast with the $g(x)$ for $p = 1$ (Fig. 7.2a), where the first maximum is located at $r = a_L$. For $p = 2$, the $g(x)$ in Fig. 7.2b has peaks with alternating heights indicating that at short distances is more likely to find a particle every second line. However, at long distances all peaks have the same height, which reflects the underlying ordering induced by the substrate. Additionally, the shortening in the height of the first peak, compared with the second one, is an evidence that particles try to push away their closer neighbors. The overall behavior of the $g(x)$ is very similar for both values of p; an increase in the substrate strength leads to an enhancement of the peak heights and a reduction in the corresponding peak widths. This indicates that particles are trapped in the substrate minima. Thus, the structural ordering along x-direction is driven by the external potential.

A completely different structural scenario for the layer 1 is observed along the fringes. Figure 7.2d shows that the $g(y)$ for $p = 2$ acquires a much less pronounced structure compared with the case $p = 1$ (Fig. 7.2c). While the peak height of the first maximum decreases with V_0^*, the height of the second peak exhibits the opposite effect. This behavior suggests a loss of correlation at very short distances. This effect is induced by the closeness of the potential fringes.

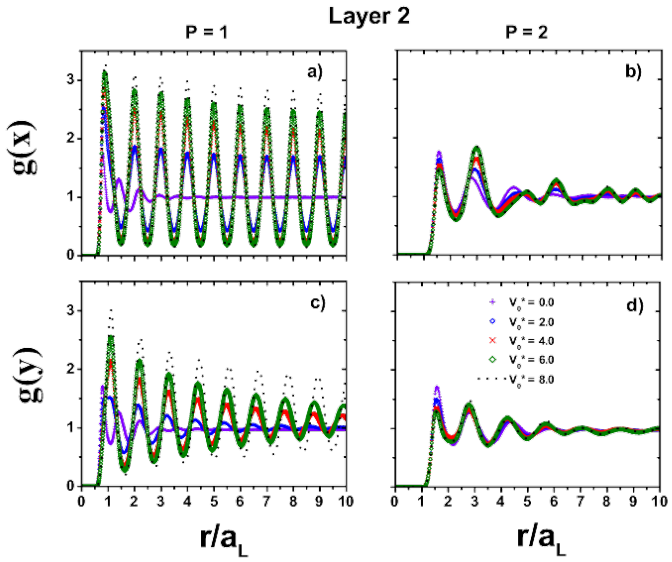

Figure 7.4: Pair distribution functions in the x- and y-directions of layer 2 as a function of $V_0^* = V_0/k_BT$. Two commensurability scenarios are analyzed, $p = 1$ (left-column) and $p = 2$ (right-column). Variable r stands for x- or y- direction, accordingly.

The neighbors in adjacent fringes of a given particle act cooperatively to push away the closest neighbors of the particle along the fringe. Thus, the colloidal correlation in any fringe is modified by the presence of particles in adjacent fringes leading to a loss of correlation. It should also be noted that while the $g(y)$ for $p = 1$ has a well-defined periodicity, for $p = 2$ there is no a characteristic length-scale. Thus, for $p = 2$ the random position of the particles in the potential minima destroys any natural periodicity and contributes to the loss of correlation at long-distances. This can be best seen in the snapshot of Fig. 7.3b.

Let us now focus on the structural behavior of the top layer. Figure 7.4 shows the pair distributions functions $g(x)$ and $g(y)$ for $p = 1$ (left-column) and $p = 2$ (right-column), respectively, as a function of the potential strength, V_0^*. Particles in this layer can, in principle, move freely in both directions because they are not coupled directly to the substrate. Thus, all structural changes are driven by the interaction among particles in the two layers. From Fig. 7.4, one can immediately observe the evolution of the static properties of the substrate-free layer. We have to point out that both $g(x)$ and $g(y)$ pair distributions, show a similar structural evolution as the one previously discussed for the bottom layer. For the upper layer the more dramatic changes are observed for $p = 1$. However, we should also stress that although the top layer is not subjected to the modulated potential, the strong coupling between layers evidently produces structural modifications on it. This illustrates the fact that the substrate induces both directly

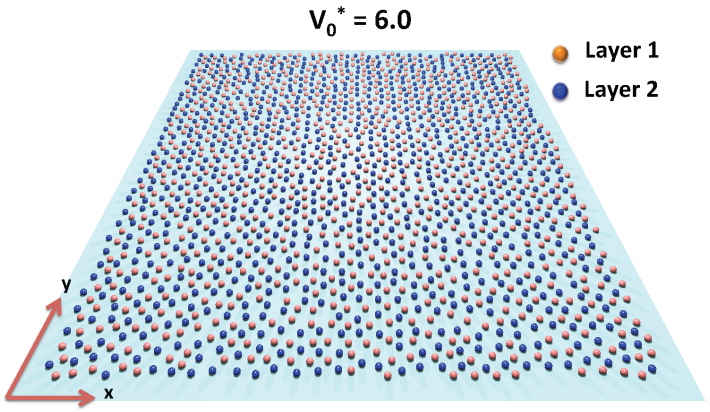

Figure 7.5: Schematic representation of the projection of particles in layer 2 on layer 1 for p = 1 and $V_0^* = 6.0$. Light brown spheres correspond to the positions of colloidal particles in the lower layer and blue spheres are the positions of colloids in the top layer projected on layer 1.

and indirectly changes in the ordering of the particles in the whole system. This is of scientific and technological importance, since, for example, the precise manipulation in the growth of crystal-like structures made of colloidal particles can be accurately controlled by simply varying the properties of the substrate.

For p = 1 (see Figs. 7.4a and 7.4c) we observe that the morphology of the substrate is transferred to the layer 2, even when such a layer is not in direct contact with the external potential; the same structural transition already discussed for layer 1 can be appreciated on the top layer. This mimicry in the structural properties can be understood only in terms of the strong correlation between layers. We argue that particles on the top layer are forced to be ordered because particles on layer 1 are restricted to move along the fringes forbidding the free movement of particles in layer 2. Thus, particles on the top layer get trapped, lying between two adjacent potential lines. This situation promotes the formation of lines particles on the top layer, which can be nicely appreciated in Fig. 7.3c. This situation is better illustrated in Fig. 7.5, where for p = 1 and $V_0^* = 6.0$ we have projected the particle positions of layer 2 on the lower layer; the light brown and blue spheres correspond to the lower and top layers, respectively. From Fig. 7.5, we can easily observe the formation of lines in both monolayers. As expected, the particles of the top layer are located in the middle of two potential troughs of the lower layer.

Despite of the similar structural behavior between monolayers, still some differences can be appreciated. First we should note that for

$p = 1$ the valleys in the $g(x)$ for layer 2 never reach the value of zero (Fig. 7.4a). This means that there is a small probability of finding particles between two lines, although particles need to surmount a huge energetic barrier imposed by the particle-particle repulsive interaction potential. Also, the peak heights in the $g(x)$ are shorter than those of layer 1. In contrast, we observe an increase in the peak heights for the $g(y)$ (Fig. 7.4c). These features can be understood as follows. Particles in layer 2 have more freedom to move in x-direction, which allows larger fluctuations perpendicular to the fringes. Thus, the probability of finding a particle at a distance x from a central particle diminish. Therefore, while the freedom of motion leads to a lower correlation along the x-direction, it increases the probability to find a particle along the channel.

For the layer 2 and commensurability factor $p = 2$, we can observe, from Figs. 7.4b and 7.4d, a completely different structural evolution of the pair distribution functions. Clearly, there is a loss of correlation at short distances and do not exist long correlations. In addition, neither the $g(x)$ nor the $g(y)$ exhibit a natural length-scale. We associate these structural features with the randomness induced by the substrate on the bottom layer. As we previously discussed, for $p = 2$ there are twice potential minima than the case $p = 1$ and, therefore, particles in layer 1 are randomly located trough the minima trying to occupy all the available fringes (see snapshot in Fig. 7.3b). This behavior disrupts the structure of the top layer destroying any well defined structure; reflected as a loss of correlation perpendicular and across the fringes. The particle arrangement in layer 2 when $p = 2$ and $V_0^* = 6.0$, can be appreciated in the snapshot of Fig. 7.3d. Then, for $p = 2$, the corrugated substrate promotes some kind of disorder transition, or an effective depinning-like transition, on the top layer.

From Figs. 7.4b and 7.4d, one can notice that upon increasing V_0^*, the probability to find the first neighbor at certain distance decreases, whereas increases for the second neighbor. Thus for higher substrate strengths is more likely to find a second neighbor. This behavior is practically the same as the one observed for the bottom layer. We also should note that in Fig. 7.4b the position of the first two maxima in the $g(x)$, corresponding to the first and second neighbors, are practically the same as in the substrate-free case. Then, at short distances, the particle distribution around a central particle barely changes with V_0^*. However as V_0^* increases, the substrate impose new correlations and a periodicity emerges at long distances ($r \geqslant 4d$). A similar behavior is observed in Fig. 7.4d for the $g(y)$, i. e., peak positions are barely affected and there is a loss of correlation at very short distances (closest neighbor). However, in contrast with the $g(x)$, after the two first peaks, the $g(y)$ has almost the same behavior as that in the substrate-free case.

To summarize, from Figs. 7.2 and 7.4 is clear that the manner in which the particles self-assemble to organize solid-like or fluid-like structures depends strongly on the properties of the substrate. Thus, it seems plausible that the substrate parameters, strength and periodicity, can be used as a control parameters to induce order-like or disorder-like particle configurations on the top layer or in systems with a finite number of layers [40].

7.3.2 *Mean-squared displacement*

Regarding the dynamical behavior, recently works on single layers subjected to external periodic potentials have elucidated some general features of diffusive processes that take place under those specific conditions [15, 27]. The strong anisotropy induced by the substrate across and along the fringes leads to different dynamical regimes [27]. Besides, it has been pointed out experimentally that the dynamics of particles in modulated potentials resembles the one of supercooled liquids [15].

In this work we have measured the MSD for both monolayers for a wide range of V_0^* values. In general, we have found that the presence of the periodic potential modulates the dynamical behavior and under certain conditions can inhibit the diffusion perpendicular to the fringes. To study the effect of the corrugated substrate on the dynamical properties of the dual-layer system, we follow the standard practice of determining the MSD's along, $W_y(t)$, and across, $W_x(t)$, the fringes [15, 27]. In the homogeneous case, $V_0^* = 0$, we checked the isotropy of the MSD in both monolayers. This means that in absence of substrate, colloids diffuse, in average, in the same fashion in any direction. In addition, for all the potential strengths simulated in this work, we have verified that $D_L < D_S$, where D_S and D_L are the short- and long-time self-diffusion coefficients, respectively. However, due to the large simulation computational cost, the temporal window in our data does not allow to capture the short-time regime where $D_0 = D_S$. For a deeper discussion of the dynamical regimes in single monolayers under the action of a modulated potential see Ref. [27] and references therein.

Figure 7.6 presents the MSD of the particles moving on the layer in direct contact with the external potential. The diffusive behavior perpendicular to the fringes, shown in Figs. 7.6a and 7.6b for $p = 1$ and $p = 2$, respectively, is very similar to the one found in single monolayers [15, 24, 27]. At sufficiently short times, where the individual particles do not feel the direct interactions with the other colloids, normal diffusion occurs and the MSD is found to be $W_x(t) \propto t$. At intermediate times the diffusion process becomes sub-diffusive and for $V_0^* < 6.0$ normal diffusion is recovered at sufficiently long times. However, for high substrates strengths $V_0^* \geqslant 8.0$ a well-defined

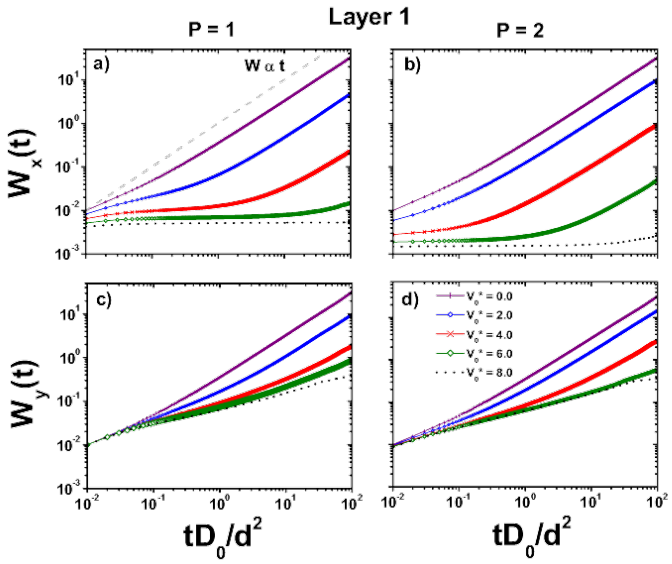

Figure 7.6: MSD as a function V_0^* of particles on the layer in contact with the corrugated substrate. Two commensurability scenarios are studied, $p = 1$ (left-column) and $p = 2$ (right-column). The dashed line in (a) is a visual guide to indicate the linear-time dependence of the MSD at long-times.

plateau is observed and normal diffusion seems to be completely suppressed in the x-direction.

The observed reduction in the MSD across the fringes is because upon increasing the substrate strength, the direct particle-substrate interaction dominates on the colloid-colloid interaction. Thus, particles must spend a longer time for crossing several substrate minima before reaching the diffusive motion. This causes that particles diffuse or oscillate around the position of each substrate minimum for a long period of time. This means that the time needed to surmount the energetic barrier increases with the substrate strength. For very high substrate strengths, $V_0^* > 8.0$, particles are no able to surmount the potential barrier, then diffusion in such direction is completely suppressed and this is evidenced by the plateau observed in Fig. 7.6 (upper row). Similar to recent experimental results, our simulation data suggest that for high strengths potentials, no long-time diffusion is observed across the fringes and the system thus appears dynamically arrested [15].

In contrast to the observed behavior in the $W_x(t)$, Fig. 7.6 (lower row) shows that the MSD along the fringes, $W_y(t)$, is not dramatically affected by the application of the external potential. Note that the presence of the corrugated substrate forces particles to form channels (see snapshots in Figs. 7.3 and 7.5), but the $W_y(t)$ is not suppressed because colloidal particles can diffuse freely inside the potential troughs where thermal fluctuations promote diffusion along y-

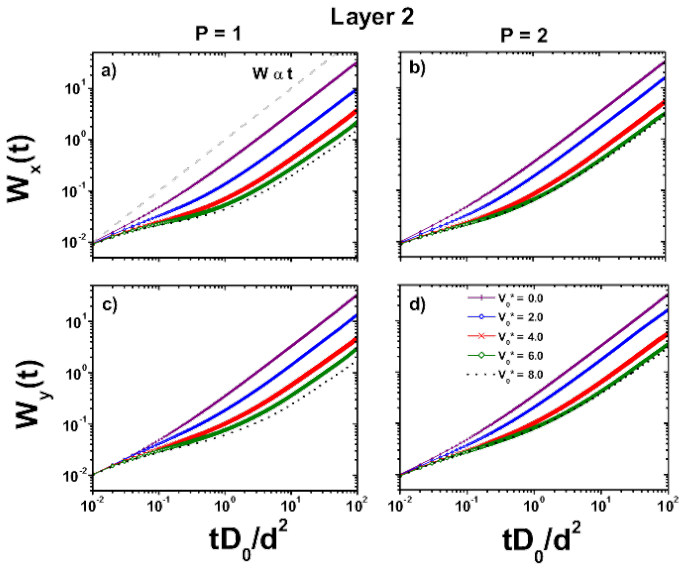

Figure 7.7: MSD as a function V_0^* of particles on the top layer, i. e., substrate-free layer. Two commensurability scenarios are studied, $p = 1$ (left-column) and $p = 2$ (right-column). The dashed line has the same meaning that in Fig. 7.6.

direction. Thus, the reduction in the MSD can be understood in terms of the confinement of colloids in q1D channels and not by direct effect of the modulated potential. We should recall that for $p = 1$ we have 30 fringes and one each is filled with approximately 30 particles (Fig. 7.3a). Thus, although colloidal particles are constrained to move in q1D channels the MSD in y-direction is still proportional to t (see dashed line in Fig. 7.6a), in clear contrast with the MSD scaling for true 1D systems [12, 27].

The dynamic behavior of the top layer is shown in Fig. 7.7. We should note that in contrast with the behavior observed in Fig. 7.6 (upper row) for the layer 1, the MSD perpendicular to the fringes in layer 2, does not exhibit a plateau neither for $p = 1$ nor $p = 2$ (Fig. 7.7 (upper row)). In addition, from Figs. 7.7a and 7.7b, we can appreciate that the $W_x(t)$ is practically the same in both commensurability scenarios for all values of V_0^*. This behavior is interesting because if we remember the structural behavior in layer 2 for $p = 1$ (Fig. 7.4a), particles seem to be strongly confined in lines. However, the $W_x(t)$ shows that particles have the same freedom to move in either the x-direction (Fig. 7.7a) or the y-direction (Fig. 7.7c). Thus, although particles in layer 2 form a well-defined strips for $p = 1$ (Figs. 7.3c and 7.5), they can go in and out perpendicular to the channels contributing to the diffusion in x-direction. Regarding the diffusion along the fringes (Fig. 7.7 (lower row)), the dynamic behavior is very similar to the one observed in layer 1. However, we can appreciate larger values of the $W_y(t)$ at long times on the top layer. This is because particles

on it are not effectively constrained to move on a line. Thus, particles exhibit larger fluctuations perpendicular to the fringes. This allows some freedom of motion along the fringes. The extra-freedom is reflected in a larger diffusion along the y-direction compared with the bottom layer.

The reduction of the MSD in the top layer is a direct effect of the correlation between layers. The induced arrangement of particles on the layer 1 modifies the motion of particles on the layer 2. Then, for $p = 1$ particles in the upper layer are forced to move inside strips (Fig. 7.3c) or for $p = 2$, they are enclosed in some region (Fig. 7.3d), reducing its diffusion. However, they can move relatively free and are able to perform random walks in any direction. This freedom is reflected in the larger values of the MSD on the top layer and the equality $W_x(t) \approx W_y(t)$ in both commensurability scenarios.

7.4 CONCLUDING REMARKS

Using BD simulations and a novel layered colloidal system [11], we have investigated the effect of a 1D periodic potential on the structure and diffusive behavior of interacting colloidal particles confined in two parallel monolayers. We have shown that the physical properties of the upper layer can be indirectly modified by the external potential, although the substrate has direct influence only on the bottom layer.

From the evolution of the pair distribution functions, it was evident that different commensurability scenarios and external potential strengths led to a rich structural landscape. One of the surprising outcomes of our work is that the top layer exhibits qualitatively the same structural behavior than the one observed in the bottom layer. Particularly important is, for example, the fact that at $p = 1$ the top layer is forced to mimic the quasi-crystal structure of the bottom layer. Thus, by simply changing the substrate parameters, either order-like or disorder-like can be imposed on the substrate-free layer. This knowledge can be used to investigate, for instance, the role of the substrate on the growth of colloidal crystals and the ordering along the z-direction in layered systems.

In contrast to the observed structural behavior when $p = 1$, the MSD perpendicular to the fringes for particles on the substrate-free layer always showed normal diffusion at long-times, whereas in the bottom layer particle dynamics was characterized by the appearance of a plateau at high substrate strengths. This means that although particles on the top layer exhibits a sort of "solidlike" ordering, they still diffuse in the same manner on x- and y-directions.

Hence, a layered system subjected to periodic energy landscapes possesses a complex liquid-solid behavior that still needs to be studied in detail. The combination of confinement and external potentials suggest that the substrate strength, V_0^*, and the commensurability

factor, p, might be the key parameters to control crystallization-like processes in the directions parallel and perpendicular to the layers.

A natural extension of the present work is the explicit inclusion of HI, which could contribute to fluidize the system along the potential fringes. In addition, there are several physical observables that merit additional attention. For example, translational and orientational order parameters, the distribution and dynamics of topological defects as well as the distribution of displacements along and across the fringes, will allow us to study in detail the rich physical properties of layered systems when the first layer is under the action of a spatially modulated light field.

Finally, while considerable knowledge about the effect of a periodic substrate on a single colloidal monolayer exists, there are no experimental studies that probe the effect of a patterned substrate in a system of parallel monolayers. Hence, it is needed the experimental contribution to corroborate our predictions and to extend our understanding of directed self-assembly controlled by modulated fields.

BIBLIOGRAPHY

[1] A. Cacciuto and D. Frenkel, *Physical Review E*, 2005, **72**, 041604.

[2] N. Vogel, C. K. Weiss and K. Landfester, *Soft Matter*, 2012, **8**, 4044–4061.

[3] M. Grzelczak, J. Vermant, E. M. Furst and L. M. Liz-Marzán, *Acs Nano*, 2010, **4**, 3591–3605.

[4] U. Gasser, *Journal of Physics: Condensed Matter*, 2009, **21**, 203101.

[5] Y. Yin and A. P. Alivisatos, *Nature*, 2004, **437**, 664–670.

[6] H. Löwen, *Journal of Physics: Condensed Matter*, 2008, **20**, 404201.

[7] H. Löwen, *Journal of Physics: Condensed Matter*, 2009, **21**, 474203.

[8] A. van Blaaderen, *Mrs Bulletin*, 2004, 85.

[9] K. Zahn and G. Maret, *Current opinion in colloid & interface science*, 1999, **4**, 60–65.

[10] R. Bubeck, P. Leiderer and C. Bechinger, *Structure and dynamics of two-dimensional colloidal systems in circular cavities*, Springer, 2001.

[11] C. Contreras-Aburto, J. Méndez-Alcaraz and R. Castañeda-Priego, *The Journal of chemical physics*, 2010, **132**, 174111.

[12] S. Herrera-Velarde, A. Zamudio-Ojeda and R. Castañeda-Priego, *The Journal of chemical physics*, 2010, **133**, 114902.

[13] M. C. Jenkins and S. U. Egelhaaf, *Journal of Physics: Condensed Matter*, 2008, **20**, 404220.

[14] A. Ashkin, *Phys. Rev. Lett.*, 1970, **24**, 156–159.

[15] C. Dalle-Ferrier, M. Krüger, R. D. Hanes, S. Walta, M. C. Jenkins and S. U. Egelhaaf, *Soft Matter*, 2011, **7**, 2064–2075.

[16] Q.-H. Wei, C. Bechinger, D. Rudhardt and P. Leiderer, *Physical review letters*, 1998, **81**, 2606–2609.

[17] A. Chowdhury, B. J. Ackerson and N. A. Clark, *Physical review letters*, 1985, **55**, 833–836.

[18] K. Franzrahe, P. Nielaba, A. Ricci, K. Binder, S. Sengupta, P. Keim and G. Maret, *Journal of Physics: Condensed Matter*, 2008, **20**, 404218.

[19] K. Franzrahe and P. Nielaba, *Physical Review E*, 2009, **79**, 051505.

[20] I. O. Götze, J. M. Brader, M. Schmidt and H. Löwen, *Molecular Physics*, 2003, **101**, 1651–1658.

[21] R. L. Vink, T. Neuhaus and H. Löwen, *The Journal of chemical physics*, 2011, **134**, 204907.

[22] R. L. Vink and A. Archer, *Physical Review E*, 2012, **85**, 031505.

[23] E. Frey, D. R. Nelson and L. Radzihovsky, *Physical review letters*, 1999, **83**, 2977–2980.

[24] J. Baumgartl, M. Brunner and C. Bechinger, *Physical review letters*, 2004, **93**, 168301.

[25] F. Bürzle and P. Nielaba, *Physical Review E*, 2007, **76**, 051112.

[26] C. Bechinger and E. Frey, *Journal of Physics: Condensed Matter*, 2001, **13**, R321.

[27] S. Herrera-Velarde and R. Castañeda-Priego, *Physical Review E*, 2009, **79**, 041407.

[28] M. I. Hoopes, M. Deserno, M. L. Longo and R. Faller, *The Journal of chemical physics*, 2008, **129**, 175102.

[29] C. Xing and R. Faller, *Soft Matter*, 2009, **5**, 4526–4530.

[30] S. Varma, M. Teng and H. L. Scott, *Langmuir*, 2012, **28**, 2842–2848.

[31] J. Dobnikar, R. Castañeda-Priego, H.-H. von Grünberg and E. Trizac, *New Journal of Physics*, 2006, **8**, 277.

[32] R. Castañeda-Priego, L. F. Rojas-Ochoa, V. Lobaskin and J. Mixteco-Sánchez, *Physical Review E*, 2006, **74**, 051408.

[33] R. Castañeda-Priego, V. Lobaskin, J. Mixteco-Sánchez, L. Rojas-Ochoa and P. Linse, *Journal of Physics: Condensed Matter*, 2012, **24**, 065102.

[34] S. Bleil, H.-H. von Grünberg, J. Dobnikar, R. Castaneda-Priego and C. Bechinger, *EPL (Europhysics Letters)*, 2006, **73**, 450.

[35] S. Herrera-Velarde and R. Castañeda-Priego, *Journal of Physics: Condensed Matter*, 2007, **19**, 226215.

[36] C. Reichhardt and C. O. Reichhardt, *Physical Review E*, 2005, **72**, 032401.

[37] Y. Enomoto, M. Sawa and H. Itamoto, *Physica A: Statistical Mechanics and its Applications*, 2005, **345**, 547–554.

[38] D. L. Ermak and J. McCammon, *The Journal of chemical physics*, 1978, **69**, 1352.

[39] A. Reinmüller, E. Oğuz, R. Messina, H. Löwen, H. Schöpe and T. Palberg, *The Journal of Chemical Physics*, 2012, **136**, 164505.

[40] E. C. E.-D. S. Herrera-Velarde, A. Delgado-González, *To be submitted*.

8

CONCLUDING REMARKS

"The science of today is the technology of tomorrow."
Edward Teller

At the present time, colloids are model systems by excellence in *Soft Matter*. One of the main goals of the colloidal systems is that the understanding of an infinite number of physical problems could only be achieved by some interesting facts about colloids: tuning the inter–colloidal interactions is relatively easy and at the lab one can directly visualize the position, the shape and the movements of the colloidal particles. On the other hand, during recent years, the interference of laser beams has been used to simulate the presence of substrates in a large variety of geometries opening up the doors of a huge set of studies about the dynamical and structural behavior of colloidal systems under the influence of such external fields. The present thesis has been developed within the use of theoretical approaches and numerical methods for the solution of the equations of motion of simple systems. Our main tool: the Brownian dynamics method for computer simulations. We developed a systematic analysis of the structural and dynamical properties of non-directly and directly-interacting colloids. For the latter case, we studied mainly two kinds of interactions, namely, Yukawa and super-paramagnetic potentials. Furthermore, we were able to study colloidal system in a wide range of different confinements achieving for each system a different dimension starting from a quasi-zero-dimension to a quasi-three-dimension passing by intermediate levels of confinement. Our results showed interesting dynamical behaviors and also a large variety of structural phases as a function of the strength and shape of the external field.

Our first topic was the study of the the hydrodynamic coupling in systems consisting of two and three colloidal particles. Here, we particularly addressed the question of the importance of a third body on the two-body correlation functions for different particle configurations. We showed that a third particle influences the self-motion of a particle, as well as the two-body cross-correlation functions, leading to very interesting and non-trivial dynamical phenomena. We found that the dynamical behaviour induced by the presence of the

third particle can be used as a novel way to tune the hydrodynamic coupling between particles. According to the relative position of the third particle, the coupled motion of the first two beads may be affected and even positive or negative correlation effects could be promoted. Therefore, the presence of more than two particles could enhance or decrease the particle diffusion. One aspect that we must highlight is that at very small particle separations lubrication forces may dominate on the particle dynamics and, in consequence, could have a strong influence on the dynamical modes. Such topic can be addressed in future works considering also with the role of rotational motion, as well as many-body forces on the hydrodynamic coupling in few-particle colloidal systems.

We also investigated, by means computer simulation techniques, the effects due to hydrodynamic interactions on the diffusive properties of repulsively interacting colloids confined in a one–dimensional channel and subjected to a periodic external potential. We performed an extensive study covering an extended parameter space that includes weak and strong couplings among particles and different values of the external potential strength. The latter led us to discuss some points about the results showed: in general, the complex dynamical scenario of both systems is basically the same because both potentials led to a correlation of the particles at long inter–particle separations. We also found that hydrodynamic interactions led to an enhancement of the particle mobility. When the external potential is switched on, the particle diffusion became sensitive to the strength and commensurability of the sinusoidal potential with the inter-particle spacing. Most of the dynamical properties can be explained in terms of collective diffusion, due to the long-range nature of the HI, and the competition between particle-particle and particle-substrate interactions. From the present work, we can suggest different scenarios that can lead to interesting phenomena, one is to investigate irrational commensurablities. We also we expect different and exciting scenarios when attractive and repulsive short-range potentials are implemented. Besides "mixtures" of different strength or types of interaction can lead to great discoveries.

Furthermore, we found structural transitions in planar interacting colloidal systems at a constant density subjected to a parabolic field applied in one direction. According with the increase in the intensity of the parabolic trap, we found loss (gain) of structure transitions classified as *melting*-like (*freezing*-like). We analyzed the ordering of the first layer of neighbors that also helped us in the characterization of the structural phase transitions, which is of crucial importance for the development of technological devices that require a precise knowledge on the localization of the particles. Moreover, we found that super-paramagnetic particles showed smooth transitions between supper–cooled liquid, cooled–liquid and liquid while

the system of Yukawa particles jumped from supper-cooled liquid to liquid (and vice versa) with a small increment of the trap strength. We were able to provide a structural phase diagram, although the complete phase diagram of the particles analyzed here would be a complement of this study and shed some light about the structural and dynamical behavior of colloidal going through non-trivial structural transitions.

Another asset reached in the present thesis was the study of the dynamical transitions of the systems previously mentioned. The inclusion of the hydrodynamic interactions allowed us to have a better scenario about the colloidal systems under confinement. According with the increase of the trap stiffness, we found that the systems present different dynamical behaviors at long times which either can be normal two-dimensional diffusion, and sub- and hyper-diffusion. Also, we found that the mobility of the particles is larger when the hydrodynamic interactions are considered. We analyzed the probability density function of a particle which is equivalent to find the solution of the coupled Smoluchowski equations for the system. Furthermore, we were able to describe the interaction of the particle with its neighbor-layer and give more light about the caging effect induced by those particles and the external field. We also found that the HI are implicitly related with the fluidization of the suspension. The complexity of the HI in such kind of systems is large and can be visualized as counter-intuitive effects. We presented a study whose discussion and results may be relevant to find an a appropriate approach to attack much more complex systems, such as the biological ones. Still, different open questions remain about self-assembly of colloids and the HI, such as the consequences of density gradients and the dynamics mixtures of several species of interacting colloidal particles.

Finally, we approached to the tree-dimensional world of colloids by studying a quasi-three-dimensional system. We have investigated the effect of a one-dimensional periodic potential on the structure and diffusive behavior of interacting colloidal particles confined in two parallel monolayers. Basically, we have shown that the physical properties of the upper layer can be indirectly modified by the external potential, although the substrate has direct influence only on the bottom layer. We found that different commensurability scenarios and external potential strengths led to a rich structural landscape. Thus, by simply changing the substrate parameters, either order-like or disorder-like can be imposed on the substrate-free layer. In contrast to the observed structural behavior for a particular case where the conmmensurabilty was $p = 1$, we found that although particles on the top layer exhibits a sort of "solid-like" ordering, they still diffuse in the same manner on x- and y-directions. A layered system subjected to periodic energy landscapes possesses a complex liquid-solid behavior that still needs to be studied in detail. The combina-

tion of confinement and external potentials suggest that the substrate strength, and the commensurability factor, might be the key parameters to control crystallization–like processes in the directions parallel and perpendicular to the layers. A natural extension of the present work is the explicit inclusion of hydrodynamic interactions, which could contribute to fluidize the system along the potential fringes. Our work is of special interest for the design of photonic crystals due to the fact that periodic arrays of spherical particles make similar arrays of interstitial voids, which act as a natural diffraction grating for light waves in photonic crystals, especially when the interstitial spacing is of the same order of magnitude as the incident lightwave.

With no doubt, one of the basic topics of the Soft Condensed Matter is the manipulation of colloids by external fields, which, as we have seen through the present thesis, still has plenty of open questions to be answered. Up to now, the state-of-the-art in the manipulation of optical tools, that several experimental research groups have reached all over the globe, makes visible the corroboration of all the results contained in the present thesis in a short-term. We invite those experimentalists to join forces and to work in these challenging topics.

Furthermore, we would like to highlight that the study of colloids involves interdisciplinary knowledge, the results can be directly addressed to the design of new technologies not only for the basic-Science interests but for several kinds of industries like medical, food and photonics, just to mention a few.

Part I

APPENDIX

A

HISTORICAL REVIEW OF BROWNIAN MOTION

"If you don't know history, then you don't know anything. You are a leaf that doe

–Michael Crichton

Here, we briefly describe the history of Brownian motion, as well as the contributions of Einstein, Sutherland, Smoluchowski, and Langevin to its theory. The present Appendix contains fragments of a more detailed historical review made by Bertrand Duplantier for the Poincaré Seminar in 2005 [1].

A.1 ROBERT BROWN

Robert Brown (1773-1858), of Scottish descent, was one of the greatest botanists of his time in Great Britain. He is renowned for his discovery of the nucleus of plant cells, for being the first to recognize the phenomenon of cytoplasmic streaming, and for the classification of several thousands dried plant specimens he brought back to England from a trip to Australia in 1801-1805 [1, 2]. In a pamphlet, dated July 30th, 1828, first printed privately [1, 3, 4], then published in the Edinburgh New Philosophical Journal later that year [1, 5], and republished several times elsewhere [1, 6–8], entitled "*A Brief Account of Microscopical Observations Made in the Months of June, July, and August, 1827, on the Particles Contained in the Pollen of Plants*" and "*on the General Existence of Active Molecules in Organic and Inorganic Bodies*" Brown reported on the random movement of different particles that are small enough to be in suspension in water. It is an extremely erratic motion, apparently without end (see Fig. A.1) . A second article, dated July 28th, 1829, was published later and bears the brief title "*Additional Remarks on Active Molecules*" [1, 4, 9, 10].

One can find examples at www.lpthe.jussieu.fr/poincare/

Brown used the wording active molecule in these titles in a sense different from its current one. It referred to earlier teaching of Georges-Louis Leclerc de Buffon (1707-1788) who introduced this word for the hypothetical ultimate constituents of the bodies of living beings. Only later with the acceptance and development of Dalton's 1803 atomic theory the word molecule was going to take on its modern mean-

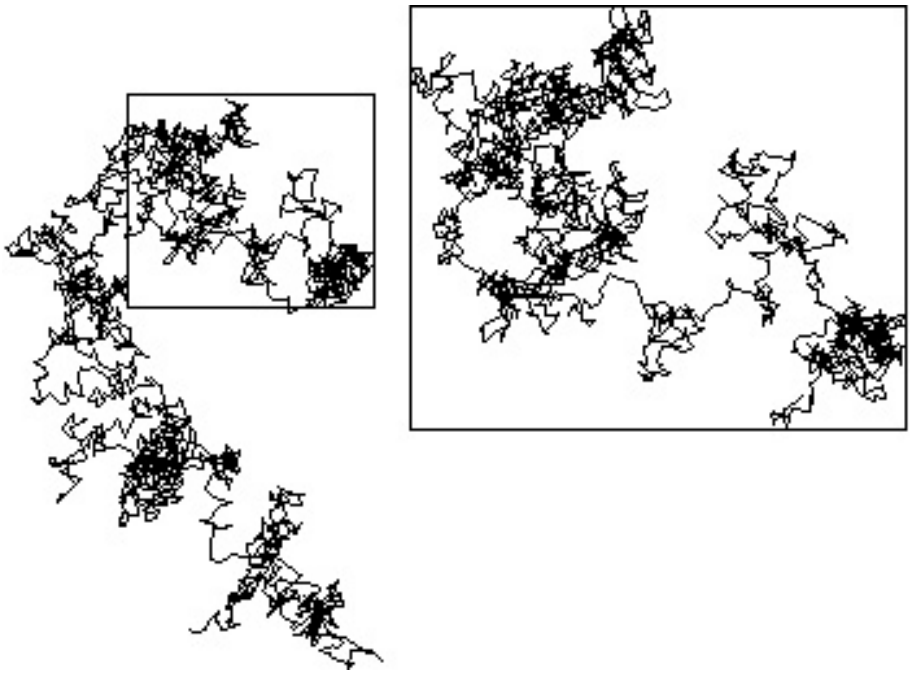

Figure A.1: Brownian motion described by a pollen granule in suspension

ing. The first plant Brown studied was Clarkia pulchella, see Fig. A.2, whose pollen grains contain granules varying

> *from nearly* 1/4000 *to about* 1/3000 *of an inch in length, and of a figure between cylindrical and oblong, perhaps slightly flattened...*

(from about six to eight microns). It is these granules, not the whole pollen grains, upon which Brown made his observations.

Brown may have not been the first, however, to observe Brownian motion. In fact, he discussed in his second article (1829) [1, 11] previous observations by others which could have been interpreted

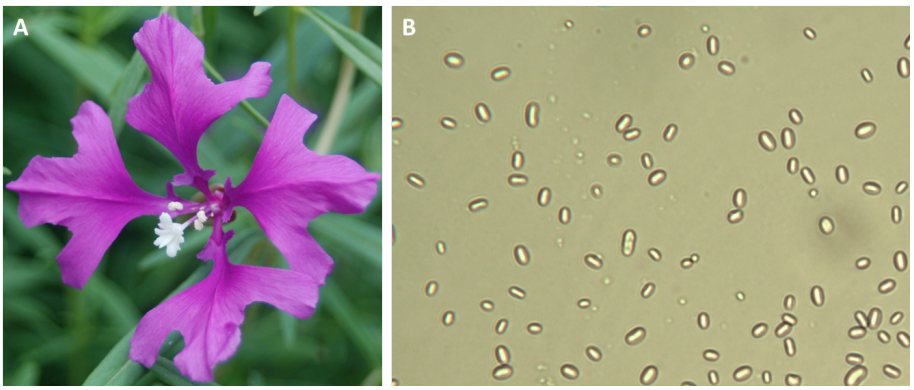

Figure A.2: A) provides an image of the Clarkia Pulchella flower used in early experiments of R. Brown, B) Amyloplasts and (a few) spherosomes from Clarkia pulchella

as prior to his. The universal and irregular motion of small grains suspended in a fluid may have been observed soon after the discovery of the microscope. The story begins with Anthony van Leeuwenhoek (1632-1723), a famous constructor of microscopes in Delft, who in 1676 was also designated executor of the estate of the no-less-famous painter Johannes Vermeer, who was apparently a personal friend . Leeuwenhoek built several hundred simple "microscopes," with which he went as far as to observe living bacteria and discover the existence of spermatozoids.

Although no document exists testifying a relationship between Vermeer and van Leeuwenhoek, it seems impossible that they did not know one another. The two men were born in Delft the same year, their respective families were involved in the textile business and they were both fascinated by science and optics. A commonly accepted and probable hypothesis is that Anthony van Leeuwenhoek was in fact a model for Vermeer, and perhaps also the source of his scientific information, for the two famous scientific portraits, The Astronomer, 1668, (Louvre Museum, Paris), and The Geographer, 1668-69, (Städelsches Kunstinstitut am Main, Frankfurt).

Brown's first publication on the erratic motion of the granules of pollen grains garnered much attention, but the use of the ambiguous terms "*active molecules*" by Brown brought him criticisms based on some misunderstanding. Indeed, under the influence of Buffon, the similar expression "*organic molecules*" represented hypothetical entities, elementary bricks all living beings would be made of. Such theories were still around at the beginning of the 19th century. His emphasis leads one to think that Brown's opinion was that the observed particles themselves were animated. Faraday himself had to defend him during a Friday night lesson he gave at the Royal Society on February 21, 1829, about Brownian motion [1, 12]. This led Brown in his Supplement Additional Remarks on Active Molecules to an apology.

Brown's merit was in gradually emancipating himself from this misconception and in making a systematic study of the ubiquity of "*active molecules*," hence of the movement named after him, with grains of pollen, dust and soot, pulverized rock, and even a fragment from the Great Sphinx! This served to eliminate the "*vital force*" hypothesis, where the movement was reserved to organic particles. As for the nature of Brownian motion, even if Brown could not explain it, he eliminated easy explanations, like those linked to convection currents or to evaporation, by showing that the Brownian motion of a simple particle stayed "*tireless*" even in a isolated drop of water in oil! On the same occasion he eliminated as well the hypothesis of movements created by interactions between Brownian particles, a hypothesis that would nevertheless reappear later.

A.2 THE PERIOD BEFORE EINSTEIN

Between 1831 and 1857 it seems that one can no longer find references to Brown's observations, but from the 1860's forward his work began to draw large interest. It was noticed soon thereafter in literary circles, if we are to judge by a passage of "*Middlemarch*" published by George Eliot in 1872, where Rev. M. Farebrother offers to make an exchange to the surgeon Lydgate:

> *I have some sea-mice- fine specimens- in spirits. And I will throw in Robert Brown's new thing - Microscopic Observations on the Pollen of Plants- if you don't happen to have it already.*

Jean Perrin wrote in his famous 1909 memoir Brownian Motion and Molecular Reality [1, 13]: In the 1860's, the idea emerged that the cause of the Brownian motion has to be found in the internal motion of the fluid, namely that the zigzag motion of suspended particles is due to collisions with the molecules of the fluid. The first name worth citing in this regard is probably that of Christian Wiener, holder of the Chair of Descriptive Geometry at Karlsruhe, who in 1863 reaffirmed in the conclusions to his observations that the motion could be due neither to the interactions between particles, nor to differences in temperature, nor to evaporation or convection currents, but that the cause must be found in the liquid itself [1, 14]. Such an explanation was criticized by R. Mead Bache, who showed that the motion was insensitive to the color of light, whether it was violet or red [1, 15]. Christian Wiener is nevertheless credited by some authors as the first to discover that molecular motion could explain the phenomenon [1, 13]. At least three other people proposed the same idea: Giovanni Cantoni of Pavia, and two Belgian Jesuits, Joseph Delsaulx and Ignace Carbonelle. The Italian physicist attributed Brownian movement to thermal motions in the liquid. The Belgian physicists published in the Royal Microscopical Society and in the Revue des Questions scientifiques, from 1877 to 1880, various Notes on the Thermodynamical Origin of the Brownian Movement. In 1888 the French physicist Louis-Georges Gouy made the best observations on Brownian motion, from which he drew the following conclusions:

- The motion is extremely irregular, and the trajectory seems not to have a tangent.
- Two Brownian particles, even close, have independent motion from one another.
- The smaller the particles, the livelier their motion.
- The nature and the density of the particles have no influence.
- The motion is most active in less viscous liquids.
- The motion is most active at higher temperatures.
- The motion never stops.

Gouy seemed, however, to claim again that one cannot explain Brownian motion by disordered molecular motion, but only by the partially organized movements over the order of a micron within the liquid. But somehow he became known as the "*discoverer*" of the cause of Brownian motion, as Jean Perrin wrote about his experimental conclusions

> *"Thus comes into evidence, in what is termed a fluid in equilibrium, a property eternal and profound. This equilibrium only exists as an average and for large masses; it is a statistical equilibrium. In reality the whole fluid is agitated indefinitely and spontaneously by motions the more violent and rapid the smaller the portion taken into account; the statical notion of equilibrium is completely illusory."*

A.3 WILLIAM SUTHERLAND

In his famous biography of Einstein, *Subtle is the Lord...* (1982), Abraham Pais noted, while describing Einstein's route to his well-known diffusion relation, that the same relation had been discovered "*at practically the same time*" by the Melbourne theoretical physicist William Sutherland, following similar reasoning to Einstein's, and had been submitted for publication to the *Philosophical Magazine* in March 1905, shortly before Einstein completed the doctoral thesis in which he first announced the relation.

Sutherland's paper to which Pais refers was actually published in June 1905 [1, 16], after Einstein completed his thesis, but shortly before he submitted it for examination. We seem to be looking here at a perfect example of effectively simultaneous discovery. However, as Rod Home notes, the story is still a little more complicated, for Sutherland had already reported his derivation over a year earlier, at the congress of the Australasian Association for the Advancement of Science held in Dunedin, New Zealand, in January 1904, and his paper had been published in the congress proceedings in early 1905! [1, 17] Unfortunately, there was a *misprint* in the crucial equation giving the diffusion coefficient of a large molecular mass in terms of physical parameters: Avogadro's constant was missing!

As R. W. Home remarks, it is clear that one is looking at a genuine misprint in the proceedings, since the preceding line was given correctly.

In 1903, Einstein and his friend Michele Besso discussed a theory of dissociation that required the assumption of molecular aggregates in combination with water, the "hypothesis of ionic aggregates," as Besso called it. This assumption opens the way to a simple calculation of the sizes of ions in solution, based on hydrodynamical considerations. In 1902, Sutherland had considered in *Ionization, Ionic Velocities, and Atomic Sizes*[1, 18] a calculation of the sizes of ions on the basis of Stokes' law, but criticized it as in disagreement with experimental data [1]. The very same idea of determining sizes of ions by means of classical hydrodynamics occurred to Einstein in his letter of 17 March 1903 to Besso [1, 19], where he proposed what appears to be just the calculation that Sutherland had performed. That Sutherland, in spite of his isolation in Melbourne, was well-known in physics circles is also evidenced by the fact that he was invited to contribute to the Boltzmann Festschrift in 1904-the only other non-European contributor being J. Willard Gibbs!.

A.4 ALBERT EINSTEIN

Einstein completed his dissertation on "*A New Determination of Molecular Dimensions*" on 30 April 1905, and submitted it to the University of Zürich on 20 July. Shortly after being accepted there, the manuscript was sent for publication to the Annalen der Physik, where it would be published in 1906 [1, 21]. On 11 May 1905, eleven days after finishing his thesis, Einstein had also sent the manuscript of his first paper on Brownian motion to the Annalen, which would publish it on 18 July 1905.

Einstein had already submitted a dissertation in 1901, on "a topic in the kinematic theory of gases". By February 1902, he had withdrawn the dissertation, possibly at his advisor's suggestion to avoid a controversy with Boltzmann. (For a detailed analysis, see [1, 20]). Nevertheless, there is no doubt that Einstein was a great admirer of Boltzmann.

Einstein's central assumption is the validity of using classical hydrodynamics to calculate the effect of solute molecules, treated as rigid spheres, on the viscosity of the solvent in a dilute solution. His method is well suited to determine the size of solute molecules that are large compared to those of the solvent, and he applied it to solute sugar molecules. As we have seen above, Sutherland published in 1905 a method for determining the masses of large molecules, with which Einstein's method shares many important elements. Both methods make use of the molecular theory of diffusion that Nernst[1, 22] developed on the basis of van 't Hoff's analogy between solutions and gases, and of Stokes' law of hydrodynamic friction.

Einstein's dissertation was at first overshadowed by his more spectacular work on Brownian motion, and it required an initiative by Einstein to bring it to the attention of the scientists of his time. The paper on Brownian motion, the first of several on this subject that Einstein published over the course of the next couple of years, actually included his first published statement of the famous relationship linking diffusion with viscosity, that he had derived in his thesis. As Abraham Pais points out in Subtle is the Lord..., this equation has found widespread applications, as a result of which Einstein's January 1906 paper in the Annalen der Physik, the published version of his dissertation, later became his most frequently cited paper! [1] As stressed by R. H. Home in his essay on Sutherland, Pais also goes on to argue that the thesis was also one of Einstein's "most fundamental papers", of comparable intrinsic significance to the other papers Einstein wrote in that year of 1905 [1]. "In my opinion," Pais writes, "the thesis is on a par with (Einstein's) Brownian motion article": indeed, "in some if not all respects, his results are by-products of his thesis work."

The 1905 article on Brownian motion

The 1905 article is entitled: "*On the Motion of Small Particles Suspended in Liquids at Rest, Required by the Molecular-Kinetic Theory of Heat.*" [23] There, Einstein tried to establish the existence and the size of molecules, and to determine a theoretical method for computing Avo-

gadro's number precisely, by using the molecular kinetic theory of heat. In fact, he concluded:

"Let us hope that a researcher will soon succeed in solving the problem presented here, which is so important for the theory of heat!"

> *Móge es bald einem Forscher gelingen, die hier aufgeworfene, für die Theorie der Wärme wichtige Frage zu entscheiden !*

Astonishingly enough, he was not yet certain that one could apply it to Brownian motion. In fact, his introduction opens with:

> *In this paper it will be shown that, according to the molecular-kinetic theory of heat, bodies of a microscopically visible size suspended in liquids must, as a result of thermal molecular motions, perform motions of such magnitude that they can be easily observed with a microscope. It is possible that the motions to be discussed here are identical with so-called Brownian molecular motion; however the data available to me on the latter are so imprecise that I could not form a judgement on the question.*

Einstein relied on the results of his thesis, that he completed eleven days before submitting his famous article on the suspensions of particles. Only later would his predictions be progressively confirmed by refined experimental data on Brownian motion [1].

A.5 MARIAN VON SMOLUCHOWSKI

Smoluchowski's name is closely attached to Brownian motion and the theory of diffusion, as we will show here. Moreover, as Marc Kac wrote about Smoluchowski,[1, 24] the latter showed through a true intellectual *tour de force*, that the notion of a game of chance lies at the heart of our comprehension of physical phenomena. We are indebted to him for his original and bold introduction of the calculus of probability in statistical physics.

This probabilistic point of view is clearly present in Smoluchowski's first article on Brownian motion, "*Essay on the theory of Brownian motion and disordered media*" 101 published in 1906 (very likely under the pressure of Einstein's publication of his first two articles), as well as in another article, about the mean free path of molecules in a gas [1, 25]. In these remarkable articles he was seemingly the first to establish the relation between *random walks* and Brownian diffusion, even though in 1900 Louis Bachelier had already introduced the model of a random walker in his thesis *The Theory of Speculation*.

Smoluchowski begins by citing Einstein's work from 1905 and writes that the latter's results

> *completely agree with those I obtained a few years ago by an entirely different path of reasoning, and that since then I have considered an important argument in favor of the kinetic nature of these phenomena.*

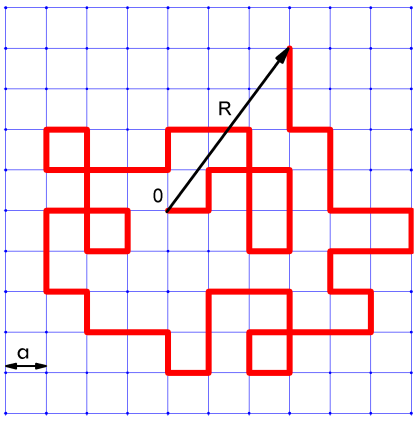

Figure A.3: Random walk on a square lattice with elementary lattice step a. We choose each step at random. In two dimensions, two equivalent methods exist. In the first one, we draw heads or tails (with a probability of $1/2$) for a direction, vertical or horizontal, and next the orientation along the chosen direction. In the second method, we draw with the same probability (with probability of $1/4$) one of the four possible directions. In the continuous limit where the lattice step goes to 0, a very long random walk will take the appearance of the Brownian motion of Fig. A.1. (Adapted figure from Ref. [1])

However, he adds further along that his own method

> *seems more direct, simpler, and perhaps more convincing than that of Einstein.*

While Einstein (like Sutherland) avoids all treatment of collisions in favor of a general thermodynamic approach, Smoluchowski has a clear kinetic vision and treats the Brownian motion as a random walk or a game of heads or tails, see Fig. A.3.

The newness and the originality of Smoluchowski's approach is in the replacement of an incredibly difficult problem (a Brownian particle which collides within a gas or liquid) by a relatively simple stochastic process. Each dynamic event like a collision is considered as a random event similar to a game of heads or tails, or to the throw of a dice, where the elementary probabilities are (to a certain extent) determined by underlying mechanical laws. This way of reasoning plays a fundamental role in mechanics and statistical physics today and, as Marc Kac noticed, it is difficult for us today to imagine the degree of Smoluchowski's intellectual boldness in starting this subject during the early years of the last century.

With Einstein, Smoluchowski shares the credit for having shown the importance of microscopic fluctuations in statistical physics, at the same time promoting the probabilistic approach. In this sense he appears as a great master inheritor in physics of the *Doctrine of Chance* of Abraham de Moivre.

In 1917, Marian von Smoluchowski had just been elected rector of the Jagellonian University in Kraków (Cracow) University, but he was never to fulfill his new task. During the summer he succumbed to an epidemic of dysentery. During his illness he complained to his wife that he could have done so much more. He died prematurely in September of 1917 at the age of forty five.

In 1973 Chandrasekhar was awarded the Marian von Smoluchowski Medal of the Polish Physical Society in appreciation of his contributions to stochastic methods in physics and astrophysics and, especially, the Review of Modern Physics 1943 article which covered Smoluchowski's contributions. In his speech at the award ceremony, Chandrasekhar noted that the Nobel prizes in chemistry awarded to R. Zsigmondy in 1925 and to T. Svedberg in 1926 were for experimental confirmation of Smoluchowski's theoretical predictions on colloidal and disperse systems and that if Smoluchowski had been still alive he would certainly have been a Nobel laureate himself [1, 24].

A.6 PAUL LANGEVIN

Langevin's scientific thought displayed an extraordinary clarity and vivacity combined with a quick and sure intuition for the essential point. Because of those qualities, his courses exerted a decisive influence on more than a generation of French theoretical physicists. ... It seems to me certain that he would have developed the special theory of relativity if that had not been done elsewhere, for he had clearly recognized its essential points.

In 1908, Langevin, whose skill in kinetic theory had first been developed when he worked on ionic transport, turned briefly to the theory of Brownian motion developed by Einstein in 1905 and, via a more direct route, by Smoluchowski in 1906. The result was simplified, still-standard treatment which, unlike Smoluchowski's, produced precisely Einstein's formula for the mean-square displacement. Subsequently Langevin took up the subject of thermodynamics and reconsidered its basic notions, starting from theories of Boltzmann and of Planck ("the physics of the discontinuous") in 1913.

A.7 JEAN PERRIN EXPERIMENTS

Jean Perrin is often cited as the one who established the Einstein-Smoluchowski-Sutherland theory by his beautiful experiments. He was also an outstanding promotor of atomistic ideas [1, 26].

He further expounded on the idea that non-differentiable continuous functions, such as the trajectory of Brownian motion, were as completely natural as differentiable functions, objects of all prior studies. In the preface of Atoms, by considering the very irregular surface of a colloid and by making the analogy with the shape of Brittany's

coast, he announced with a dazzling geometric intuition the ideas of Lewis Fry Richardson on Hausdorff anomalous dimensions, which would later be developed by Benôit Mandelbrot [1, 27].

The beautiful experiments of 1908-1909 by Perrin and his students, on emulsions of gum-resin ("gamboge") or of mastic, are described in detail in his review article Brownian Motion and Molecular Reality, which appeared in Annales de Chimie et Physique in 1909 [1, 28], and the results are published in several Notes *aux Comptes Rendus*. The same material is also summarized in his book Atoms. Perrin began by verifying the exponential distribution of the density of n particles in a suspension, as a function of the height h in a gravitational field g, a formula that generalizes the barometric formula for the atmosphere.

He built as well an apparatus for fractioned centrifugation to produce emulsions of uniform size, a key element of his success. Using three independent processes to measure the radius of particles, one of which went via Stokes' law, he could verify the validity of the latter for particles in suspension. It was in fact one of the weak points of the theoretical proofs, because the continuity conditions required by hydrodynamics were far from being clearly fulfilled in the case of small spheres in very active Brownian motion [1].

BIBLIOGRAPHY

[1] B. Duplantier, in *Einstein, 1905–2005*, Springer, 2006, pp. 201–293.

[2] D. T. Moore, *TASFORESTS-HOBART-*, 2000, **12**, 123–146.

[3] R. Brown, *The Philosophical Magazine, or Annals of Chemistry, Mathematics, Astronomy, Natural History and General Science*, 1828, **4**, 161–173.

[4] R. Brown, *The miscellaneous botanical works of Robert Brown*, Published for the Ray society by R. Hardwicke, 1866, vol. 1.

[5] R. Brown, *Edinburgh New Phil. J.*, 1828, **5**, 358–371.

[6] R. Brown, *Ann. Sci. Naturelles (Paris)*, 1828, **14**, 341–362.

[7] R. Brown, *Phil. Mag.*, 1828, **4**, 161–173.

[8] R. Brown, *Ann. d. Phys. u. Chem.*, 1828, **14**, 294–313.

[9] R. Brown, *Edinburgh Journal of Science (new series)*, 1829, **1**, 314–319.

[10] R. Brown, *Phil. Mag.*, 1829, **6**, 161–166.

[11] R. Brown, *The Philosophical Magazine, or Annals of Chemistry, Mathematics, Astronomy, Natural History, and General Science*, 1829, **6**, 161–166.

[12] S. G. Brush, *The kind of motion we call heat*, North-Holland Amsterdam, 1976, vol. 2.

[13] J. Perrin, Annales de Chimie et de Physique, 1909, pp. 5–104.

[14] C. Wiener, Ann. d. Physik, 1863, p. 79.

[15] R. M. Bache, *Proceedings of the American Philosophical Society*, 1894, **33**, 163–177.

[16] W. Sutherland, *The London, Edinburgh, and Dublin Philosophical Magazine and Journal of Science*, 1905, **9**, 781–785.

[17] W. Sutherland, Report of the 10th Meeting of the Australasian Association for the Advancement of Science, Dunedin, 1904, p. 117.

[18] W. Sutherland, *The London, Edinburgh, and Dublin Philosophical Magazine and Journal of Science*, 1902, **3**, 161–177.

[19] A. Einstein, M. A. Besso and P. Speziali, *Albert Einstein, Michele Besso, correspondence, 1903-1955*, Hermann, 1972.

[20] M. J. Klein, A. Kox, J. Renn and R. Schulmann, *The collected papers of Albert Einstein*, 1993, **5**, year.

[21] A. Einstein, *Annalen der Physik*, 1906, **324**, 289–306.

[22] W. Nernst, *Zeitschrift Fur Physikalische Chemie–Stochiometrie Und Verwandtschaftslehre*, 1905, **53**, 235–244.

[23] A. Einstein, *Annalen der Physik*, 1905, **322**, 549–560.

[24] S. Chandrasekhar, M. Kac and R. Smoluchowski, *Marian Smoluchowski, His Life and Scientific Work*, Polish Scientific Publishers, PWN, Warszawa, 2000.

[25] M. R. von Smolan Smoluchowski, Bulletin International de l'Académie des Sciences de Cracovie, 1906, pp. 202–213.

[26] S. Chandrasekhar, M. Kac and R. Smoluchowski, *Les Atomes*, Félix Alcan, 1913.

[27] J.-F. Gouyet and B. Mandelbrot, *Physics and fractal structures*, Masson Paris, 1996.

[28] J. Perrin, *Ann. Chim. Phys.*, 1909, **18**, 1–114.

B

CURRICULUM VITAE

Edith Cristina Euán Díaz

Contact information

Institute: División de Ciencias e Ingenierías.
Campus León. Universidad de Guanajuato.
and
Condensed Matter Group. Physics Department.
University of Antwerp.

Address:	University of Guanajuato	University of Antwerp
	Loma del Bosque 103	Groenenborgerlaan 171
	Lomas del Campestre	Antwerp
	Leon, Guanajuato, Mexico	Belgium
	37150	BE-2020
Phone:	+52 (477) 788-5100	+32 3 265 36 64
Fax:	+52 (477) 788-5100	+32 3 265 35 42

e-mail: edith@fisica.ugto.mx, editheuan@gmail.com.

Personal Information

Date of birth:	June 23rd, 1986.	
Address:	319 de los Manzanos	59 Oude-Godstraat
	99059	BE-2650
	Fresnillo,Mexico.	Edegem, Belgium.

Languages: Spanish (Native), English (Proficient User), German (Basic).

Research interests: Soft matter, complex fluids, biological systems, applied physics.

Education

2010-2014	PhD degree in Physics. (Joint-PhD)
	División de Ciencias e Ingenierías. Campus León. Universidad de Guanajuato. Mexico.
	and
	Condensed Matter Group. University of Antwerp. Belgium
	Thesis: *Structural and dynamical properties of colloids on substrates.*
2009	Master degree in Physics.
	División de Ciencias e Ingenierías. Campus León. Universidad de Guanajuato. Mexico.
	Thesis: *Colloidal suspensions, the role of hydrodynamic interactions.*
2007	Bachelor degree in Physics.
	Unidad Académica de Física. Universidad Autónoma de Zacatecas. Mexico.
	Thesis: *Substrate effect on a multilayered colloidal system.*

Publications

1. "Single-file diffusion in periodic energy landscapes: The role of hydrodynamic interactions", **Edith C. Euán-Díaz**, Vyacheslav R. Misko, Francois M. Peeters, Salvador Herrera-Velarde and Ramón Castañeda-Priego, *Physical Review E*, 2012, **86**, 031123.

2. "Directed Self-Assembly of Colloids on Parallel Layers by a One-Dimensional Modulated Substrate", Salvador Herrera-Velarde, Alexandra Delgado-González, **Edith C. Euán-Díaz** and Ramón Castañeda-Priego, *Journal of Nanofluids*, 2012, **1**, 44–54.

3. "Hydrodynamic correlations in three-particle colloidal systems in harmonic traps", Salvador Herrera-Velarde, **Edith C. Euán-Díaz**, Fidel Córdoba-Valdés and Ramón Castañeda-Priego, *Journal of Physics: Condensed Matter*, 2013, **25**,325102.

4. "Structural phases and dimensional variations induced by a parabolic potential in colloidal systems", **Edith C. Euán-Díaz**, Salvador Herrera-Velarde, Vyacheslav R. Misko, Francois M. Peeters and R. Castañeda-Priego, *To be submitted*.

5. "Self-diffusion of interacting colloids in a parabolic potential", **Edith C. Euán-Díaz**, Salvador Herrera-Velarde, Vyacheslav R. Misko, Francois M. Peeters and R. Castañeda-Priego, *To be submitted*.

6. "Single-file diffusion: The role of the attractive interactions", **Edith C. Euán-Díaz**, Salvador Herrera-Velarde and R. Castañeda-Priego, *To be submitted*.

Awards

2013 *Carl Storm International Diversity Fellowship*
Gordon Research Seminar: Soft Condensed Matter Physics
Colby-Sawyer College, New London, NH, USA

Invited Talks

2013 *Structural and dynamical properties of colloids under confinement.*
Gordon Research Seminar: Soft Condensed Matter Physics. Colby-Sawyer College, NH, USA.

2013 *Structural and dynamical properties of colloids under confinement.*
Statistical Physics Seminar. Physics Institute. Universidad Autónoma de San Luis Potosí. San Luis Potosí, Mexico.

Talks, Posters and Workshops

2013 *Poster:* Directed self-assembly of interacting colloids by a parabolic potential. Gordon Research Conference: Soft Condensed Matter Physics.
Colby-Sawyer College, NH, USA.

2013 *Poster:* Directed Self-Assembly of Colloids on Parallel Layers by a One-Dimensional Modulated Substrate.
Soft Condensed Matter Mexican Network, Second general meeting. Guanajuato, Mexico.

2013 *Poster:* Single file diffusion in colloidal systems: the role of hydrodynamic interactions.
Soft Condensed Matter Mexican Network, Second general meeting. Guanajuato, Mexico.

2012 *Poster:* Single file diffusion in colloidal systems: the role of hydrodynamic interactions.
Belgian Physical Society. General meeting. Brussels, Belgium.

2009 *Workshop:* Development of scientific outreach workshops.
16th National Week of Science and Technology. XXVI Anniversary of the Science Museum of the Universidad Autónoma de Zacatecas. Zacatecas, Mexico.

2008 *Workshop:* Development of scientific outreach workshops.
XXIII National Scientific Outreach Meeting. Zacatecas, Mexico.

2007 *Poster:* Substrate effects on charged colloids distributed on parallel layers.
XXXVII Winter Meeting on Statistical Physics. Taxco, Mexico.

2006 *Workshop:* Development of scientific outreach workshops.
Project: "Quark: Developing young science" ("Quark: Haciendo Ciencia Joven"), supported by INJUZAC. Zacatecas, Mexico.

2006 *Workshop:* Development of scientific outreach workshops.
XXVI National Congress of the Mexican Society of Surfaces and Materials Science. Puebla, Mexico.

2006 *Talk:* Analysis of crystallization by Brownian dynamics simulations.
XXVI National Congress of the Mexican Society of Surfaces and Materials Science. Puebla, Mexico.

2006 *Talk:* Analysis of crystallization by Brownian dynamics simulations.
XLIX National Congress on Physics. San Luis Potosí, Mexico.

2006 *Talk:* The Glories of the sky.
IV International Congress on Science Teaching and IX International Workshop on the Teaching of Physics. Havana, Cuba.

2005 *Poster:* Elastic constants tensor for cubic and hexagonal lattices.
XLVIII National Congress on Physics. Guadalajara, Mexico.

2005 *Workshop:* Development of scientific outreach workshops.
XXV National Congress of the Mexican Society of Surfaces and Materials Science. Zacatecas, Mexico.

2005 *Workshop:* Development of scientific outreach workshops.
Celebration of 15 Years of Children's Science Club of the Science Museum of the Universidad Autónoma de Zacatecas. Zacatecas, Mexico.

Research Visits

2013 Condensed Matter Theory Group. University of Antwerp. Belgium.

Topics: Structural and dynamical properties of colloids under confinement.

2011-2012 Condensed Matter Theory Group. University of Antwerp. Belgium.

Topics: Structural and dynamical properties of colloids under confinement.

2011 Condensed Matter Physics Laboratory. University of Düsseldorf. Germany.

Topics: Hydrodynamics in colloidal suspensions, external fields and their effects in dynamical and structural properties of colloids.

2010 Chemical Engineering Department. University of Delaware. USA.

Topics: Hydrodynamics in colloidal systems, effects of the interaction of external fields with colloidal suspensions.

2010 Universidad de las Américas, Puebla and Benemérita Universidad Autónoma de Puebla. México.

Topics: General Theory of tracer particles on colloidal suspensions and Espresso Programming.

2006 University of Guanajuato. Mexico.

Summer Research National Program supported by Mexican Academy of Sciences. *Project:* Colloidal dynamics of charged layered colloidal systems under the influence of external laser fields.

Academic Experience

Tutor

2012 *Physics III.* División de Ciencias e Ingenierías. Campus León. Universidad de Guanajuato.

2010 *Physics I.* División de Ciencias e Ingenierías. Campus León. Universidad de Guanajuato.

2008 Calculus I. División de Ciencias e Ingenierías. Campus León. Universidad de Guanajuato.

2007 *Physics I.* División de Ciencias e Ingenierías. Campus León. Universidad de Guanajuato.

Additional Experience

2006 *Delegate.* IV International Congress on Science Teaching and IX International Workshop on the Teaching of Physics. Havana, Cuba.

Organization and Logistics

2009 Organization and Logistics, collaborator 16th National Week of Science and Technology and XXVI Anniversary of the Science Museum of the Universidad Autóma de Zacatecas. Zacatecas, Mexico.

2008 Organization and Logistics of the XXIII National Scientific Outreach Meeting. Zacatecas, Mexico.

2006 Organization of the course: Initiation in the Popularization of Science through Recreation Workshops. Zacatecas, Mexico.

Additional Courses

2002 *Intermediate communicative English*. Sistema Educativo Nacional. Centro de capacitación para el trabajo industrial número 163. Fresnillo, Mexico.

2006 *Advanced English* (720 hours). Language Center. Universidad Autónoma de Zacatecas. Zacatecas, Mexico.

2006 *How to promote the scientific culture in young people between 15 and 18 years old? A didactic based proposal* (Cómo promover la cultura científica en los jóvenes de 15 a 18 años? Una propuesta didáctica fundamentada). By Beatriz Macedo, delegate of UNESCO in Latin America. Havana, Cuba.

2013 *Some Applications of Statistical Physics in Biology.* By Prof. Meheran Kardar (MIT). Institute for Intensive Theoretical Studies. Katholieke Universiteit Leuven.

Professional Societies

2009-present American Physical Society (APS). Student Member.

Technical Skills

Scientific Software: Mathematica, OriginPro, Latex, VMD, Espresso, Matlab.
Programming Languages: Fortran, TCL.
Operating Systems: Microsoft Windows, Linux, Macintosh.

C

APPROVAL LETTERS

León, Guanajuato, a 25 de noviembre de 2013

Director Dr. Guillermo Mendoza Díaz
División de Ciencias e Ingenierías
PRESENTE

Estimado Dr. Mendoza Díaz:

Por medio de la presente le informo que he leído y revisado detalladamente el contenido de la tesis titulada *"Structural and dynamical properties of colloids under confinement"* desarrollada por la **M. en F. Edith Cristina Euán Díaz** y dirigida por su servidor y co-dirigida por el Prof. Francois M. Peeters, y el Dr. Salvador Herrera Velarde. En su proyecto de investigación, Edith estudió, mediante la técnica de Dinámica Browniana, los sistemas coloidales de baja dimensión en presencia de campos externos periódicos. Los resultados y la calidad del trabajo que realizó Edith culminaron en la publicación de varios artículos de investigación, otros más están en proceso de escritura, y, principalmente, se obtuvo un convenio de doble titulación que nuestra Universidad compartirá con la Universidad de Antwerpen (Bélgica).

Por otro lado, le informo que la tesis está bien escrita y es auto-contenida. Esto favorece su fácil lectura y la comprensión de la misma. Considero que la tesis reúne, y por mucho, los requisitos de calidad para ser defendida por Edith, por lo que doy mi anuencia para formar parte del jurado de esta tesis, la cual puede defenderse en la fecha que sea más conveniente.

Atentamente,

Dr. Ramón Castañeda Priego
Profesor Titular B
Departamento de Ingeniería Física

DIVISIÓN DE CIENCIAS E INGENIERÍAS, CAMPUS LEÓN

Loma del Bosque 103, Fracc. Lomas del Campestre C.P. 37150 León, Gto., Ap. Postal E-143 C.P. 37000 Tel. (477) 788-5100 Fax:(477) 788-5100 ext. 8410, http://www.ifug.ugto.mx

Noviembre 28, 2013

Director Dr. Guillermo Mendoza Díaz

PRESENTE

Estimado Dr. Mendoza Díaz:

Por medio de este conducto le informo que estoy de acuerdo con el contenido de la tesis titulada "S***tructural and dynamical properties of colloids under confinement***", que para obtener el grado de Doctor en Física presenta la **M. en F. Edith Cristina Euán Díaz**. En dicha tesis se presenta un estudio sistemático de las propiedades estructurales y de transporte de sistemas coloidales con interacciones repulsivas; en la simulación molecular se toma en cuenta de manera explícita las interacciones hidrodinámicas así como diversos tipos y grados de confinamiento. Parte de los resultados obtenidos han sido publicados en revistas internacionales mientras que otros se encuentran bajo proceso de arbitraje en una revista internacional indexada. De esta forma, Edith C. Euán Díaz cumple con los requisitos académico-administrativos para llevar a cabo la defensa de su trabajo doctoral.

Sin otro particular por el momento, me despido enviándole un cordial saludo.

Atentamente,

Dr. Salvador Herrera Velarde

Profesor-Investigador

Subdirección de Posgrado e Investigación

INSTITUTO TECNOLÓGICO SUPERIOR DE XALAPA
Sección 5a de la Reserva Territorial s/n. Col. Santa Bárbara. C.P. 91096. Xalapa, Ver.
Tel: 01 (228) 1 65 05 25 www.itsx.edu.mx

Universiteit Antwerpen

Departement Fysica

FDFYS - GROENENBORGERLAAN 171, 2020 ANTWERPEN, BELGIE
Director Dr. Guillermo Mendoza Díaz
Division of Science and Engineering

Campus Groenenborger
Gebouw U
Groenenborgerlaan 171
2020 ANTWERPEN, BELGIE

Tel. 03/265.36.64
Fax 03/265.35.42

UW KENMERK

ONS KENMERK

DATUM
2 december 2013

BIJLAGE

Dear Dr. Mendoza Díaz,

Herewidth, I confirm that I have read and reviewed the PhD thesis "Structural and dynamical properties of colloids under confinement" by Edith Cristina Euán Díaz that was supervised by Prof. Ramón Castañeda Priego, Dr. Salvador Herrera Velarde, Dr. Vyacheslav Misko and myself.
In this thesis, Edith investigated low-dimensional colloidal systems in the presence of external fields by using Brownian dynamics simulations. This research resulted in several publications in international peer reviewed journals. Some of the work is still in the reviewing process and some of it has still to be submitted.
The thesis is well written and self-contained. In particular, I enjoyed also reading the historical part. The work is rather complete. Part of the work was done while Edith was a visiting scholar in my group at the University of Antwerp. This entitles her to obtain a joint PhD with our university.
I find the work is of high quality. The thesis meets all the requirements in order for Edith to be allowed for the defense of her PhD thesis. I agree to be a member of the Jury of this thesis and I am looking forward to her defense.

Sincerely yours,

Prof. Dr. François Peeters
Head of the research group CMT

Prof. dr. Francois Peeters
University of Antwerp (CGB)
Condensed Matter Theory
Department of Physics
Groenenborgerlaan 171
B-2020 Antwerpen

Universiteit Antwerpen
Faculteit Wetenschappen
Departement Fysica

Dr. V.R. Misko, PhD, Leader of ND-NANO Research Project "Odysseus" of the Flemish Government and FWO-Flanders

CMT, Department of Physics (U215)
University of Antwerp (CGB)
Groenenborgerlaan 171
B-2020 Antwerpen
Belgium
Tel: +32-(0)3-265.34.84, Fax: +32-(0)3-265.35.42
Email: Vyacheslav.Misko@uantwerpen.be

Date: December 3, 2013

Dr. Guillermo Mendoza Diaz
Director of Division of Science and Engineering

Dear Dr. Mendoza Diaz,

Hereby I confirm that I have read and reviewed in detail the content of the thesis entitled *"Structural and dynamical properties of colloids under confinement"* prepared by Ms. Edith Euán Cristina Diaz under supervision of Dr. Ramón Castañeda-Priego, Dr. Salvador Herrera Velarde (University of Guanajuato), Prof. Francois M. Peeters and myself (Universiteit Antwerpen), in accordance with the Agreement of a Joint PhD between the University of Guanajuato (Maxico) and Universiteit Antwerpen (Belgium).

In his thesis, Ms. Edith Euán Cristina Diaz studied the structural and dynamical properties of colloids in presence of periodic external fields, using Brownian dynamics simulations, with a special focus on the role of hydrodynamic interactions. The high quality of the research is confirmed by the fact that the obtained results have been published in recognized international journals in the field, plus other manuscripts are in preparation.

As regards the quality of the thesis, it is a well-written and self-consistent text, with a good balance between a general introduction and the original chapters. As such, the thesis by Edith, in my opinion, meets all the criteria for PhD works, and thus I recommend this work for the presentation to the jury members with a subsequent defense of the thesis.

Yours sincerely,

V.R. Misko

Universidad de Guanajuato

León, Gto., a 2 de diciembre de 2013

Asunto: Tesis
Edith Cristina Eún Díaz

DR. GUILLERMO MENDOZA DÍAZ
DIRECTOR DE LA DIVISIÓN DE CIENCIAS E INGENIERÍAS
CAMPUS LEÓN
P R E S E N T E

Por medio de la presente le informo que he leído y revisado detalladamente el contenido de la tesis titulada "Structural and dynamicalproperties of colloidsunderconfinement" desarrollada por la M. en F. Edith Cristina Euán Díaz y encuentro que los resultados así como las publicaciones en que culminaron sus trabajos son de alta calidad por lo que considero que el documento sometido reúne los requisitos para ser defendida por la M. en F. Euán.

Agradezco de antemano la atención brindada a la presente y aprovecho para enviarle un cordial saludo.

ATENTAMENTE
"LA VERDAD OS HARA LIBRES"
EL PROFESOR INVESTIGADOR

DR. JOSÉ LUIS LUCIO MARTÍNEZ

C.c.p. Archivo.

DIVISIÓN DE CIENCIAS E INGENIERÍAS, CAMPUS LEÓN
Loma del Bosque 103, Fracc. Lomas del Campestre C.P. 37150 León, Gto., Ap. Postal E-143 C.P. 37000 Tel. (477) 788-5100 Fax:(477) 788-5100 ext. 8410,
http://www.ifug.ugto.mx

Universidad de Guanajuato

CAMPUS LEÓN
DIVISIÓN DE CIENCIAS E INGENIERÍAS
DEPARTAMENTO DE INGENIERÍA FÍSICA

León, Gto. 2 de Diciembre del 2013

Dr. Teodoro Córdova Fraga
Coordinador de los PE del Posgrado en Física
División de Ciencias e Ingenierías.

Por medio de la presente le informo que doy mi aval para que Edith Cristina Euán Díaz , estudiante del Programa de Doctorado en Física, presente el examen de grado para la defensa de su trabajo de tesis que lleva por título ***Structural and dynamical properties of colloids under confinement***, una vez que la estudiante ha cumplido de manera satisfactoria el procedimiento de revisión y entrevista del trabajo de tesis.

Agradeciendo su atención, quedo a su órdenes para cualquier aclaración

Dr. Alejandro Gil-Villegas
Departamento de Ingeniería Física.

Loma del Bosque # 103, Col. Lomas del Campestre, León, Gto., México, C.P. 37150
Tel. 01 (477) 788 5100 Ext.8472, 8411, Fax. Ext. 8410
www.ugto.mx

UNIVERSIDAD AUTÓNOMA
DE SAN LUIS POTOSÍ

27 de Noviembre de 2013.

Dr. Guillermo Mendoza Díaz
Director de la División de Ciencias e Ingenierías
Universidad de Guanajuato
PRESENTE

Estimado Dr. Mendoza Díaz:

Por medio de la presente le informo que he leído y revisado el contenido de la tesis titulada "Structural and dynamical properties of colloids under confinement" desarrollada por la M. en F. Edith Cristina Euán Díaz.

Considero que este trabajo reúne los requisitos de una tesis doctoral, por lo que doy mi anuencia para formar parte del jurado de la misma, la cual puede defenderse en la fecha que sea más conveniente.

Atentamente,

Dr. Bernardo José Luis Arauz Lara

UASLP
Instituto de Física
INSTITUTO DE FÍSICA
"Manuel Sandoval Vallarta"
Álvaro Obregón 64, Zona Centro
CP 78000 • San Luis Potosí, S.L.P.
tel. (444) 826 2362 al 65
fax. (444) 813 3874
www.uaslp.mx
www.ifisica.uaslp.mx

UNIVERSIDAD NACIONAL
AUTONOMA DE MEXICO

INSTITUTO DE FISICA
Departamento de Física Teórica
Apartado Postal 20-364, 01000 México, D.F., ☎ (525)622-5014, 622-5020
FAX (525) 622-5015

México D.F. a 3 de diciembre de 2013

Director Dr. Guillermo Mendoza Díaz
División de Ciencias e Ingenierías
PRESENTE

Estimado Dr. Mendoza Díaz:

Por medio de la presente le informo que he leído y revisado detalladamente el contenido de la tesis titulada "*Structural and dynamical properties of colloids under confinement*" desarrollada por el **M. en C. Edith Cristina Euán Díaz** y dirigida por el Dr. Ramón Castañeda Priego.

La tesis está bien escrita y es auto-contenida. Esto favorece su fácil lectura y la comprensión de la misma. Por otro lado, considero que la tesis reúne, y por mucho, los requisitos de calidad para ser defendida por Edith, por lo que doy mi anuencia para formar parte del jurado de esta tesis, la cual puede defenderse en la fecha que sea más conveniente.

Atentamente,

Dra. Karen Patricia Volke Sepúlveda
Investigador Titular B
Departamento de Física Teórica, Instituto de Física
Universidad Nacional Autónoma de México